

**THREE DIMENSIONAL BIOMETRIC GUIDE IN  
DETERMINING MAXILLARY TOOTH POSITION AND  
ARCH FORM**

**OMAR FAROUQ TAWFIQ**

**FACULTY OF DENTISTRY  
UNIVERSITY OF MALAYA  
KUALA LUMPUR**

**2020**

**THREE DIMENSIONAL BIOMETRIC GUIDE IN  
DETERMINING MAXILLARY TOOTH POSITION AND  
ARCH FORM**

**OMAR FAROUQ TAWFIQ**

**THESIS SUBMITTED IN FULFILMENT OF THE  
REQUIREMENTS FOR THE DEGREE OF DOCTOR OF  
PHILOSOPHY**

**FACULTY OF DENTISTRY  
UNIVERSITY OF MALAYA  
KUALA LUMPUR**

**2020**

**UNIVERSITY OF MALAYA**  
**ORIGINAL LITERARY WORK DECLARATION**

Name of Candidate: OMAR FAROUQ TAWFIQ

Registration/Matric No: DHA110006

Name of Degree: DOCTOR OF PHILOSOPHY (Ph.D)

Title of Thesis:

THREE DIMENSIONAL BIOMETRIC GUIDE IN DETERMINING  
MAXILLARY TOOTH POSITION AND ARCH FORM

Field of Study: Restorative Dentistry (Prosthodontics)

I do solemnly and sincerely declare that:

- (1) I am the sole author/writer of this Work;
- (2) This Work is original;
- (3) Any use of any work in which copyright exists was done by way of fair dealing and for permitted purposes and any excerpt or extract from, or reference to or reproduction of any copyright work has been disclosed expressly and sufficiently and the title of the Work and its authorship have been acknowledged in this Work;
- (4) I do not have any actual knowledge nor do I ought reasonably to know that the making of this work constitutes an infringement of any copyright work;
- (5) I hereby assign all and every rights in the copyright to this Work to the University of Malaya ("UM"), who henceforth shall be owner of the copyright in this Work and that any reproduction or use in any form or by any means whatsoever is prohibited without the written consent of UM having been first had and obtained;
- (6) I am fully aware that if in the course of making this Work I have infringed any copyright whether intentionally or otherwise, I may be subject to legal action or any other action as may be determined by UM.

Candidate's Signature

Date:

Subscribed and solemnly declared before,

Witness's Signature

Date:

Name:

Designation:

# **THREE DIMENSIONAL BIOMETRIC GUIDE IN DETERMINING MAXILLARY TOOTH POSITION AND ARCH FORM**

## **ABSTRACT**

In complete denture fabrication, when pre-extraction records are lacking, determining the denture teeth positions to where the natural predecessors occupied is essential yet challenging. Although several biometric guides were suggested to position teeth for dentures, none is providing three-dimensional (3D) positions of teeth that can be used in the recently developed computer designed digital dentures. The aim of this study was to develop new biometric guides to determine the original 3D positions of the maxillary teeth and dental arch form individualised for each given dentate or edentulous maxillary cast based on selected intraoral landmarks. The objectives were to investigate the relationship between measurements of selected maxillary anatomical landmarks, to verify the accuracy of the relationship equations in predicting tooth position; to predict teeth positions for edentulous casts; to investigate the dental-arch curves morphological relationship with HNR-curve and predictability of dental arch for dentulous casts from HNR-curve.

Ninety-two Malaysian adults (20-35 years old) who had class I dental and skeletal relationships, well-aligned teeth and minimal attritions were selected for the study. Maxillary stone-casts were obtained, digitised and standardised. The points' 3D Cartesian-coordinates were converted into spherical-coordinates for statistical analyses. The dentate sample (n=92) was subdivided randomly into control group (n=70) and dentate verification group (n=22). The

control group was used to investigate linear regressions and functional circular relationships to generate equations, while the verification group was used to compare the coordinates of teeth predicted by the relationship equations with the measured coordinates in each cast of the group using paired *t*-test. Dental arch curves and hamular-notch rugae-point curve (HNR-curve) were fitted to polynomial-fourth-degree equations and compared for shape-similarity using Z-test ( $\alpha = 0.05$ ). Then artificial neural network (ANN) was used to generate dental arch curves by HNR-curves for dentate casts, verify the prediction accuracy of the method before application on edentulous casts. Thirty-four maxillary edentulous casts were obtained, digitised, standardised and had the triangular pyramid landmarks coordinates similar to the dentate casts registered and used to predict teeth positions. The results showed high correlation coefficients between the landmarks and teeth positions ( $0.5 \leq r \leq 0.9$ ,  $p < 0.05$ ). Fifty-four regression and circular relationship equations were derived to predict the teeth positions ( $0.89 \leq R^2 \leq 0.998$ ). No significant differences were found between the existing and predicted coordinates of teeth through the verification group subjects ( $p > 0.05$ ). When the arch forms were compared for similarity with HNR-curve; Z-test values (*SD*) were 0.894(0.64), 0.705(0.51), 0.382(0.31) for buccal, middle and lingual dental arches respectively. Within the limitations of this study, predicted teeth positions showed non-significant difference with the natural teeth positions when verified in new dentate sample. Furthermore, predicted teeth positions for edentulous sample showed statistical equivalence with the range of the natural teeth positions in dentate sample. Additionally, the predicted dental arch forms for verification dentate group showed no significant difference with the original dental arches. Conclusively, the maxillary teeth 3D-points together with the dental arch form may suggest

acceptable guide for digital dental rehabilitation for edentulous patients using the latest digital denture manufacturing technology based on stable intraoral anatomical landmarks with strong coefficients.

**Keywords:** Complete denture, Biometric guides; dental arch form; 3D tooth position; CAD/CAM complete denture.

Universiti Malaya

# **PANDUAN BIOMETRIK NOVEL DALAM MENENTUKAN BENTUK ARKUS MAKSILA DAN KEDUDUKAN 3D GIGI-GIGI BAGI PESAKIT BERGIGI DAN EDENTULUS**

## **ABSTRAK**

Dalam fabrikasi dentur penuh, penentuan kedudukan gigi-gigi palsu berdasarkan kedudukan gigi terdahulu adalah penting namun mencabar terutama dengan kekurangan rekod pra-cabutan. Walaupun beberapa panduan biometrik telah dicadangkan untuk memposisikan gigi-gigi palsu, tiada yang menyediakan kedudukan gigi palsu berdasarkan posisi tiga- dimensi (3D) yang dapat digunakan sejajar dengan perkembangan teknologi reka bentuk dentur digital. Tujuan kajian ini adalah untuk membangunkan panduan biometrik baru bagi menentukan kedudukan 3D gigi-gigi maksila dan arkus gigi bagi setiap tuangan bergigi dan edentulus berdasarkan kepada penanda aras intraoral yang dipilih. Objektifnya adalah untuk menyiasat hubungan penanda aras intraoral terpilih bagi mengesahkan ketepatan hubungan persamaan ramalan kedudukan gigi; untuk meramalkan kedudukan gigi pada tuangan edentulus; untuk menyiasat persamaan morfologi antara lengkung arkus gigi dan lengkung arkus yang dicadangkan, juga lengkung arkus gigi dari lengkung HNR tuangan edentulus.

Sembilan puluh dua orang dewasa warga Malaysia (20-35 tahun) yang mempunyai hubungan pergigian dan skeletal kelas I dengan gigi sejajar dan atrisi yang minimum telah dipilih untuk kajian ini. Tuangan kajian maksila diperolehi, didigitalkan dan diselaraskan. Titik koordinat Cartesian 3D ditukar menjadi koordinat sfera untuk analisis statistik. Sembilan puluh dua sampel pesakit bergigi dibahagi secara rawak kepada dua kumpulan, 70 dalam

kumpulan kawalan dan 22 dalam kumpulan verifikasi. Kumpulan kawalan digunakan untuk menyiasat regresi linear dan hubungan berfungsi sirkular untuk menghasilkan persamaan, manakala kumpulan verifikasi digunakan untuk membandingkan koordinat gigi yang diramalkan oleh hubungan persamaan dengan koordinat yang diukur pada setiap tuangan di dalam kumpulan menggunakan ujian-*t* berpasangan. Lengkung arkus gigi dan lengkung HNR dipadankan pada persamaan polinomial-darjah-keempat dan dibandingkan untuk bentuk-kesamaan menggunakan ujian *Z* ( $\alpha = 0.05$ ). Kemudian ANN digunakan untuk menghasilkan lengkung arkus gigi mengikut lengkung HNR bagi tuangan bergigi. Ini adalah untuk mengesahkan ketepatan kaedah ramalan sebelum diaplikasikan pada tuangan edentulus. Tiga puluh empat tuangan maksila edentulus diperolehi, didigitalisasi, diseragamkan dan ditandakan dengan tanda-tanda mercu tanda piramid yang serupa dengan yang terdapat pada tuangan bergigi yang didaftarkan untuk meramalkan kedudukan gigi. Hasilnya menunjukkan pekali korelasi yang tinggi di antara mercu tanda dan kedudukan gigi ( $0.5 \leq r \leq 0.9$ ,  $p < 0.05$ ). Lima puluh empat persamaan relasi regresi dan hubungan berfungsi sirkular diperolehi untuk meramalkan kedudukan gigi ( $0.89 \leq R^2 \leq 0.998$ ). Tidak terdapat perbezaan yang ketara antara koordinat gigi yang sedia ada dan yang diramalkan berdasarkan sampel kumpulan verifikasi ( $p > 0.05$ ). Apabila bentuk lengkung arkus dibandingkan dengan lengkung HNR; Nilai ujian *Z* (*SD*) masing-masing ialah 0.894 (0.64), 0.705 (0.51), 0.382 (0.31) bagi lengkung arkus pergigian bukal, tengah dan lingual. Berdasarkan batasan kajian ini, ramalan kedudukan gigi menunjukkan perbezaan yang tidak signifikan dengan kedudukan gigi semula jadi apabila disahkan menggunakan sampel bergigi yang baru. Tambahan pula, ramalan kedudukan gigi bagi sampel edentulus menunjukkan kesetaraan statistik

dengan julat kedudukan gigi semula jadi dalam sampel bergigi. Di samping itu, bentuk lengkung arkus gigi yang diramalkan untuk kumpulan verifikasi bergigi tidak menunjukkan perbezaan yang signifikan dengan lengkung arkus pergigian asal. Secara keseluruhannya, titik 3D gigi maksila bersama-sama dengan bentuk lengkung arkus pergigian yang dicadangkan berdasarkan penanda aras anatomi intraoral yang stabil dengan pekali yang kuat ini mungkin dapat menjadi panduan yang boleh diterima untuk rehabilitasi digital bagi pesakit edentulus dengan menggunakan teknologi terkini pembuatan gigi palsu digital.

**Kata kunci:** Gigi palsu lengkap, Panduan biometrik; bentuk arkus pergigian; Kedudukan gigi 3D; CAD / CAM gigi lengkap.

## ACKNOWLEDGEMENTS

I would like to thank Allah S.W.T. for giving me the health and ability to complete this work. I dedicate this work to my very supportive parents and wonderful wife who sacrificed the most to enable me to complete this long journey.

I would like to thank my lovely sisters and only brother, Ali. They were my inspiration and support throughout the study.

My appreciation goes to my advisors Associate Prof. Dr Zakiah, Associate Prof. Dr Norasmatul Akma Ahmad, Associate Prof. Dr Eshamsul Sulaiman, Dr Norli Anida, and Associate Prof. Dr Hamid Jalab.

I would like to thank Prof Datuk Dr Khairiya Abd Almuttalib and Prof Dr Norsiah Yunus for the great support they provided. Special thanks to Prof Wong Kok Sheik Prof, Dr Yong Zulina, Prof Dr Phrabhakaran, Dr Azwatee, Dr Siti Fauzza, Dr Mohideen, Dr Omar Rijal, Dr Norliza for their guidance, motivation and knowledge they have given to me.

I wish to extend my thanks to my awesome friends Dr Okba, Dr Aymen, Dr Iqbal, Dr Hasan, Dr Anwar, Dr Chalabi, Dr Maath, Mr Mustafa, Dr Ayad, Dr Belal, Mr and Mrs Konno, Dr Kumar, Dr Srinivas, Dr Suchismita, Dr Indumathi and Ms Helen. I would like to thank Ms Junaidah, Ms. Zuraida, admin staff in restorative department: Mrs Sauda, Ms Masitah, Mrs Roslina,, Mrs Norhayati, the dental technicians Mr Rosli, Mr Najib, Ms Rozlina, Ms Suthashini and last but not least to Madam Alina for her wonderful help and to all the participants and patients involved in the study.

This study was supported by MOSTI scientific project number 02-01-03-SF0384, Faculty of Dentistry, University of Malaya, Kuala Lumpur, Malaysia

## TABLE OF CONTENTS

THREE DIMENSIONAL BIOMETRIC GUIDE IN DETERMINING MAXILLARY TOOTH POSITION AND ARCH FORM.....	iii
Abstract .....	iii
PANDUAN BIOMETRIK NOVEL DALAM MENENTUKAN BENTUK ARKUS MAKSILA DAN KEDUDUKAN 3D GIGI-GIGI BAGI PESAKIT BERGIGI DAN EDENTULUS .....	vi
Abstrak .....	vi
Acknowledgements .....	ix
Table of Contents .....	x
List of Figures .....	xviii
List of Tables.....	xxiii
List of Symbols and Abbreviations.....	xxv
List of Appendices .....	xxviii
<b>CHAPTER 1 .....</b>	<b>1</b>
<b>CHAPTER 1: INTRODUCTION.....</b>	<b>2</b>
1.1 Background of the study .....	2
1.1.1 Alveolar ridge resorption .....	3
1.1.2 The rehabilitation of edentulous arch: The evolution .....	4
1.2 Problem statement and significance of the research.....	7
1.3 Hypothesis .....	9
1.4 Aim of the study .....	9
1.5 Objectives of the study .....	9
<b>CHAPTER 2 .....</b>	<b>11</b>



2.7	Digital and computerised dentistry .....	46
2.7.1	Digital dental cast analysis and research.....	46
2.7.2	The geometrical coordinate systems .....	46
2.7.3	The Cartesian coordinate system.....	47
2.7.3.1	The transformations of coordinates in the Cartesian system.....	48
2.7.3.2	Three-dimensional coordinate systems .....	49
2.7.4	The spherical coordinate system .....	50
2.7.4.1	The radius ( $l$ ) .....	52
2.7.4.2	The azimuth angle ( $\theta$ ) .....	52
2.7.4.3	The elevation angle ( $\phi$ ) .....	53
2.7.5	Angular and circular data analysis .....	53
2.7.6	Computer guided complete denture technology.....	54
2.7.6.1	Advantages of CAD/CAM complete dentures.....	56
2.7.6.2	Commercially available CAD/CAM complete denture systems .....	57
2.8	Form of dental arch in literature .....	62
2.8.1	Significance of the dental arch form .....	62
2.8.2	The need for dental arch form in dental application .....	65
2.8.2.1	In orthodontics.....	65
2.8.2.2	In prosthodontics .....	66
2.8.2.3	In oral surgery .....	67
2.8.3	Reference points used to define the dental arch form .....	67
2.8.4	Digitising and comparing dental arches .....	68
2.8.5	Mathematical representation of dental arch form .....	69
2.9	The position of teeth in dental arch .....	70
2.10	Statistical analysis in dental research .....	72

2.10.1	The Pearson product moment correlation .....	72
2.10.2	Regression analysis .....	73
2.10.2.1	Regression model assumptions .....	73
2.10.2.2	Simple linear regression model (SLRM) .....	74
2.10.2.3	Multiple linear regression model (MLRM).....	75
2.10.2.4	Simple functional linear relationship in circular data .....	77
2.10.3	Assessing goodness-of-fit of regression models .....	77
2.10.3.1	Coefficient of determination $R^2$ .....	77
2.10.3.2	Weighted least squares regression.....	78
2.10.3.3	Multicollinearity and variance inflation factor (VIF) .....	79
2.10.3.4	Identify the important variables in the multiple regression model .....	81
2.11	Computer artificial intelligence (AI) .....	81
2.11.1	Artificial Neural Networks (ANN) .....	81
2.11.1.1	Back-propagation artificial neural network (ANN) .....	82
2.11.1.2	Advantages and disadvantages of the AI highlighted by the literature .....	83
2.11.1.3	Application of artificial intelligence on complete denture .....	83
<b>CHAPTER 3 .....</b>		<b>85</b>
<b>CHAPTER 3: MATERIALS AND METHODS .....</b>		<b>86</b>
3.1	Sample of the study .....	86
3.1.1	The dentate sample.....	86
3.1.2	The edentulous sample .....	88
3.2	Ethical approval and patient consent .....	89
3.3	Study flow charts .....	90
3.4	Dental cast collection and standardisation.....	91

3.4.1 Dentate arch impressions .....	91
3.4.2 Dentate cast preparation .....	92
3.4.3 Edentulous arch impressions .....	93
3.4.4 Edentulous cast preparation .....	93
3.4.5 Digitising the dental casts into three-dimensional digital casts .....	94
3.4.6 Standardising the digital casts before measurements .....	97
3.4.6.1 Registering the landmarks .....	98
3.4.6.2 Aligning the digital casts to Cartesian XY plane (Phase I).....	103
3.4.6.3 Coordinates' transformation to standardise cast position (Phase II) .....	112
3.4.6.4 Integrity of digital measurements (error of the measurements).....	121
3.5 First objective: Three-dimensional tooth position in relation to landmarks.....	121
3.5.1 The sample of the first objective .....	121
3.5.2 Study flow chart (first objective) .....	123
3.5.3 Converting the Cartesian coordinates to spherical coordinate system.....	124
3.5.4 Linear radial distance of the tooth ( $\ell$ ) .....	127
3.5.5 The azimuth ( $\theta$ ) and the elevation ( $\varphi$ ) angles of spherical coordinate system .....	130
3.5.6 Data analysis (objective 1a) .....	132
3.5.6.1 Statistical analysis .....	132
3.5.6.2 Calculating the radial distance ( $\ell$ ).....	133
3.5.6.3 Calculating azimuth angle ( $\theta$ ) .....	135
3.5.6.4 Calculating elevation angle ( $\varphi$ ) .....	137
3.5.7 The verification of the method in first objective (objective 1b) .....	137
3.5.8 Regression analysis to investigate the relationship between variables .....	139

3.5.8.1	Residual plots .....	139
3.5.8.2	Weighted least squares regression.....	140
3.5.9	Determining maxillary teeth positions for new independent dentate sample .....	140
3.5.10	Determining maxillary teeth position for edentulous patients (objective 1c).....	141
3.6	Second objective: The relationship between the form of palatal vault and the form of the dental arch.....	144
3.6.1	Dental arch form.....	144
3.6.2	Sample and materials .....	146
3.6.3	Study flow chart (second objective).....	146
3.6.4	Identifying the curves of dental arch.....	147
3.6.4.1	The palatal vault curve (HNR curve) .....	147
3.6.4.2	The dental arch curves.....	150
3.6.5	Digitising the dental arch curves .....	153
3.6.5.1	Fitting mathematical functions to the dental arch curves.....	156
3.6.6	Similarity between the curves (hypothesis test).....	157
3.6.7	Predicting the dental curve from the HNR curve.....	158
3.6.8	Predicting dental arch for dentate sample .....	159
3.6.9	Verification test of the method in second objective.....	159
3.6.10	Predicting the form of maxillary dental arch for edentulous cases .....	160
<b>CHAPTER 4 .....</b>		<b>162</b>
<b>CHAPTER 4: RESULTS.....</b>		<b>163</b>
4.1	Introduction on results .....	163
4.2	3D position of maxillary teeth .....	163

4.2.1	Descriptive statistics.....	163
4.2.1.1	Cartesian coordinates .....	163
4.2.1.2	Spherical coordinates .....	167
4.2.2	Analysis to determine position of teeth in dentate subjects .....	171
4.2.2.1	The radius coordinate analysis of the teeth .....	171
4.2.2.2	The azimuth angle determination.....	179
4.2.2.3	Elevation angle determination.....	182
4.2.3	Determining maxillary teeth positions for the edentulous sample.....	186
4.2.4	Equivalence test results .....	191
4.2.5	Results of integrity of study's digital measurements (error of measurements).....	193
4.3	Results of maxillary dental arch curve reconstruction .....	194
4.3.1	Verification results .....	194
4.3.2	The comparison between the forms (form similarity test) .....	194
4.3.3	Prediction of dental arch curve based on palatal curve.....	195
4.3.4	Verification of the dental arch prediction method .....	199
4.3.5	Application on edentulous casts: prediction dental arch curves for edentulous cast .....	202
<b>CHAPTER 5</b>	<b>.....</b>	<b>204</b>
<b>CHAPTER 5: DISCUSSION</b>	<b>.....</b>	<b>205</b>
5.1	The selection of study sample.....	207
5.2	Data collection.....	208
5.3	The variables used in the study.....	209
5.3.1	The landmarks selected for this study analysis .....	209
5.3.1.1	Hamular notches.....	209
5.3.1.2	Incisive papilla .....	211

5.3.1.3	Rugae lines, midpalatal raphe and rugae point (R-point).....	211
5.3.1.4	Points representing tooth position .....	213
5.4	Tooth position determination for dentate and edentulous arch .....	214
5.4.1	Determination of teeth positions for edentulous sample.....	220
5.4.2	The current CAD/CAM complete denture systems and their method for teeth selection.....	221
5.5	Reconstructing the maxillary dental arch form .....	222
5.5.1	Application on edentulous cases .....	223
<b>CHAPTER 6</b>	.....	<b>225</b>
<b>CHAPTER 6: CONCLUSIONS</b>	.....	<b>226</b>
6.1	Limitations of the study .....	226
6.2	Conclusions .....	227
6.2.1	Summary and potential future benefits of this research.....	228
6.3	Recommendations for further study .....	230
REFERENCES	.....	231
Appendices	.....	252
Appendix A	.....	253
Appendix B	.....	258
Appendix C	.....	260
Appendix D	.....	261
Appendix E	.....	268
Appendix F	.....	274
Appendix G	.....	276
Appendix H	.....	286

## LIST OF FIGURES

Figure 2.1: Suggested distance between incisive papilla and labial surface of central incisors. Blue line shows the suggested relation between intercanine line and incisive papilla.....	35
Figure 2.2: Measurements of the buccolingual breadth (BLB) in the anterior and posterior teeth before extraction. Adopted from Nomura et al. (1991) .....	42
Figure 2.3: Illustration showing the lingual gingival vestige and the suggested horizontal buccal breadth in denture flanges to restore cheek support. Dotted line is the farthest distance of the flanges .....	43
Figure 2.4: Diagram showing the elements of the spherical coordinate system in presenting the Cartesian point $P(x, y, z)$ .....	50
Figure 2.5: Illustration showing the spherical and Cartesian coordinates for a 3D point .....	51
Figure 2.6: Comparison between angles of 30 measured in radians and degrees.....	54
Figure 2.7: Current arbitrary alignment of teeth in DRCD that need to be adjusted individually by the dentist or technician (Masri & Driscoll, 2015) .....	55
Figure 2.8: Basic elements of an artificial neuron (adopted from Tayşi (2010)).....	82
Figure 3.1: The overall flow chart of the study based on objectives .....	90
Figure 3.2: Preparing the casts to ensure trimming the base on a level parallel to the occlusal plane.....	92
Figure 3.3: (A) Standardising edentulous cast to have the hamular incisive papilla plane parallel to the horizon using a surveyor and tripodding technique (B) following HNIP, tripodding three vertical lines of 20mm were marked on the cast using a carbon marker .....	94
Figure 3.4: Maestro 3D dental scanner machine. MDS200 model.....	95
Figure 3.5: Occlusal view of anterior part of the 3D digitised dentate (above) and edentulous (below) casts showing the triangles mesh acquired by the 3D dental scanner.....	96
Figure 3.6: Software settings to view and align the digital dental cast in Cartesian coordinate system.....	98

Figure 3.7: Tracing the rugae lines and assigning R-point on dentate (above) and edentulous (below) digital casts .....	101
Figure 3.8: Digital cast and the landmarks registration in 3D analyser software. Hamular notches (LHN & RHN) and the incisive papilla (IP) were used to align the casts to Cartesian coordinate system; 22 selected points were illustrated in the diagram.....	102
Figure 3.9: Triangular biometric pyramid illustrated on edentulous digital cast showing the essential lines used as predictors extending between the the four selected landmarks .....	102
Figure 3.10: (A) Flat 2D image (brown) opened in the Cartesian system (VAM software) and selection of circle shape (green) was made on the centre of the plane. (B and C) Selection was inversed; (B and D) selected area was deleted.....	106
Figure 3.11: Introducing the digital cast next to the prepared XY plane before Phase I alignment .....	107
Figure 3.12: Projecting (cloning) the selected landmarks on the XY plane and reading the landmarks' coordinates before registering surfaces.....	108
Figure 3.13: Register and transform the digital cast to superimpose the landmarks to the corresponding one on the plane.....	109
Figure 3.14: The digital cast aligned in phase II before translation.....	110
Figure 3.15: Digital cast in phase I processing using VAM software, HNIP plane alignment with XY plane (yellow surface). The 3D coordinates are displayed on the right pane of the screen .....	111
Figure 3.16: The clockwise rotation of the dental cast to get the RHN and LHN aligned to X-axis .....	114
Figure 3.17: The counterclockwise rotation of the dental cast to align RHN and LHN to X-axis.....	114
Figure 3.18: The digital cast is aligned according to phase II processing .....	115
Figure 3.19: Final translation of the digital cast on Y and Z axes to have R-point as the Cartesian origin .....	116
Figure 3.20: When R-point is origin, all the other landmarks will have positive z coordinates .....	118
Figure 3.21: Final standardised position for digital cast where R-point become the origin (0, 0, 0) and HNIP plane is parallel to XY plane.....	118

Figure 3.22: Screenshot for the Excel sheet sample used for coordinate transformation (rotation) in phase II.....	119
Figure 3.23: Screenshot for sample Excel sheet showing final coordinate translation to standardise R-point as the origin.....	120
Figure 3.24: Flow chart for the study (objective 1) .....	123
Figure 3.25: Diagram showing the direction of measuring the azimuth angle ( $\theta$ ) of spherical coordinates of the teeth in dental arch. Example of right canine is given .....	126
Figure 3.26: Diagram showing the spherical coordinates for right central incisor tooth (RCI): radius ( $\ell$ ) in yellow and elevation angle in pink ( $\phi$ ).....	126
Figure 3.27: Linear measurements obtained for first objective: (red) is HNIP plane and distances between RHN, LHN and IP, (black) radial distances of teeth from R-point, (yellow) distance between IP and R-point, (pink) distance between LHN and R-point, (green) distance between RHN and R-point and, (blue) depth of R-point from HNIP plane .....	128
Figure 3.28: Biometric triangular pyramid illustrated on maxillary digital cast where: the base (grey) is HNIP plane, the slanting (red) lines are the distances between R-point and each of LHN, RHN and IP respectively. The (blue) line is the vertical height of HNIP plane from R-point .....	129
Figure 3.29: Side view showing triangular pyramid: (red) HNIP plane, (yellow) IP-R line, (green) LHN-R, (white) RHN-R and (blue) is R-point depth from HNIP.....	129
Figure 3.30: The angles of elevation $\phi$ of teeth measured .....	131
Figure 3.31: The measurement of azimuth angles $\theta$ in counter clockwise direction....	131
Figure 3.32: The calculation of azimuth angle in Cartesian system .....	136
Figure 3.33: The azimuth angle is representing the position of the tooth from (+ve) x-axis on a counter clockwise direction .....	136
Figure 3.34: Digital cast aligned by having R-point as the origin (0, 0, 0). Red, yellow and black lines are the Cartesian X, Y and Z axes respectively .....	141
Figure 3.35: Triangular pyramid measurements on maxillary edentulous cast .....	142
Figure 3.36: The observed similarity between the forms of the dental arches and the HNIR curve .....	145
Figure 3.37: Flow chart for the study (objective 2) .....	146

Figure 3.38: Landmarks registration and HNR curve formation .....	148
Figure 3.39: Digitising HNR curve by making points to fit polynomial curve equation .....	149
Figure 3.40: Palatal vault curve (HNR curve) in edentulous maxillary cast .....	150
Figure 3.41: Dental arch curves: (A) buccal cusps curve T <sub>1</sub> , (B) fossae curve T <sub>2</sub> and (C) lingual cusps curve T <sub>3</sub> .....	152
Figure 3.42: Buccal dental curve (T <sub>1</sub> ) in green, central fossae curve (T <sub>2</sub> ) in maroon and lingual dental curve (T <sub>3</sub> ) in blue.....	154
Figure 3.43: Digitising the palatal and dental curves in 2D image using GetData software.....	155
Figure 3.44: Example of fitting the buccal cusps curve (T <sub>1</sub> ) to 4 <sup>th</sup> degree polynomial equation. R <sup>2</sup> is indicating the percentage of the curve fitting the 18 points.....	157
Figure 3.45: Neural network training tool flow .....	159
Figure 4.1: Occlusal view of average 3D tooth position points for dentate sample plotted on Cartesian graph .....	166
Figure 4.2: Frontal view of average of 3D tooth position points for dentate sample plotted on Cartesian graph .....	166
Figure 4.3: Right side view of average 3D tooth position points for dentate sample plotted on Cartesian graph .....	167
Figure 4.4: Rose graph showing the means and standard deviations of the azimuth angles measured in experiment dentate group (n = 70) .....	170
Figure 4.5: Front view of average predicted 3D tooth position points for edentulous sample compared to dentate sample plotted on Cartesian graph .....	189
Figure 4.6: Right side view of average predicted 3D tooth position points for edentulous sample compared to dentate sample plotted on Cartesian graph.....	190
Figure 4.7: Occlusal view of average predicted 3D tooth position points for edentulous sample compared to dentate sample plotted on Cartesian graph.....	190
Figure 4.8: Rose graph showing the range of azimuth angles of the maxillary teeth in dentate sample (n = 92) compared to the range of azimuth angles of the correspondent teeth predicted for edentulous sample (n = 34).....	192

Figure 4.9: The training data were given to the ANN as 2D coordinates in millimetre: 18 points of HNR curve (T <sub>0</sub> ) as original curve; 18 points of T <sub>1</sub> ; 18 points of T <sub>2</sub> and 18 points for T <sub>3</sub> as target curves.....	195
Figure 4.10: The neural network training dataset after training completion.....	196
Figure 4.11: Performance plot for ANN with 7 Epochs showing the iteration at which the validation performance reached a minimum MSE as 0.65 at epoch 4.....	197
Figure 4.12: Regression plots of training, validation, testing and total data and fitting lines with coefficients of determinations of the proposed ANN.....	198
Figure 4.13: Histogram showing the error instances between the predicted output and the target curves .....	199
Figure 4.14: Verification predicted dental arch curves (red) shown in comparison to the (green) actual dental arch curves (A)T <sub>1</sub> buccal cusps curve, (B)T <sub>2</sub> fossae curve and (C)T <sub>3</sub> Palatal cusps curve for dentate subjects predicted using the palatal vault curve, HNR-curve (blue) through the ANN.....	201
Figure 4.15: Predicted dental arch curves for edentulous casts by given T <sub>0</sub> curve, T <sub>1</sub> , T <sub>2</sub> and T <sub>3</sub> were predicted.....	202
Figure 4.16: ANN system application to predict dental arch curves for given HNR curve of edentulous cast. (A) predicting the buccal cusps curve T <sub>1</sub> , (B) predicting the central fossae curve T <sub>2</sub> and (C) predicting the lingual cusps curve T <sub>3</sub> .....	203
Figure 6.1: Occlusal view for four cases showing extensive hyperplastic changes in the palatal mucosa. Image taken from Rao et al. (2014).....	227

## LIST OF TABLES

Table 2.1: Descriptive statistics for measurements representing breadth of the residual ridge measured the horizontal distance between the lingual gingival margin and the mid-buccal point of the teeth regions in 100 patients (Watt & MacGregor, 1976) .....	41
Table 2.2: Comparison of various types of currently available CAD/CAM completed denture systems and manufacturers .....	59
Table 3.1 Modified <i>t</i> -tests applied to compare palatal curves and dental arches.....	158
Table 4.1: Means and standard deviations of the Cartesian coordinates ( <i>x, y, z</i> ) of the biometric triangular pyramid points (in mm).....	165
Table 4.2: Means and standard deviations of the Cartesian coordinates ( <i>x, y, z</i> ) (in mm) of the teeth and landmarks of the experiment dentate groups ( <i>n</i> = 70) .....	165
Table 4.3: Means and standard deviations of the spherical coordinates ( $\ell, \theta, \varphi$ ) of the biometric triangular pyramid points.....	168
Table 4.4: Means and standard deviations of the spherical coordinates ( $\ell, \theta, \varphi$ ) that represent the location of the teeth and landmarks in relevance to the origin (R-point) 168	168
Table 4.5: Pearson correlation coefficient values for correlation analysis between the teeth radial distance and landmarks measurements .....	172
Table 4.6: Summary of one or more predictors out of Table 4.5 that are eligible and recommended to use for regression relationship analysis to find the radius ( $\ell$ ) values for the teeth .....	173
Table 4.7: Weighted simple regression models, coefficients of determination and variance inflation factors for predicting the radial element ( $\ell$ ) of spherical coordinates for maxillary left and right of anterior teeth points in relevance to R-point.....	174
Table 4.8: Weighted simple and multiple regression models, coefficients of determination and variance inflation factors for predicting the radial element ( $\ell$ ) of spherical coordinates for the maxillary left and right posterior teeth points in relevance to R-point .....	175
Table 4.9: Descriptive statistics, means and standard deviations of the spherical coordinates ( $\ell, \theta, \varphi$ ) of the biometric triangular pyramid points of the verification sample ( <i>n</i> = 22) .....	176

Table 4.10: Descriptive statistics of the spherical coordinates ( $\ell$ , $\theta$ , $\varphi$ ) that represent the location of the teeth and landmarks with relevance to the origin (R-point) in the verification sample (n = 22) .....	177
Table 4.11: Means, standard deviations and $p$ -values of paired $t$ -tests comparing the predicted and measured radial coordinates ( $\ell$ ) values of the verification new dentate group (n = 22) .....	178
Table 4.12: Functional linear relationship models for predicting the azimuth angle ( $\theta$ ) spherical coordinate measured in radians for the left and right anterior and posterior maxillary teeth positions in relation to R-point .....	179
Table 4.13: Means, standard deviations and $p$ -values of paired $t$ -test comparing the predicted and measured values of the azimuth angle spherical coordinate ( $\theta$ ) of the verification new dentate group (n = 22) .....	181
Table 4.14: Functional linear relationship models for predicting the elevation angle ( $\varphi$ ) spherical coordinate measured in radians for the left and right anterior and posterior maxillary teeth positions in relation to R-point .....	183
Table 4.15: Means (standard deviations) of the measured and predicted elevation angles for the teeth with $p$ -values for paired $t$ -test for each comparison between the angles $\varphi$ with confidence interval of 95% for verification sample (n = 22) .....	185
Table 4.16: Spherical coordinates of the biometric triangular pyramid of edentulous sample (n = 34) application sample .....	186
Table 4.17: Predicted spherical coordinates for teeth position for edentulous sample (n = 34) application sample .....	187
Table 4.18: Cartesian coordinates' means and standard deviations version of the biometric triangular pyramid for application sample (n = 34) of edentulous subjects .	188
Table 4.19: Cartesian coordinates' means and standard deviations version of the predicted coordinates of teeth for application sample (n = 34) of edentulous subjects	188
Table 4.20: Means (standard deviations) and paired $t$ -test value for the digital and manual measurement on Error! Reference source not found. ....	193
Table 4.21: Summary statistics of one sample $z$ -test comparing the difference in the dentate sample between the palatal curve ( $T_0$ ) and buccal ( $T_1$ ), central ( $T_2$ ) and lingual ( $T_3$ ) dental arch curves by $Z_1$ , $Z_2$ and $Z_3$ respectively (n = 92) .....	194

## LIST OF SYMBOLS AND ABBREVIATIONS

Abbreviation	Full name
AI	: Artificial intelligence
ANN	: Artificial neural network
$\theta$	: Azimuth angle of the spherical coordinates system
BPN	: Back-propagation neural networks
BLB	: Buccolingual breadth
Z	: Coefficient of Z test (modified <i>t</i> -test)
CD	: Complete denture
CAD/CAM	: Computer aided design / Computer aided manufacturing
CECD	: Computer engineered complete denture
CCD	: Conventional complete denture
DCD	: Digital complete denture
*.stl	: Digital stereolithographic binary format
$\phi$	: Elevation (polar) angle of the spherical coordinates system measured from a fixed zenith direction
IP	: Incisive papilla
L1PM	: Left first premolar buccal cusp tip
L2PM	: Left second premolar buccal cusp tip
LC	: Left canine cusp tip
LHN	: Left hamular notch

LDb1M	:	Left disto-buccal cusp tip of first molar
LDb2M	:	Left disto-buccal cusp tip of second molar
LMb1M	:	Left mesio-buccal cusp tip of first molar
LMb2M	:	Left mesio-buccal cusp tip of second molar
MSE	:	Mean standard error
LCI	:	Middle of the incisal edge of left central incisor
LLI	:	Middle of the incisal edge of left lateral incisor
RCI	:	Middle of the incisal edge of right central incisor
RLI	:	Middle of the incisal edge of right lateral incisor
$mod\ 2\pi$	:	Modular arithmetic
-ve	:	Negative
OP	:	Occlusal plane
OVD	:	Occlusal vertical dimension
O	:	Origin in Cartesian coordinates system (0, 0, 0)
R-point	:	Point of junction between the midpalatal raphe with the line joining the medial points of the left and right third rugae lines
PDL	:	Periodontal ligament
+ve	:	Positive
RP	:	Rapid prototyping
RRR	:	Residual ridge resorption
R1PM	:	Right first premolar buccal cusp tip
RC	:	Right canine cusp tip

RDb1M	:	Right disto-buccal cusp tip of first molar
RDb2M	:	Right disto-buccal cusp tip of second molar
RHN	:	Right hamular notch
RMb1M	:	Right mesio-buccal cusp tip of first molar
RMb2M	:	Right mesio-buccal cusp tip of second molar
SD	:	Standard deviation
DALY	:	The disability-adjusted life-years
TMJ		Temporomandibular joint
HNR	:	The plane on the cast that extends through the hamular-notches and R-point.
HNIP	:	The plane on the cast that extends through the incisive papilla and left and right hamular notches.
$\ell$	:	The radial distance of point from the origin in spherical coordinates system
3D	:	Three-dimensional
VIF	:	Variance inflation factor
obj	:	Wavefront OBJ (obj) attribute computer file

## LIST OF APPENDICES

Appendix A: Participant information and consent sheet	253
Appendix B: Matlab algorithm code for the simple circular analysis	258
Appendix C: Selected scatter plots for variables	260
Appendix D: Normality tests for the variables used for regression	261
Appendix E: Regression analysis residual VS fit plots for regression analysis	268
Appendix F: Comparison study data for digital VS manual measurements	274
Appendix G: Equivalence plots for Two-Sample Equivalence	276
Appendix H: Polynomial fourth-degree equations	286

# **CHAPTER 1**

---

## Introduction

---

Universiti Malaya

## CHAPTER 1: INTRODUCTION

### 1.1 Background of the study

Edentulism is still a high prevalence and is expected to keep being high in elderly population (Schimmel et al., 2019). Conventional removable complete denture is the most common treatment modality for rehabilitation of edentulous patients (Kutkut et al., 2018). In order to achieve the optimal aesthetics, phonetics and stability of denture during function, the denture teeth should be positioned in the optimal places which are the positions previously occupied by natural teeth (Watt, 1978). In the absence of pre-extraction records, various biometric guides were suggested to determine the optimal position of the teeth that subsequently lead to the optimal dental arch form, occlusal plane orientation, vertical dimension of occlusion, aesthetics, phonetics and function (Scandrett et al., 1982; Devlin & Hoad-Reddick, 2001). However, dental literature often considered the currently known biometric guides as unstable guides longitudinally and having questionable reliability due to reference points' inconsistency and instability (Watt & Likeman, 1974; Ortman & Tsao, 1979; Mavroskoufis & Ritchie, 1981).

Recently, digital technology has offered faster and more accurate approach in the fixed and removable complete denture field. The teeth positions in the modern treatment approach are the basic and essential as long as they are the final outcome in the treatment and careful planning for the digital denture design and/or supporting implants positions became due (Masri & Driscoll, 2015).

### **1.1.1 Alveolar ridge resorption**

It is well known that after any tooth extraction, reduction in the quality and quantity of the supporting alveolar bone will occur on the site of extraction in both buccolingual and apicocoronal directions in accordance with Wolff's law, which states that every change in the function of bones is followed by definite changes in their internal architecture and external shape (Amin, 2010). This reduction happens gradually and it is known as residual ridge resorption (RRR) (Lam, 1960; GPT-9, 2017). The ridge resorption may continue even after healing of the extraction socket and may become extreme when periodontal, periapical or bone defect occur in the extraction site (Araújo & Lindhe, 2005; GPT-9, 2017). In edentulous arch, RRR become more extensive. Atwood (1971) described the resorption as a cumulative multifactorial entity that involves bone loss in various rates and amounts from individual to individual, within the same individual at different times, and even at the same time in different parts of the ridge. Due to the progression of RRR in edentulous patient, the remaining alveolar residual ridges may provide insufficient support for the cheeks and lips horizontally and inter-arch occlusal stop vertically. This lack of support may lead to reduction in lower face height, temporomandibular joint disorders, and progressive anatomical, physiological and psychological changes to the patient. Further instability, lack of retention to the prostheses and unnatural patient's appearance may result ever since the patient starts to lose teeth (Atwood & Coy, 1971; Atwood, 1979; Doundoulakis et al., 2003; Divaris et al., 2012; Misch, 2014).

### **1.1.2 The rehabilitation of edentulous arch: The evolution**

Since the discovery of acrylic around 80 years ago, the denture base material has shown advancement in properties that made it almost ideal denture base material. This reflected a significant improvement in retention, stability and support of dentures and helped to conceptualise what is now known as conventional complete denture (CCD). The CCD has become the most common treatment option prescribed to rehabilitate an edentulous arch because of its non-invasiveness, cost-effectiveness, compatibility, relative simplicity, and convenience for most patients (Johnson, 1959; Zarb et al., 2013). However, restoration of the edentulous mouth is considered as one of the most difficult and challenging dental procedures. Hawkinson (2005) described the creation of complete denture (CD) and full mouth rehabilitation as “starting with nothing”; The denture construction poses challenges to the dentists in determining many important decisions such as the proper extension to restore facial support, the proper vertical dimension, the position, size and form of the teeth and involve multiple steps and visits to resolve the final prosthesis design that can fulfil both aesthetic and functional needs for individual patients. Due to limited and regressive denture bearing tissues remaining after RRR and related changes taking place in edentulous arch, the prosthesis may witness limited mucosal quality and support, less stability, and less mucosal retention during function and action of the muscles of the lips, cheeks, tongue and other surrounding muscles, especially in mandibular CD (Winkler, 1988).

Due to the alveolar ridge resorption, retention, support and stabilisation for the dentures became difficult on the edentulous arches, especially lower dentures (Winkler, 1988). Because of this, to minimise these disadvantages,

conventional complete denture had critical limitations in positioning the teeth and certain concepts for designing the denture and setting the teeth were developed and coined such as balanced occlusion (Zarb et al., 2013), setting lower teeth on the crest of the residual ridge first and customising the upper teeth positions to fit (Winkler, 1988) and arranging the artificial teeth in the neutral zone away from the natural teeth positions (Beresin & Schiesser, 2006; Rahn et al., 2009).

The discovery of endosseous dental implants and their incorporation in complete overdenture support have improved largely the denture's retention, stability, support and patient's comfort. Both dental implants and bone grafting have helped many edentulous patients who were unable to wear complete denture due to severe bone resorption (Doundoulakis et al., 2003; Zarb et al., 2013). In addition, new treatment options became available for edentulous cases such as the implant supported fixed or removable complete dentures. Dental implants and bone grafting may not be the best solution for all the edentulous cases. However, the successful implant borne prosthodontics definitely have superior biomechanics, greater biting forces and masticatory efficiency compared to the CCD (Prithviraj et al., 2014); this allowed the prosthesis to carry artificial teeth in a cantilevered position if the design planned to apply stresses on the implants within the acceptable physiological limits. Nevertheless, the methods and procedures of complete denture construction especially in occlusion, determining the occlusal plane (OP) orientation, the occlusal vertical dimension (OVD) and teeth arrangement were maintained the same as in CCD (Kim et al., 2005; Misch, 2014).

The extension of computer aided design/computer aided manufacturing (CAD/CAM) and rapid prototyping (RP) technologies to the fabrication of removable prosthodontics such as digital complete denture (DCD) / computer engineered complete denture (CECD) have been developed albeit slower than in the fixed prosthodontics; Through the last decade, many studies have contributed to developing the technology to reduce significantly the number of clinical appointments from lengthy 5 or 6 visits to 2 or 3 short appointments (Bidra et al., 2016). Retention, stability, support and comfort were significantly improved, and patient preference was achieved compared to the CCD (Maeda et al., 1994; Zhang et al., 2002; McLaughlin & Ramos, 2015; Bilgin et al., 2016; Kattadiyil & AlHelal, 2017). However, in designing CECD, traditional 2D and arbitrary guides and concepts are still followed besides difficulty reported in reading a digital preview in CECDs that is identified as a unique complication limiting the outcome (AlHelal et al., 2017b; Kattadiyil et al., 2017).

Recently, many studies and research projects were dedicated for tissue engineering, tissue specialisation and tooth regeneration: dentin regeneration, periodontal ligament (PDL) regeneration and guided alveolar bone regeneration using human mesenchymal stem cells and other techniques (Takahashi et al., 2013; Lee & Kim, 2014; Ono et al., 2017; Sheikh et al., 2017; Kawai et al., 2018). Currently, progress in making the first clinical trials on human case reports were published in endeavours to restore the lost teeth and resorbed supporting structures (Katagiri et al., 2016; Buduru et al., 2019). However, this field of research is still very costly and not yet fully developed.

The long-term success of dental implants has given dentists the chance to overcome many problems related to function and satisfaction that were previously causes of contraindication or failure in making complete denture. The CAD/CAM success, bone regeneration technologies and 3D automatic teeth placement and teeth milling hold promise as factors to put the teeth in original position in future prostheses with better outcome (Adell et al., 1981; Zarb & Schmitt, 1990).

In the last few decades, dental technologies evolved; treatment options faced demand for fast fabrication of prosthesis at lower cost, with higher properties and aesthetic quality (Gonzalez, 2014; Jazayeri et al., 2018). Dental implantology, bone regeneration, CAD/CAM technology in complete denture treatment have improved denture biomechanics, speed of fabrication, accuracy and dimensional properties significantly (Infante et al., 2014; Petre et al., 2019). The necessity for making comprehensive and practical 3D biometric guides to be employed by computerised technology to produce teeth positions that individually match the given case and compatible for CAD/CAM manufacturing is justified.

## **1.2 Problem statement and significance of the research**

In dental prostheses, optimal aesthetic, phonetics and soft tissue support can be achieved when artificial teeth especially anterior teeth are placed in the original position of the natural teeth (Devlin & Hoad-Reddick, 2001; Zarb et al., 2013). However, this concern is frequently overlooked and questionable landmarks such as the resorbed residual ridges or unstable structures are used as the primary indicator for tooth position which may lead to extreme changes in shape and size, function or aesthetic of teeth in dentures (Waliszewski,

2005). The currently known biological and biometric guides for complete denture design have several limitations in different perspectives: 1- Geometrically, they are limited to two-dimensional level that is very challenging to standardise or implement on 3D application such as having the straight horizontal or vertical distance between points. 2- Longevity or in other words, long term positional stability of the landmarks; for example, the questionable reliability that is observed in incisive papilla and lingual gingival vestige after teeth extraction and residual ridge resorption. 3- Depth of statistical analysis; the guides of the current landmarks are limited to mere correlation relationship level and often with weak correlation coefficients reported. 4- The number of teeth investigated; only maxillary central incisor and canine were investigated in most of the studies. Fabrication of the relatively new conceptual fixed or removable computer engineered complete denture (CECD) requires robust three-dimensional (3D) biometric guides that can help in achieving reliable individualised data to make important decisions regarding the denture design such as orientation of occlusal plane, the optimal arch form and the proper size and position of artificial teeth. Kojima et al. (2003) expressed the difficulty in establishing coordinate system for 3D dental cast analysis unless an individual plane is specified by landmarks on soft tissue that has an almost constant relationship to the occlusal plane of subjects with normal occlusion established. To date, objective three-dimensional biometric guides are lacking for accurately helping in designing and positioning teeth in the CECDs. The current available guides are two-dimensional and suggested since a long time before 3D scanners existed (Waliszewski, 2005). Although the available guides for teeth position have been used since about 80 years ago, these guides are still being used in CECD construction depending largely on

the manual adjustments by the dentist or dental technician to customise the tooth position, gingival contour, occlusal plane orientation and the dental-arch form following the form of the resorbed ridge. Dissatisfaction by both the patients and the dentists using the CECD systems were reported recently with relation to the form of the dental arch and orientation of occlusal plane due to errors in teeth positioning. Consequently, additional (third) clinical visit was advised to allow chance for adjustment and verification to these subjective settings before confirmation and processing and issuing the prosthesis (AlHelal et al., 2017b; Kattadiyil et al., 2017; Yilmaz et al., 2017).

### **1.3 Hypothesis**

The biometric guides suggested in this study can provide an accurate and reliable references to determine the 3D position of the teeth and the form of dentate and edentulous maxillary dental arch compared to the currently available guides.

### **1.4 Aim of the study**

This study is aimed at providing reliable and objective biometric guides to determine three-dimensional positions of the dental arch form and artificial teeth in close approximation to the positions previously occupied by their natural predecessors. It uses geometrical and statistical relationships detected between the natural teeth positions and longitudinally stable landmarks in dentate population.

### **1.5 Objectives of the study**

- 1) Three-dimensional positions of teeth:

- a) To determine the relationship between anatomical landmarks' measurements and the 3D teeth positions in the control group of dentate subjects (control group).
- b) To verify this relationship in a new group of dentate subjects (verification group)
- c) To apply the verified relationship equations on edentulous casts to predict the position of artificial teeth for edentulous patients (application group).

2) Dental arch form:

- a) To test the shape similarity between the dental arch curves and the palatal vault curve.
- b) To develop an artificial neural network (ANN) code that predicts the curve of the dental arch for a given dentate or edentulous maxillary cast using the palatal vault curve.

## **CHAPTER 2**

---

Literature review

---

Universiti Malaya

## CHAPTER 2: LITERATURE REVIEW

### 2.1 Background of edentulism

When natural teeth are lost, resorption to the alveolar bone and supporting structures will occur followed by tissue remodelling as a part of the healing process. This process is found to be continuous and very rapid in the first few months after tooth loss (Atwood, 1979; Misch, 2014). Unlike the other bones in the human body, the alveolar process has an exceptional behaviour in terms of repair and sustainability; once the resorption takes place there will be no repair or return to initial status regardless of patient age or status of dentate or edentulism (Jo, 1970). When the entire dentition is missing, the remaining residual alveolar ridge will not provide any stable occlusal stop for the lower face and the temporomandibular joint (TMJ) for the edentulous patient (Kumar, 2014).

Edentulism is regarded as a general public health problem, social disability and handicap (Polzer et al., 2010). Compared to dentate, edentulous patients lose the ability to cut and grind the food efficiently, lose vertical height of lower face, experience alterations to temporomandibular joint, pronunciation and speech impairments which may lead directly to anatomical, physiological and psychological impairment and indirectly affecting the patient's quality of life (Douglass et al., 2002; Walls & Steele, 2004; Emami et al., 2013).

### 2.2 Consequences of tooth loss, edentulism and aging population

According to Atwood (1971), the edentulism and RRR are “major oral disease entity that causes physical, psychological, and economical problems for

millions of people all over the world” making the patient dentally handicapped, ultimately resulting in “dental cripple”. When natural teeth are lost, resorption to the alveolar bone and supporting structures will occur in two phases. The early phase of resorption is remodelling as a part of the healing process. It is found to be continuous and very rapid in the first few months after tooth loss and the second phase is in slower rate, inevitable but continues indefinitely (Craddock, 1956; Zarb et al., 2013; Misch, 2014). Other factors may contribute to the speed and amount of bone resorption such as mineral index in patient body, age, gender and the condition of prostheses in the mouth and stresses applied on supporting structures of the denture bearing area (Harper, 1948; Atwood, 1979).

For better understanding of changes occurring in the alveolar bone after extraction immediately and during edentulism, a few longitudinal studies observed and followed-up the 2D and 3D morphological changes in extraction sites, alveolar bone and supporting structures after teeth loss in certain intervals for durations ranging between 2.5 to 17 years after extraction (Likeman & Watt, 1974; Watt & MacGregor, 1976; Atwood, 1979; Watt, 1987). These studies described clearly and summarised the changes happening following the tooth extraction. The most rapid changes occur in the first 6 months to 2 years, but in many individuals, changes continue apparently through the patient’s life, resulting in loss of massive amounts of jaw structure. As described by Elaskary (2008), immediately after extraction, a blood clot forms and fills the extraction socket. In the next 48 to 72 hours, inflammatory cells including monocytes, granulocytes, neutrophils, and fibroblasts migrate into the wound site along the fibrin network. Slowly, granulation tissue replaces the clot from apical to coronal direction. At 96 hours, oral epithelium is formed and at the same time

osteoclasts are observed in margins of the alveolar bone. Later in around seven days, young connective tissue and primary alveolus osteoid and epithelial proliferation occur. Only at 21 days were formation of connective tissue, mineralisation of osteoid, and re-epithelialisation noted. At six weeks after extraction, wound closure with soft tissue and woven bone (primary bone, immature bone) formation was found. Bone continues to model and remodel to form lamellar bone (secondary bone or mature bone) and bone marrow (Elaskary, 2008). This process can take up to six months. According to Atwood (1979) the continuous bone resorption / remodelling of the denture bearing structures is considered naturally happening for every patient. It would require multiple retreatments even when the dentures are made very well; this constitutes a major socio-economic problem.

The pattern of bone resorption in the maxillary arch is believed to be in upwards inwards direction while for the mandibular arch, the direction of resorption is downwards outwards. This resorption starts by thinning of the bone labio-/bucco-lingually followed by vertical reduction. In presence of additional factors of resorption, this might extend until the basal bone of the jaw and in some instances result in dehiscence of mandibular nerve or mandibular nerve canal (Atwood, 1979).

With the improvement of the general and oral health awareness and medical control for most of the medial and pathological conditions, the average life among the elder population has increased in the last few decades. The percentage of elderly people in the United States stood at 12.6% in 2000, compared with only 4.1% in 1900 and a projected increase to 20% by 2030. As life expectancy has increased in the last few decades more rapidly since 1960

than at any other time in history and as long as tooth loss is known as directly related to age, the number of adults missing teeth is expected to increase.

Although the percentage of patients with total edentulism is decreasing globally because of the baby-boomer population, the total number of edentulous patients is expected to increase in future. This is because the population worldwide is aging and they have improved overall health and healthcare services. It is expected that by the year 2025, the number of adult population older than 60 years will increase 87% compared to the number in 2000. The expected chances for a healthy 65-year-old senior to live until 85 is 50% (Misch, 2014; Resnik, 2020).

### **2.3 The prevalence of edentulism**

In the literature, edentulism used to be presented as a phenomenon associated with aging, dental health education and patient's or population's socio-economic level. The expected large number of edentulous patients in every population will need more attention and prosthodontic services for partially and completely edentulous dentitions. The need for service will also increase in both quantity and quality and also treatment option variety (Olofsson et al., 2018). According to the disability-adjusted life-years (DALY), edentulism occupied more than one third (7.6 million) among oral disorders disability burden, globally (Kassebaum et al., 2016). It has been estimated that every 10 years, the rate of edentulism increases about 4% in early adult years and in those above 70, the increase exceeds 10% per decade (Feine & Carlsson, 2003).

Average total edentulous rate worldwide for patients aged 60 and above varies significantly between countries; for China, Qi (2008) reported that in 2005, 6.82% of elders aged from 65 to 74 who are about seven million patients were edentulous, while the total edentulous rate in Kenya and Nigeria was 0% for patients group aged 65- to 74-years. The Netherlands and Iceland have a 65.4% and 71.5% rate, respectively. The health promotion survey in Canada in 1990 revealed that the edentulous Canadian rate was 47% for seniors at ages between 65 to 69 years and 58% for patients at age range between 70 to 98 years (Resnik, 2020).

According to the world health organisation's global oral health data bank, the prevalence (percentage) of edentulousness in the elderly patients who are 65 years and above was reported in Malaysia as 57%, and it is the highest percentage among the Western Pacific and South-East Asia countries (Petersen et al., 2005; Resnik, 2020).

#### **2.4 Progression of prosthodontic treatment options for edentulism**

Dental research has a good understanding of most edentulousness problems; However, the suggested rehabilitation solutions for edentulism are still lacking consensus on certain occlusal scheme or robust theory for teeth positioning. To achieve the optimal treatment success for edentulous patient, satisfaction in quality of life including chewing ability, biting efficiency, pronunciation and aesthetic outcome should be fulfilled. Although the best position for artificial teeth should be in the exact or very close to the position occupied by natural teeth, it was found challenging to fulfil both biomechanical and biometric requirements in CCD. Therefore, new biomechanical concepts were introduced with the conventional complete and partial dentures such as neutral zone,

phonetic and lip guidance, balanced, legalised, monoplane posterior and buccalised occlusion concepts to overcome the limitations of retention, stability and support of conventional removable prostheses (Zarb et al., 2013; Shirani et al., 2014; Resnik, 2020). The implant supported prostheses associated with the new technologies may exhibit higher biomechanical performance (Misch, 2014).

Based on the amount of bone resorption, the crown height and the space measured from the occlusal plane to the crest of the bone, five types of treatment options for implant supported prostheses were suggested; three of which are fixed and the remaining two are removable prostheses. In order to restore the original teeth height, an indirectly proportional relationship between the crown height required and the available bone height is calculated. The greater the bone loss, the higher the crown required to compensate and reproduce the original height. Wide and angulated implant fixtures may be used in less resorbed ridges (Misch, 2014).

#### **2.4.1 Conventional complete removable denture**

The CCD did not have many changes in concepts, design, materials and techniques. With the methyl methacrylate denture base material, although the complete denture become less bulky, more rigid and stable in the patient mouth, the retention ever since is depending on adhesion, atmospheric pressure and coordination of oral musculature (Johnson, 1959; Zarb et al., 2013).

Retention, stability and support for this type of denture are based on several factors such as the negative atmospheric pressure between the denture base and the denture bearing mucosa, the fit of the denture base to the tissues, and the

saliva physical prosperities. The retention in this type of prosthesis mainly depends on the peripheral seal and suction-cup concept made by negative pressure on denture-bearing areas that is sealed by the denture boundaries. Following these concepts, overextending or underextending the denture-base in relation to the denture limiting structures may violate optimal performance of denture retention (Shillingburg et al., 1997).

The support of this type of denture is focused on the primary and secondary stress bearing areas in the upper and lower jaws. The primary stress bearing area in the upper jaw is the posterolateral portion of the residual ridge and posterior part of hard palate. The stability is enhanced by parallelism of the primary denture bearing areas. When natural teeth contact in centric occlusion, the surfaces of the maxillary and mandibular arches are, in effect, parallel which makes for a very stable relationship. Even though denture teeth will be set to contact evenly in centric occlusion, the surface of the arches supporting the dentures may not be parallel because of bone resorption. This diminishes denture stability because vertical loads will acquire a horizontal component due to ridge angulation. The problem can be severe where the ridges offer little resistance to horizontal denture displacement and must be identified at examination for consideration in denture design (Zarb et al., 2013).

#### **2.4.2 Implant supported complete denture**

The dental implant is a prosthetic device made of alloplastic material(s) implanted into the oral tissues beneath the mucosal and/or periosteal layer, and on/or within the bone to provide retention and support for a fixed or removable dental prosthesis; it is a substance that is placed into or/and upon the jaw bone to support a fixed or removable dental prosthesis.

Recently, computer-guided planning for denture for edentulous maxilla was deemed to be considered as priority for best outcome in prosthodontic driven implant placement for rehabilitating edentulous patient (Katsoulis et al., 2009). The prosthodontic planning for implant/teeth position may not always coincide with the surgical opinion for the optimal implant location based on the available supportive bone and the bone quality. Therefore, the ideal location of the final tooth position as individual or in denture must be determined before deciding implant positioning considering the available bone at the same time. Without a known prosthetically driven location, the implant may often end up in a surgically wrong position, leading to prosthesis biomechanical failure and future complications. Radiographic survey is a must in achieving the relationship between the implant and final prosthesis location. Ideal location of the planned implants may be made by either using radio opaque radiographic templates or using virtual restorations in implant planning software (Resnik, 2020).

Advancement in technology, diagnosis and pre-treatment preparation capabilities such as bone grafting, guided alveolar bone regeneration and tissue engineering may provide better chance to position the teeth in positions closer to the original natural positions to better satisfy prosthodontic and aesthetic requirements. Limitation of the implant placement such as the reduced maxillary bone thickness in the molar and premolar areas close to the maxillary sinus or thin mandibular bone in the premolar and molar areas that makes the implant close to the inferior alveolar dental nerve may require modification in the implant fixture design such as angulated or wider diameter implant fixture to allow more surface area of osseointegration between bone and implant and

improve the physical properties of the restoration and avoid more invasive options (Lorenz et al., 2019; Nag et al., 2020).

Despite the facts stated before, there is still no distinctly superior treatment option that is always advantageous for rehabilitation of edentulous arch. Multiple factors such as physiological, economical, anatomical and psychological factors play an important role in deciding what treatment options can be offered for edentulous patients (MacEntee & Walton, 1998).

### **2.4.3 Computer assisted complete denture prostheses**

Through the recent 100 years, only in the last two decades, significant changes have occurred in the removable complete denture fabrication technology; although it has been 25 years since the first attempt to implement computer aided design / computer aided manufacturing (CAD/CAM) technology in making completed denture (Maeda et al., 1994). This technology is developing slowly to enhance the accuracy, speed, and quality in denture manufacturing and denture material. The implementation was extended to involve production of removable and fixed complete dentures (Bidra et al., 2013; AlHelal et al., 2016). New terms ever since have been introduced to dental practice to describe specifically the computer guided complete denture making such as CAD/CAM denture, computer-engineered complete dentures (CECDs) and digital removable complete denture (DRCD) (Bidra et al., 2013; Kattadiyil & AlHelal, 2017; Özkan et al., 2018). Recently, the industry of digital complete denture has been improved in accuracy, speed of preparation, design and consequently patient satisfaction, retention, uniform support and stability. The digital denture acceptance among dentists and patients is expected to improve with reduced fabrication time and cost (Maeda et al.,

1994; Kawahata et al., 1997; Zhang et al., 2002; Kojima et al., 2003; Yamamoto et al., 2014; Srinivasan et al., 2019). However, review articles were published later revealing errors in certain areas such as tooth placement, denture base fitting and major shortcomings in CECD. Some suggested addition of trial and review visits to improve the outcome and patient satisfaction (McLaughlin & Ramos, 2015; Bidra et al., 2016; Bilgin et al., 2016; AlHelal et al., 2017b; Kattadiyil et al., 2017; Yilmaz et al., 2017).

The advantages of the CECDs include a reduced number of visits required (Steinmassl et al., 2017), improved retention, accuracy and fit due to less polymerisation shrinkage (AlHelal et al., 2017a). The CECDs allow electronic archiving and easy replacement or production of duplicate dentures for the patient (Russo & Salamini, 2018). However, patient and some clinicians' dissatisfaction has been reported with CECDs, which may be attributed to the lack of a trial placement appointment, aesthetics and optimal occlusal assessment, lip support and poor tooth arrangement, misaligned occlusal plane, and inappropriate denture base characteristics (Kattadiyil et al., 2017). Adding a trial-denture clinical step and several guidelines were recommended to verify the vertical occlusal dimension and reduce or eliminate the complications and dissatisfactions (AlHelal et al., 2017b; Yilmaz et al., 2017).

#### **2.4.4 Guided bone regeneration and ridge augmentation**

Often prior to or during the placement of osseointegrated dental implant, bone graft is used to enhance the amount of bone surrounding the implant to be placed for buccolingual thickening of recipient site, residual ridge augmentation or maxillary sinus lifting to reinforce and improve the foundation supporting the endosseous implants (Boronat et al., 2010). In the literature,

various surgical approaches have been proposed to enhance the alveolar bone volume including ridge splitting, distraction osteogenesis, onlay placement or particulate bone grafts with or without membranes and autogenous bone, harvested from extraoral and intraoral donor sites, have been extensively used (Hämmerle et al., 2008; Boronat et al., 2010).

Guided bone regeneration is the most common technique for localised bone augmentation. It involves application of cell occlusive membranes that mechanically exclude non osteogenic cells from the surrounding soft tissues; it has become well-documented, classified and shown highly successful procedure for augmenting the height and width of the atrophic jaw foundation before implant placement as compared to using bone grafts alone (Urban et al., 2013; Khojasteh et al., 2017).

#### **2.4.5 Tooth and tissue regeneration and stem cell banking**

In addition to the alveolar bone guided regeneration, standard procedures were successfully developed recently in isolating, identifying and differentiating and regenerating dental and periodontal stem cells such as the outer layers of tooth; enamel of the crown, cementum of the root and an inner layer of dentin or the pulpal soft tissue. In addition, other stem cells were needed that are essential for developing what is termed as “the dental pulp-dentin complex”, alveolar bone and tooth root such as the specialised PDL that links the bone to the tooth cementum derived from apical papilla (Shuai et al., 2018). However, this technology is still striving to overcome challenges such as legislation, bio-insurance and the long period procedure of tooth extraction, primary culture and in vitro cell expansion that limits their usage at the time of clinical requirements. Solutions such as ability to preserve the cells and

relevant structures in long term storage and timely application of dental stem cells remain to be settled.

Liu et al. (2019) reviewed developments in regenerating teeth and surrounding tissues. They reported development of novel approaches in regeneration such as a tri-layered nano-scaffold having cementum, fibrous PDL, and alveolar bone with growth factors achieved recently and made full defect closure and healing, with new cancellous-like tissue 3D printed scaffold as in microcomputed tomography analyses, cell homing solution to avoid the ethical problems of using embryonic stem cells, and to prevent the potential immune rejection, development of gene therapy that could precisely target the microenvironment of the defect and combinational methods that develop simultaneously the biomimetically regenerate periodontal structures completely. In addition, recently, dental stem cell banking has been emerging based on regenerative medicine. Several banks providing dental stem cells have emerged. A National Dental Stem Cells Bank has been established in the People's Republic of China, which is the first high-tech organisation of dental stem cells research, storage and development of the dental follicle which is a loose ectomesenchyme connective tissue, surrounding tooth germ during tooth development and playing important roles in tooth eruption and tooth root development (Shuai et al., 2018).

Basic researches and clinical pilot studies in regenerative medicine highlight the promise of dental stem cells dependent translational medicine. Although the frame of dental stem cells dependent translational medicine has been primarily and successfully constructed, a proper quality control and efficacy in the clinic, and a better understanding of underlying mechanisms regulating

dental stem cells regenerative capacity, including the direction and quantity of regenerated tissue needed and the location of regenerated teeth are generally regarded as problems requiring urgent solution (Shuai et al., 2018).

## **2.5 Issues related to fabrication of complete denture**

According to the glossary of prosthodontic terms (GPT-9), complete prosthetics is defined as “the replacement of the natural teeth in the arch and their associated parts by artificial substitutes” (Zarb et al., 2013; GPT-9, 2017). In the context of this definition and as agreed by many, the replacement must mimic as closely as possible the original in shape, size and position as it is generally agreed by dental literature to achieve optimum aesthetic, lips and cheek support, phonetics, functional and physiological harmony. Therefore, the artificial teeth should be placed in positions where the natural teeth used to occupy before extraction (Watt, 1978; Winkler, 1988; LaVere et al., 1992a, 1992b; Devlin & Hoad-Reddick, 2001; Zarb et al., 2013). Pre-extraction records were suggested. These records can help in determining the positions of the artificial teeth on the denture to occupy the same position as they were before extraction and reproduce the same aesthetic, phonetic and for some extent the functional performance (Bissasu, 2004).

While in the lack of pre-extraction records, existing dentures or the patient does not want to use the existing denture as template, several biometric guides have been suggested to help achieve optimal aesthetics and function (Bissasu, 1992; Fu et al., 2007b; Alhadjj et al., 2017).

Majority of these earlier mentioned guides are based on naturally existing relationships found between the teeth and craniofacial and anatomical

landmarks and measurements obtained from dentate control using radiographs, photography or dental cast models (Zarb et al., 2013). Some guides were based on clinical and aesthetic observations (Watt et al., 1967; Likeman & Watt, 1974) or denture space and neuromuscular determination (Beresin & Schiesser, 2006). Many textbooks suggested guides known by the majority of clinicians and widely used in dental practice. Several subsequent studies, however, have expressed disagreement and concerns regarding the validity of these guides when they verified the theories and applied them in clinical practice (Waliszewski, 2005). It is well documented that the majority of the currently known biometric guides suggested for complete denture fabrication are not only inconsistent and lacking reliability, they suggest average values derived from the observed patients and refer to landmarks with questionable stability, inaccuracy in measurement or lack of correlation (Watt & Likeman, 1974; Bell, 1978; Ortman & Tsao, 1979; Mavroskoufis & Ritchie, 1981; Sellen et al., 1998). Such guides are referring to movable landmarks, concluded based on weak relationships or simply expressing average values that may be inapplicable when applied on larger patients' group (Ismail & Bowman, 1968; Likeman & Watt, 1974; Watt & Likeman, 1974; Murray, 1977; Monteith, 1985; Nissan et al., 2003; Waliszewski, 2005). This has made the guides subjective especially when they are needed in constructing the recently evolved CECD prostheses that require rapid, automatic and digital three-dimensional information for their designing.

With relevance to the CECDs, Yamamoto et al. (2014) have commented that positioning the artificial teeth, currently placed offset on the milled prefabricated acrylic denture base, is posing a unique challenge in CECD

fabrication; the exact location for the tooth should be known to enable correct positioning in implementation.

To the best of the researcher's knowledge, to date, no study has empirically investigated and explained the three-dimensional geometrical and linear relationship that justifies the individual anterior or posterior tooth position with relevance to fixed reference landmark or plane in the dental cast. This relationship can help to predict the accurate and unique 3D tooth position in the dental arch using cast measurements that are unaffected if teeth are missing or not.

### **2.5.1 Artificial teeth and their positions**

In order to obtain patient's acceptance and adaptability to the partial or complete prosthesis offered, restoration of the pre-prosthetic original appearance should be made to the patient. This restoration cannot be achieved without positioning the upper artificial teeth and dental arch form to their original settings. Majority of clinicians and dental researchers have consensus that the artificial teeth should be placed in the exact or approximate locations where the natural teeth occupied before (Murray, 1977; Zarb et al., 2013). To achieve that, biometric guides were suggested to help provide support for the lips and cheeks as when the natural teeth were present. This would also result in patient's psychological satisfaction, upper and lower face height harmony, phonetics and maintaining the TMJ and overall oral health.

### **2.5.2 The application of dentate relationships on edentulous patients**

Following teeth extraction, the basal bone is not changing after residual ridge resorption takes place (Cawood & Howell, 1988). For the American

College of Prosthodontists, McGarry et al. (1999) have developed a classification for complete edentulism to ease the understanding of the conditions and limitations of the denture bearing foundation. The classification defined four categories ranging from class I that has adequate alveolar bone, well defined hamular notches and no palatal tori. While class IV has the most challenging situation from the multifactorial perspective. The patient class IV has gag reflex, hypersensitive tongue, insufficient interarch space, acquired or congenital maxillofacial defects and extensive resorption to alveolar ridge that cannot provide resistance for the proposed prosthesis. This classification enabled achieving reasonable prognosis, treatment planning and suggesting proper treatment options for the edentulous patients.

Several biometric guides were suggested to help in deciding the position of the artificial teeth, occlusal plane orientation and overall design of complete dentures. These guides were inspired from what was found in natural healthy dentition and are considered very helpful in dental practice (Devlin & Hoad-Reddick, 2001; Zarb et al., 2013). Examples of such guides are height of the lower lip in relation to the incisal edges of the lower anterior teeth, Stensen's duct opening in relation to height of the maxillary molars in occlusal table, height of the posterior reference of occlusal plane and the retromolar pad and the labio-lingual position of anterior teeth to the incisive papilla.

## **2.6 Artificial teeth positioning and guides in complete denture**

As generally agreed, the optimal position of the artificial teeth is where it was occupied by natural teeth if the patient used to have healthy, aesthetic and well-aligned dentition (Sharry, 1974; Watt, 1978). In the literature, it is believed that knowing an anatomical cranial or craniofacial reference that has a

constant relationship with the natural teeth positions or occlusal plane that is stable after teeth extraction would provide significant help in edentulous patient's rehabilitation (Kapur et al., 1982; Misch, 2008). Various reference anatomical landmarks or structures such as incisive papilla and crest of the residual ridge average distance with natural teeth have been suggested in the literature to guide the restoration of the form and angulation of the dental arch and form and position of the artificial teeth to a setting similar to that previously occupied by natural predecessors (Ortman & Tsao, 1979; Devlin & Hoad-Reddick, 2001; Amin et al., 2008; Guldag et al., 2008; Zarb et al., 2013).

The size and shape of the teeth and arch form are very important to fulfil the optimum requirements of aesthetics, facial tissue support, phonetics, mastication and preservation of the healthy condition of TMJ and oral tissues and function; in order to achieve that, artificial teeth must be selected and arranged in places as similar as possible to the natural missing teeth in form, dimensions and position in the oral cavity (Misch, 2014).

Currently, although retention, stability and support has significantly improved using the latest surgical and computer guided technology, the concepts in teeth arrangement are still bound to the old guides established for conventional complete denture that were meant to be supported by the resorbed mucosa. The concepts of teeth positioning especially the maxillary teeth are still confined buccolingually to be close to the crest of the resorbed alveolar ridge and aligned on certain scheme such as the group function, balanced, lingualised and monoplane occlusion concepts suggested for the limited mucosa support and limited mucosa suction retention due to resorbed bearing ridges (Ohkubo et al., 2018).

Various theories have been suggested and discussed for the optimal position of the artificial teeth in edentulous patient's mouth.

### **2.6.1 Neuromuscular concept (neutral zone) and pronunciation**

Although it is agreed that the optimal position of the artificial teeth is where the natural teeth were previously occupied, the concept of “denture space” or “neutral zone” is widely accepted and used in removable conventional completed dentures especially when severe resorbed ridges exist and the patient cannot undergo an implant overdenture therapy (Fish, 1933; Yeh et al., 2013). Position of the teeth was suggested under this concept to be in relation to the duration of edentulism, residual ridge crest location or patient age. Porwal et al. (2016) have noted controversy and erroneous methods used in projecting guides related to neutral zone by previous studies and concluded that neutral zone has no relationship with patient age, residual ridge crest or duration of being edentulous. Certain labial and lingual sounds are suggested to determine the anterior teeth position (Goodacre et al., 2012). The upper lip length and commissures during relaxation and smiling were suggested to guide positioning the anterior teeth in complete denture (Winkler, 1988; Mack, 1996).

In severe residual ridge resorbed cases where the denture become unstable due to muscular activity of the muscles of lips, cheeks from a side and the tongue from the opposite side, neutral zone or what is also called the “denture space” concept was developed and suggested by some studies, case reports and textbooks to reduce the interference with normal oral muscular functions especially with greater residual alveolar ridge loss. Therefore, in severe RRR

cases, positioning the teeth in the neutral zone is part of the solution (Beresin & Schiesser, 2006; Yeh et al., 2013).

### **2.6.1.1 Denture space or neutral zone concept**

The neutral zone is defined in GPT-9 (2017) as “the potential space between the lips and cheeks on one side and tongue on the other, that area or position where the forces between the tongue and cheeks or lips are equal”. Some references named this zone as “dead space” or “zone of minimal conflict”. (Beresin & Schiesser, 2006). It is commonly agreed in the literature that, to achieve the required denture stability and retention, the denture design should harmonise with the patient’s physiological oral neuromuscular system. Therefore, positions of the artificial teeth especially the mandibular were suggested to be set buccolingually on the crest of the ridge in the denture base in order to occupy the neutral zone and avoid dislodging forces applied by the surrounding musculature during function. However, the relationship between the residual ridge crest and neutral zone is found varying significantly from person to person and from time to time depending on the musculature and the resorption pattern when comparative study was made in groups of patients with different duration of being edentulous (Bhorgonde et al., 2014). This is perhaps due to the ridge resorption rates in the mandibular jaw being faster and more extensive compared to the maxillary jaw (Atwood & Coy, 1971).

Apart from the differences between the phonetic type of neutral zones and the swallowing type to be recorded, the neutral zone may undergo morphological and positional variation in the same patient when different materials are used to record or record was made in different duration of

edentulousness (Lammie, 1956; Fahmi, 1992; Makzoumé, 2004). Fahmi (1992) traced the neutral zone position in two edentulous subjects and found a significant difference in the neutral zone position of subjects who had been edentulous for more than two years compared to the position in subjects who had history of being edentulous for less than two years, and concluded that the neutral zone moves lingually.

### **2.6.2 Anatomical landmarks and biometric guides suggested for teeth position**

In the absence of pre-extraction records, to achieve optimum aesthetics, phonetics, function and comfort, several anatomical and biometric guides have been suggested to help determine the position of artificial teeth in complete denture (Devlin & Hoad-Reddick, 2001). In the dental literature, the biometric guides suggested to position the teeth can be divided into two types: the extraoral facial guides and the intraoral mucosal guides. The extraoral guides stemmed from clinical observations of relationships between some facial soft tissue landmarks and teeth in good-looking subjects such as the average upper lip position in relation to the maxillary incisors, maxillary incisors following the curvature of the lower lip, the canine as constant position to the upper lip in both genders and in different age groups (Misch, 2008). maxillary incisors should touch the lower lip in repose position, smile that displays maxillary teeth up to the second premolar, and the line descending from the inner-canthus of each side and touching the ala of the nose should pass through the tip of the maxillary canines. These findings were concluded as widely variable and different in various ethnic and age groups and no single method has found practical application of relationships (Pellacani & Seidenari, 1999; Devlin &

Hoad-Reddick, 2001; De Menezes et al., 2011). Some landmarks have been proposed as biometric guides and used by various studies for orientation of occlusal plane such as ala-tragus line (Camper's plane), crest of residual ridges, buccinator grooves and the commissure of lips, retromolar pad, condylar path, parotid papilla and the lateral border of the tongue.

### **2.6.2.1 Hamular notches**

Hamular notch also called pterygomaxillary notch is defined by Scheid & Weiss (2017) as “a notch that separates the maxillary tuberosity of each maxilla from the posterior located pterygoid process of the sphenoid bone” It is a mucosal depression composed of loose connective tissue about 2 mm wide, situated between the posterior end of tuberosity and the pterygoid hamulus of the medial pterygoid plate forming the distal limit of the buccal vestibule. The pterygomandibular raphe is attached to the hamulus to form the upper connection of the raphe. The hamulus serves as a fulcrum for the tensor veli palatini muscle during its function. The muscle descends almost vertically and slightly anteriorly from its attachment to the cartilaginous portion of the auditory tube giving a tendon that courses diagonally through the notch around the hamulus before it extends attachments to the horizontal shelves of the palatine bone and meet an aponeurosis from the contralateral muscle in the soft palate. Clinically, fracturing the hamulus is almost impossible through dental treatment. This gives the hamular notch its anatomical permanency and eligibility to be used as a stable intraoral anatomical landmark (Linkow, 1977; Özkan et al., 2018). The hamular notch is a palpable structure as its mucous membrane consists of a thick submucosa made up of loose areolar tissue. In

conventional removable complete denture, the left and right hamular notches are agreed to be the posterior limits of the denture base including the notches as part of posterior palatal seal, the tissues in the notch should be displaced by the posterior palatal border of the denture to achieve a posterior palatal seal, but overextension causes trauma to the mucosa (Zarb et al., 2013).

### **2.6.2.2 Incisive papilla**

The incisive papilla is a prominence in the anterior lingual part of the central incisor area known also as palatine papilla. It was described by smooth pear or oval-shaped prominence of mucosa that covers the incisive foramen. Histologically, the papilla is formed of dense connective tissue and contains blind ducts of varying length lined by simple or pseudostratified columnar epithelium, rich in nasopalatine ducts (Kumar, 2019).

In the literature, incisive papilla (IP) is the most extensively studied intraoral landmark for its guidance in positioning central incisors or canines for maxillary complete dentures. Many publications investigated the horizontal two-dimensional distance between the incisive papilla and the labial surface of the central incisors in dentate subjects and suggested positioning central incisor 8 to 12mm anterior to the incisive papilla (Harper, 1948; Kumar, 2019). It was also suggested that a virtual horizontal line passing through the incisive papilla will pass over the maxillary left and right canine tips (Mavroskoufis & Ritchie, 1981). However, controversy occurred when different researchers supported various reference points on the IP (i.e. anterior, middle or posterior part of the papilla) in relevance to this guide (Ortman & Tsao, 1979; Grave & Becker, 1987; Fu et al., 2007b). Significant change in the shape and forward and

upwards movement in the position of the IP occur with the RRR of the maxillary edentulous arch (Watt & Likeman, 1974).

Incisive papilla is the most famous and most often studied intraoral landmark in the prosthodontic dental literature. Many studies investigated the relationship between the incisive papilla and the buccolingual position of maxillary central incisors or canines in dentate population in order to give guidance for placement of artificial teeth in edentulous population (Ehrlich & Gazit, 1975; Huang et al., 2004; Fu et al., 2007b; Zia et al., 2009).

Harper (1948) stated that the incisive papilla did not change position for up to 7 years after a tooth was extracted, but he did not present enough evidence to support this conclusion (Lau & Clark, 1993). In follow up longitudinal study Watt & Likeman (1974) studied the patterns of alveolar ridge resorption for 2.5 years and found that on average the papilla moved forward about 1.6 mm (range 0.76 to 2.77 mm) and upward about 2.3 mm (range 1.3 to 4.0 mm).

According to Said, Lau & Clark (1993) it would be unwise for a dentist to follow this rule strictly for every patient treated; individual variations must be considered and dentists are advised to use a combination of biometric guides, phonetic tests, and denture space identification to reproduce the relationships established between natural teeth and the orofacial investing tissue.

**(a) *Anatomical overview of incisive papilla***

The incisive papilla is elevation of soft tissue covering the foramen of the incisive or nasopalatine canal (GPT-9, 2017). In other definition, the incisive papilla is described as a pad of fibrous connective tissue overlying the orifice

of the nasopalatine canal carrying the nasopalatine vessels and nerves and located usually in the median line between the central incisors.

(b) *Incisive papilla-central incisor distance*

The straight distance between the incisive papilla and the labial surface of central incisors was suggested as biometric guide to position the artificial teeth in complete and partial denture on a position closer to the natural tooth positions (Harper, 1948; Ortman & Tsao, 1979; Grave & Becker, 1987). In the literature, various reference points of the incisive papilla were used for measuring distance with the teeth. Studies examining the relationship between the middle of incisive papilla and the labial surface of the maxillary central incisor suggested that the labial surfaces of the natural upper central incisors should be at 8-10mm in front of the middle of the incisive papilla (Figure 2.1), (Hickey et al., 1962; Murray, 1977; Amin et al., 2008). Mersel & Ehrlich (1981) found that this measurement varies in different arch forms (oval, squared and tapered) where it was found 5mm in squared arch form; 6mm in ovoid arch, and 7mm, in tapered arch form. Studies that measured the incisive papilla posterior border also have considered that it is the least affected part of the papilla after teeth extracted remodelling. They suggested distance ranges of (Ortman & Tsao, 1979; Amin et al., 2008).

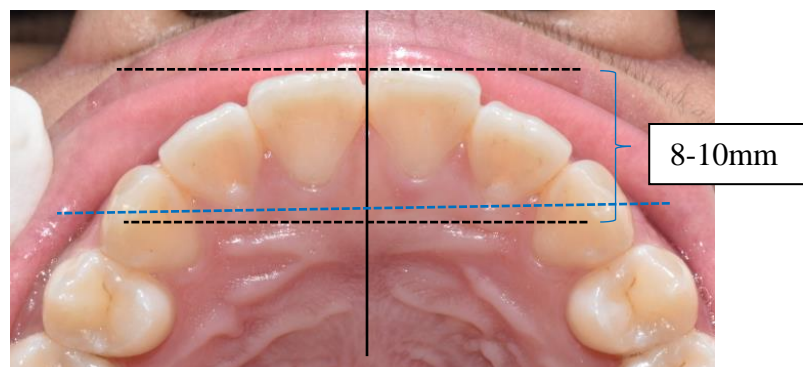


**Figure 2.1: Suggested distance between incisive papilla and labial surface of central incisors. Blue line shows the suggested relation between intercanine line and incisive papilla**

Watt & Likeman (1974) observed migration and changes in the shape of the incisive papilla during recession of the alveolar ridge after teeth extraction. They reported that the papilla alters its relation to the incisive foramen and migrates within 2.5 years an average of 1.6 mm forward (0.76 to 2.77 mm) and 2.3 mm upward (1.3 to 4mm). They advised to consider migration of the papilla position in case the papilla is used as guide for arranging of anterior teeth for dentures.

(c) *Incisive papilla- canine position*

The incisive papilla distance to the canine-tips were studied and measured. Schiffman (1964) studied 507 casts with various arch forms and found that the arch form has no effect on the relation between the incisive papilla and the line passing through the tips of the maxillary canines (Figure 2.1), and concluded that this horizontal biometric method is stable. In agreement with Schiffman, Mavroskoufis & Ritchie (1981) reported that incisive papilla is situated on the line passing through the tips of the canines in the dentate person and that may give guidance for canine teeth placement in the edentulous mouth.

**2.6.2.3 Rugae area**

The palatal rugae are also known as plicae palatinae transversae, transverse palatine folds and rugae palatine are “irregular elevations of the mucosa composed of firm connective tissue located in the anterior 1/3 of the palate” (Lysell, 1955; Özkan et al., 2018). The area has irregular, sometimes branching ridges that are laterally extending with various distances from the incisive papilla and the palatal raphe. These hard ridges, which contain a core of dense connective tissue, are usually concentrated in the anterior portion of the palate,

particularly around the incisive papilla. They are the vestigial remains of an auxiliary masticatory apparatus.

The clinical significance of rugae lines in dental practice and research is mostly in forensic and orthodontic disciplines. In restorative and prosthodontic dentistry, however, no relevance or use of the palatal rugae area was highlighted in terms of treatment planning and treatment procedures except in considering it as a secondary stress bearing area and in designing complete denture, it is believed that the replication of the rugae lines in the denture baseplate may enhance chewing ability and food stability for denture wearers during mastication and in removable partial denture designing, covering unnecessarily the rugae area by the denture base is not advisable as it may interfere with the patient's comfort and phonetics (Zarb et al., 2013).

(a) ***Rugae lines***

In glossary of prosthodontic terms (GPT-9, 2017), rugae lines were defined as anatomic folds or wrinkles composed of irregular fibrous connective tissue ridges located in the anterior third of the hard palate. Rugae lines are transversally extending directed toward the midpalatal raphe. The shapes and dimensions of these lines are found to be different in different individuals and they are unique but stable so they can be used as identification features for a person in forensic dentistry. However, the rugae lines are always aligned in similar pattern anterioposteriorly as three or more horizontal rows on each side extending from the medial to lateral lining of the premaxilla. This gives this area uniqueness as an identification feature in forensic dentistry (Allen, 1888).

Lysell (1955) studied the palatal rugae in detail and developed a classification and method to ready and classify the rugae lines. He concluded

that although the posterior rugae are not symmetrical, they have the most bilateral symmetry among the rugae lines; they may move distally up to age 20 years. Although he concluded that the rugae cannot be as efficient as fingerprints in identification nor can be used for establishing paternity, Lysell believed that the rugae represents a valuable identity of a person if detailed system of recording was used (Lysell, 1955; Salzmann, 1955).

Forensic studies considered the rugae lines as stable structures possessing the individuality and unicity. Like in fingerprints and chiloscopy, unicity can be found even in identical twins (Bansode & Kulkarni, 2009; Taneva et al., 2017).

**(b) *Stability of rugae area***

Several studies have evaluated the palatal rugae stability throughout orthodontic treatment. They found that in patients treated with a functional appliance or headgear, the medial ruga points appeared more stable than the lateral ruga point (Almeida et al., 1995; Bailey et al., 1996; Abdel-Aziz & Sabet, 2001; Hoggan & Sadowsky, 2001; Jang et al., 2009; Ganzer et al., 2017).

In cephalometric longitudinal studies, the area where the third pair of rugae lines exist were identified as the most stable landmarks and suggested for use as reference points for tooth movement before and after orthodontic treatment (Hoggan & Sadowsky, 2001; Christou & Kiliaridis, 2008).

It has been well documented in longitudinal studies on dimensional and morphological changes occurred in maxillary denture bearing area after teeth extraction, the area around medial points of the third palatal rugae was the

most stable and least affected by extraction (Watt & Likeman, 1974). This finding was confirmed by orthodontic longitudinal studies that used the midpoint between the right and left medial points of the third rugae lines as stable landmark and reliable enough for maxillary dental cast superimposition before and after treatment even if teeth extraction was involved in follow-up studies confirmed that the medial area between the third rugae lines have been suggested as the most stable rugae (Bailey et al., 1996; Christou & Kiliaridis, 2008; Jang et al., 2009; Chen et al., 2011).

(c) ***Rugae lines as guide for teeth positioning***

Some studies suggested rugae lines as guides for positioning the teeth in edentulous patients. Rangarajan & Padmanabhan (2017) suggested to use labial surface of the canine to be placed at 10.5 mm from the lateral aspect of the first large pair of anterior rugae. In an attempt to use the palatal rugae lines as guide for teeth positions, Panjwani et al. (2013) investigated the relationship between the rugae line length, the distance between the rugae lines and the distance between the lateral end of first rugae line to tips of canine on left and right sides. Although they found very weak relationships, they concluded that the correlations found do not have significant clinical application value.

Peavy & Kendrick (1967) observed the effects of orthodontic repositioning of maxillary anterior teeth on the rugae lines nearby; they found that the lateral terminal points of rugae lines are unreliable as reference points especially those closer to anterior teeth. However, they have recommended using the midsagittal plane of the palatal raphe area as a stable and reliable area for serial cast studies. All studies evaluating stability of the palatal rugae throughout orthodontic treatment, before and after extraction of the maxillary teeth or

during wearing complete dentures had consensus on the medial ruga points and area being more stable than the lateral ruga points and area or other parts on the maxillary mucosa (Watt & Likeman, 1974; Almeida et al., 1995; Bailey et al., 1996; Abdel-Aziz & Sabet, 2001; Hoggan & Sadowsky, 2001; Jang et al., 2009).

#### **2.6.2.4 Vestige of linguogingival margin (lingual gingival margin line)**

The remnant of the lingual/palatal gingival margin/vestige is a cord-like elevation of the mucosa near the crest of the residual ridge as described by Watt & MacGregor (1976). The buccolingual breadth (BLB) of the residual alveolar ridge (the horizontal distance between the lingual gingival margin to the mid-buccal point that touches the cheek in the corresponding region of each of the anterior and posterior tooth) were measured in 100 patients (Watt et al., 1967). In a longitudinal study for up to 14- and 17-years, Likeman & Watt (1974) tracked the morphological changes occurring to the maxillary denture bearing area of a 25-patient sample after teeth extraction throughout 2.5 years. The study hypothesised that when the sulcus breadth of the dentulous cast can be clearly recognised, adding space extending from the outer surface of the sulcus as average coronally or sagittally may represent the cheek position (Table 2.1). Later, in another study, Watt (1987) made mucosal tattoo spots near the buccal and linguogingival margins of the teeth decided for extraction. BLB measurements were collected before and after extraction in 25 patients at varying intervals. Serial casts for every patient were made, sagittal and coronal measurement for BLB in anterior and posterior teeth regions were made respectively. The study concluded that the lingual gingival margin remnants

moved after extraction to positions that are buccal and superior to the positions before extraction. The amount of movement was found less in incisors than in molar region. They suggested subtracting the average amount of movement from the average BLB obtained before extraction in order to estimate the flange width in the maxillary complete denture and position of the teeth. They concluded that the average pre-extraction BLB can be transferred directly to the edentulous casts to guide the breadth of the flange of the complete upper denture, estimate the amount of tissue loss, buccal changes that have taken place and the sulcus breadth required for the edentulous patient especially when pre-extraction records are unavailable (Table 2.1 and Figures 2.2 & 2.3).

**Table 2.1: Descriptive statistics for measurements representing breadth of the residual ridge measured the horizontal distance between the lingual gingival margin and the mid-buccal point of the teeth regions in 100 patients (Watt & MacGregor, 1976)**

Position and plane of measurement	Direction	Average changes (SD) mm
Central incisor	Sagittal	6.3 (0.91)
Canine	Coronal	8.5 (1.06)
First premolar	Coronal	10.0 (1.03)
Second premolar	Coronal	10.6 (1.40)
First molar	Coronal	12.8 (0.98)
Second molar	Coronal	11.6 (1.14)
Third molar	Coronal	10.1 (1.33)

Nomura et al. (1991) measured the bucco-lingual breadth (BLB) of the dentate alveolar process of maxillary study casts in Japanese population. They found that the BLB is smaller by 0.5–1.00mm in incisor and canine region and larger by 0.6-0.8mm in the premolar and molar regions when compared to Scottish population studied by Watt & MacGregor (1976).

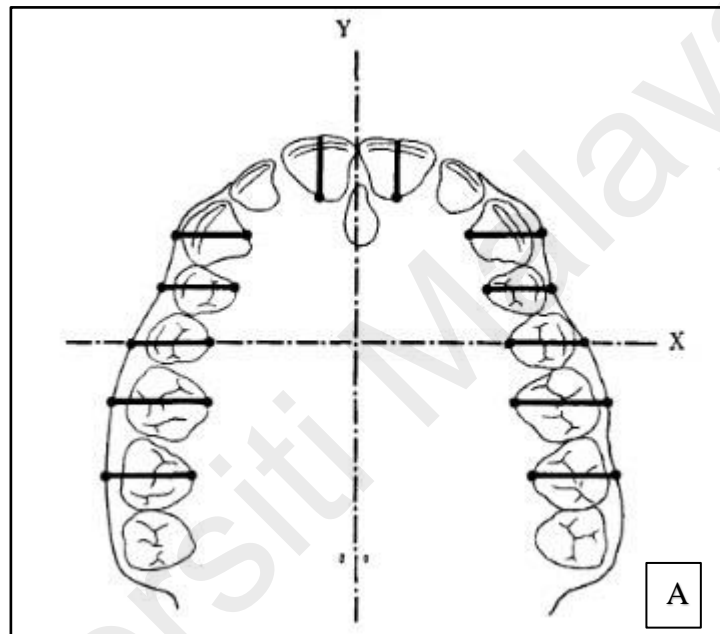


**Figure 2.2: Measurements of the buccolingual breadth (BLB) in the anterior and posterior teeth before extraction. Adopted from Nomura et al. (1991)**

Overall, the dental literature has contrasting opinions regarding the palatal gingival vestige significance; some studies have observed its movement and continuous instability during the continuous bone resorption of the supportive alveolar bone (Jahangiri et al., 1998). Additionally, the palatal gingival vestige was detected in patients who never had teeth before in their lives such as the neonatal children before teeth eruption and patients diagnosed with anodontia. Therefore, the assumption that it is the remnant of the palatal gingival margin is distanced (Devlin & Hoad-Reddick, 2001; Devlin, 2002).

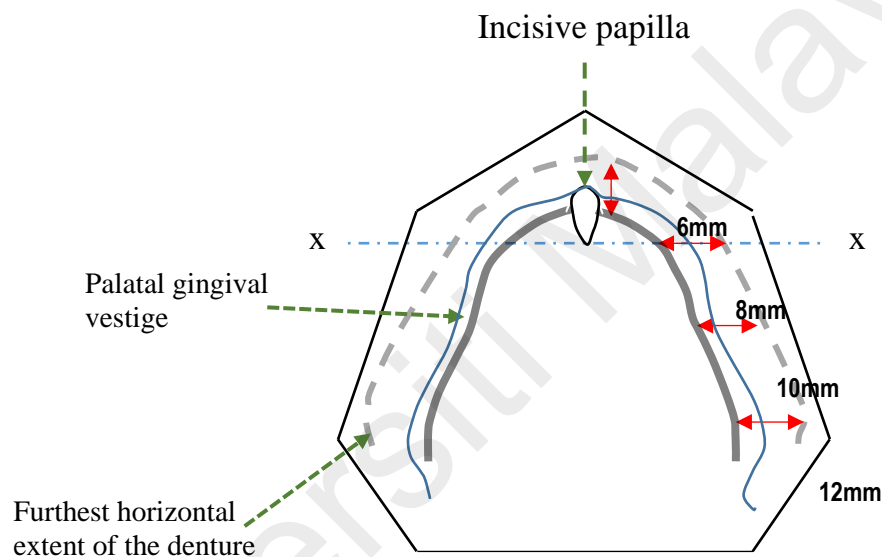


**Figure 2.3: Illustration showing the lingual gingival vestige and the suggested horizontal buccal breadth in denture flanges to restore cheek support. Dotted line is the farthest distance of the flanges**

#### 2.6.2.5 The crest of alveolar residual ridges

During mastication using conventional complete denture, in order to avoid denture displacing forces and subsequent further residual ridge resorption and at the same time ensure teeth positions close to the neutral zone, some studies suggested setting denture's artificial teeth especially the posterior upper and lower teeth in places directly over the crest of the ridges following

the resorbed maxillary and mandibular alveolar ridge forms whether or not this setting may lead to teeth set in cross-biting relationship (Weinberg, 1958; Jain et al., 2015).

Longitudinal studies that followed up changes in the alveolar ridges after teeth extraction and denture wearing observed that the ridge crest varies greatly during alveolar ridge resorption. They found that the ridge crest moves posteriorly and lingually at unpredictable rate along the advancement of the alveolar bone resorption and that bone resorption is enhanced in denture wearers compared to non-denture wearers (Jo, 1970; Watt & MacGregor, 1976; Van der Weijden et al., 2009).

#### **2.6.2.6 Canine eminence**

The maxillary canine eminence region is formed by the support of bone between the large canine socket anteriorly and the smaller first premolar socket posteriorly and located just lateral to the lateral pyriform rim of the nose; it often offers the greatest height of available bone in the maxillary anterior region that may serve as good foundation for implant placement (Razavi et al., 1995; Misch, 2014). The canine eminences are not always found in the edentulous arch; they may be found distal to the true canine position and when they are used as landmark that guides the teeth position, they may result in placing the six maxillary anterior teeth in the space between the distal of the right canine eminence and the distal of the left canine eminence (Watt & Likeman, 1974).

### **2.6.2.7 The parotid papilla**

Winkler (1988) suggested to set the occlusal surface of maxillary first molar teeth at 6 mm below the parotid papilla. Others have suggested that parotid papilla must be at 3.3 to 4.0 mm above the occlusal plane when they used measurements with a different reference for the occlusal plane (Lundquist & Luther, 1970; Foley & Latta, 1985; Shigli et al., 2005).

In the literature inconsistency exists in position of the parotid papilla, ranging from 2.56 mm to 6.0 mm, above the occlusal plane in dentulous subjects. Hence this landmark alone is an inaccurate guide for occlusal plane orientation (Shigli et al., 2005).

### **2.6.2.8 Hamular incisive papilla plane (HIP or HNIP plane)**

The hamular incisive papilla plane (HNIP) is the geometrical plane that consists of the three intraoral landmark points: the left and right hamular notches and the incisive papilla. Despite the fact that the incisive papilla is expected to be round and migrate geometrically upward and forward after extraction of maxillary anterior teeth (Watt & Likeman, 1974), many studies supported the concept of parallelism between the occlusal plane (OP) and the HNIP plane (Cooperman, 1975; Rich, 1982; Fu et al., 2007a; Jayachandran et al., 2008).

## **2.7 Digital and computerised dentistry**

### **2.7.1 Digital dental cast analysis and research**

The structured-light scanner is a type of noncontact active scanner that reconstructs 3D surfaces based on triangulation. The active projector device emits a structured-light pattern that forms an illusion of texture on an object. This increases the number of unique definitions of matching object points, corresponding to every unitary position in the image, thus enabling 3D object reconstruction by matching of the projected and recorded patterns (Hassan et al., 2016).

Advances in technology, materials science and development of innovative clinical techniques such as computerised treatment plans for implant supported prostheses, cone beam computed tomography analysis, CAD/CAM technology to fabricate complete prosthesis and the rapidly increasing progress in stem cell tooth regeneration and alveolar bone regrowth have demanded higher quality oral rehabilitation and treatment techniques. Therefore, higher level of technology integration in dental research is needed to reveal new concepts by providing guides for tooth selection, position and restoration of occlusion and aesthetics for edentulous patients.

### **2.7.2 The geometrical coordinate systems**

In order to describe object or shape in space, coordinates system was found to give relevant numerical spatial relationship described between two points in space (Stewart et al., 2016). In this study, we considered the teeth as vectors arose in three-dimensional directions from the origin point that is the most stable and reliable landmark in the dentate and edentulous patients. R-point was chosen to be that origin.

Two additional coordinate systems are common in three dimensions: “cylindrical” and “spherical” coordinates. All three systems can be illustrated onto the Cartesian system.

Often in the literature, the teeth position was managed as linear 2D or linear 3D distances and when angular analysis was performed, the angles were managed as linear without considering their directional component (Jayachandran et al., 2008).

### **2.7.3 The Cartesian coordinate system**

Just as points on a line can be identified with real numbers to form the coordinate line, points in a plane can be identified with ordered pairs of numbers to form the coordinate plane or what is called as the Cartesian coordinate system. It is simply made up of a point in a plane, called the origin, and two perpendicular axes intersecting through that origin; one axis is horizontal and one is vertical. Any point in the plane can be reached from the origin by travelling a certain distance  $x$  along the horizontal axis and a certain distance  $y$  along the vertical axis. The numbers  $(x, y)$  are the coordinates of the point. The origin itself has coordinates  $(0, 0)$ . The part of the horizontal axis (also called the  $x$ -axis) that lies to the left of the origin and the part of the vertical axis (the  $y$ -axis) below the origin are described by negative numbers (Stewart et al., 2016).

Cartesian system uses orthogonal axis vectors,  $\vec{e}_x$ ,  $\vec{e}_y$  perpendicular to each other as its basic platform and in 3D Cartesian type the  $\vec{e}_z$  vector is the third basic axis in the system. All of the vectors are originating from one origin of that system in a point of origin. This coordinate system is used primarily for

systems with rectangular shape, for example, microfluidic channels with rectangular cross-section (Rapp, 2017).

The two axes are dividing the plane into four quadrants, labelled I, II, III, and IV. Any point  $P$  in the coordinate plane can be located by a unique ordered pair of numbers, the first number  $a$  is called the x-coordinate of  $P$ ; the second number  $b$  is called the y-coordinate of  $P$ . We can think of the coordinates of  $P$  as its “address,” because they specify its location in the plane (Stewart et al., 2016).

### 2.7.3.1 The transformations of coordinates in the Cartesian system

#### (a) *Translation*

“A translation moves a shape by sliding it up, down, sideways or diagonally, without turning it or making bigger or smaller”. It is a type of transformation. Translation can also be defined as the movement of the object along one axis such as x or y axis without other transformation. An example for translation in geometry is moving the object forward, backwards, left or right on one direction only, all the coordinates should maintain the same values except for the coordinate of the translation (Stewart et al., 2016).

#### (b) *Rotation*

Turning a shape in a clockwise or anti-clockwise angle about a fixed point or axis called centre of rotation. When a shape rotates, all of its points are rotating by the same angle except the centre of rotation.

#### (c) *Reflection*

“in a line produces a mirror image in which corresponding points on the original shape and the mirror image are always the same distance from the mirror line.”

(d) ***Enlargement or scaling***

“is a transformation. However, it is different from reflection, rotation and translation because it changes the size of an object” (Stewart et al., 2016).

### **2.7.3.2 Three-dimensional coordinate systems**

In three dimensions, we need to specify three numbers to describe the position of an object (e.g., a bird flying in the air). The planes determined by the coordinate's axes are the XY-plane, whose standard equation is  $z = 0$ ; the YZ-plane, whose standard equation is  $x = 0$ ; and the XZ-plane, whose standard equation is  $y = 0$ . The planes meet at the origin  $(0, 0, 0)$ . The origin is also identified by the symbol  $O$  or sometimes the letter  $O$ .

The three coordinate planes  $X = 0$ ,  $Y = 0$ , and  $Z = 0$  divide space into eight cells called octants. The octant in which the point coordinates are all positive is called the first octant; there is no convention for numbering the other seven octants. The points in a plane perpendicular to the X-axis all have the same  $x$  coordinate, this being the number at which that plane cuts the X-axis. The  $y$  and  $z$  coordinates can be any numbers. Similarly, the points in a plane perpendicular to the Y-axis have a common  $y$  coordinate and the points in a plane perpendicular to the Z-axis have a common  $z$  coordinate (Hass et al., 2018).

Compared to 2D, in three-dimensional (3D) Cartesian coordinate system, we simply add a third axis, Z, that is mutually perpendicular to both X and Y. The position of an object can then be specified by using the three coordinates,  $x$ ,  $y$ , and  $z$ . By convention, we use the Z axis to be the vertical direction in 3D.

### 2.7.4 The spherical coordinate system

Spherical coordinate system is a system of curvilinear coordinates that are natural for describing positions on a sphere or spheroid. In this system; Theta ( $\theta$ ) is the azimuthal angle in the XY-plane from the x-axis with  $0 \leq \theta < 2\pi$  and Phi ( $\varphi$ ) is the polar angle (also known as the zenith angle) and colatitude, with  $\varphi = 90^\circ - \delta$  where  $\delta$  is the latitude from the positive side of Z-axis with  $0 \leq \varphi \leq \pi$ , and  $\ell$  to be distance (radius) from a point to the origin. This is the convention commonly used in mathematics (Wolfram Mathworld) (Figure 2.4).

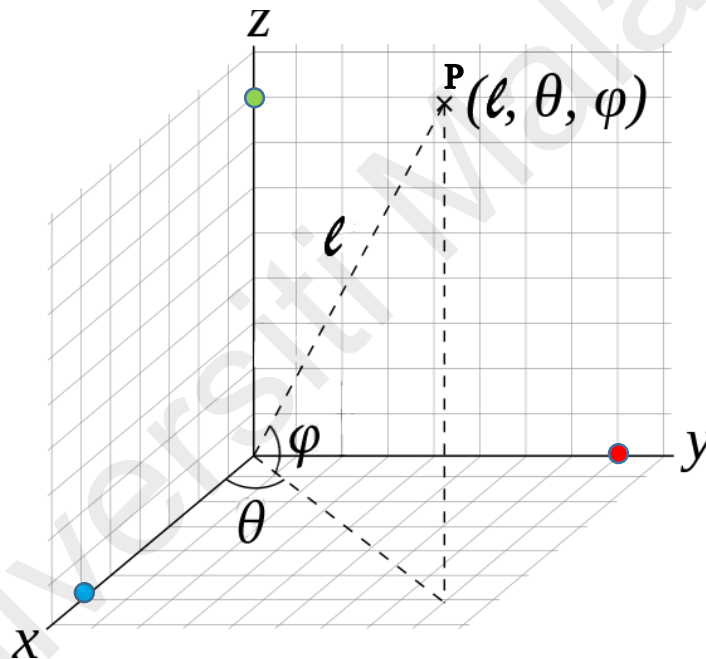


**Figure 2.4: Diagram showing the elements of the spherical coordinate system in presenting the Cartesian point  $P(x, y, z)$**

Some studies used the spherical coordinates to investigate facial symmetry or to track changes after orthognathic surgery (Yoon et al., 2011; Yoon et al., 2013; Yoon et al., 2014).

The spherical coordinates can be interchanged with the Cartesian coordinates  $(x, y, z)$  when desired (Figure 2.5) by the following procedures:

The spherical coordinates  $(\ell, \theta, \varphi)$  are related to the Cartesian coordinates  $(x, y, z)$  by the following equations:

$$\ell = \sqrt{x^2 + y^2 + z^2}$$

$$\theta = \tan^{-1}\left(\frac{y}{x}\right)$$

$$\varphi = \cos^{-1}\left(\frac{z}{\ell}\right)$$

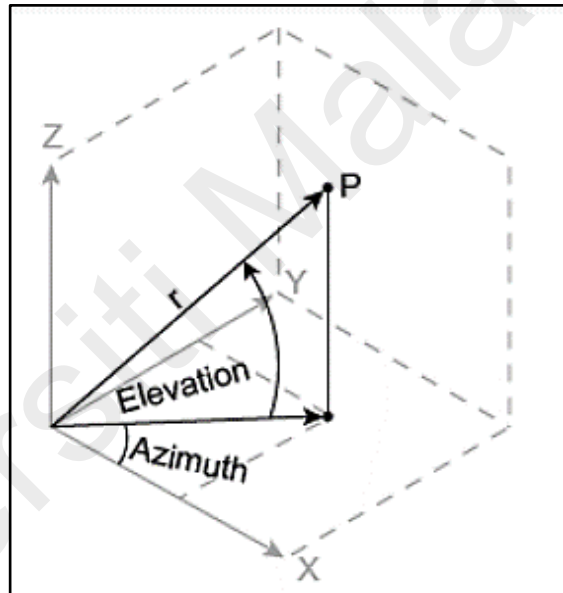


**Figure 2.5: Illustration showing the spherical and Cartesian coordinates for a 3D point**

The Cartesian coordinates can be converted to spherical coordinates in three-dimensional form as in the following equations:

$$x = \ell * \cos(\varphi) * \cos(\theta)$$

$$y = \ell * \cos(\varphi) * \sin(\theta)$$

$$z = \ell * \sin(\varphi)$$

Example for converting the spherical coordinates to Cartesian coordinates for RCI:

$$\begin{array}{ccc}
 \text{Spherical } (\ell, \theta, \varphi) & & \text{Cartesian } (x, y, z) \\
 \text{RCI } (27.50, 78.81, 36.12) & \begin{array}{l} \xrightarrow{x = 27.5 * \text{COS}(36.12) * \text{COS}(36.12)} \\ \xrightarrow{y = 27.5 * \text{COS}(36.12) * \text{SIN}(36.12)} \\ \xrightarrow{z = 27.5 * \text{SIN}(36.12)} \end{array} & \text{RCI } (4.31, 21.79, 16.211)
 \end{array}$$

Like the Cartesian coordinate system, the spherical coordinate system has three elements:

#### 2.7.4.1 The radius ( $\ell$ )

The shortest straight distance of a point from the origin  $O = (0, 0, 0)$  in the three-dimensional Cartesian coordinate system is called the radius; it is calculated by standard Euclidean straight distance equation (Fisher et al., 1993)

#### 2.7.4.2 The azimuth angle ( $\theta$ )

The azimuth angle is the counter-clockwise directed angle in the x-y plane that is measured in radians from the positive x-axis. Or in other words, it is the angle measured counter-clockwise between the vector  $\overrightarrow{Ox}$  and the projection of the vector  $\overrightarrow{OP}$  as shown in Figures 2.5 and 2.6. This angle is always measured starting from the positive x and it ranges between:

$$0^\circ \leq \theta \leq 360^\circ$$

### 2.7.4.3 The elevation angle ( $\varphi$ )

Is the angle measured between the vector  $\overrightarrow{OZ}$  and the vector  $\overrightarrow{OP}$  (Figure 2.5). This elevation angle is confined between 0-90 degrees

$$0^\circ \leq \varphi \leq 90^\circ$$

### 2.7.5 Angular and circular data analysis

In some statistical problems, when the data is directional (measured by angles), the simple linear functional relationship model is no longer appropriate for determining relationships between the angular values or the units of the circle. Circular data can be represented as angles or as points on the circumference of a unit of a circle (Jammalamadaka & Sengupta, 2001). The data refer to a set of observations measured by angles in the intervals of (0 -  $2\pi$  radians) or (0 -  $360^\circ$ ) (Figure 2.6). When the data are circular or directional, the simple linear functional relationship is no longer appropriate for their analysis. Relationships between variables that are not linear such as angles are not possible to be determined by regression analysis or simple correlations

- Conversion of angles from degrees to radians:

$$360^\circ = 2\pi \text{ radians}$$

We can use the relationship to develop a method for converting between degrees and radians as follows.

$$1^\circ = \frac{\pi}{180} \text{ radian} \qquad 1 \text{ radian} = \frac{180^\circ}{\pi}$$

If the angle measure presented with no unit specified, then radian measure is understood.

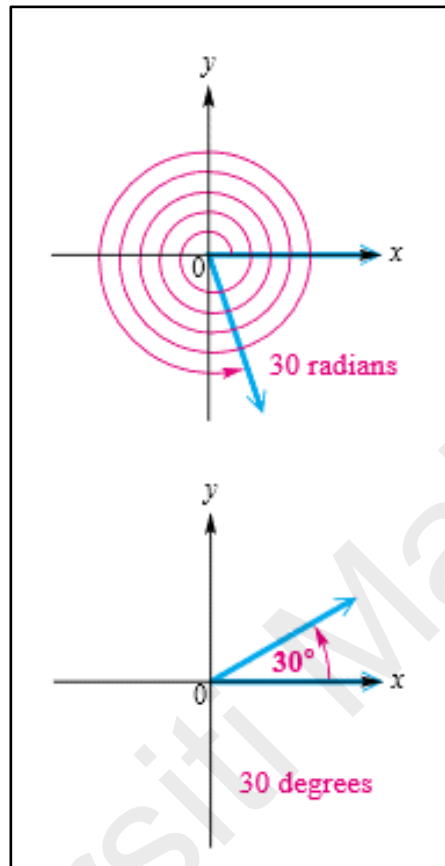


**Figure 2.6: Comparison between angles of 30 measured in radians and degrees**

### **2.7.6 Computer guided complete denture technology**

The last two decades witnessed an important upgrade in the computer aided designing / computer assisted manufacturing (CAD/CAM) industry when the early attempts to make removable prostheses started rather than being confined to fixed restorations. Although progress in developing removable CAD/CAM prostheses was slow compared to the CAD/CAM development, Maeda et al. (1994) had initiated early attempts to make complete CAD/CAM dentures, established a prototype system and concept for denture fabrication and they positioned the artificial teeth in what they named as “the proper stress

distribution among denture-supporting tissues” which is recommended by studies based on finite element analysis of stress distribution of teeth in complete dentures. In the finite element analysis, assumptions for the supportive structures (mucosa and underlying bone) behaviours under stress application were suggested a few years later (Zhang et al., 2002). Digital archivability and portable data on patient and prosthesis became available.

Sun et al. (2009) established a trial prototype for teeth alignments as a surface that is formed by connecting the centre curves of the alveolar ridge of the maxilla and mandible, which is intersecting the occlusal plane.

Automatic default setting of teeth is suggested in the CAD software with the scanned dental cast and the data required along with the algorithms for analysis would result in positioning that is in biometric relation to the palatal landmarks measurements and arch form. Figure 2.7 shows current arbitrary alignment of teeth that need to be adjusted individually by the dentist or technician.



**Figure 2.7: Current arbitrary alignment of teeth in DRCD that need to be adjusted individually by the dentist or technician (Masri & Driscoll, 2015)**

The denture artificial teeth can be delivered to the denture in three forms: individual CAD-CAM-bonded teeth having premanufactured acrylic teeth bonded into the milled

denture base; CAD-CAM monolithic teeth, in which the denture teeth are milled as part of the denture base and the one-set aligned artificial teeth (ISA) that are made in one set of linked teeth made by CAD/CAM subtraction or rapid prototyping (Bilgin et al., 2015; Goodacre et al., 2018).

#### **2.7.6.1 Advantages of CAD/CAM complete dentures**

Besides the reduced number of clinical visits and speed in fabricating the dentures, several comparison studies were conducted to test the critical aspects that can show the distinction of CAD/CAM dentures apart from the conventional complete dentures. Two-dimensional discrepancy comparison was made by Steinmassl et al. (2018) to test the difference between the CCD and the DCD dentures; they found that the DCD have more stable and accurate fitting to the denture bearing tissue and higher dimensional stability because no or minimal polymerisation shrinkage may occur in prefabricated acrylic blocks and subtractive procedures compared to conventional polymerised acrylic material. Moreover, when compared to the three available types of acrylic denture bases, CAD/CAM denture bases showed better colour stability compared to other denture base types used for fabricating complete dentures (Dayan et al., 2019).

Compared to the conventional complete denture's five or six appointments, the digital dentures appointments were reduced to as little as two only (Steinmassl et al., 2017; Hirayama, 2019), the clinical procedures and clinical recordings were confined into one appointment only and duration of patient visits to one or two hours (Kattadiyil et al., 2013).

The various DCD systems have introduced procedures, materials and instruments to the basic fabrication steps that were not used in CCD procedures to improve the fabrication speed and practicality. Examples are Dentca detachable tray and Wagner EZ tray for preliminary impressions, prefabricated acrylic blocks, monolithic teeth sets and so forth (Hirayama, 2019). Almost all the procedures in making the complete denture have been improved and modified slightly to accommodate the need for DCD fabrication such as recording the intra-occlusal record (IOR), occlusal vertical dimension (OVD), teeth arrangement, mounting the casts to virtual articulator were improved and facilitated. However, after final impression and occlusal relationship are uploaded into the design software, the anatomical landmarks plotted, and the denture border is determined; the CAD/CAM software propose initial teeth setup for the denture in DCD. The proposed teeth setup is still subjective and created based on average values of two-dimensional tooth position in relation to anatomical landmarks and acquired information such as lip support, maxillary incisal teeth position, occlusal plane, and so forth. If the proposed digital teeth setup position, digital gingival contour, and digital gingival wax-up are satisfactory and approved by the dentist, a final DRCD or a try-in denture would be produced (Hirayama, 2019).

#### **2.7.6.2 Commercially available CAD/CAM complete denture systems**

Until the early 2010s, Dentca™ and AvaDent™ were the only companies claiming the ability to make complete dentures in two visits. Over the years, they have found difficulties in the manufacturing process and developed additional steps to rectify the limitations. Later on, several software

development companies developed DCD CAD software compatible with multiple manufacturing options. To the author's knowledge, to date, only a few available CAD/CAM systems are capable of designing and assisting in manufacturing removable complete dentures (Steinmassl et al., 2017). Currently dentists have two main options for fabricating DCD: Direct centre system, direct account with AvaDent or Dentca (Masri & Driscoll, 2015) or laboratory system: through a dental laboratory as one of the following:

(a) AvaDent or Dentca through the dental laboratory

(b) Combination of software and material companies: Dentsply Sirona, AvaDent, Kulzer, Dentca, Ivoclar, 3Shape, Mertz Baltic denture system, Amman Girschbach, and so forth.

(c) In laboratory software system: 3Shape, Dental Wing, Exocad, Stoneglass Industries (de Mendonça et al., 2016; Hirayama, 2019)

In Table 2.2, comparison between the available CAD/CAM complete denture systems in terms of biometric guides used, number of visits needed and other details are presented.

**Table 2.2: Comparison of various types of currently available CAD/CAM completed denture systems and manufacturers**

<b>Detail</b> <b>System</b>	<b>Company</b>	<b>Country of origin</b>	<b>Number of visits (excluding try-in)</b>	<b>Type of teeth used</b>	<b>Fabrication technology</b>	<b>Landmarks used for teeth position guidance</b>
<b>AvaDent digital dentures</b>	Global Dental Science	USA	3 (2)	Individual teeth pre-manufactured	Full-subtractive Manufacturing	Incisive papilla Inter alar width Lip length Interpupillary distance
<b>Baltic Denture System</b>	Merz Dental GmbH	Germany	2	bonded into the sockets	Full-subtractive Manufacturing	Maxillary Tuberosities Canine eminence Premolar position on the ridge Hamular notches
<b>Dentca</b>	Dentca Inc. Los Angeles, CA	USA	3 (2)	bonded into the sockets	Rapid prototyping (Additive Manufacturing)	Incisive papilla edentulous alveolar ridges
<b>WholeYou Nexteeth</b>	Whole you Inc.	USA	3 (2)	bonded into the sockets	Full-subtractive Manufacturing	Lip length
<b>Vita Vionic (Ceramill FDS)</b>	VITA Zahnfabrik	Germany	3(2)	bonded into the sockets	Full-subtractive Manufacturing	Crest of alveolar ridge line Incisive papilla

<b>Exocad</b>	Exocad	Germany	Software: Compatible with many systems	bonded into the sockets	Full-subtractive Manufacturing	Incisive papilla
<b>Ivoclar digital</b>	Ivoclar Vivadent	Germany	4 (3)	bonded into the sockets	Full-subtractive Manufacturing	Incisive papilla  Crest of alveolar ridge line  Maxillary Tuberosities
<b>Wieland digital denture</b>	Ivoclar Vivadent Group.	Germany	4 (3)	bonded into the sockets	Full-subtractive Manufacturing	occlusal plane  midline,  lip closure line  shapes of anterior rims of maxilla and mandible
<b>3Shape Dental system</b>	Trios 3Shape	Denmark	Software: Compatible with many systems	bonded into the sockets	Full-subtractive Manufacturing	Incisive papilla  Crest of alveolar ridge line  Maxillary Tuberosities
<b>Dental wings</b>	Dental Wings Inc. Montréal, Québec	Canada	3	one-set aligned artificial tooth bonded into groove	Full-subtractive Manufacturing	Incisive papilla  Maxillary Tuberosities  Canine eminence

						Interalar width Hamular notches (pterygo mandibular folds) Crest of alveolar ridge line
<b>Ceramill Full Denture System</b>	Amann Girschbach AG	Austria	4 (3)	bonded into the sockets	Semi-subtractive manufacturing	Incisive papilla edentulous alveolar ridges Tuberosities Frenula
<b>Zirkonzahn Denture</b>	Zirkonzahn, Inc	Italy	4 (3)	bonded into the sockets	Full-subtractive Manufacturing	scan the patients' face

\*Data were obtained from online tutorials, webinars, product manuals of user guides and (Steinmassl et al., 2017)

## **2.8 Form of dental arch in literature**

Lammie (1959) described the importance of the arch form and position of anterior teeth as the most important factor in good appearance. Ideally, prosthodontic rehabilitation is not limited to restoring the missing teeth but extends to replacing the missing supporting tissues and reconstruction of the occlusal plane, phonetics, aesthetics, mastication and preservation of the remaining healthy condition of the patient's TMJ. This can be achieved only by the proper knowledge of the position, size and shape of the missing original teeth and arch form, and oral tissues and function to select and arrange the artificial teeth in places as similar as possible to the natural missing predecessors (Bissasu, 1992; Misch, 2014).

Restoring the original or ideal form of the dental arch is crucial for ideal aesthetics, stability and optimal functionality of the dentition. Many studies attempted to quantify the dental arch form and aimed at better understanding and planning for treatment especially in orthodontic patients (Currier, 1969; Wakabayashi et al., 1997; Cassidy et al., 1998; Ling & Wong, 2009). However, to date, no one global model can justify the variability in the forms of the dental arches in dentate individuals. Each arch has its independent characteristic pattern (Ferrario et al., 1994).

### **2.8.1 Significance of the dental arch form**

Dental arch form plays a very important role in the biomechanics and design of prostheses especially implant-supported prostheses for edentulous maxillary arch (Sagat et al., 2010). Whether fixed or removable prosthesis was planned, the number of implants needed to support prostheses in edentulous patients depends on several factors including the bone quality, the expected forces

applied on the prosthesis and the relationship between the residual ridge shape and the dental arch form. The ultimate form of the resorbed residual ridge in an edentulous arch is a result of the non-uniform resorption of the extraction sockets and healing after extraction; it would not necessarily represent the original or ideal form of the dental arch of the same specific patient (Misch, 2014; Fonseca, 2017).

Digital curve-fitting for dental arch to quantify arch forms for both clinical and research purposes has become the field of interest of many studies in orthodontics, maxillofacial surgery and prosthodontic disciplines (AlHarbi et al., 2008). Linear measurements such as arch width, depth, and circumference were the methods used to describe arch shapes. However, they were regarded as insufficient to describe the shape of the dental arch accurately. In natural dentition, five types of dental arch forms are known in the literature: normal, ovoid, narrow ovoid, tapered and narrow tapered (Ricketts, 1990). It was believed that these were integrated with the depth and the width of the arch (Wakabayashi et al., 1997; Jivraj et al., 2006).

Disagreement in opinion is detected in the literature regarding the ideal dental arch form for the artificial teeth alignment in the completed denture and reconstructive procedures. Zarb et al. (2003) stated, “the form of the palatal vault gives an indication as to the original form of the dental arch before removal of the natural teeth and resorption of the residual ridge” and it serves as the key for the artificial teeth arranged form. Another consideration, the “neutral zone” is key to the ideal dental arch form (Beresin & Schiesser, 2006; Zarb et al., 2013). At the same time some researchers argued that the neutral zone is varying in the same patients in different point of time following the

resorption of the residual ridge, the surrounding muscle activity and the period of being edentulous (Lammie, 1959). In contrast, a third opinion sees the existing form of the residual ridge in a point of time as a result of resorption or trauma and suggests to follow arbitrary measurements with relatively stable landmarks such as incisive papilla and mid palatal suture (Misch, 2014; Resnik, 2020).

Due to the discrepancy in teeth positioning that leads to improper form of the dental arch, many cases had negative feedback by the dentist and the patient when teeth are arranged based on the current available guidelines. Therefore, to overcome this complication, AlHelal et al. (2017b) suggested utilising additional visit to perform secondary impression and maintain jaw relation records.

To the author's knowledge, the earliest attempt to predict the form of the dental arch was made by Preti et al. (1986). They used regression analysis to suggest the curved distance over the alveolar process between the maxillary left and right buccal frenae to predict the parabolic curve that represents the outer form of anterior dental arch of the maxillary teeth based on centre of incisive papilla landmark to serve as biometric guides for edentulous patients. The objective of this study was to find the relationship between intraoral anatomical landmarks and the curve of the dental arch, generate relationship model and verify the predictability on independent group of dentate subjects, and then predict dental arch form for edentulous cases.

In both the fixed and removable prosthodontic rehabilitation for edentulous patients, deciding the ultimate form of the dental arch is crucial to achieve aesthetics, proper tissue support and enhance the biomechanical properties of

the prosthesis (Zarb et al., 2013; Misch, 2014). Valenzuela et al. (2001) suggested that Fourier series describes the differences in dental arch form and size more precisely. However, AlHarbi et al. (2008) compared multiple mathematical analyses to represent the dental arch curvature and found that the polynomial function was the best predictor of the individualised ideal arch for each particular patient.

To quantify and prove this similarity, the curves must be standardised, identified and extracted before being compared and matched to each other using proper systematic mathematical procedures (such as regression analysis or Procrustes analysis). Finally, it is necessary to check whether any relationship exists between each other that may lead to predict one by the other.

## **2.8.2 The need for dental arch form in dental application**

### **2.8.2.1 In orthodontics**

The importance of knowing the ideal or ultimate dental arch form in orthodontic cases is very important in order to get the arch wire prepared and to plan for the treatment and maintenance for the patient based on the suitable arch form (Chuck, 1934).

### **2.8.2.2 In prosthodontics**

To rehabilitate the aesthetic, function and the proper TMJ function, the prosthesis should follow the proper original arch form uniquely for the given patient's case.

#### **(a) *In conventional complete denture prosthesis***

The recommended dental arch form and size for the conventional complete denture is directly related and affected by the size and form of the edentulous residual ridges as they appear from an occlusal viewpoint especially in the anterior premaxillary area. Both the mandible and the maxillae size, form and horizontal relation to each other may affect the teeth size selection and the teeth arrangement as long as a certain occlusal scheme is required; retention and support are very limited in CCD. Asymmetric arches may create problems in tooth arrangement and occlusion (Zarb et al., 2013).

#### **(b) *CAD/CAM prostheses***

The computer-guided manufacturing needs computer rated data that is accurate enough to guide robotic computer information to direct the 3D printer in creating the wax rim, denture base, transferring and registering the jaw relation or setting teeth. However, the current practice has the dental arch designing performed by the dental technician in a semi-automatic procedure based on information provided by the dentist. The dentist obtains the information such as jaw relation, tooth position, tooth support to lips and cheeks manually and directly on the patient's mouth by trial and error or arbitrarily following the classical known occlusal principles of dental arch form and size determination in CCD even for fixed CAD/CAM dentures. Often practitioners are placing anterior teeth in incorrect positions far from the natural tooth position in CCD, following the same positions in CAD/CAM

dentures that are fixed or having very much higher retention, stability and support that would lead to incorrect other subsequent steps and failure in OVD, mandibular anterior tooth position, and posterior occlusal planes (Misch, 2014; Resnik, 2020).

### **2.8.2.3 In oral surgery**

For rehabilitation of fractured jaw (especially mandible) and in orthognathic surgical rehabilitation, knowledge of the dental arch form would help in achieving successful reconstruction or reduction for the fractured bone (Markiewicz et al., 2020).

### **2.8.3 Reference points used to define the dental arch form**

Scheid & Weiss (2017) described the dental arch in the ideal alignment of teeth when viewed from the occlusal aspect as three U-shaped or parabolic curves. The incisal edges and the buccal cusp tips follow a curved line around the outer edge of the dental arch, the lingual cusp tips of the posterior teeth follow a curved line nearly parallel to the buccal cusp tips and a sulcular groove curve that runs between the buccal and lingual curves.

Common anatomical reference points on the teeth such as the incisal edges, incisal corner and cusp-tips were suggested in various studies and used for measuring, comparing, classifying and digitising the dental arches. Incisal edges of anterior teeth, canine tips and buccal cusp-tips are used to represent the buccal dental arch in studies; mesiobuccal and distobuccal cusp-tips of the first and second molars are also used as they are wider teeth mesiodistally (Kasai et al., 1995). The central fossae of the maxillary posterior teeth were

used and linked in representation to the normal line of occlusion in the maxillary teeth. Cingulae of the anterior teeth and the lingual/palatal cusps of the posterior teeth were suggested to create a lingual dental arch. Mesiolingual and distolingual cusp-tip were used for the molars, as they are wider mesiodistally (Biggerstaff, 1972; BeGole & Lyew, 1998; Fujita et al., 2002; AlHarbi et al., 2008; Ling & Wong, 2009).

#### **2.8.4 Digitising and comparing dental arches**

Various studies attempted to quantify the dental arch form for better understanding of the pattern and classification. The arch as a curve may be represented by a simple curve or as the composite structure of the natural dentition. The arch curve was commonly indicated by a series of landmarks on the teeth in some biologically-meaningful way (Dryden & Mardia, 2016). To digitise the dental arch, some studies used two-dimensional digital photography captured by medium-to-high resolution digital cameras with certain calibration reference to reproduce the measurements in digital method (AlHarbi et al., 2008). Other studies have used three-dimensional scanners and utilised 3D images to perform their digital analysis on the dental arch (Mina et al., 2017). The nature of the data used for the two approaches is a bit different in terms of coordinates, the 2D uses (x, y) while the 3D uses (x, y, z) coordinates to represent the dental arch. If accuracy is a concern, acquiring data for both the 2D or 3D dental arch has its challenges; in the 2D acquisition, the settings for image calibration must be carefully designed to avoid perspective distortion (Soycan & Soycan, 2019) while for 3D imaging, the occlusal plane should be acquired or projected from an aspect perpendicular to the average plane of occlusion (Živković et al., 2019). In studies, various number and

locations of reference points were selected on the teeth to represent the anatomical dental arch for digital replication. Some have used the midincisal point of incisors and canine cusp tip as anterior tooth references while others used buccal cusp tips as posterior tooth references to represent the dental arch (Braun et al., 1998; AlHarbi et al., 2008). Other studies used the corners of incisal edges as reference for anterior teeth or contact points between teeth or incisal corners (Ling & Wong, 2009) or lingual fossae of the anterior. Posterior were represented by buccal cusps, lingual cusps, central fossae or combinations of the same to represent the dental arch (Ling & Wong, 2009). Some studies picked four points to represent the dental arch such as left and right second molars and canines (Noroozi et al., 2001).

To the best knowledge of the researcher, to date, no known study has investigated numerically the relationship between the form of dental arch and the palatal vaults form. No attempts were carried out to predict the individualised form of the dental arch from the palatal measurements or using intraoral or extraoral landmarks or anatomical features.

### **2.8.5 Mathematical representation of dental arch form**

To describe the dental arch curvature Begole (1980) suggested that mathematical curve with flexibility to fit any size asymmetries or shape of the dental arch should be used. Various methods were suggested to describe the dental arch curvature through time in the dental literature such as catenary curves by MacConaill & Scher (1949), elliptic curves and paraboloid by Currier (1969), spline curves by Begole (1980), conic sections by Biggerstaff (1972) and Sampson (1983), and the beta function by Braun et al. (1998). In dental research, least square polynomial curve fitting was tested in fitting the

dental arch on up to polynomial 12<sup>th</sup> degree ( $x^{12}$ ) equations. However, the best fitting curve for the dental arch is the polynomial fourth-degree ( $x^4$ ) when simple representation is required (Staley et al., 1985; AlHarbi et al., 2008; Adaškevičius & Vasiliauskas, 2009; Kim & Lee, 2011).

## **2.9 The position of teeth in dental arch**

One of the most important concerns in designing complete dentures is the artificial teeth arranging and positioning on the denture. The denture teeth are the part of the prostheses not only responsible for aesthetic, phonetics and chewing rehabilitation for the edentulous patient but they also restore the occlusion, regulate the jaw relation and mandibular movements during function (Basker et al., 2011). In conventional complete denture the artificial teeth also play a role in establishing occlusion and stability (Peroz et al., 2003). Due to several constraints in artificial teeth positioning, the teeth positions must be confined to certain zones that may help in sustaining the biomechanical requirements of the CCD; these constraints may be applied on computer engineered complete dentures as well (Jain & Rathee, 2019).

With technology advancement, the prosthodontic treatment options and techniques have improved significantly. Implementation of endosseous implant supporting fixed and removable prosthodontics has improved the retention, stability and support of the dental prostheses and enabled dentists to restore the aesthetics by placing the anterior teeth closer to original natural position. The osseointegrated titanium fixtures not only provide retention, support and stability to the prosthesis, they also generate internal stresses to the harbouring bone that can guarantee the survival and turnover according to the physiological need theory (Zarb et al., 2013). It is universally agreed that to

replace the missing teeth, the best position for the artificial teeth is where the natural predecessors occupied. In fixed prosthodontics rehabilitating edentulous arch, the artificial teeth may occupy the correct functional and biological natural teeth positions with normal physiological location. The locations of the teeth that can perform the best for certain dental arch are not investigated in depth in the literature (Sabir et al., 2019).

Now, when CAD/CAM technology is involved in fabricating CD and the CECD is implemented, the retention speed, precision and fit have improved and patient expectations have increased too. The first attempts in several studies faced some limitations such as difficulty in establishing OVD and retention (Kawahata et al., 1997). Slow development in this field took place through several studies in the currently available CAD/CAM systems that make removable complete conventional or implant supported denture prostheses; yet the arrangement of the artificial teeth is still following the traditional concepts in teeth arrangement. The teeth positioning is designed and made manually following questionable two-dimensional anatomical guides (Kattadiyil et al., 2013).

Progression in guided alveolar bone reconstruction and third generation of dentition research using stem cell and tissue regeneration research is ongoing. Many studies are being conducted toward regaining bone, periodontal ligament and new tooth development in missing tooth site. However, these technologies are considered costly and still facing some obstacles that are expected to be solved by time (Lee & Kim, 2014; Cucchi et al., 2017; Sheikh et al., 2017; Zeitlin, 2020).

## 2.10 Statistical analysis in dental research

Many studies investigated the relationship between anatomical landmarks, measurements of anatomical structures in order to relate them to each other or to guide in restoring the size, form or the position of missing tooth. However, majority of these studies have reported weak relationships and non-verified observations. The understanding of the mathematical relationships, the requirements for each step and the proper analysis method are very important factors for successful investigation. Misinterpretation of regression analysis, correlation or presentation of mere average values observed may not provide valuable information to the literature (Waliszewski, 2005; Isa et al., 2010).

### 2.10.1 The Pearson product moment correlation

For given series of  $n$  measurements of  $x$  and  $y$  that were written as  $x_i$  and  $y_i$  where  $i = 1, 2, \dots, n$ , the Pearson product-moment correlation coefficient can be used to estimate the correlation of  $x$  and  $y$ . The Pearson coefficient is also known as the "sample correlation coefficient". This coefficient is used to indicate the linear association between two random variables. It is expressed as a single numerical value between +1 and -1. A positive value means that when one measurement increases in value, the other one also increases. A negative value means that when one measurement increases in value, the other one decreases. The Pearson product moment correlation is defined as follows:

$$r_{x,y} = \frac{\sum_{i=1}^n (x_i - \bar{x})(y_i - \bar{y})}{\sqrt{\sum_{i=1}^n (x_i - \bar{x})^2 \sum_{i=1}^n (y_i - \bar{y})^2}}$$

where  $x_i$  and  $y_i$  are the individual observations from sample  $x$  and  $y$  respectively and  $\bar{x}$  and  $\bar{y}$  are the samples' averages.

To ensure that correlations actually reflect “meaningful” relationships, a regression analysis is used to establish relationships that make it possible to predict one or more variables in term of others. The first step is to consider the simplest type of regression analysis (i.e., the Simple Linear Regression Model, SLRM) and consequently a more complex model, the Multiple Linear Regression Model (MLRM).

## **2.10.2 Regression analysis**

### **2.10.2.1 Regression model assumptions**

When using regression as a statistical model, a few classical assumptions are involved; the assumptions are:

**SA1)**  $n > \rho$ , where  $\rho$  is the number of parameters

**SA2)**  $x_i$  is given, and dependent variables must be linearly independent, in other words it must not be possible to express any predictor as a linear combination of the others.

**SA3)**  $E(\varepsilon_i | x_i) = 0$ , error is assumed to be a random variable with a mean of zero, conditional on the dependent variables.

**SA4)**  $\text{Var}(\varepsilon_i | x_i) = \sigma^2$ , the variance of the error is constant across observations (homoscedasticity).

**SA5)** The error terms are uncorrelated, that is, the variance-covariance matrix of the errors is diagonal and each non-zero element is the variance of the error.

**SA6)**  $\varepsilon_i \sim N(0, \sigma^2)$  The errors are distributed according to a normal distribution.

### 2.10.2.2 Simple linear regression model (SLRM)

The general SLRM for a given sample  $(y_i, x_i), i = 1, 2, \dots, n$ , is basically a straight line where the equation is given by:

$$y_i = \alpha + \beta x_i + \varepsilon_i \quad (1)$$

in which  $y_i$  is the observed (dependent) variable,  $\alpha$  is the y intercept,  $\beta$  is the gradient or slope of the line,  $x_i$  is the independent variable and  $\varepsilon_i$  is the error of each observation.

To estimate the parameters of equation (1), the method of ordinary least squares is used. This method is useful in the sense that the method finds the line that minimises the sum of the squares of errors  $\sum_{i=1}^n \varepsilon_i^2$ . The estimates for  $\alpha$

and  $\beta$ ,  $\hat{\alpha}$  and  $\hat{\beta}$  are can be calculated using the equations given:

$$\hat{\beta} = \frac{\sum_{i=1}^n (x_i - \bar{x})(y_i - \bar{y})}{\sum_{i=1}^n (x_i - \bar{x})^2}$$

$$\hat{\alpha} = \bar{y} - \hat{\beta} \bar{x}$$

After using the ordinary least squares method, the model now becomes a function of a predicted variable  $\hat{y}_i$  as described by the estimates given in the equations. Equation (1) now becomes

$$\hat{y} = \hat{\alpha} + \hat{\beta}x_i$$

with the error terms now having an expected value of zero. The error or residual is defined as

$$\hat{\varepsilon}_i = y_i - \hat{y}_i.$$

### 2.10.2.3 Multiple linear regression model (MLRM)

Consider a MLRM with  $k$  explanatory variables. The general form of the MLRM is:

$$y = \beta_0 + \beta_1x_1 + \beta_2x_2 + \dots + \beta_kx_k + \varepsilon.$$

In a given experiment, one value for each of  $y, x_1, x_2, \dots, x_k$  is obtained.

Suppose the experiment is repeated  $n$ -times yielding:

$$\begin{aligned} y_1 &= \beta_0 + \beta_1x_{11} + \beta_2x_{12} + \dots + \beta_kx_{1k} + \varepsilon_1 \\ y_2 &= \beta_0 + \beta_1x_{21} + \beta_2x_{22} + \dots + \beta_kx_{2k} + \varepsilon_2 \\ &\vdots \\ y_i &= \beta_0 + \beta_1x_{i1} + \beta_2x_{i2} + \dots + \beta_kx_{ik} + \varepsilon_i \\ &\vdots \\ y_n &= \beta_0 + \beta_1x_{n1} + \beta_2x_{n2} + \dots + \beta_kx_{nk} + \varepsilon_n \end{aligned}$$

All of these equations can be represented in matrix form as follows:

$$y = X\beta + \varepsilon$$

where

$$\mathbf{y} = \begin{bmatrix} y_1 \\ y_2 \\ \vdots \\ y_n \end{bmatrix} \quad \mathbf{X} = \begin{bmatrix} 1 & x_{11} & x_{12} & \cdots & x_{1k} \\ 1 & x_{21} & x_{22} & \cdots & x_{2k} \\ \vdots & \vdots & \vdots & \ddots & \vdots \\ 1 & x_{n1} & x_{n2} & \cdots & x_{nk} \end{bmatrix}$$

$$\boldsymbol{\beta} = \begin{bmatrix} \beta_0 \\ \beta_1 \\ \vdots \\ \beta_k \end{bmatrix} \quad \boldsymbol{\varepsilon} = \begin{bmatrix} \varepsilon_1 \\ \varepsilon_2 \\ \vdots \\ \varepsilon_n \end{bmatrix}$$

$\mathbf{X}$  is an  $n \times (k+1)$  matrix consisting essentially of the given values of the  $x$ 's, with the columns of 1's appended to accommodate the constant terms whereas  $y$ ,  $\beta$ , and  $\varepsilon$  are column vectors of the observed values  $y_i$ , the true regression coefficients and the error terms, respectively.

The least squares estimate of the MLRM is given by

$$\hat{\beta} = (X'X)^{-1}X'y$$

where  $X'$  is the transpose of  $X$  and  $(X'X)^{-1}$  is the inverse of  $X'X$ . Again, as with the SLRM, the average error terms after the estimation is zero and the model equation becomes

$$\hat{y} = X\hat{\beta}$$

#### **2.10.2.4 Simple functional linear relationship in circular data**

The relationship between angles cannot be made with linear methods; therefore, circular functional relationships were suggested to find the relationship between angular data (Jammalamadaka & Sengupta, 2001).

#### **2.10.3 Assessing goodness-of-fit of regression models**

##### **2.10.3.1 Coefficient of determination $R^2$**

The most standard method of estimating a straight line is by the method of least squares (Scheaffer & McClavei, 1990; Tsai et al., 1998). This involves calculating the distance ( $d$ ) of each point from the line, in such a way that the sum of  $d^2$  is minimised (fitting a line by the method of least squares). After obtaining the least squares estimate of the regression model, it is prudent to determine whether the model is a 'good' fit to the data. To do so, the coefficient of determination, squared correlation coefficient between the actual  $y$  and its approximation value  $R^2$  is used as an indicator of the proportion of variability accounted by a statistical model or regression model,  $R^2 \in [0, 1]$ . In other words, a larger  $R^2$  value indicates that the model is more representative. It is a statistical measure of how well the regression line approximates the real data points. An  $R^2$  of 1.0 indicates that the regression line perfectly fits the data. The  $R^2$  is calculated from the sum of squares. The term "sum of squares" refers to the sum of the squares of the vertical distances that measure the distance of each point to the line that best predicts X from Y (Dielman, 2001).

Let a data set have values  $y_i$  which is the observed value measured from the sample and also  $f_i$ , the predicted value calculated from the fitted regression

model for every individual  $i$ . From these values the Total Sum of Squares (SST), Regression Sum of Squares (SSR), and the Error Sum of Squares (SSE) were computed. The sum of squares is defined as follows:

$$SST = \sum_{i=1}^n (y_i - \bar{y})^2$$

$$SSR = \sum_{i=1}^n (f_i - \bar{y})^2$$

$$SSE = \sum_{i=1}^n (y_i - f_i)^2$$

In these equations,  $\bar{y}$  and  $\bar{f}$  are the means of the observed and predicted values respectively. From these values, the  $R^2$  can be calculated using:

$$R^2 = \frac{SSR}{SST} = 1 - \frac{SSE}{SST}$$

since  $SST = SSR + SSE$ . In case of a SLRM, fitted by least squares,  $R^2$  equals the square of the Pearson product-moment correlation coefficient.

### 2.10.3.2 Weighted least squares regression

The weighted least squares (WLS) method is usually used when the constant error variances (homoscedasticity) is violated or used often as the basis for performing “robust” regression in which outliers are given less weight than points that are not outliers.

### 2.10.3.3 Multicollinearity and variance inflation factor (VIF)

Multicollinearity refers to a computational problem where predictors are correlated with other predictors in the same model. It occurs in MLRM when the model includes multiple factors that are correlated not just to the response variable, but also to each other. Multicollinearity increases the standard errors of the coefficients. It does not affect the goodness of fit and the goodness of prediction. In severe multicollinearity when the variance of the MLRM coefficients increased in the regression, the standard errors become unstable and make it more difficult to interpret the coefficients (Dielman, 2001; Thompson et al., 2017).

One of the best techniques for measuring the multicollinearity is by obtaining the variance inflation factor (VIF). A VIF can be computed for each explanatory variable. It is a measure of the strength of the relationship between each explanatory variable and all other explanatory variables in the regression. Thus, pairwise correlations are taken into account as well as more complex relationships with two or more of the other variables.

Let  $x_1, \dots, x_k$  be the  $K$  explanatory variables in a regression. Perform the regression for  $x_j$  on the remaining  $K-1$  explanatory variables and call the coefficient of determination from this regression  $R_j^2$ . The VIF for the variable  $x_j$  will be

$$\text{VIF}_j = 1/(1 - R_j^2).$$

The value  $R_j^2$  measures the strength of the relationship between  $x_j$  and the other  $K-1$  explanatory variables. If there is no relationship (an ideal case), then

$R_j^2 = 0.0$  and  $VIF_j = 1/(1 - 0) = 1$ . As  $R_j^2$  increases,  $VIF_j$  increases also. For example, if  $R_j^2 = 0.9$ , then  $VIF_j = 1/(1 - 0.9) = 10$ ; if  $R_j^2 = 0.99$ , then  $VIF_j = 1/(1 - 0.99) = 100$ . A large  $VIF_j$  suggests a serious multicollinearity problem where  $x_j$  may be highly correlated to other explanatory variables. There is no specific VIF value that suggests a problem; there are, however, two suggested guidelines given to help in overcoming the problems as in the following:

- 1- If any individual  $VIF_j > 10$  that indicates that multicollinearity may be influencing the least squares estimates of the regression coefficients.
- 2- If the average  $VIF_j$  is considerably  $> 1$  then serious problem may exist.

$$\text{Average } VIF_j, \quad \overline{VIF} = \sum_{j=1}^k VIF_j / k$$

$\overline{VIF}$  indicates how many times larger the error sum of squares for the regression is due to multicollinearity than it would be if the variables were uncorrelated.

- 3- The cut off value of VIF in the MLRM that is indicating multicollinearity is not consistent in all studies. Some studies considered values more than 4 as multicollinear indicators while other studies used 10 as high to conclude multicollinearity between the independent variables (O'Brien, 2007). In this study, the  $VIF \geq 4.0$  was considered high and alerting multicollinearity.

The VIFs for regression coefficients can be calculated from Minitab Statistical Software (Dielman, 2001; Minitab-Blog, 2013).

### **2.10.3.4 Identify the important variables in the multiple regression model**

Placing the variables one by one in the model is one of the methods to know which variable is most important. Change in  $R^2$  can be observed when the variable is added to the model. Multiple regression using “Minitab's Assistant” menu includes a useful analysis information. It calculates the increase in  $R^2$  that each variable produces when it is added to a model that already contains all of the other variables. The change in  $R^2$  represents the amount of unique variance that each variable explains above and beyond the other variables in the model (Minitab-Blog, 2016).

## **2.11 Computer artificial intelligence (AI)**

### **2.11.1 Artificial Neural Networks (ANN)**

Artificial neural networks (ANNs) can briefly be defined as “A neural network is a massively parallel distributed processor made up of simple processing units, which has a natural propensity for storing experiential knowledge and making it available for use. It resembles the brain in two respects: 1) Knowledge is acquired by the network from its environment through a learning process and 2) Interneuron connection strengths, known as synaptic weights, are used to store the acquired knowledge.” (Haykin, 1999). Neural networks are organised in layers having a number of interconnected “nodes”, which contain an “activation function”. Figure 2.8 shows the basic elements of a neuron. It has weight, bias, and an activation function. Patterns are presented to the network via the “input layer”, which communicates to one or more 'hidden layers’ where the actual processing is done via a system of weighted “connections”. The hidden layers then are linked to an “output layer” where the answer is output as shown on the right in the graphic. Artificial Neural Network (ANN) can predict any data based on feedback previously

given to it as an example. The more the examples the more reliable and accurate the results; it is working as the thinking human brain.

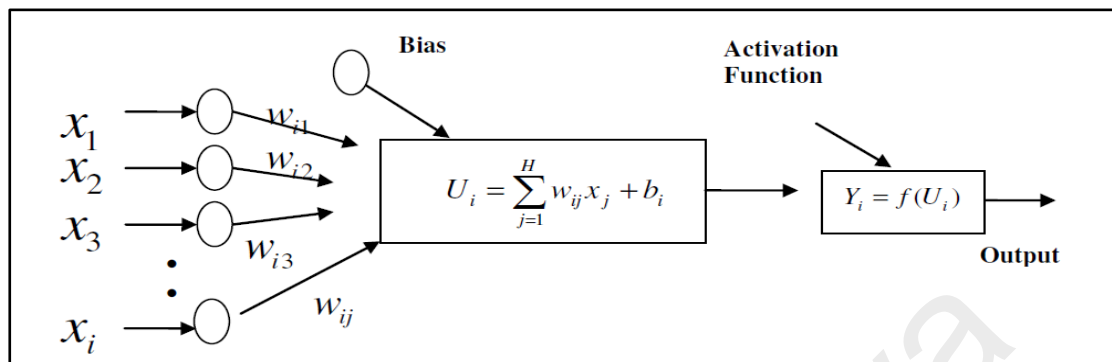


**Figure 2.8: Basic elements of an artificial neuron (adopted from Tayşi (2010))**

ANN is a computer processors' complex network similar to the human neurological systems. As in the human brain, it requires learning and it has interneuron connecting strengths known as synaptic weights used to store the knowledge.

Many layers of computer processors perform parallel computations for data processing for the function of such networks. Each of these interconnected units is known as “neurons”, each neuron has a link and numerical weight associated with it. The computer network learns through repeated adjustments of these weights (Gali, 2020).

### 2.11.1.1 Back-propagation artificial neural network (ANN)

A type of artificial neural network is called “Back-propagation Neural Networks” (BPN) was first described by Paul Werbos in 1974 (Werbos, 1990). The BPN learning is where the computer can learn from newer information to

understand diseases, diagnose them early, and to treat them effectively (Rumelhart et al., 1988; Tayşi, 2010). BPN is one of the most widely used supervised training methods for training multilayer neural networks (NN) due to its simplicity and applicability. As this is a supervised learning algorithm, it has a pair of inputs and corresponding output. The algorithm is based on a weight and consists of two passes: a forward pass and a backward pass. In the forward pass, first, the weights of the network are randomly initialised and an output set is obtained for a given input set where weights are kept as fixed. The error between the network output and the target value is propagated backward during the backward pass and used to update the weights of the previous layers (Gasteiger & Zupan, 1993).

#### **2.11.1.2 Advantages and disadvantages of the AI highlighted by the literature**

The AI is a very helpful system to determine and apply relationships between any two variables. However, it can be a misleading tool for data prediction if the variables are not carefully selected. Correlation between the variables perhaps must be checked before introducing the data in the AI system (May et al., 2011).

#### **2.11.1.3 Application of artificial intelligence on complete denture**

AI helps in predicting orthodontic teeth movement based on patient ethnicity and anthropological background. With the development of automation, robotics and artificial intelligence, focus must be on eliminating

the technical challenges involved in denture fabrication at the rural settings. Robotic systems for teeth arrangement, tooth ablation, chewing robot for testing dental materials and dental implant placement have been explored (Gali, 2020).

Several factors must be considered to claim long term successful rehabilitation of edentulous dental arch. Recently, in the currently available CECD systems, some dissatisfaction was reported by clinicians and patients that led to recommended additional visit to improve quality of the outcome (AlHelal et al., 2017b). However, some earlier steps performed during the first visit and in the lab preparations such as orientating the occlusal plane, deciding the proper dental arch form and selecting and arranging the artificial teeth in the computer designed denture base still need a lot of arbitrary and manual adjustment for attaining the optimum settings. This chapter has elaborated on application of biometric guided semi-automatic techniques to predict the orientation of occlusal plane, the proper form of the dental arch and high accuracy of three-dimensional coordinates for the artificial teeth positions that can be implemented more easily with little modifications on 3D printer and DCD.

# CHAPTER 3

---

Materials and methods

---

Universiti Malaya

## CHAPTER 3: MATERIALS AND METHODS

### 3.1 Sample of the study

The overall study sample is composed of fully dentate and edentulous dental casts collected from the study subjects. The total number of subjects recruited in this study was 126 (92 dentate and 34 edentulous). This sample size number was determined from Jan & Shieh (2019), where power of study of 0.9029 at critical value of 0.05 can be achieved having minimum sample size of 56 subjects.

In the literature, similar studies investigating guides for positioning teeth had a sample size close to the sample selected for this study (Grave & Becker, 1987; Fu et al., 2007b; Park et al., 2007). All the participants were interviewed by the researcher before they participated in this study.

#### 3.1.1 The dentate sample

Ninety-two dentate subjects (37 men and 55 women) were examined and selected to participate in this study based on the following inclusion criteria:

- a. The subjects were Malaysian male and female adults descending from ethnic Malay or Chinese backgrounds (Lu et al., 2017).
- b. Age between 20 and 35 years at the time of the study (Carter & McNamara, 1998; Jonsson & Magnusson, 2010).
- c. Having naturally well aligned natural teeth with Class-I skeletal and dental relationships according to Angle's Classification (Littlewood & Mitchell, 2019).

d. Having good oral hygiene

The subjects who had any of the following exclusion criteria were not considered to participate in the study:

- a. Any missing tooth, except for third molars.
- b. Abnormality in tooth morphology.
- c. Participant with history of large or proximal contact extended restorations, prostheses, severe attrition, over eruption, congenital missing, impaction or extraction related to maxillary or mandibular teeth, except for the 3rd molars.
- d. History or indication for surgery or orthodontic treatment such as orthognathic surgery or palatal expansion.
- e. Periodontal diseases caused pathological tooth migration, having gingival inflammation (swelling) or recession that is beyond the cemento-enamel junction or tooth mobility.
- f. Crowded teeth, teeth with spacing, malalignment, or malposition in maxillary or mandibular jaws.

Dental stone casts of maxillary and mandibular arches were obtained from patients who fit the inclusion criteria.

After completion of raw data acquisition, Microsoft Excel (Microsoft Office 2013) randomisation function was used to divide the dentate sample into two groups randomly; a study group (n = 70) and verification group (n = 22). The study group was dedicated to investigating the relationship between the landmarks' measurements and the position of teeth (objective 1a), while the verification group was used to verify the accuracy and reproducibility of predicted data from the established relationships found in the study group. The

predicted values were then compared with the actual observed corresponding values in the verification group (objective 1b).

### **3.1.2 The edentulous sample**

Among the patients who attended the polyclinics in the Faculty of Dentistry, University of Malaya seeking for treatment, 34 edentulous patients were selected after interview by the researcher individually following the questions listed in the participant information sheet (Appendix A). All selected patients were briefed and given written information about the study and their expected role as participants. Patients who agreed to participate were checked for eligibility according to the inclusion/exclusion criteria. Patient information including dental history, age, family ethnic background and duration of being edentulous were collected in the interview with the researcher and each patient was asked to fill and sign the participant's consent form of this study before clinical intraoral examination was made.

The inclusion criteria used in selecting the patients were:

- a. The patient should be Malaysian with Chinese or Malay ethnic ancestry (Lu et al., 2017).
- b. Should have maxillary edentulous arch for a duration not less than one year from the last extraction.
- c. Should have the hamular notches, incisive papilla and rugae lines anatomical structures intact.

Patient who have any of the following exclusion criteria points was not included in the study:

- a. Inherited or acquired defect in the hard palate,
- b. Fracture or anomaly in relation to maxillary tuberosity or pterygoid hamulus which result in unidentified hamular notch.
- c. History of surgery, trauma in the maxillary alveolar or palatal areas, unsupported (flabby) ridges, implant-supported restorations.
- d. Severe resorption in maxillary arch according to McGarry et al. (1999).
- e. Very large palatal torus that is extended to the rugae lines anteriorly.

Final impression for maxillary edentulous arch was performed for the patients included in this study to obtain the edentulous stone cast as explained in 3.4.3 and 3.4.4.

### **3.2 Ethical approval and patient consent**

Medical-Ethics Committee approval was attained for this study from the Faculty of Dentistry, University of Malaya. Approval number for the project was “DF PD0704/0011 (P)”.

Before starting collection of clinical data, all the dentate and edentulous subjects in this study were interviewed, informed by both verbal and written means about the study project and about their expected role if they participate in the study to obtain the participants’ consent (Appendix A).

### 3.3 Study flow charts

To give simplified idea on the study's major steps, the first and second objectives of the study, the flow chart (Figure 3.1) showed the common steps made for both dentate and edentulous samples' subjects.

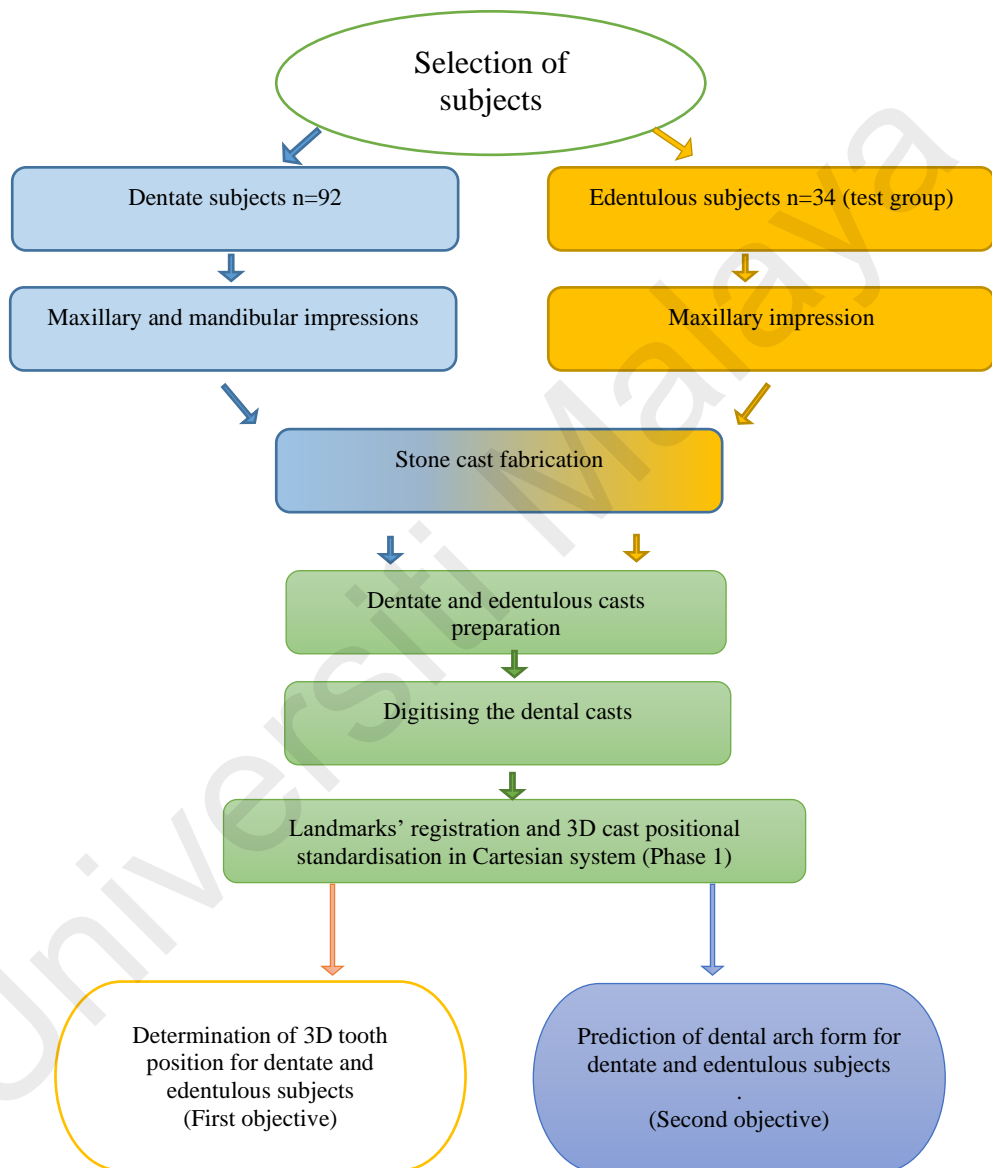


**Figure 3.1: The overall flow chart of the study based on objectives**

### **3.4 Dental cast collection and standardisation**

#### **3.4.1 Dentate arch impressions**

Maxillary and mandibular alginate impressions were made for each subject using metal stock impression trays using irreversible hydrocolloid impression material (Duplast fast set alginate impression material; Dentsply Dental Co Ltd, Tianjin, China) following the manufacturer's instructions. Before the impression was made, a second intra oral examination was performed to confirm that the patient fulfils the requirements of the study, (i.e., class I occlusion and integrity of the landmarks). Impression was rinsed under running tap water, inspected to ensure that the required details were recorded with no obvious defect. Unsatisfactory impression was repeated. The impression was then soaked in disinfectant solution (2% Perform ®– ID Schülke and Mayr, Germany) for 10 minutes and rinsed under running tap water. Immediately, dental stone (type III dental stone, Moldano; Heraeus Kulzer GmbH, Hanau, Germany) was manually mixed using a rubber bowl and spatula according to the manufacturer's instructions, then poured into the impression with the aid of vibrator to reduce bubbles in the stone cast. After complete setting of stone, casts were separated from alginate and inspected carefully and defective casts were excluded from the study.

### 3.4.2 Dentate cast preparation

Each cast was allowed to dry for 24 hours before a base of plaster of Paris was made for each cast (Donovan et al., 2019). The plaster bases were then marked and trimmed in a standardised manner to uniform the height and orientation following a procedure described by Omar (2004). A flat plastic board was used as reference board where a geometrical compass with a pencil were attached to it and adjusted to have the marker 30mm higher than the board. The stone casts were positioned to have the incisal edges and occlusal surfaces touching the board and rotated to let the marker draw a circumferential line on the plaster base for trimming (Figure 3.2). The cast base was then trimmed following the circumferential line that was made parallel to the occlusal plane.

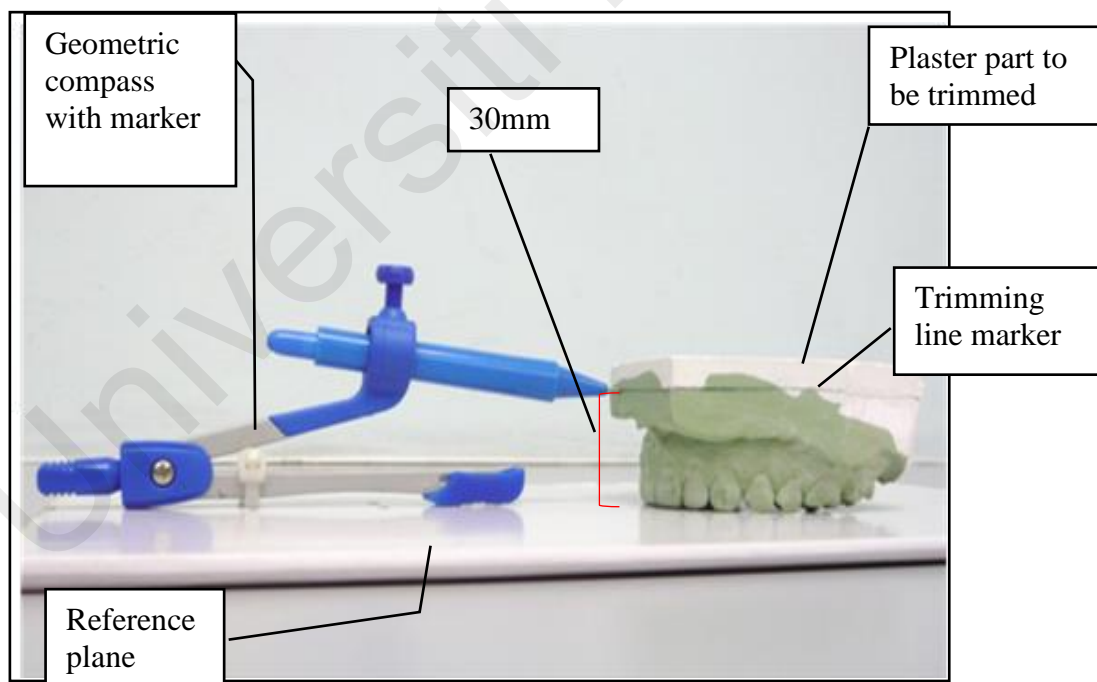


**Figure 3.2: Preparing the casts to ensure trimming the base on a level parallel to the occlusal plane**

Before scanning, the cast surface details such as occlusal grooves, palatal fossae, palatal rugae, gingival sulci and hamular notches were carefully inspected and any detected stone nodules were removed. The casts were

labelled according to participant's number following the letter 'D' for 'dentate' for digital tabling record and then kept in dental cardboard boxes for further steps. On each cast, teeth, rugae lines, midpalatal raphe and landmarks of incisive papilla (IP), left hamular notch (LHN), right hamular notch (RHN) were inspected. The left and right canine tips were marked for the comparison study of manual and digital measurements to assure the integrity of the study measurements as explained in 3.4.6.4 on page 121.

### **3.4.3 Edentulous arch impressions**

Final impressions were made for maxillary edentulous arches using special trays as a standard protocol for removable conventional complete denture fabrication. Light curing acrylic was used (Shandong Huge Dental Material Corp. Rizhao, China) to fabricate close-fitting custom trays for the impressions. After border moulding using green stick compound (Hoffman Harvard Denta GmbH Germany), all impressions were made by the same operator using Zinc Oxide Eugenol impression paste material (Impression paste, SS White, Gloucester, UK) and evaluated by the supervisor.

### **3.4.4 Edentulous cast preparation**

Edentulous impressions were poured immediately following the same as in 3.4.2. The base of the edentulous cast was trimmed parallel to the hamular incisive papilla plane using a dental surveyor and tripodding technique. The position of the cast was adjusted until the surveyor's analysing tip can touch the incisive papilla, left and right hamular notches while maintaining the same height (Figure 3.3, A). Tripodding technique was for determining the final orientation of the cast on the surveyor's occlusal table. Analysing rod was used to locate the trimming plane by drawing three lines of 20mm on the sides

of the cast's temporary base using a carbon marker. The tool fixed to the surveying arm has 20mm of parallel shaft from the hold point to surveyor arm to the point it starts to taper (Figure 3.3, B). A flexible ruler was then used to link the tips of the three vertical lines and make a horizontal circumference line that guides the trimming of the cast base parallel to HNIP. Casts were labelled according to the subject's number following the letter 'E' for 'edentulous' then kept in the dental cardboard box for further use.

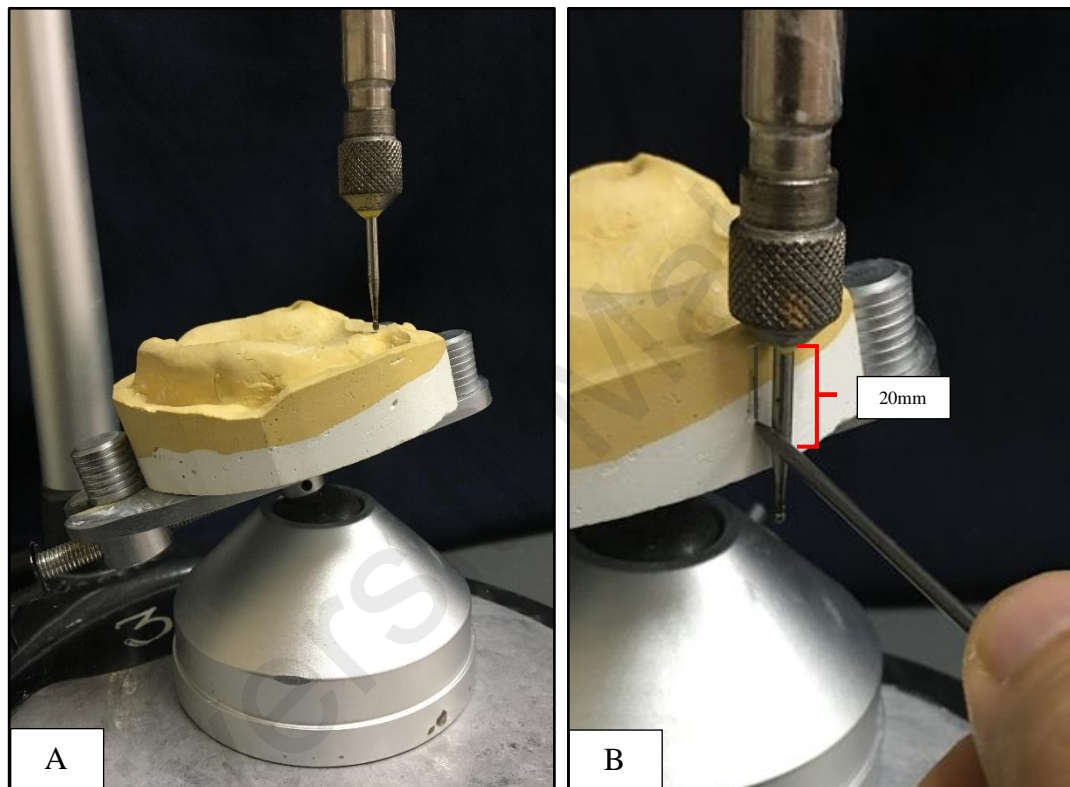


**Figure 3.3: (A) Standardising edentulous cast to have the hamular incisive papilla plane parallel to the horizon using a surveyor and tripping technique (B) following HNIP, tripping three vertical lines of 20mm were marked on the cast using a carbon marker**

### **3.4.5 Digitising the dental casts into three-dimensional digital casts**

The dental stone casts were scanned and digitised into three-dimensional digital meshes that accurately reproduce the dental casts for further analyses (Hassan et al., 2016). A 3D non-contact structured light projection triangulation scanner system Maestro 3D dental scanning machine (MDS200,

AGE Solutions, Italy) was used (Figure 3.4). The scanner's scanning accuracy is 10 microns (0.01 mm); the resolution was  $< 0.07\text{mm}$ . Calibration was done following the user guide provided by the manufacturer. Each cast was placed on the machine's integrated rotary table. Blue sticky tack was used to secure the casts in position and prevent any undesired movements during scanning. The scanning was set to use "Arc with palate" option with ten acquisitions on  $360^\circ$  rotary table turn (scanning different view of the cast at every  $36^\circ$  of horizontal rotation) in addition to one acquisition for the palate and lingual surface of the cast at  $45^\circ$  projection to the scanner's table. To standardise the projection of the cast through the last acquisition, two plastic geometric  $45^\circ$  rulers were glued parallel to each other by a block of cork and fixed as a jig to mount the cast at  $45^\circ$  on the rotary table.



**Figure 3.4: Maestro 3D dental scanner machine. MDS200 model**

Three-dimensional triangulated mesh image composed of 250,000 triangles was produced for each dentate and edentulous dental stone cast (Figure 3.5). The acquisitions were then rendered using “Postprocessing (convert the data acquired in a 3D cast)” adjusted to “Method V1” option and exported to save as digital stereolithographic binary (\*.stl) file format with disk size about 12MB for each digital cast by Maestro 3D easy dental scan software (AGE Solutions, Italy). The \*.stl files were saved following code given for each case.

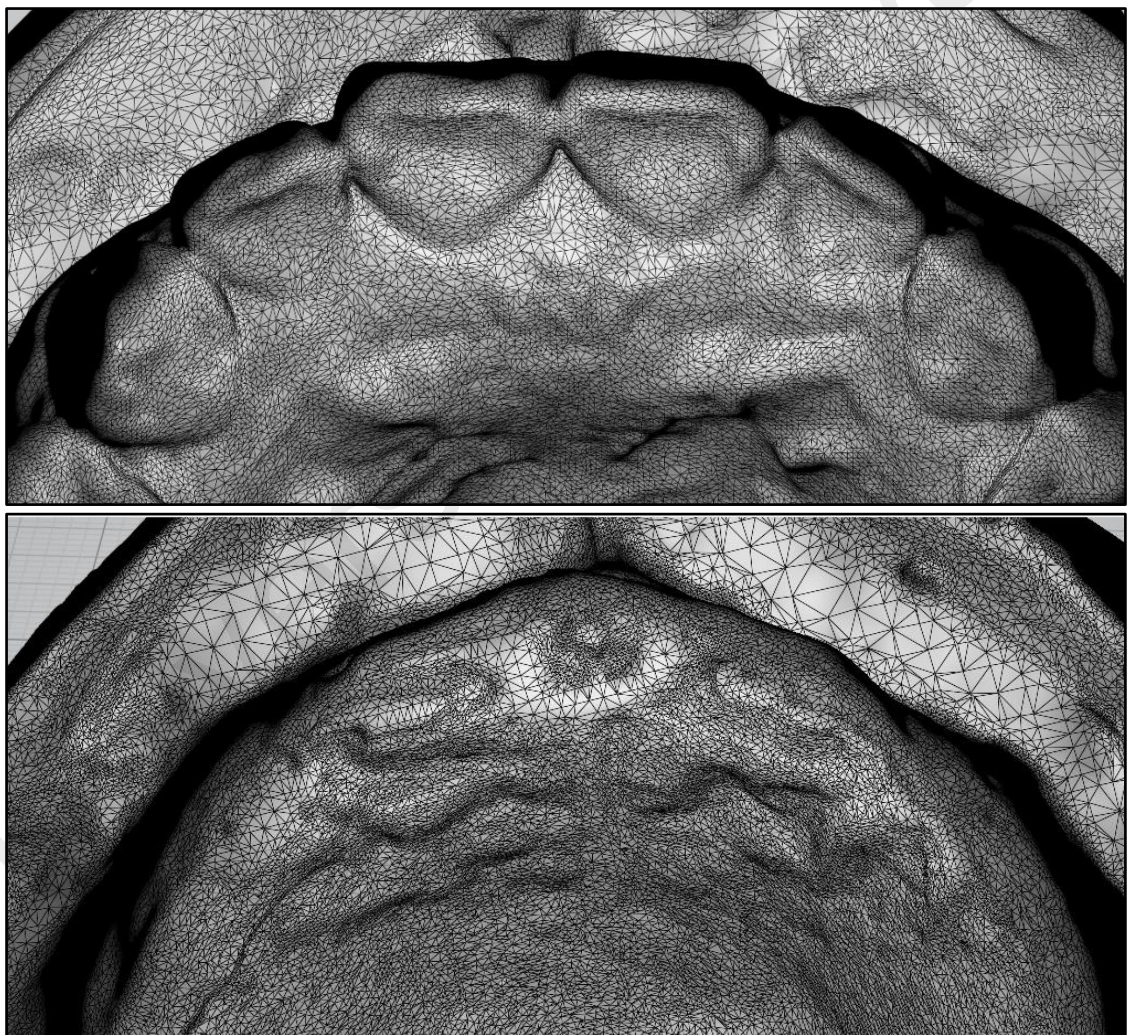


**Figure 3.5: Occlusal view of anterior part of the 3D digitised dentate (above) and edentulous (below) casts showing the triangles mesh acquired by the 3D dental scanner**

### 3.4.6 Standardising the digital casts before measurements

The digital cast position in the Cartesian coordinate system had to be standardised to enable comparison and avoid variation such as contrast for all the casts. The landmarks were marked, their coordinates were extracted and processed in serial steps to align the digital casts in a standard position using a uniform geometrical origin in the Cartesian system that is related to certain 3D coordinates selected landmarks. The standardisation was aimed at getting all the IP landmarks aligned with the Y axis ( $x = 0$ ), all the left and right hamular notches aligned with the X axis ( $y = 0$ ) on each side and at the same time, the three of the landmarks aligned on the XY plane ( $z = 0$ ). Ultimately, all the dentate and edentulous digital casts in the study were standardised by having the same origin and position in the Cartesian coordinate system based on their anatomical landmarks. Although the digital casts were positioned in the above-stated alignment by the mouse-adjusted 3D software tools (Figure 3.6); the coordinate values of the landmarks were not standardised and aligned in accuracy higher than two decimal places. Therefore, certain processing procedures were applied on both the dentate and edentulous digital casts through two sequential processing phases to achieve standardised coordinates with accuracy within 12 up to 17 decimal places (example  $z = 0.00000000000000027574$ ). In the first processing phase, geometrical tools and functions were used in the 3D analysis software while, in the second phase, geometrical concepts were used in Microsoft Excel application.

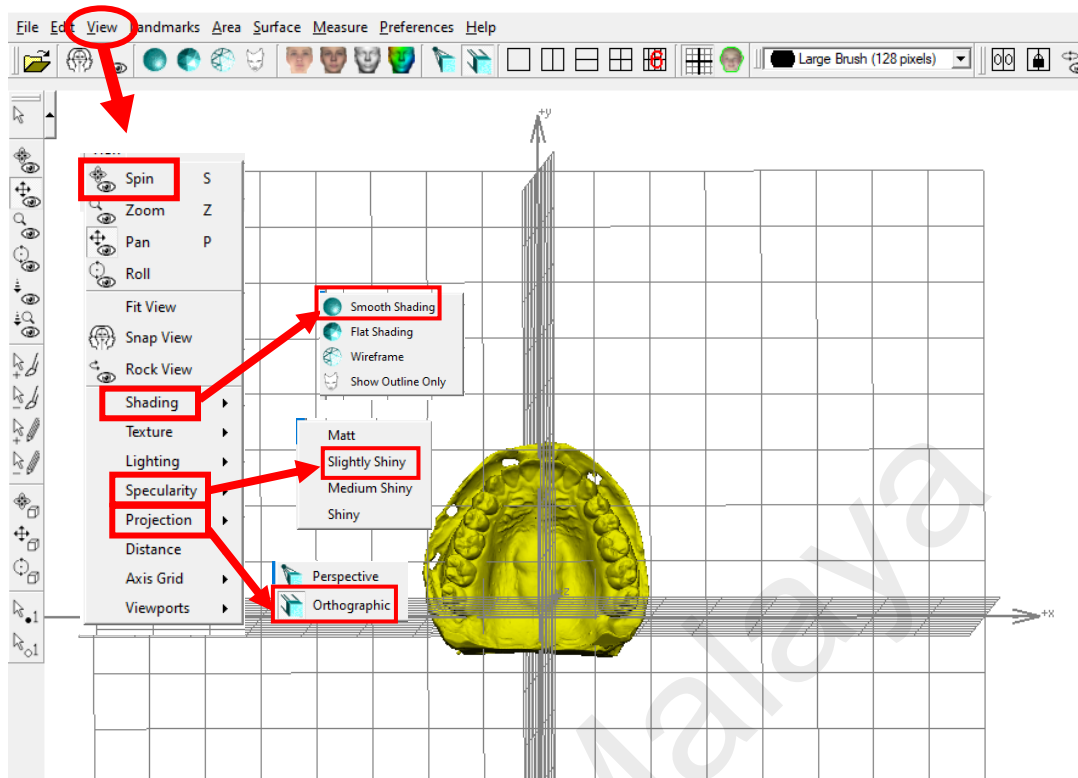


**Figure 3.6: Software settings to view and align the digital dental cast in Cartesian coordinate system**

### 3.4.6.1 Registering the landmarks

The digital casts were downloaded into a 3D analysis software (VAM, Vectra 3D, Canfield Scientific Inc., USA) to register the points representing the anatomical landmarks, the teeth and align the casts before extracting the 3D coordinates of the registered points and making measurements to perform the data analyses. Each digital cast was opened in VAM software and viewed according to the following settings from the main menu. Under “view” drop-down list → (1) “shading” → select “smooth shading” option was selected, (2) “Specularity” → “Slightly Shiny” option was selected, (3) “Projection” → “Orthographic” option was selected. The positions of the 3D casts were aligned initially to be viewed from occlusal aspect using “Spin” tool to explore the landmarks and identify the primary palatal rugae lines. Rugae were identified

as the first, second, and third rugae sequentially from anterior to posterior and rugae points were registered on the 3D dentate and edentulous casts according to Lysell (1955) and Jang et al. (2009) as shown in Figure 3.7.

With the help of “Place Landmarks” tool, landmarks and points were identified and registered in each dentate and edentulous digital dental cast (Figures 3.7 - 3.9):

(a) **Landmarks**

The following 4 landmarks were registered on both dentate and edentulous casts:

- The centre of the incisive papilla (IP),
- Left and right hamular notches (LHN & RHN) respectively
- The point on the palate that lies at the intersection between the line joining the left to right medial ends of the third primary rugae lines and the sagittal line on the midpalatal raphe that extends from the middle of IP perpendicular on the line joining LHN and RHN is registered as R-point. The R-point is having the same x coordinate as and x of IP (Figures 3.7, 3.8 and 3.9).

(b) **Points**

18 additional landmarks and points were assigned for the dentate digital casts only:

- The centre points of the incisal edge of each of the left and right central and lateral incisor teeth (LCI, RCI, LLI and RLI) respectively
- The left and right canine tips (LC and RC)
- The left and right buccal cusp-tips of the first and second premolars (L1PM, R1PM, L2PM and R2PM) respectively and

- The mesio-buccal and disto-buccal cusp-tips of the left and right first and second molars (LMb1M, LDb1M, RMb1M, RDb1M, LMb2M, LDb2M, RMb2M and RDb2M) respectively.

Universiti Malaya

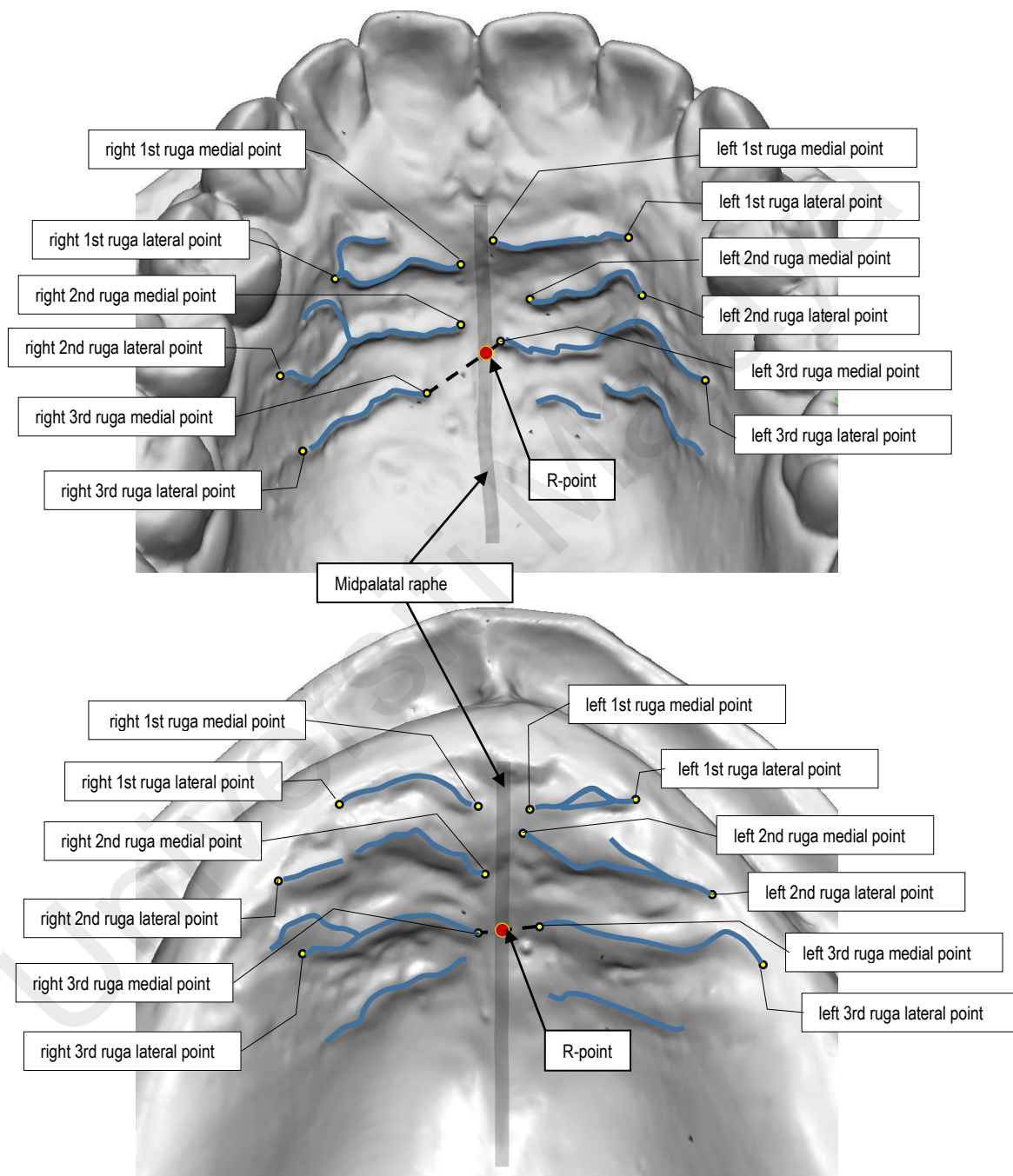


**Figure 3.7: Tracing the rugae lines and assigning R-point on dentate (above) and edentulous (below) digital casts**

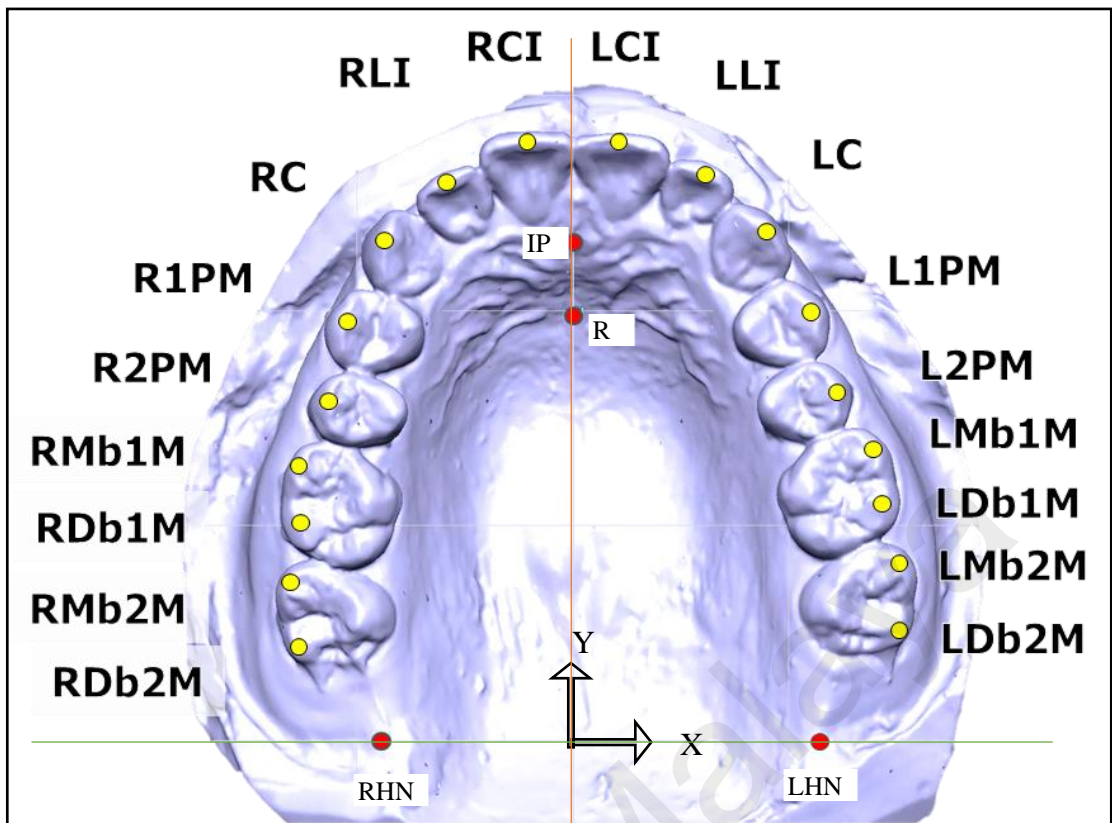


**Figure 3.8: Digital cast and the landmarks registration in 3D analyser software. Hamular notches (LHN & RHN) and the incisive papilla (IP) were used to align the casts to Cartesian coordinate system; 22 selected points were illustrated in the diagram**

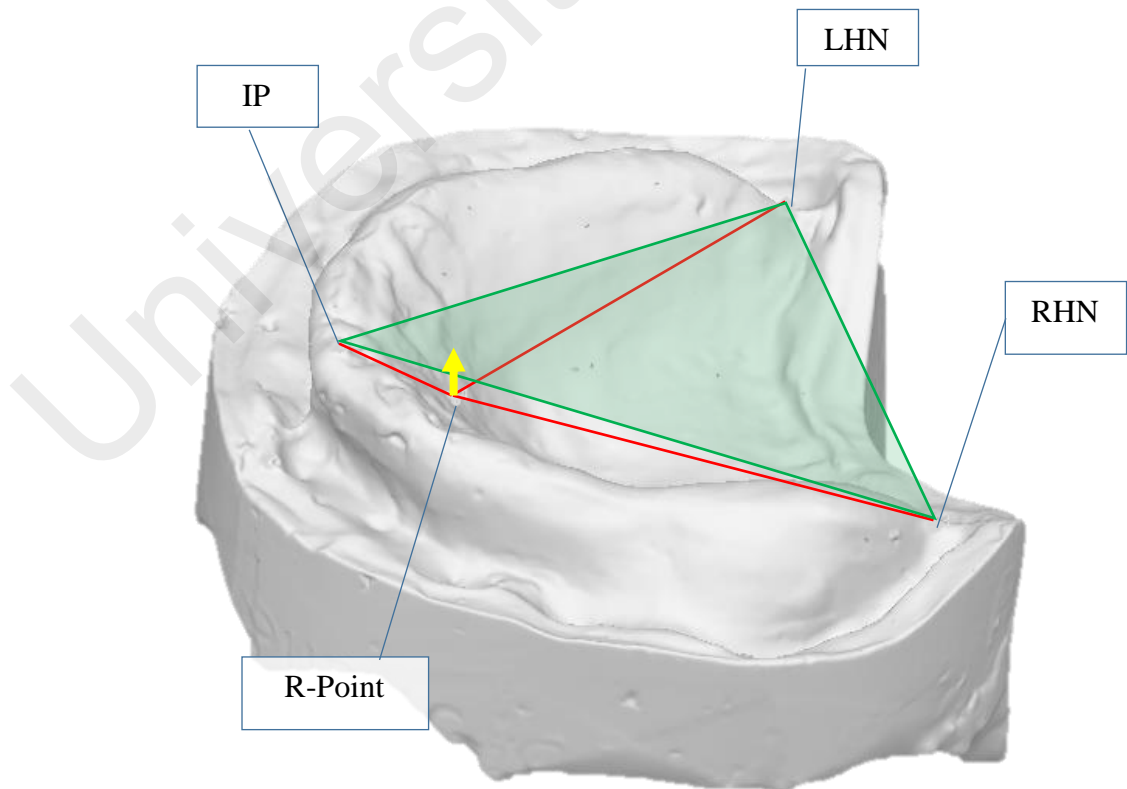


**Figure 3.9: Triangular biometric pyramid illustrated on edentulous digital cast showing the essential lines used as predictors extending between the the four selected landmarks**

### 3.4.6.2 Aligning the digital casts to Cartesian XY plane (Phase I)

In this phase, the hamular-incisive papilla plane of all the digital casts in the study were aligned on the Cartesian XY plane. This can be done by having the  $z$  coordinate of the three landmarks of IP, LHN and RHN as zero. A two-dimensional (2D) plane surface was created and introduced to the 3D Cartesian setting with the digital cast in VAM software to serve as a reference surface on the XY plane. The 2D surface was made by importing a 2D image from the main menu under “File” drop-down menu → option “Open Image as a Flat Surface” was selected and the “surface plane” as “XY” was chosen in the details to open the image in superimposition with the XY Cartesian plane. From “view” drop-down menu → “Axis Grid” category → “Show Axis Grids” should be selected to show the 3D Cartesian grid. The XY plane-image was then cropped to a smaller circle-shape plane for convenience by choosing “Area” from main menu panel → “Tools” → “Paint Area Selection” and “Large Brush (128 pixels)” options then with one click the centre area of the Cartesian axis grids was painted (Figure 3.10). Using “Area” → “Select” drop-down menu → “Inverse” tool, the undesired area of the image was selected and deleted by “Area” → “Delete Selected Area” option. The circular plane was then saved as Wavefront OBJ (obj) attribute computer file with the name of XY plane for further use (Figure 3.10). The landmarks of IP, LHN and RHN were selected on the digital cast using the “Landmarks” from main menu → “Tools” → “Select Landmarks” option then click on the landmark by mouse while holding “shift key” and then by using “Landmarks” from main menu → “Project Selected Landmarks” option, three new points corresponding to the selected landmarks were created (projected) on the XY plane. The new points carried the same  $x$  and  $y$  coordinates of the original points from the cast but

their  $z$  coordinate was zero. The projected landmarks on the XY plane and the original points on the cast; IP, LHN and RHN were selected and main menu option “Surface” → “Register Surfaces...” tool was opened. In the settings options of “Register Surfaces...” tool, the digital cast was selected in “Move this surface” pane, the XY plane was selected in “to fit this surface” pane and from “Calculate alignment using:” list, the option “landmarks with corresponding names” was selected. The researcher ensured that no other landmarks were present in the XY plane than the three corresponding to IP, LHN and RHN to avoid wrong alignment order. By using the above-mentioned procedure, all the dentate and edentulous digital casts in this study were aligned in a standard position where the landmarks of IP, LHN and RHN were on the XY plane having their  $z = 0$  (i.e.  $(x, y, 0)$ ). In other words, the HNIP planes of all the casts were standardised to superimpose the XY plane (Figures 3.12 - 3.15).

The Cartesian coordinates  $(x, y, z)$  for all the points and landmarks were projected and copied using “Display coordinates” command. Coordinates were transferred to the Excel sheet as set of three numbers of four decimal places separated by comma for each point, first number was  $x$ , second was  $y$  and third was  $z$  coordinates as shown in Figure 3.15. Comma separated file management of imported data function was used to transfer the data in Excel to allocate a cell for each individual element of the three.

The 22 points’ coordinates were obtained from each cast and transferred into a text document and imported to Excel sheet. Each point had three separated coordinates  $(x, y$  and  $z)$  under its name that was saved in an individual column using data transfer option of “get external data from text

file” in Microsoft Excel application and values were exported as “Comma-separated values” for easy management of any geometrical transformation. The described procedure was applied on the 92 dentate casts; the coordinates were collected, tabled in Excel spread sheets and saved for further 2D /3D standardisation, processing, measurements and analysis. The digital casts were saved in obj file format; the obj files are storing the Cartesian position of the cast in the system for future use. After Phase I, the software has limitation of inability to move individual points by dictating where the point is supposed to be; therefore, it was not possible to perform other transformations in high accuracy in Phase I. In Phase II using Microsoft Excel, further transformations can be made.

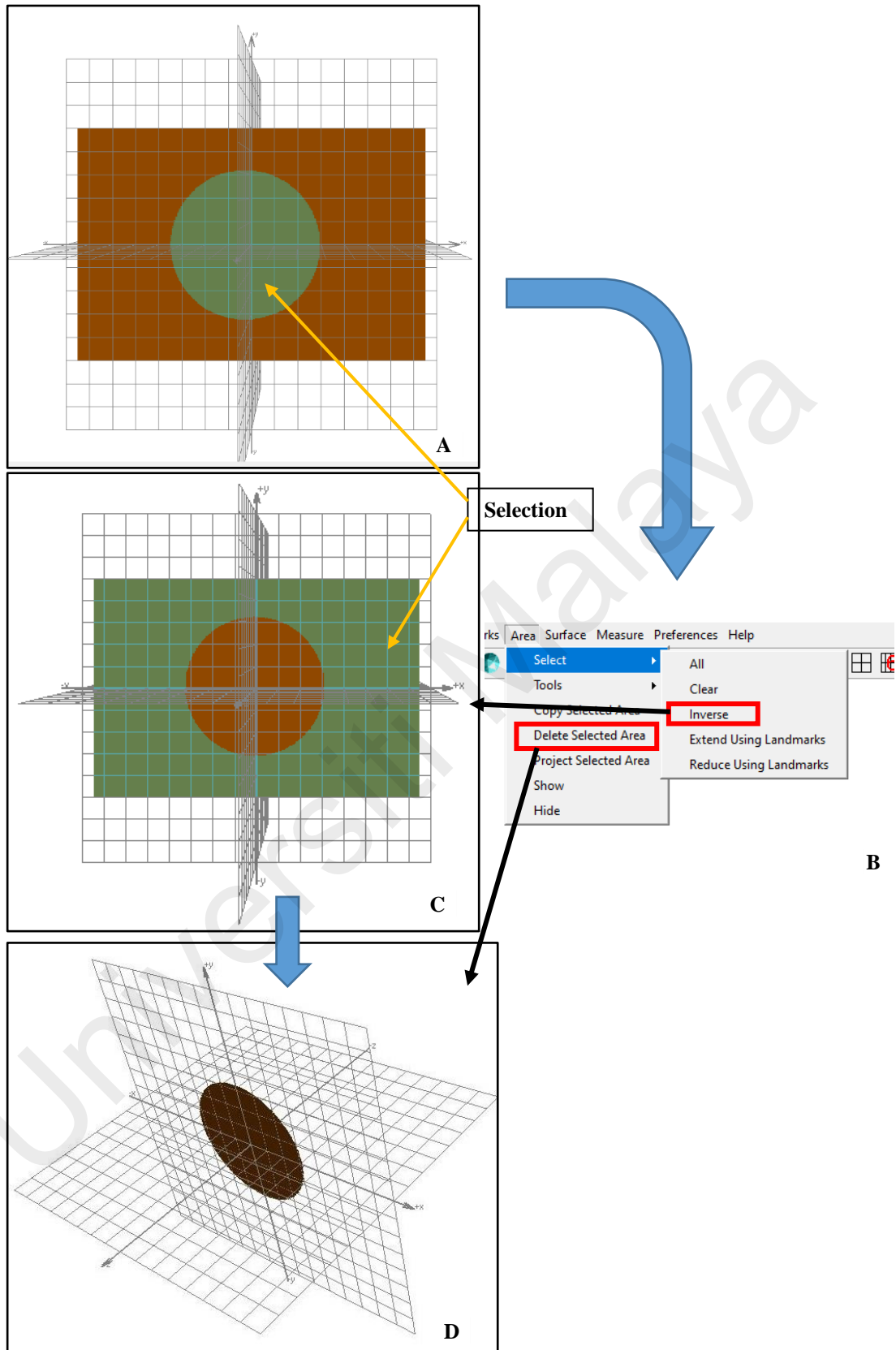


**Figure 3.10: (A) Flat 2D image (brown) opened in the Cartesian system (VAM software) and selection of circle shape (green) was made on the centre of the plane. (B and C) Selection was inverted; (B and D) selected area was deleted**

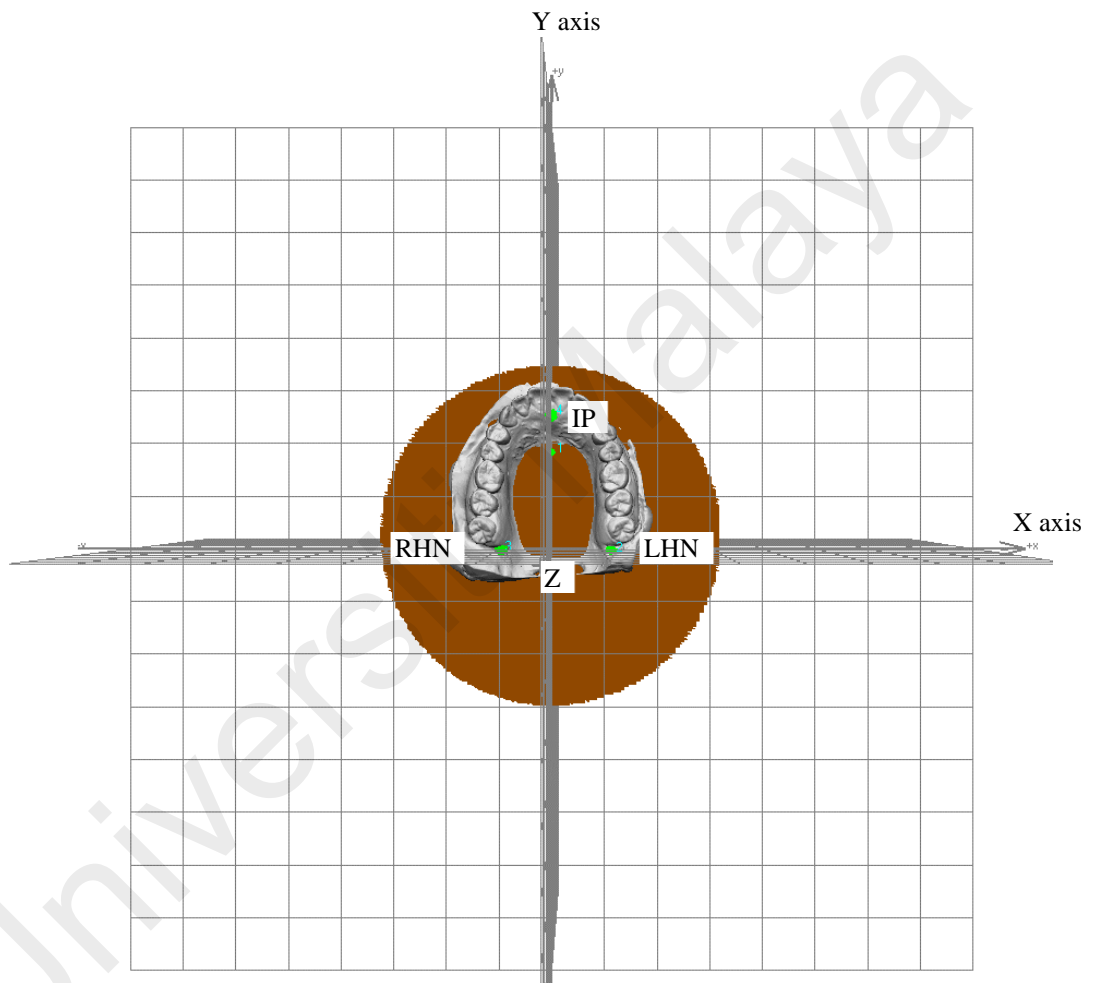


**Figure 3.11: Introducing the digital cast next to the prepared XY plane before Phase I alignment**

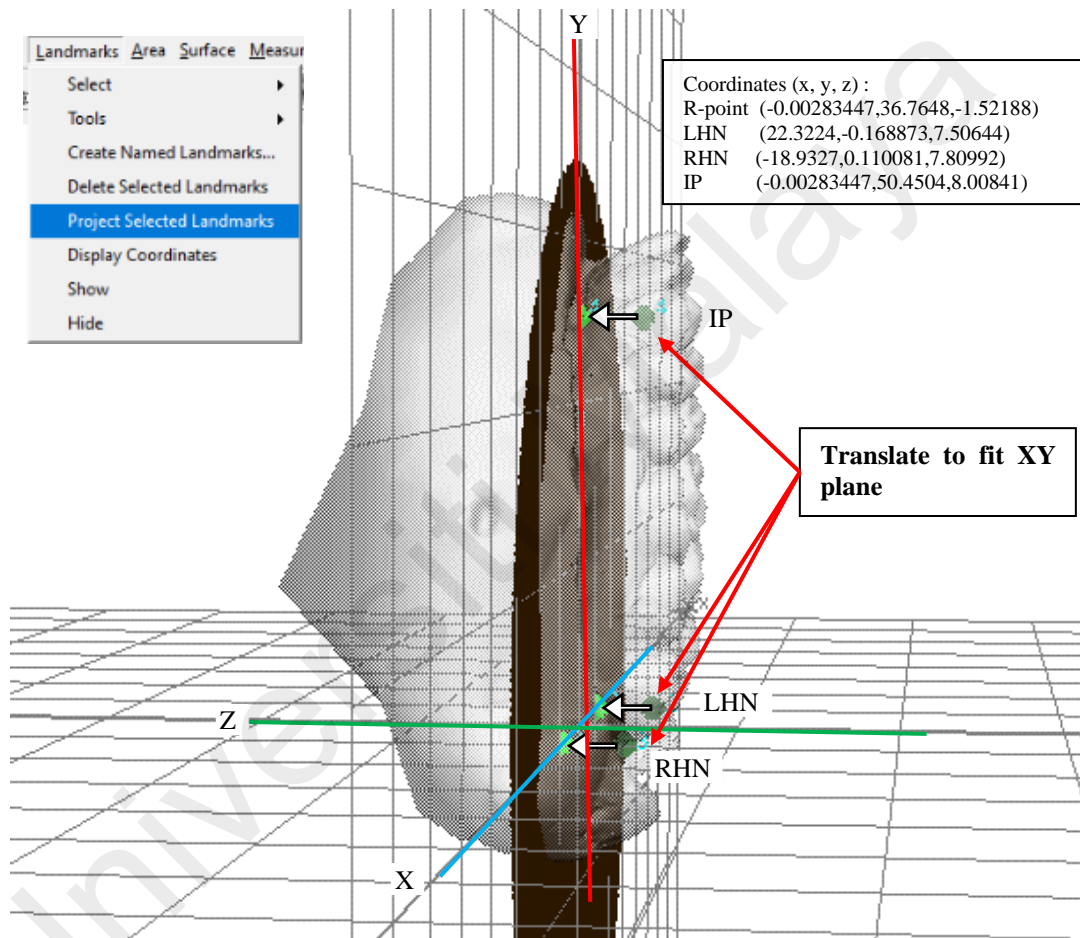


**Figure 3.12: Projecting (cloning) the selected landmarks on the XY plane and reading the landmarks' coordinates before registering surfaces**

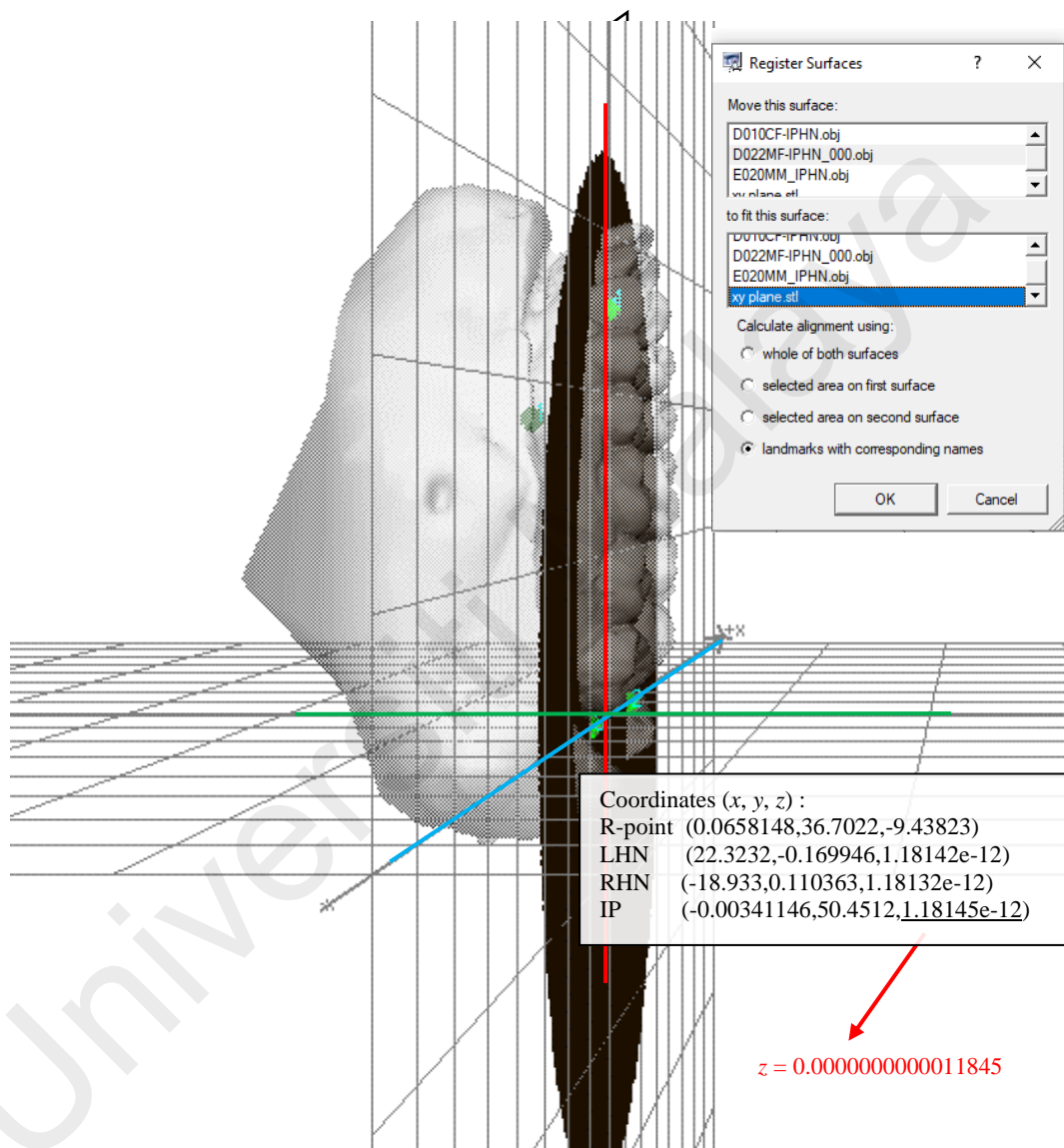


**Figure 3.13: Register and transform the digital cast to superimpose the landmarks to the corresponding one on the plane**

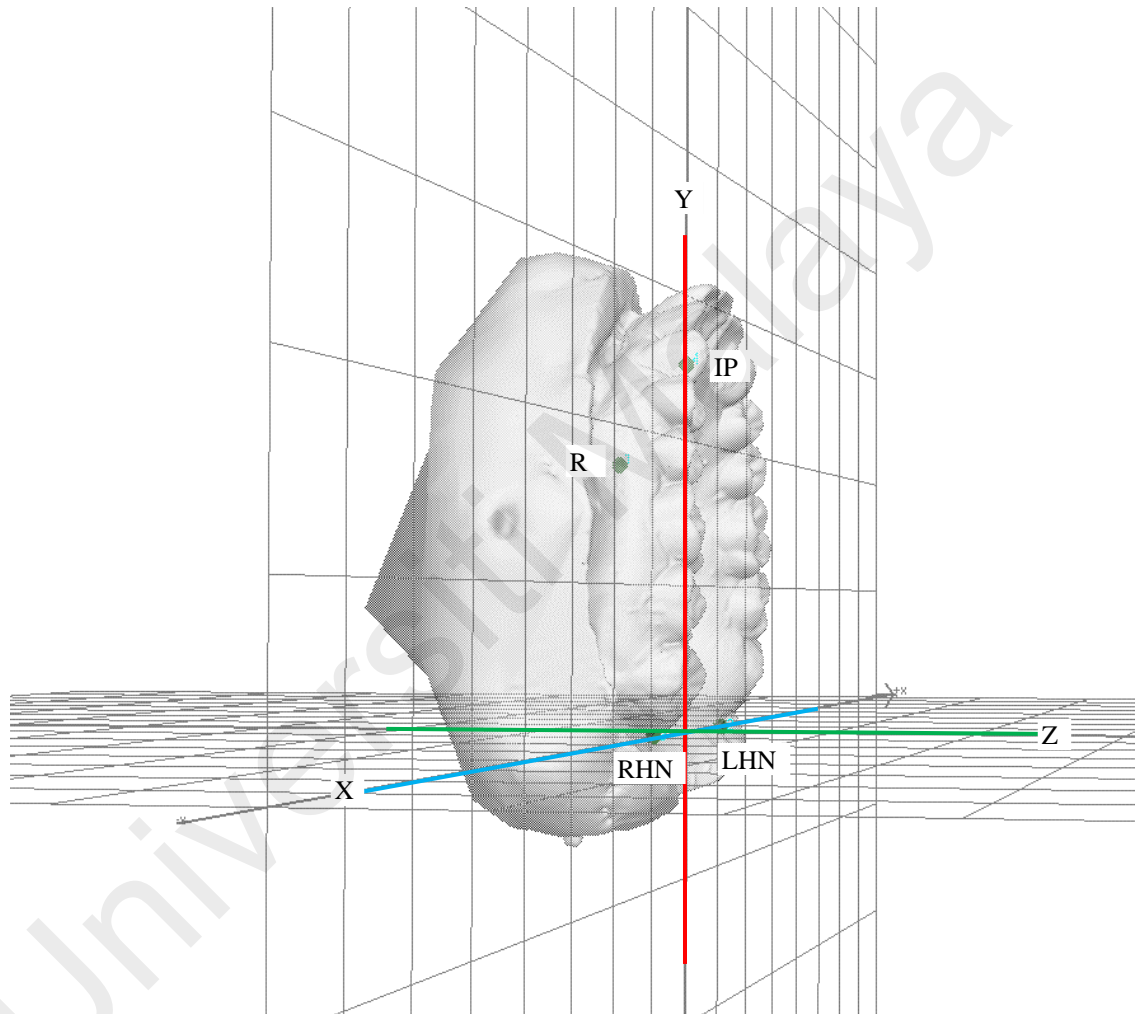


**Figure 3.14: The digital cast aligned in phase II before translation**

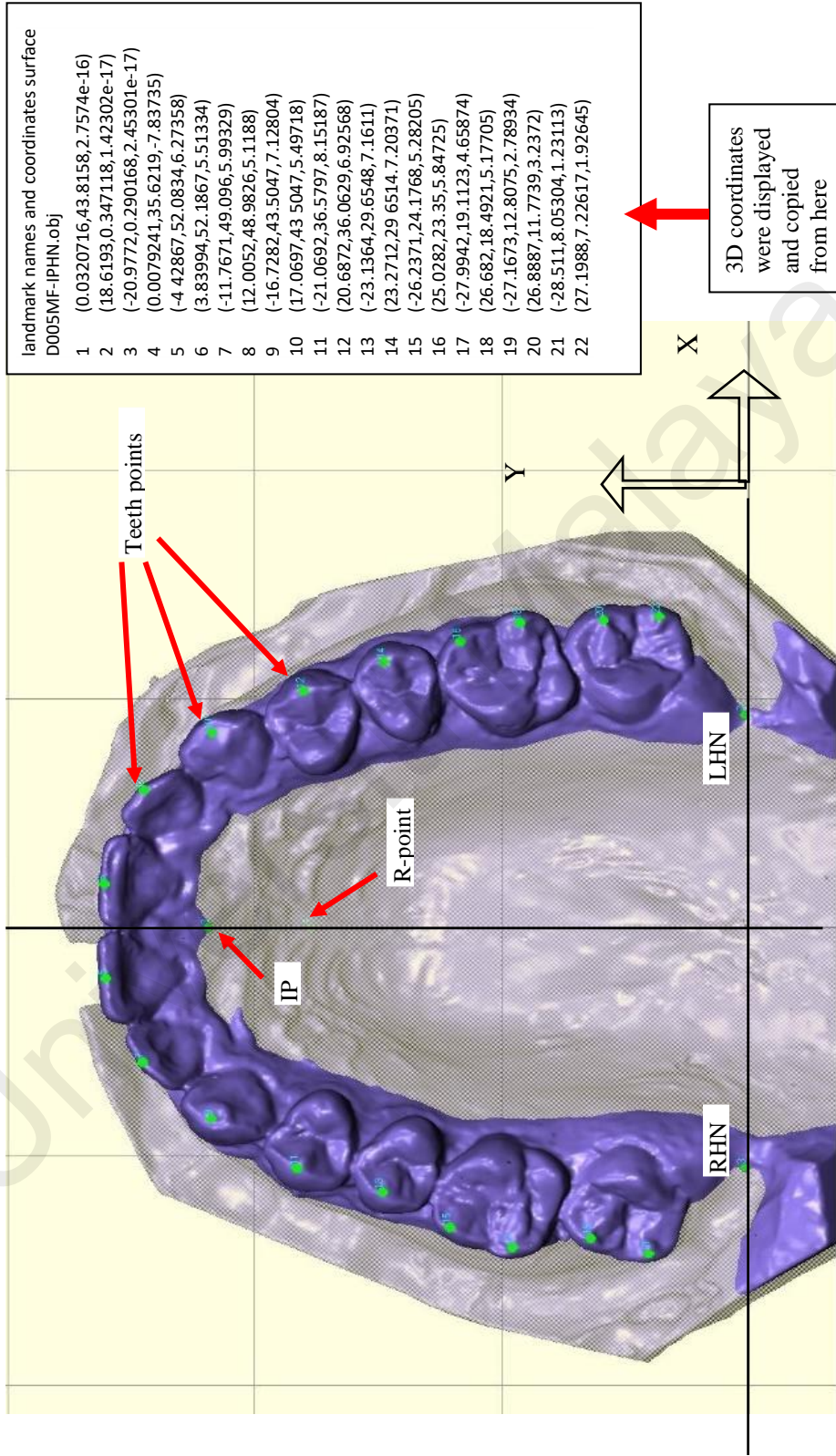


Figure 3.15: Digital cast in phase I processing using VAM software, HNIP plane alignment with XY plane (yellow surface). The 3D coordinates are displayed on the right pane of the screen

### 3.4.6.3 Coordinates' transformation to standardise cast position (Phase II)

After the HNIP plane had been aligned with the XY plane and the  $z$  coordinate of the plane's three landmarks had been uniformed to zero ( $z = 0$ ); the subsequent phase in standardising the cast position involved translating the cast on XY plane to move the RHN to the origin (0, 0, 0), rotate (in 2D) the cast about the origin on the XY plane to get the other hamular notch (LHN) aligned with the X axis (having  $y = 0$ ) simultaneously with the RHN. Finally, the cast was translated on the X axis to get the IP point superimposed on the Y axis ( $x = 0$ ) as shown in Figure 3.15. The following sequential procedures were made using Microsoft Excel application to perform these transformations:

#### (a) *Translating RHN point to the origin (0, 0, 0)*

This translation was made by subtracting the values of the RHN's  $x$  and  $y$  coordinates from the  $x$  and  $y$  coordinates of each of the 22 points of a given cast respectively including the RHN point itself using the following functions:

$$x'_i = x_i - x_{RHN}$$

$$y'_i = y_i - y_{RHN}$$

Where  $i$  is from 1 to 22,  $x'$  and  $y'$  are the new  $x$  and  $y$  coordinates of the points  $x$  and  $y$  respectively after translation and the constant  $x_{RHN}$  and  $y_{RHN}$  are the  $x$  and  $y$  coordinates of the RHN point respectively.

Having the RHN as origin, the RHN became aligned on the X axis by default.

(b) **Rotation to get the LHN aligned to the X axis along with RHN**

Two-dimensional geometrical rotation was made about the origin for the triangle composed of the two hamular notches and the IP landmarks. The coordinates underwent a rotation function on a clock-wise or counter-clock-wise direction based on Pythagorean Theorem, the sine and cosine values related to the angle between the RHN - LHN line and the X axis (Figures 3.16 and 3.17). “SIN” and “COS” functions in Microsoft Excel were used to return the sine and cosine of the above-mentioned angle respectively according to the following equations:

$$x'_i = x_i \cdot \cos \beta - y_i \cdot \sin \beta$$

$$y'_i = x_i \cdot \sin \beta + y_i \cdot \cos \beta$$

Where  $I = 1$  to 22,  $x'$  and  $y'$  are the new coordinates of  $i$  point after rotation and  $\beta$  is the angle desired for rotation. A negative (-ve) value if  $y$  coordinate of LHN ( $y_{LHN}$ ) was in; a counter-clock-wise direction rotation is needed using the sine value of angle ( $\beta$ ) in (+ve). However, if  $y_{LHN}$  was in (+ve) value, a clock-wise direction rotation is needed,  $\beta$  and sine values should be used in (-ve) in Excel functions (Figures 3.16 and 3.17).

The straight distance between LHN and RHN was calculated using the Euclidean equation of straight distance between two points to compute the sine and cosine values:

Straight distance between (A) LHN ( $x_1, y_1, z_1$ ) and (B) RHN ( $x_2, y_2, z_2$ )

$$AB = \sqrt{(x_2 - x_1)^2 + (y_2 - y_1)^2 + (z_2 - z_1)^2}$$

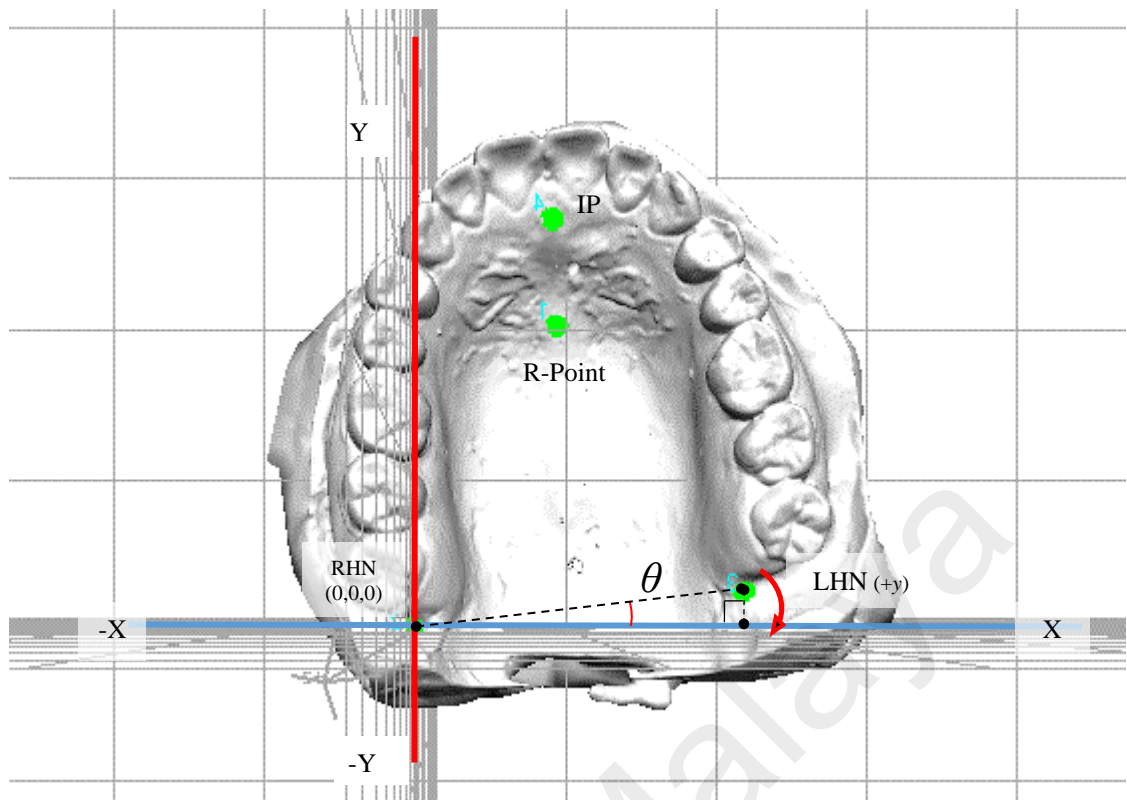


**Figure 3.16: The clockwise rotation of the dental cast to get the RHN and LHN aligned to X-axis**

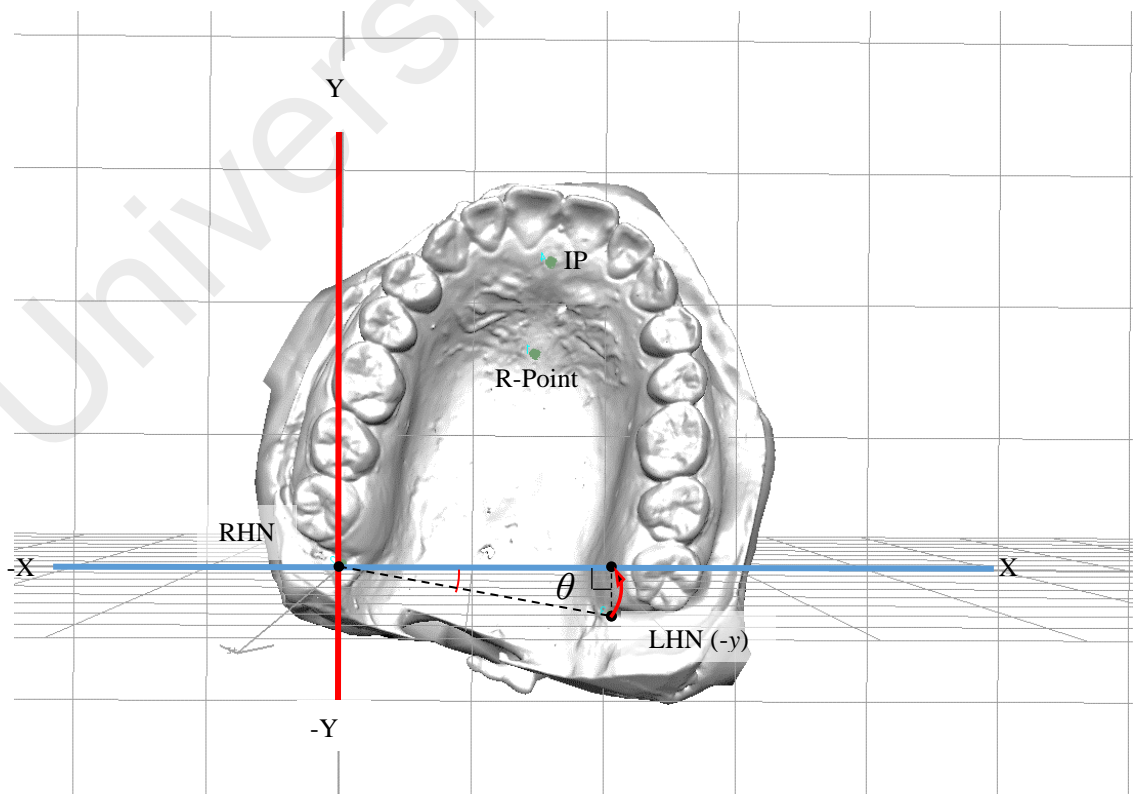


**Figure 3.17: The counterclockwise rotation of the dental cast to align RHN and LHN to X-axis**

Next, a second translation was made to the digital cast by subtracting the value of  $x_{IP}$  coordinate from all the  $x$  coordinates of the points and landmarks of the cast including  $x_{IP}$  itself to translate the cast on the XY plane and get IP point aligned with the Y axis ( $x_{IP} = 0$ ) while maintaining the  $z$  coordinates of IP, RHN and LHN as ( $z = 0$ ). Positioning the digital cast in the above-stated setting made the origin point (0, 0, 0) at the intersection between the line passing on Y axis through the IP and the line passing on X axis through both RHN and LHN simultaneously (Figure 3.18).

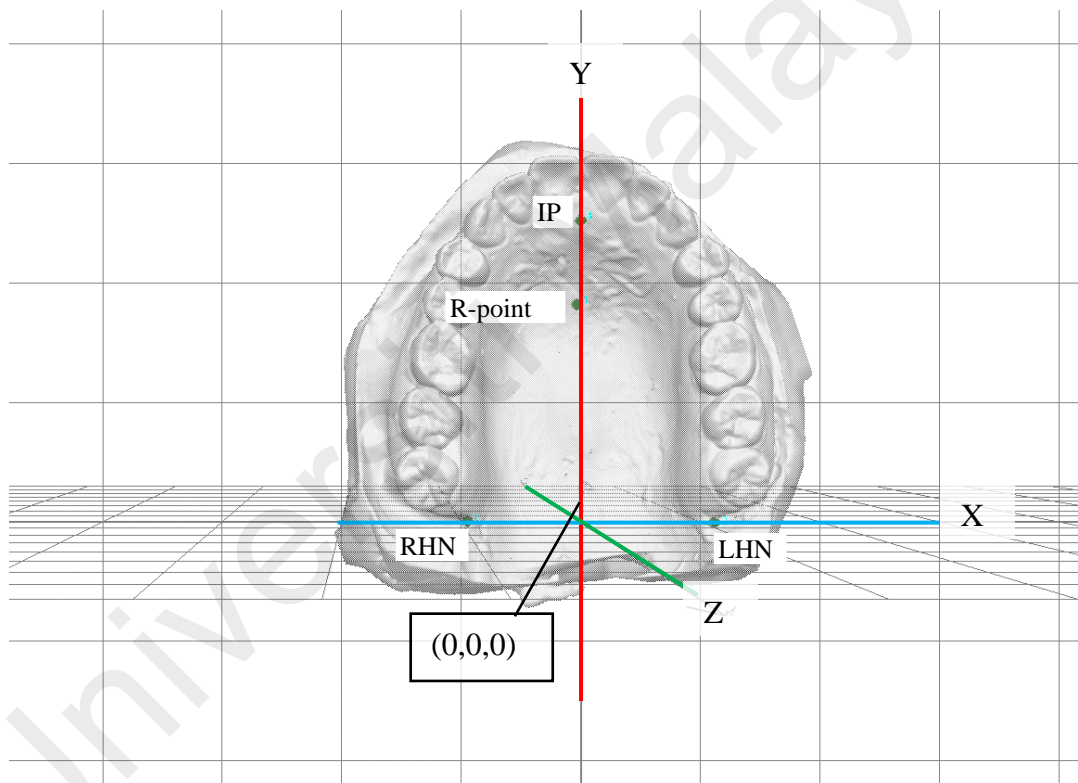


**Figure 3.18: The digital cast is aligned according to phase II processing**

(c) *Translation to make R-point as the origin*

A third sequential translation was performed to make R-point as the origin R (0, 0, 0) of the 3D Cartesian coordinates system (Figure 3.19). This translation was the final in the serial translations includes moving all coordinates to make R-point coordinates to (0, 0, 0). The translation was made by subtracting the values of R-point coordinates ( $x_{R-point}, y_{R-point}, z_{R-point}$ )

from the corresponding coordinates  $(x, y, z)$  of all the 22 points including R-point respectively in Excel sheet according to the following equations:

$$x'_i = x_i - x_{R\text{-point}}$$

$$y'_i = y_i - y_{R\text{-point}}$$

$$z'_i = z_i - z_{R\text{-point}}$$

where  $i$  is 1-22,  $x'$ ,  $y'$  and  $z'$  are the new coordinates of the points in the digital cast when R-point is on the origin and  $x$ ,  $y$  and  $z$  are the digital cast coordinates of points before translation.

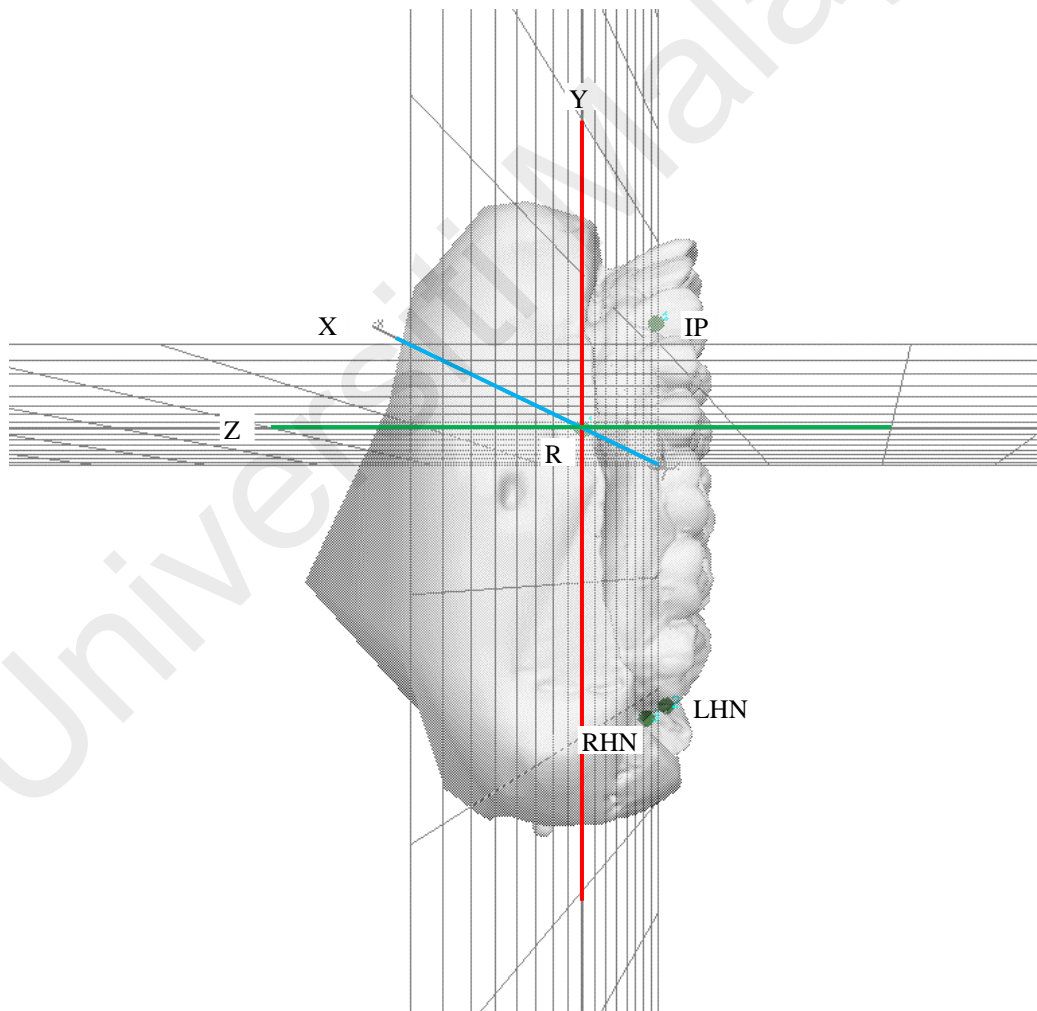


**Figure 3.19: Final translation of the digital cast on Y and Z axes to have R-point as the Cartesian origin**

The above-mentioned steps of transformations (3 translations and 1 rotation) made all the coordinates of interest in the cast have positive value of z coordinates as the origin R-point has become the deepest point in the measured palatal structures (Figures 3.20 and 3.21). These procedures were applied on all the 92 digital dentate casts and similar transformations were made for the 34 edentulous digital casts considering the difference of skipping the 18 points coordinates related to the teeth. All the coordinates were tabulated and saved in Excel sheets for further processing, measurements and analysis (Figures 3.22 and 3.23).

Universiti Malaysia

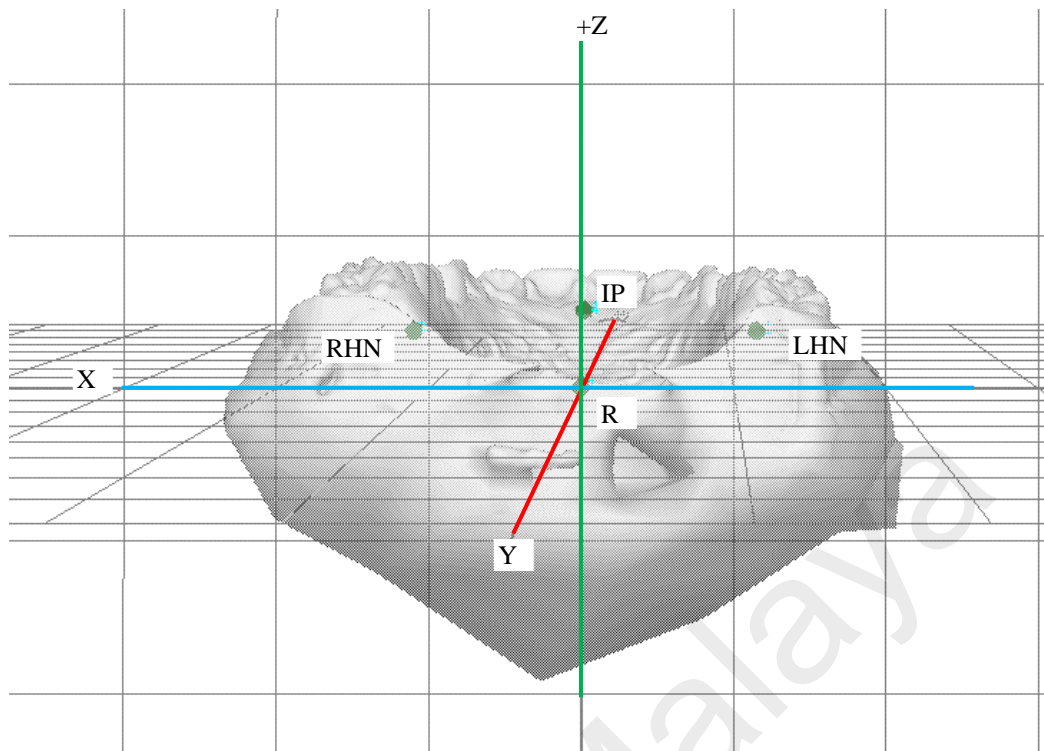


**Figure 3.20: When R-point is origin, all the other landmarks will have positive z coordinates**

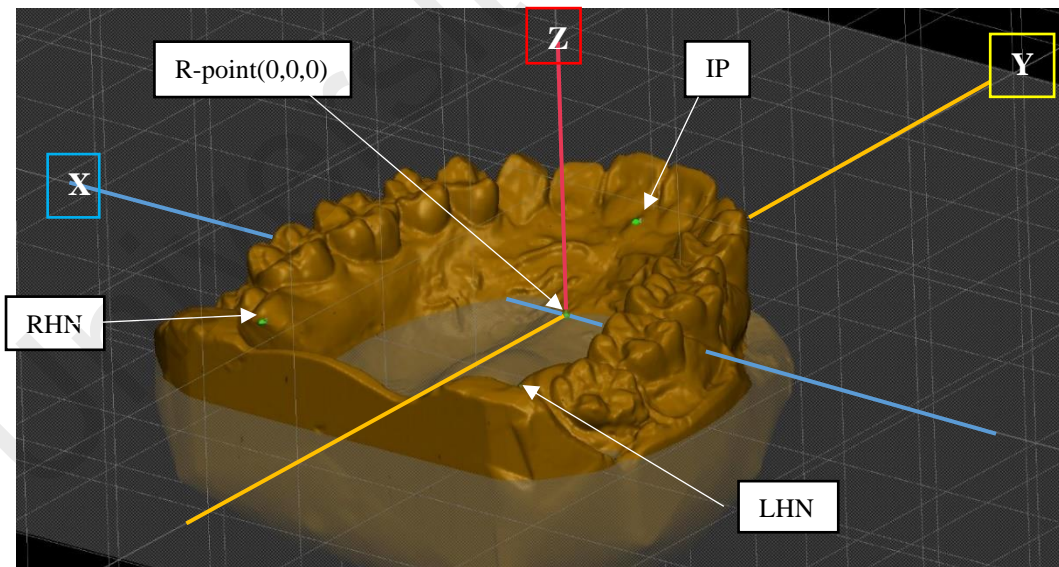


**Figure 3.21: Final standardised position for digital cast where R-point become the origin (0, 0, 0) and HNIP plane is parallel to XY plane**

the application	X	Y	Z	NAME	POINT	X	Y	Z	TRANSLATION 3 TO (0,0,0)	DISTANCE	sin rad	cos	radian	degree	clockwise(+) anticlockwise(-)	Y'	Z'	X'=x cosθ - y sinθ	Y'=x sinθ + y cosθ	distance after rotation	finally translation to make 1(0,0)	X	Y	Z
1 D001MM	1	-0.019	44.496	0.000	IP	1	23.056	43.965	0.000	1 TO 2	48.118	0.002147	0.9999977	0.002147	22.961	44.014	0.000	1	48.118	IP	1'	0.000	44.014	0.000
	2	19.331	0.440	0.000	LHN	2	42.406	-0.091	0.000	1 TO 3	49.644	0.002147	0.9999977	0.002147	42.406	0.000	0.000	2	49.644	LHN	2'	19.445	0.000	0.000
	3	-23.075	0.531	0.000	RHN	3	0.000	0.000	0.000	2 TO 3	42.406				0.000	0.000	0.000	3	42.406	RHN	3'	-22.961	0.000	0.000
	4	-0.034	31.238	-9.215	3RP	4	23.041	30.707	-9.215						22.975	30.757	-9.215	4		3RP	4'	0.013	30.757	-9.215
	5	3.475	56.952	6.617	LCI	5	26.550	56.421	6.617						26.429	56.478	6.617	5		LCI	5'	3.468	56.478	6.617
	6	11.532	52.229	6.538	LLI	6	34.607	51.698	6.538						34.496	51.772	6.538	6		LLI	6'	11.535	51.772	6.538
	7	18.108	46.024	7.060	LC	7	41.183	45.493	7.060						41.085	45.581	7.060	7		LC	7'	18.123	45.581	7.060
	8	22.460	37.596	8.222	LIPM	8	45.535	37.065	8.222						45.456	37.163	8.222	8		LIPM	8'	22.494	37.163	8.222
	9	24.776	30.095	8.498	L2PM	9	47.851	29.564	8.498						47.787	29.667	8.498	9		L2PM	9'	24.826	29.667	8.498
	10	26.813	23.520	7.280	UMB1M	10	49.888	22.989	7.280						49.838	23.096	7.280	10		UMB1M	10'	26.877	23.096	7.280
	11	26.628	17.778	7.321	LDB1M	11	49.703	17.247	7.321						49.666	17.354	7.321	11		LDB1M	11'	26.704	17.354	7.321
	12	28.880	12.576	5.712	UMB2M	12	51.955	12.045	5.712						51.929	12.156	5.712	12		UMB2M	12'	28.967	12.156	5.712
	13	29.216	7.444	4.984	LDB2M	13	52.291	6.913	4.984						52.276	7.026	4.984	13		LDB2M	13'	29.315	7.026	4.984
	14	-4.955	56.232	6.338	RCI	14	18.140	55.701	6.338						18.020	55.740	6.338	14		RCI	14'	-4.941	55.740	6.338
	15	-12.926	51.185	6.780	RLI	15	10.149	50.654	6.780						10.040	50.676	6.780	15		RLI	15'	-12.922	50.676	6.780
	16	-18.478	44.708	7.173	RC	16	4.597	44.177	7.173						4.502	44.187	7.173	16		RC	16'	-18.459	44.187	7.173
	17	-22.516	37.054	7.600	R1P	17	0.559	36.523	7.600						0.481	36.524	7.600	17		R1P	17'	-22.481	36.524	7.600
	18	-26.217	29.567	7.860	R2P	18	-3.142	29.036	7.860						-3.204	29.029	7.860	18		R2P	18'	-26.166	29.029	7.860
	19	-27.394	23.679	7.148	RMB1M	19	-4.320	23.148	7.148						-4.369	23.139	7.148	19		RMB1M	19'	-27.331	23.139	7.148
	20	-28.151	18.043	6.770	RDB1M	20	-5.077	17.512	6.770						-5.114	17.501	6.770	20		RDB1M	20'	-28.075	17.501	6.770
	21	-30.507	13.501	4.992	RMB2M	21	-7.432	12.970	4.992						-7.460	12.954	4.992	21		RMB2M	21'	-30.421	12.954	4.992
	22	-31.096	7.613	4.215	RDB2M	22	-8.021	7.082	4.215						-8.036	7.064	4.215	22		RDB2M	22'	-30.997	7.064	4.215

Landmark's name

The coordinates x, y, z

(-ve) y coordinate of LHN requires counter clockwise rotation of object

Figure 3.22: Screenshot for the Excel sheet sample used for coordinate transformation (rotation) in phase II

	A	B	C	D	G	L
1						
2	the application					
3						
4	1 D001MM					
5		1 IP				48.118
6		2 LHN				49.644
7		3 RHN				42.406
8		4 SRP				
9		5 LCI				
10		6 LLI				
11		7 LC				
12		8 L1PM				
13		9 L2PM				
14		10 LMB1M				
15		11 LDB1M				
16		12 LMB2M				
17		13 LDB2M				
18		14 RCI				
19		15 RLI				
20		16 RC				
21		17 R1PM				
22		18 R2PM				
23		19 RMB1M				
24		20 RDB1M				
25		21 RMB2M				
26		22 RDB2M				
27						
28						
29	2 D002MF					
30		1				46.455
31		2				46.562
32		3				42.966
33		4				
34		5				

	A	B	C	D	G	L
1						
2						
3						
4						
5						
6						
7						
8						
9						
10						
11						
12						
13						
14						
15						
16						
17						
18						
19						
20						
21						
22						
23						
24						
25						
26						
27						
28						
29						
30						
31						
32						
33						
34						

The landmarks (points)

The coordinates rotated x, y, z

translation to make R as origin

translation to make R as origin

Figure 3.23: Screenshot for sample Excel sheet showing final coordinate translation to standardise R-point as the origin

#### **3.4.6.4 Integrity of digital measurements (error of the measurements)**

To confirm the accuracy and reproducibility of digital 3D measurements on digital casts, compared to the traditional direct digital calliper measurements, the intercanine distance was measured twice in 41 randomly selected dental stone casts by digital calliper (Series 500 calliper, Mitutoyo, Kawasaki, Japan). The same distance (the straight distance between the left and right canine tips) was then measured digitally on the digital 3D image of each of the casts by the 3D analysis software using the coordinates twice and average was considered for each cast on the two methods.

Paired *t*-test was conducted to test the hypothesis of existence of significant difference between the two measurements within the confidence level of 95%. The null hypothesis for the test was set to assume that the mean difference between the two measurements is not equal to zero.

### **3.5 First objective: Three-dimensional tooth position in relation to landmarks**

#### **3.5.1 The sample of the first objective**

The subjects of this objective are the 92 digital dental casts that were collected, digitised and standardised as described in section 3.1. The sample was divided into two subgroups; study group and verification group as described in 3.1.1.1. The study group ( $n = 70$ ) was used to find the relationship between the positions of teeth and selected intraoral landmarks. To test the predictability of the mathematical models generated by the study group, the models were used to predict coordinates for the teeth position for independent

individuals in the verification subgroup ( $n = 22$ ) by fitting independent measurements in the models to obtain the coordinates. Statistical tests were then used to compare and measure the difference between the predicted coordinates and the existing teeth coordinates in the verification sample.

Pearson correlation, simple and multiple regression analyses were used for finding the relationships in this objective. Certain requirements and assumptions had to be checked and fulfilled before statistical procedures started. Details regarding the requirements, assumptions and procedures for the proper statistical analysis pertaining to Pearson correlation were explained earlier in chapter 2, in 2.10.1.

### 3.5.2 Study flow chart (first objective)

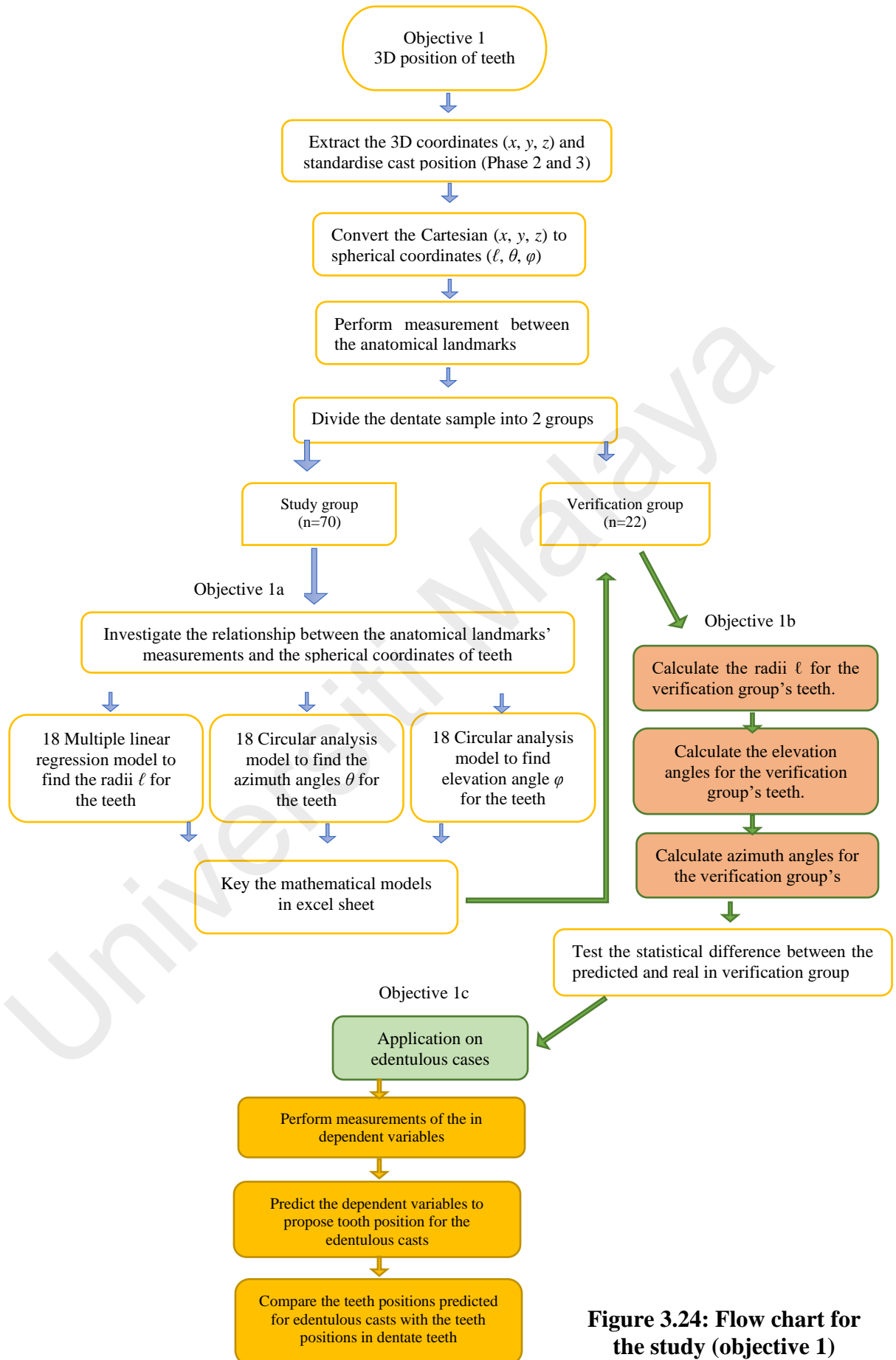


**Figure 3.24: Flow chart for the study (objective 1)**

### 3.5.3 Converting the Cartesian coordinates to spherical coordinate system

In order to describe the position of teeth from the origin and analyse the relationship between the positions and other predictors, 3D coordinate system ( $x, y, z$ ) may be used to describe the tooth location from the origin. The Cartesian coordinate elements such as  $x, y$  or  $z$  coordinates cannot individually express the position of a point in space as  $x$  alone cannot give meaningful value for the position of the tooth in relevance to a point specially when the reference point is standardised in position with value of 0 in  $x, y$  or  $z$  coordinate in all the sample.

The flow chart for the first objective (Figure 3.24) was followed to investigate the relationship between the tooth position and the anatomical landmark measurements; the points representing the tooth positions should be converted to the spherical coordinate system, as it is impossible to run statistical analysis using the Cartesian coordinates. For instance, if the central incisor was located on a point (3, 26, 16) away from the origin (0, 0, 0); 3 does not represent a meaningful value such as distance that can be used to find the average and standard deviation to then investigate the relationship between other variables to predict it for the other sample. Therefore, the traditional 3D Cartesian coordinates should be converted into other coordinates form, namely spherical coordinates ( $\ell, \theta, \varphi$ ) to describe the location of a point from origin as distance and two angles (Stewart et al., 2016). The standardisation (alignment) of the landmark coordinates would ease calculation of the distances between the points and comparison between the subjects. However, having uniform  $z$  coordinates for IP, LHN and RHN, uniform  $y$  coordinates for LHN and RHN

and  $x = 0$  IP in all the casts would make it impossible to find the relationships between the landmarks and predict the teeth coordinates. Therefore, spherical coordinate system was considered instead of the Cartesian coordinate system to find the relationships. The spherical coordinate system is composed of  $(\ell, \theta, \varphi)$ : a line (distance) and two angles (azimuth and elevation) rather than  $(x, y, z)$ . Mathematically, the two systems are interchangeable and they are only two ways of describing the point position in 3D space. However, using the spherical coordinate system would allow application of regression analysis and finding the relationship between the variables tested due to the proportional values of distance from the origin  $\ell$  and angles that represent the elevation and azimuth in relevance to specific planes  $\theta, \varphi$  respectively.

For instance, the point of left central incisor tooth in Cartesian coordinates (3, 26, 16) is represented as (30, 82, 31) in the spherical coordinate system and would be more meaningful for descriptive statistics and statistical analyses where (30) represents the magnitude of the vector (the straight distance) between the tooth and the origin without direction, (82) represents the angle of the tooth vector in degrees directed in anti-clockwise direction starting from right x axis as 0 degrees when the arch is viewed from occlusal view (Figure 3.25) and (31) represents the elevation angle of the tooth vector in degrees started from the horizon as 0 degrees (Figure 3.26).

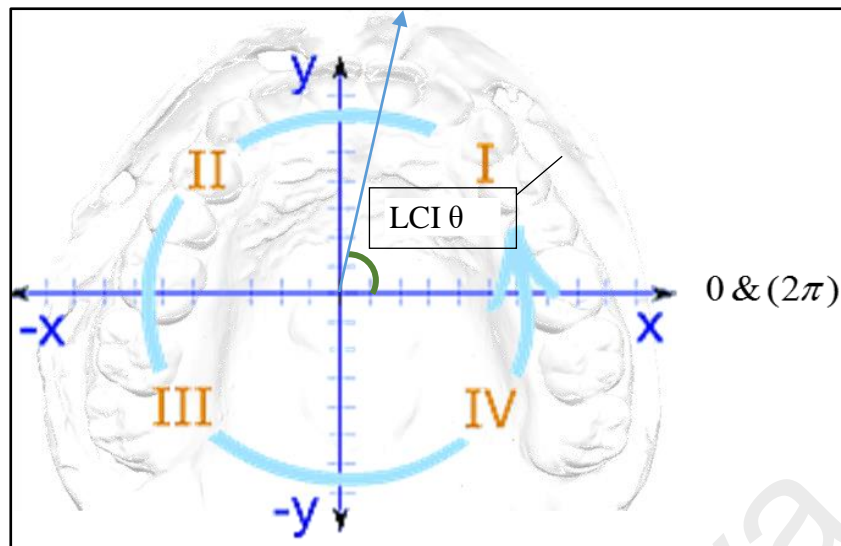


**Figure 3.25: Diagram showing the direction of measuring the azimuth angle ( $\theta$ ) of spherical coordinates of the teeth in dental arch. Example of right canine is given**

Running statistical tests and analysis between the spherical coordinates is possible and logical but should be carefully managed. The two angles ( $\theta$  and  $\phi$ ) are circular variables; treating the angles as linear variables in statistics may not be appropriate.

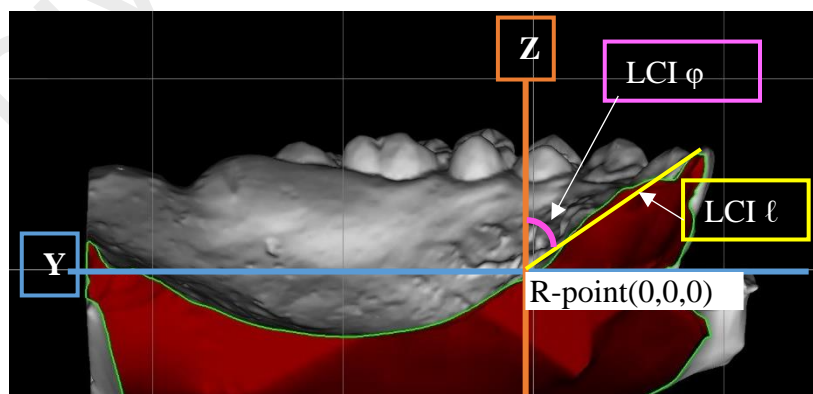


**Figure 3.26: Diagram showing the spherical coordinates for right central incisor tooth (RCI): radius ( $\ell$ ) in yellow and elevation angle in pink ( $\phi$ )**

### 3.5.4 Linear radial distance of the tooth ( $\ell$ )

Twenty-two straight distances measurements (in millimetres) were obtained (Figure 3.27):

1. Centre of the incisive papilla (IP) and R-point (IP-R)
2. Left hamular notch (LHN) and R-point (LHN-R)
3. Right hamular notch and R-point (RHN-R)
4. Height of the hamular incisive papilla plane from R-point (HNIP-height)
5. Left central, lateral incisors and canine and R-point (LCI-R, LLI-R, LC-R) respectively.
6. Left first and second premolars and R-point (L1PM-R & L2PM-R)
7. Mesio Buccal and distobuccal cusp tips of left first and second molars and R (LMb1M-R, LDb1M-R, LMb2M-R, LDb2M-R) respectively.
8. Right central, lateral incisors and canine and R-point (RCI-R, Right central RLI-R, RC-R) respectively.
9. Buccal cusp tips of the right first and second premolars and R-point (R1PM-R & R2PM-R) respectively.
10. Mesio Buccal and distobuccal cusp tips of right first and second molars and R-point (RMb1M-R, RDb1M-R, RMb2M-R, RDb2M-R) respectively.

The measurements were calculated mathematically in Microsoft Excel by applying the Euclidean straight distance equation between two points A ( $x_1, y_1, z_1$ ) and B ( $x_2, y_2, z_2$ ) in 3D as shown in the following:

$$AB = \sqrt{(x_2 - x_1)^2 + (y_2 - y_1)^2 + (z_2 - z_1)^2}$$

The first coordinate (radial distance) in the spherical system was then calculated using the following equation:  $\ell = \sqrt{x^2 + y^2 + z^2}$

Collectively, the lines measured between the selected anatomical landmarks on the maxillary digital cast are forming a triangular pyramid structure that has the HNIP as base and R-point as the peak (Figures 3.28 and 3.29 ).

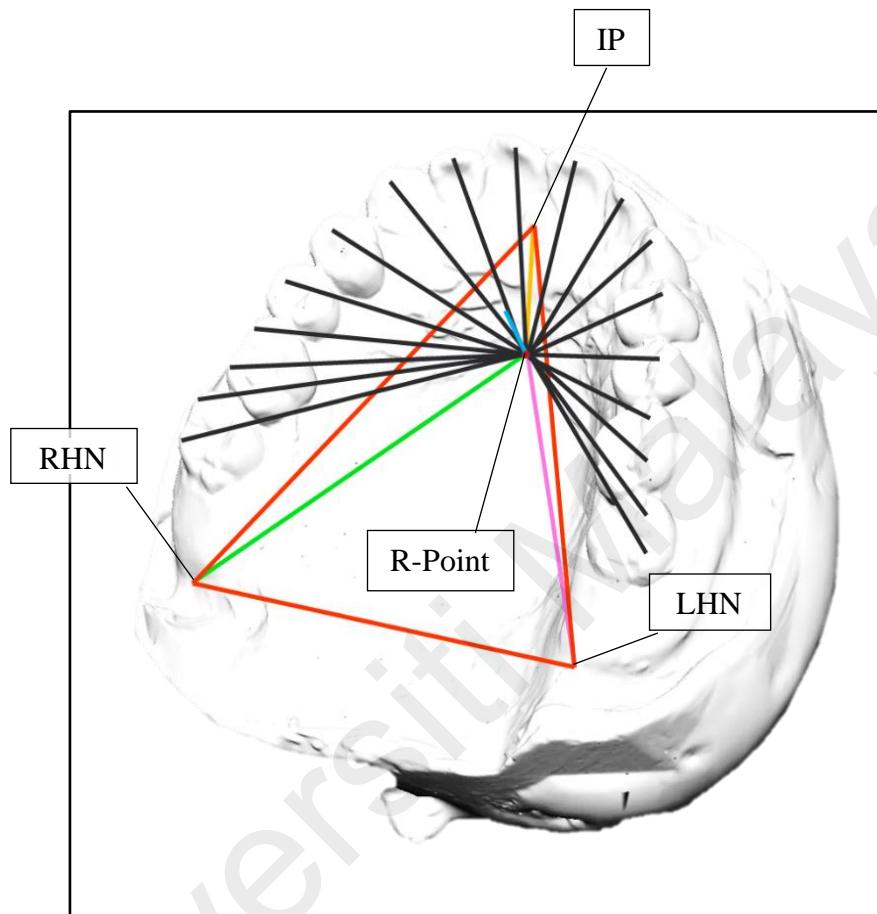


**Figure 3.27: Linear measurements obtained for first objective: (red) is HNIP plane and distances between RHN, LHN and IP, (black) radial distances of teeth from R-point, (yellow) distance between IP and R-point, (pink) distance between LHN and R-point, (green) distance between RHN and R-point and, (blue) depth of R-point from HNIP plane**

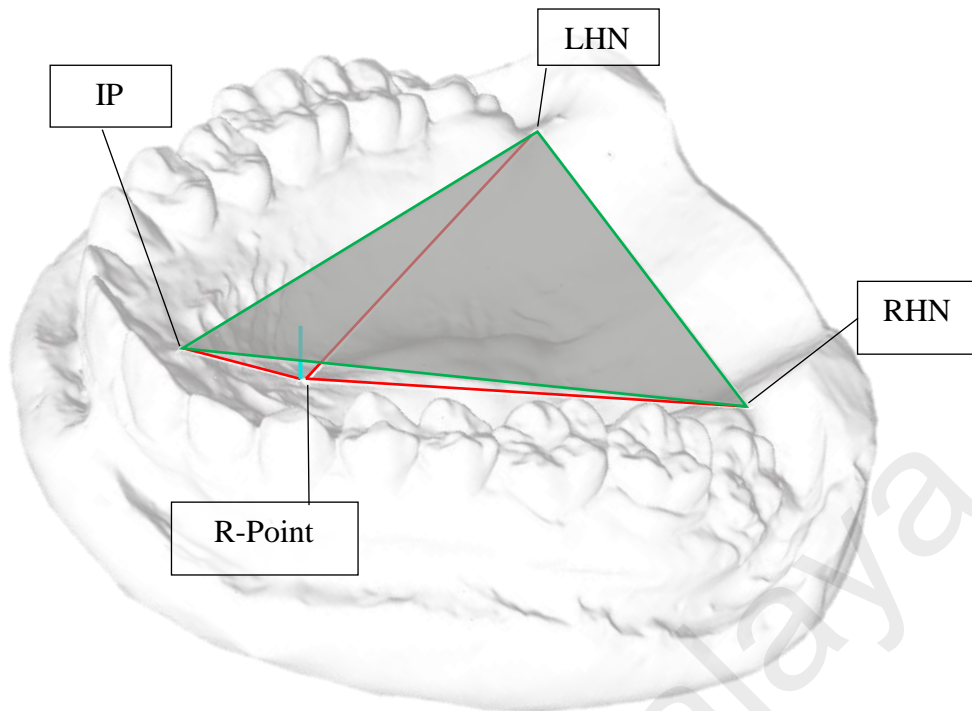


**Figure 3.28: Biometric triangular pyramid illustrated on maxillary digital cast where: the base (grey) is HNIP plane, the slanting (red) lines are the distances between R-point and each of LHN, RHN and IP respectively. The (blue) line is the vertical height of HNIP plane from R-point**

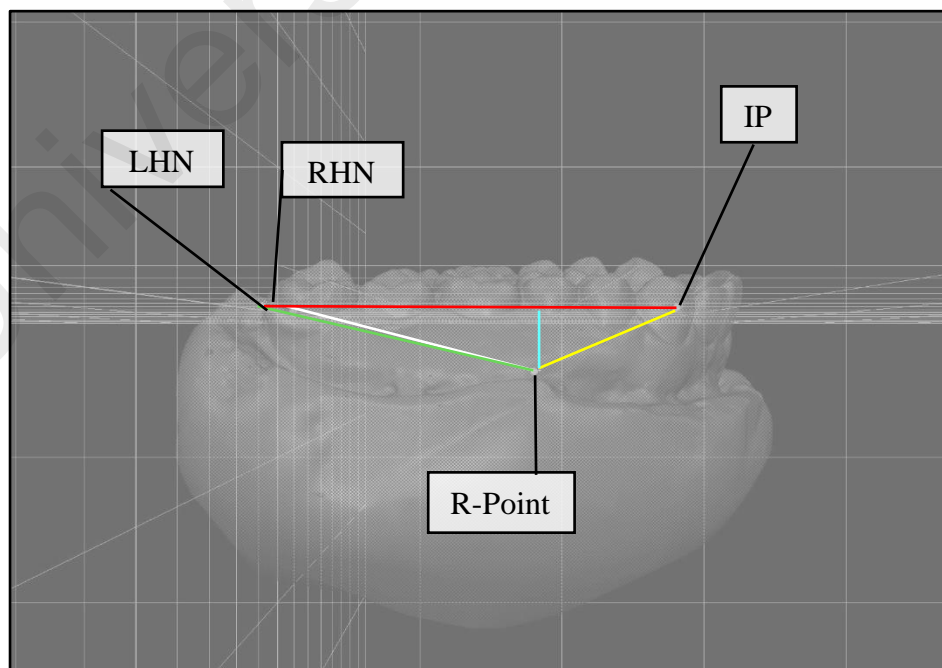


**Figure 3.29: Side view showing triangular pyramid: (red) HNIP plane, (yellow) IP-R line, (green) LHN-R, (white) RHN-R and (blue) is R-point depth from HNIP**

### 3.5.5 The azimuth ( $\theta$ ) and the elevation ( $\varphi$ ) angles of spherical coordinate system

To obtain the second and the third spherical coordinate elements, namely the azimuth and elevation angles; 41 angles were calculated from each 3D dental cast: 21 (elevation angles  $\varphi$ ) measured from the zenith and 20 (Azimuth angles  $\theta$ ) that represent the 18 angles of the teeth vector's for the second molar to second molar teeth points in addition to the left and right hamular notches obtained. Each angle starts from the positive quadrant of the X-axis (Figures 3.31 and 3.30).

Measurements were obtained after collecting all the landmarks' coordinates in the form of  $(x, y, z)$  and then defined using Microsoft Excel functions to calculate the radial distance ( $\ell$ ) from the origin to the landmark as straight distance, the polar angle ( $\theta$ ) and the azimuthal angle ( $\varphi$ ) using the following equations:

$$\theta = \tan^{-1} \left( \frac{y}{x} \right)$$

$$\varphi = \cos^{-1} \left( \frac{z}{\ell} \right)$$

The edentulous casts were marked and scanned to produce digital edentulous casts in a similar procedure as done to the dentate casts. Digitally, the casts were standardised in position, landmarks were registered and coordinates were collected in the same protocol as in dentate casts. Only the four landmarks (IP, LHN, RHN and R-point) forming the palatal triangular pyramid were marked and registered in the digital edentulous casts. The casts were aligned and coordinates were extracted and saved in Excel sheet where

the distances (such as IP-R, LHN-R, RHN-R and HNIP-height) and angles (such as  $\theta$  of LHN and RHN and  $\varphi$  of LHN, RHN and IP) within the triangular pyramid were calculated.

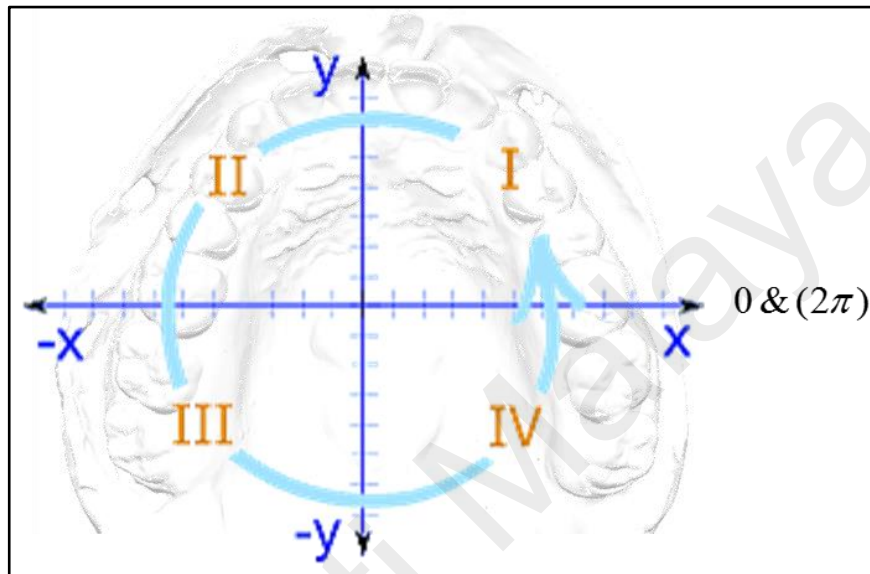


**Figure 3.31: The measurement of azimuth angles  $\theta$  in counter clockwise direction**

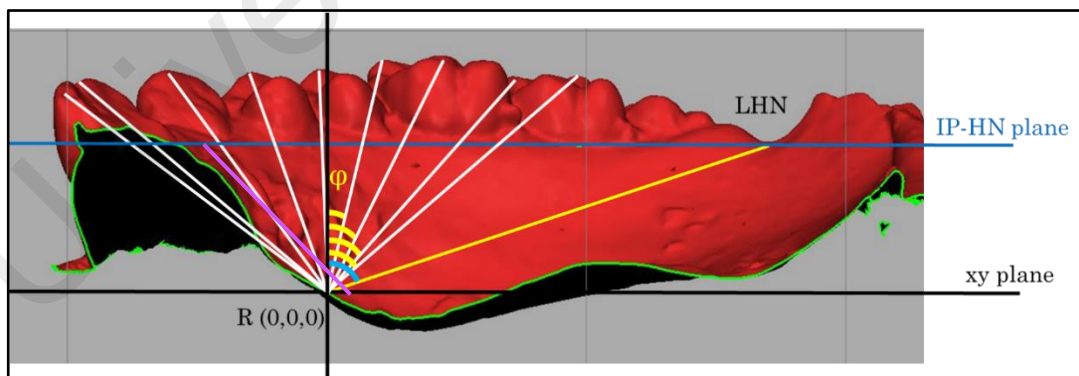


**Figure 3.30: The angles of elevation  $\varphi$  of teeth measured**

### 3.5.6 Data analysis (objective 1a)

#### 3.5.6.1 Statistical analysis

##### (a) *Correlations between the teeth and the predictor variable(s)*

The second element of spherical coordinates ( $\theta$ ) was checked for circular correlation with the independent variable of ( $\theta$ ) for the corresponding side LHN $\theta$  or RHN $\theta$ .

The third coordinate of the teeth ( $\phi$ ) was checked for circular correlation with the independent variable of the elevation angle ( $\phi$ ) of the corresponding side (LHN $\phi$  or RHN $\phi$ ).

The equation for the correlation coefficient is:

$$\text{Correl}(X, Y) = \frac{\sum(x - \bar{x})(y - \bar{y})}{\sqrt{\sum(x - \bar{x})^2 \sum(y - \bar{y})^2}}$$

Where  $\bar{x}$  &  $\bar{y}$  are the means of the sample (average of array 1) and (average of array 2)

##### (b) *Simple linear regression analysis*

The radius ( $\ell$ ) of each tooth was tested for relationship with multiple independent variables (IP-R, LHN-R, RHN-R and HNIP-height). However, the variance inflation factor VIF test was used to decide whether the best model was the simple or multiple regression model. Either way, the coefficient of determination  $R^2$  would be the indicator for the power of the relationship regressed. The residuals VS fit scatter plot was demanded in the settings of the regression to assure integrity of the regression procedure.

(c) *Multiple linear regression analysis*

In multiple regression analysis, the variance-inflation factor was used to confirm that the predictors used in the equations are independent before implementation and proceeding to calculate teeth positions. The usage of VIF was described as the simplest and most effective direct measure of the harm on the equations produced by collinearity (Fox & Monette, 2002).

(d) *Circular analysis*

Simple linear circular analysis was made to calculate the  $\alpha$  and kappa values for the models using Matlab algorithm code (Appendix B). The model stated in 3.5.6.3 was used to calculate the azimuth angle and the model in 3.5.6.4 was used to calculate the elevation angle for each point that represent tooth position in the dental arch.

**3.5.6.2 Calculating the radial distance ( $\ell$ )**

To investigate relationship between two or more variables, the most common techniques used are correlations and linear regressions. Correlations show the quantity of the linear relationship strength between variables, whereas regression expresses the relationship in the form of an equation (Bewick et al., 2003). The first step was to explore the data visually on a graphical scatter diagram. The diagram may reveal if any suggested linear relationships between the variables exist. The closer the points to a straight-line alignment the more likely the strong linear relationship between them.

Correlation analysis was used (as described in 2.10.1) to explore and quantify the strength of potential relationship by reading the product moment

correlation coefficient ( $r$ ).  $r$  value can represent the strength of the relationship. The closer the  $r$  value to 1, the stronger the positive or negative linear relationship between the two variables. Minitab 17 software (Minitab statistical software for windows. Minitab Inc. USA 2014) was used to make scatter diagrams and investigate the possible linear relationships between each tooth spherical coordinate to straight and angular measurements in the palatal triangular pyramid (Appendix C).

The correlation between the radial straight distance ( $\ell$ ) of each tooth and each of IP-R, LHN-R, RHN-R and HNIP-height was calculated. The strongest correlations were filtered to proceed with the regression analysis.

In order to investigate which of the measured variables is having reasonable relationship with the first spherical coordinate of the teeth positions, correlation analysis was made between the teeth and the potential predictor variable(s)

Using S-plus statistical software, the relationship between the dependent (tooth position) and independent variables (HNIP-height, IP-R, LHN-R and RHN-R) was investigated through multiple regression analysis and standardised weighted least squares. The required assumptions for regression analysis were verified, checked and fulfilled (Appendix D and Appendix E). To compute the radial distance of each tooth to R-point, 18 multiple linear regression equations were generated in the following form:

$$y = \beta_0 + \beta_1x_1 + \beta_2x_2 + \dots \beta_kx_k + u$$

Where:

$y$  is the dependent variable (radial distance ( $\ell$ ) coordinate of the tooth)

k is the number of independents (k = 4 in this study)

u is the model error in R-point

Each equation can predict the distance ( $\ell$ ) of its corresponding tooth from R-point in the specific dental cast.

### 3.5.6.3 Calculating azimuth angle ( $\theta$ )

Simple linear functional relationship was used to investigate the circular (azimuth angles) relationship between the left hamular notch and the left side teeth and the right hamular notch and the right side teeth to generate models that can estimate azimuth angle of each of the 18 maxillary teeth points bases on the azimuth angle of the corresponding side hamular notch. The model format was as the following:

$$y_{\theta} = \alpha + x_{\theta} \pmod{2\pi}$$

where  $y_{\theta}$  is the azimuth angle of the left or right tooth in radian units,  $\alpha$  is a constant value in the equation and  $x_{\theta}$  is the  $\theta$  of LHN for left side teeth  $\theta$  prediction or it is the  $\theta$  of RHN for the right- side teeth  $\theta$  prediction ( $y_{\theta}$ ).

The azimuth angles of the left side teeth were predicted by the azimuth angle of the left hamular notch and the angles of the right-side teeth from the azimuth angle of the right hamular notch. All the angles used for this model were measured in radian units and were counted starting from the positive x axis (Figures 3.32 and 3.33).

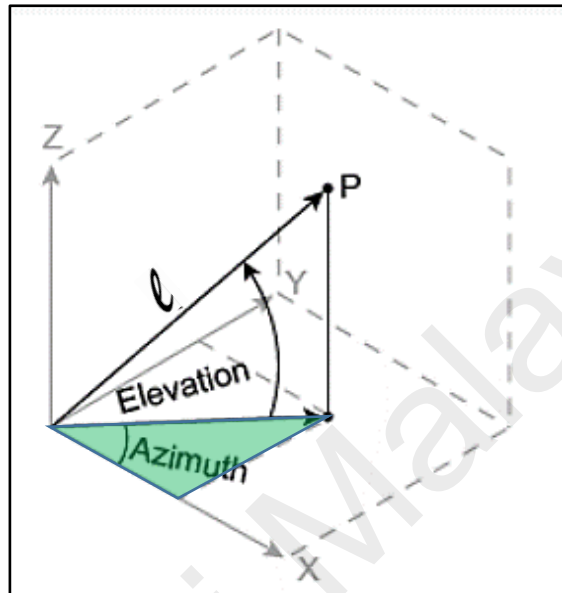


Figure 3.32: The calculation of azimuth angle in Cartesian system

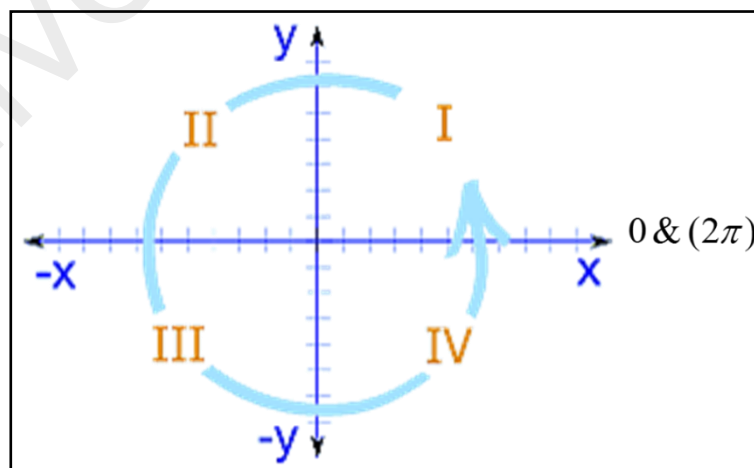


Figure 3.33: The azimuth angle is representing the position of the tooth from (+ve) x-axis on a counter clockwise direction

#### 3.5.6.4 Calculating elevation angle ( $\varphi$ )

Similar to the azimuth angle calculation process, simple linear functional relationship was used to calculate the elevation angle of each individual tooth using the elevation angle of the hamular notch in the corresponding-left or right side of that tooth in a given cast as in the following equation:

$$y_{\varphi} = \alpha + x_{\varphi} (\text{mod}2\pi)$$

Where  $y_{\varphi}$  is the elevation angle of left or right tooth in radian units,  $\alpha$  is a constant value in the equation,  $x_{\varphi}$  is the  $\varphi$  of LHN for left side teeth  $\varphi$  prediction or it is the  $\varphi$  of RHN for the right-side teeth  $\varphi$  prediction ( $y_{\varphi}$ ).

#### 3.5.7 The verification of the method in first objective (objective 1b)

The statistical models were used to predict the spherical coordinates ( $\ell$ ,  $\theta$ ,  $\varphi$ ) that represent the positions of the teeth in relation to R-point for verification dentate group (22 dentate sample). Paired  $t$ -test was used in Minitab software to compare the predicted and the real (measured values from the existing teeth) teeth positions of the 22 subjects with confidence interval of 95%. The  $p$ -value was then compared to the critical value of 0.05 to accept or reject the null hypothesis: “no significant difference between the values” If  $p > 0.05$ , the null hypothesis can be accepted and a conclusion of not enough evidence to support the existence of statistically significant difference between the variables can be obtained.

The verification data were composed of two groups, measured and estimated angles from 22 three-dimensional scanned maxillary dental casts.

The estimated angles were calculated after finding the relationship between the anatomical landmarks and the teeth of 70 other study casts.

They are:

A. Azimuth angle Theta ( $\theta$ ) (in radians) is the angle between the positive x axis and the point of landmarks or tooth measured on anti-clockwise direction from zero to 360 (occlusal view)

The established simple linear functional relationship models were used to estimate the azimuth angles of the maxillary teeth for the verification group based on the azimuth angle of the corresponding side hamular notch.

The azimuth angles of the left side teeth are found by the left hamular notch azimuth angle and vice versa for right side. The angles used for this model are in radians and are calculated from the positive x axis.

B. Elevation angle Phi ( $\varphi$ ) (in radians) is the angle between the vertex (Z-axis) and the point of landmark or tooth seen by side view of the cast.

Similar to the azimuth angle calculation, the elevation angle of each tooth will be calculated by the simple linear functional relationship to use the corresponding side hamular notch elevation angle in the estimation of the elevation angle of the tooth in the corresponding side using the form of the following equation:

$$y_{\varphi} = \alpha + x_{\varphi}(\text{mod}2\pi)$$

### **3.5.8 Regression analysis to investigate the relationship between variables**

Through correlation tests, strong and significant correlations may suggest presence of relationship between the correlated variables. The relationship between the palatal triangular biometric pyramid points measurements, LHN, RHN, IP and HNIP-height and the teeth radial distance from R-point were selected for simple linear regression analysis as they revealed the highest correlation coefficient among the correlations tested (Table 4.6). Before applying the regression analysis, the six classical standard assumptions (SA1-SA6) of simple linear regression analysis were verified and confirmed unviolated. The regression analysis was applied using S-Plus software ( $\alpha = 0.05$ ) (Isa et al., 2010).

If all of these assumptions were met, then the estimates are known as the best linear unbiased estimates and thus the model they estimate is called the “best” model.

#### **3.5.8.1 Residual plots**

To assure the validity of some of the regression assumptions, the residual plot vs fit was generated for the regression. The settings were adjusted to show the three most extreme residuals for showing outliers. The plots should show no certain pattern for the residuals plotted, no unreasonably extreme outliers and no obvious curvature for the line of regression.

### 3.5.8.2 Weighted least squares regression

To improve the regression models, make them more immune from distorting effects of autocorrelation and correct the problem of non-constant variances, generalised least squares method, specifically the weighted least squares (WLS) method was used (Draper & Smith, 2014; Welc & Esquerdo, 2017). Weighted least squares regression method was applied in this study following Isa et al. (2010), by obtaining the residuals from the ordinary least squares estimation, standardising the residuals  $\hat{e}_i$  using the following equation

$$\hat{e}_i = \frac{e_i - E(e_i)}{\sqrt{\text{Var}(e_i)}};$$

calculating the weights applying the following equation in Excel sheet:

$$\text{weight} = \frac{1}{\hat{e}_i^2};$$

Then the weighted regression analysis was run using the weighted least squares (WLS) in S-plus statistical software (S-Plus 8.0 for Windows; Insightful Corp). The regression models and  $R^2$  values were stored and used for further investigation in this study.

### 3.5.9 Determining maxillary teeth positions for new independent dentate sample

The sample in this part of the study was the verification dentate subgroup (n = 22). The predictor variables, namely the IP  $\ell$ , LHN  $\ell$ , RHN  $\ell$  and HNIP-height were used according to the suggested equations earlier to predict the 3D coordinates of teeth positions for the subjects (Figure 3.34). The predicted

distances and angles were compared with the measured existing angles in the sample using paired *t*-test with confidence of 95%.

$$H_0: \mu_P \neq \mu_o$$

$$H_1: \mu_P = \mu_o$$

Where  $\mu$  is the mean,  $p$  is the predicted value and  $o$  is the observed value.

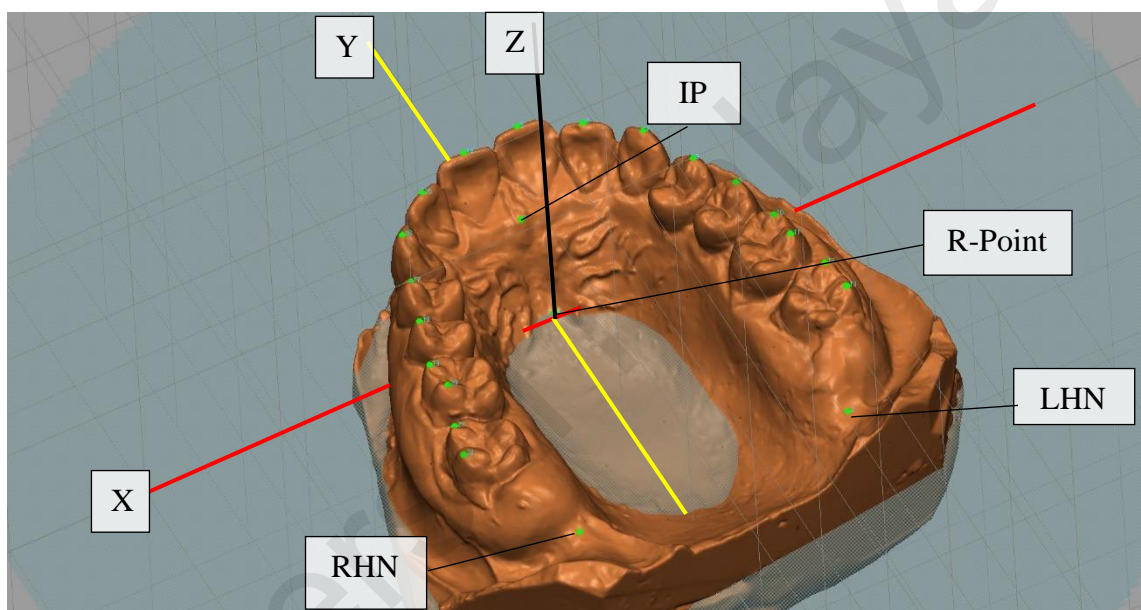


**Figure 3.34: Digital cast aligned by having R-point as the origin (0, 0, 0). Red, yellow and black lines are the Cartesian X, Y and Z axes respectively**

### **3.5.10 Determining maxillary teeth position for edentulous patients (objective 1c)**

Similar to the dentate sample, the edentulous maxillary stone master casts were digitised to 3D dental casts using Maestro 3D scanner (Maestro 3D dental scanner, Pizza, Italy). Image processing procedures were made as in dentate casts, the digital casts were standardised, followed by registration of the landmarks, coordinates collection and measurements of biometric triangle of landmarks obtained (Figure 3.35).

The digital casts were downloaded into a 3-dimensional analysis software (Vectra 3D, Canfield. USA) and the anatomical landmarks marked on the digital edentulous cast and registered were the centre of incisive papilla (highest point occlusally) (IP), deepest points on left and right hamular notches (LHN and RHN) respectively and the R-point. The height of HNIP plane from R-point (HNIP-height) was represented by the z coordinate of IP, LHN or RHN as long as R-point z is zero and HNIP was transformed to have uniform z

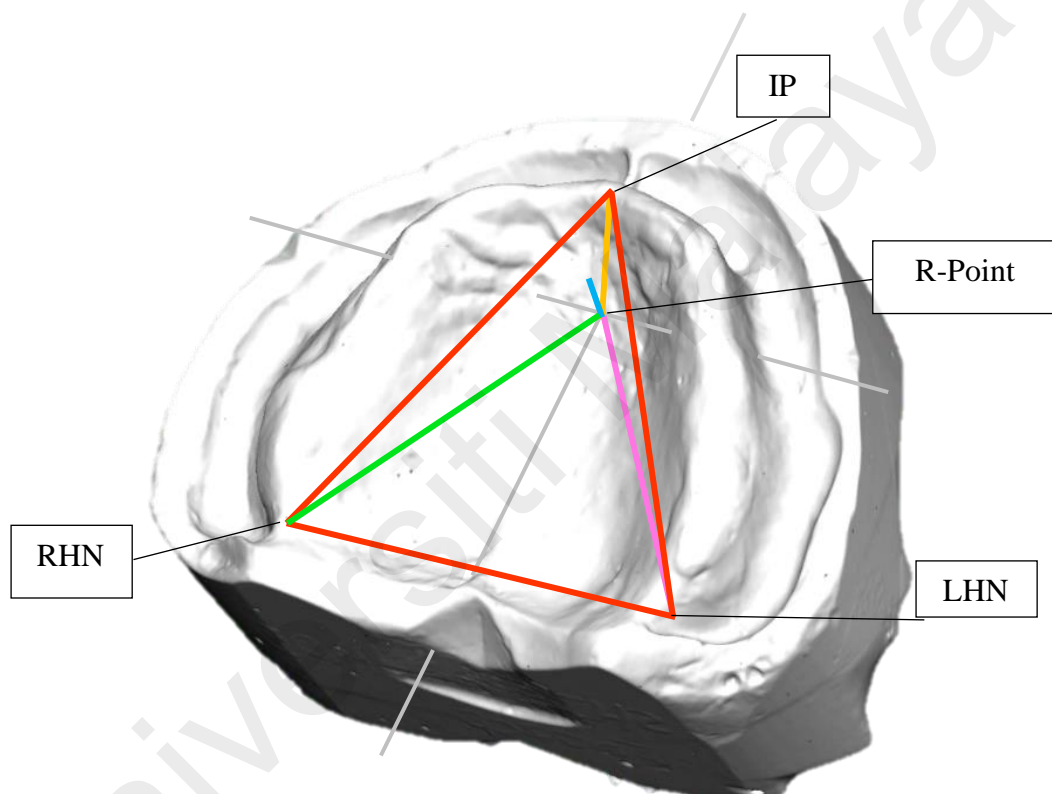


**Figure 3.35: Triangular pyramid measurements on maxillary edentulous cast** coordinates in phase I of the cast positioning.

The verified mathematical models were used to predict teeth positions for the edentulous sample using coordinates and measurements on the biometric triangular pyramid points of the edentulous casts (Figure 3.35). In order to perfect the guide for restoring the maxillary dental arch overall dental arch form is needed to fit the predicted points especially for anterior teeth as the points in the middle if the incisal edge may accept rotation about the long axis of the tooth.

When needed, the spherical coordinates can be converted to Cartesian coordinates for illustration and description purposes as will be shown in the results part in 4.3 and related plotting.

Universiti Malaya

### **3.6 Second objective: The relationship between the form of palatal vault and the form of the dental arch**

#### **3.6.1 Dental arch form**

In this objective of the study, the similarity between the form of the natural dental arch and the independent curve formed on the palatal vault by a secant plane passing through stable intraoral landmarks (Hamular Notches and Rugae point). The researcher determined the relationship and the possibility to reproduce the form of the dental arch based on the given form of the palatal arch, verified the validity of the method with independent dentate sample and then applied on edentulous cases with different resorption rates.

Matlab software (MATLAB and Statistics Toolbox Release 2013b, The MathWorks, Inc., Natick, Massachusetts, United States) was used to generate automatically four mathematical fourth-degree polynomial equations for each dental cast. The curves were introduced to the software as two-dimensional coordinate data to generate a best-fit curve representing the arch. In Matlab, algorithms can be designed to run a series of complicated mathematical processes to come up with high precision data in an exceptional short time. One brilliant application by Matlab is the artificial intelligence or neural network that could solve complicated problems by training and application process similar to human brain learning (Agatonovic-Kustrin & Beresford, 2000).

This objective is to use biometric guides to reconstruct the form of the maxillary dental arch by finding the mathematical relationship between the form of the palatal vault and the form of the arch of natural well-aligned teeth.

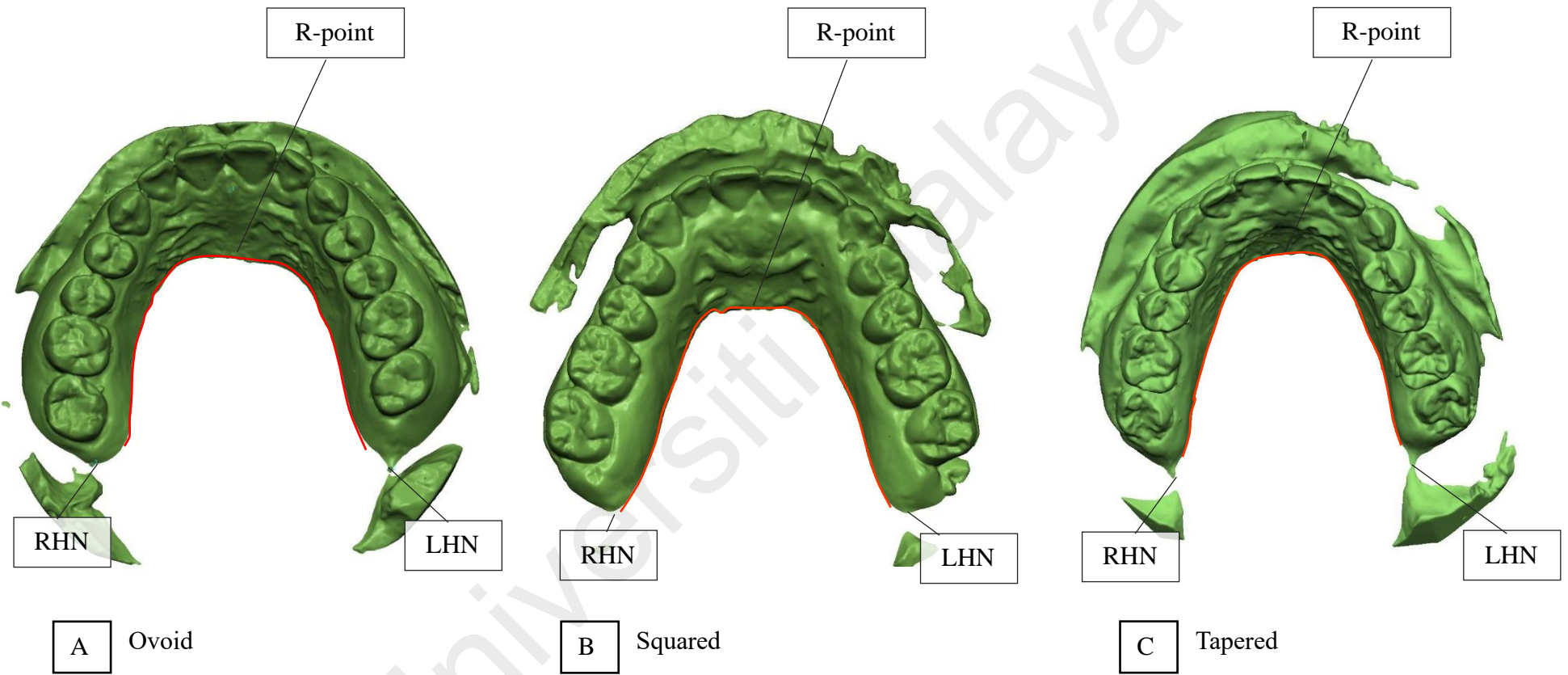


**Figure 3.36: The observed similarity between the forms of the dental arches and the HNIR curve**

### 3.6.2 Sample and materials

The number of dentate subjects and the raw data collection was explained earlier.

### 3.6.3 Study flow chart (second objective)

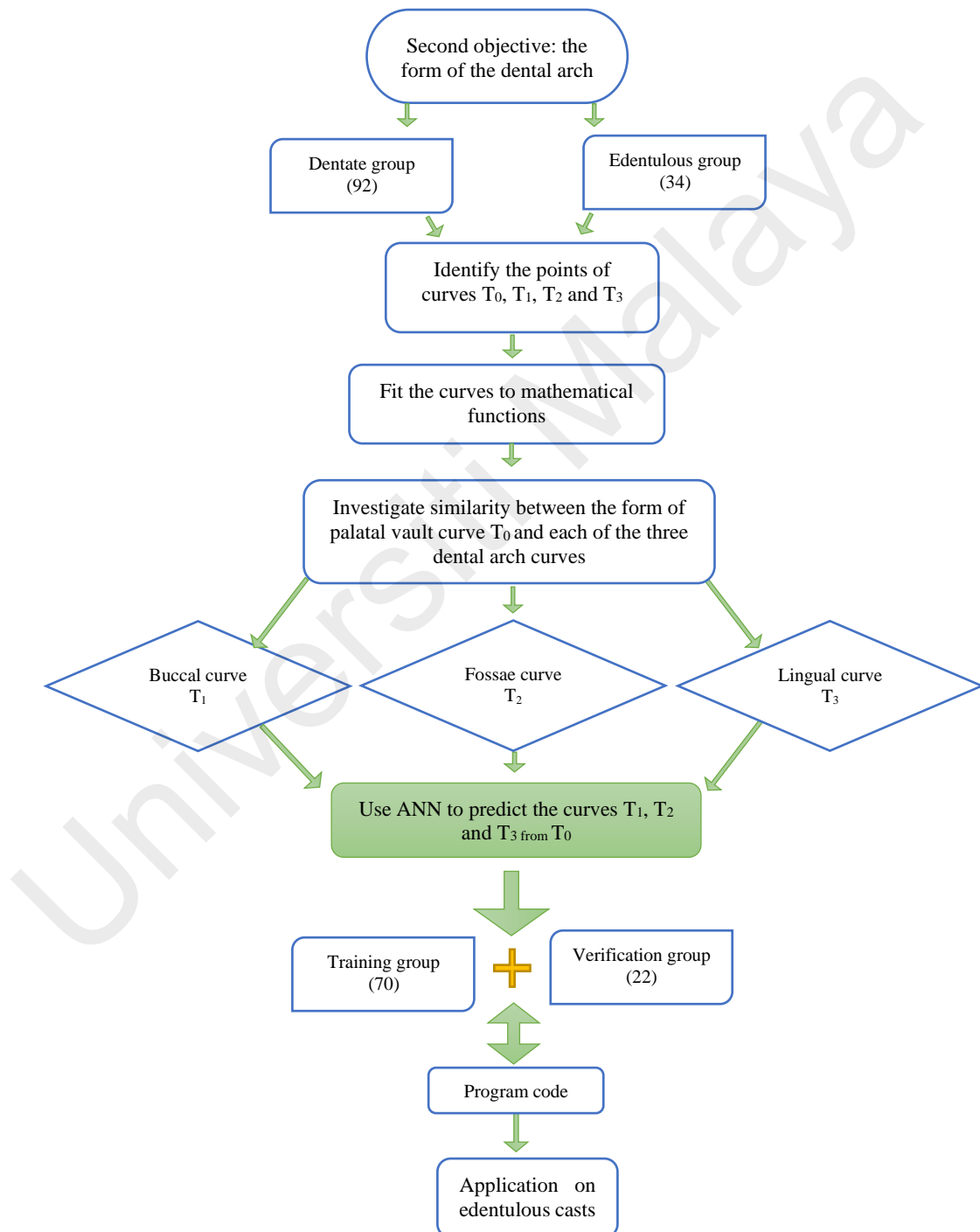


Figure 3.37: Flow chart for the study (objective 2)

### **3.6.4 Identifying the curves of dental arch**

Following the flow chart for the study (Figure 3.37), The dental arch can be represented in three forms based on the reference points selected on the teeth: the labial and buccal points are forming “buccal arch”; the middle fossae of the teeth are forming “fossae arch”; while the palatal cingulae and palatal cusps of the teeth are forming the “palatal arch”.

#### **3.6.4.1 The palatal vault curve (HNR curve)**

When maxillary dentate stone casts were projected from occlusal view, similarity in the form was observed between the curve of the dental arch made by joining the incisal and occlusal-tip points on the teeth and a curve generated across the palatal vault by an intersecting secant plane across the digital cast passing through the left and right hamular notches and the midpoint between the medial ends of the third rugae lines. In this study, this curve will be referred to as the “HNR curve” or “palatal vault curve”.

Palatal vault curve (HNR curve) is the curve extending on the palate from left to right hamular notches through the R-point created by the secant line on the palate horizontally on the surface of the palate extending from the left hamular notch to the right hamular notch passing through the point on the midline between the medial-end-points of the third ruga pair of lines (R-point) (Figure 3.38).

In the 3D image analyser VAM application version 2.8.3 (Canfield Scientific Inc., Fairfield-NJ, USA), the landmarks LHN, RHN and R-point, were registered and by choosing the task “split at plane, 3 landmarks” from the drop down menu under “surface” in the application taskbar; a circumferential line in light green will appear extending over

the dental cast running horizontally along the surface between the three landmarks R-point, LHN and RHN (Figure 3.38).

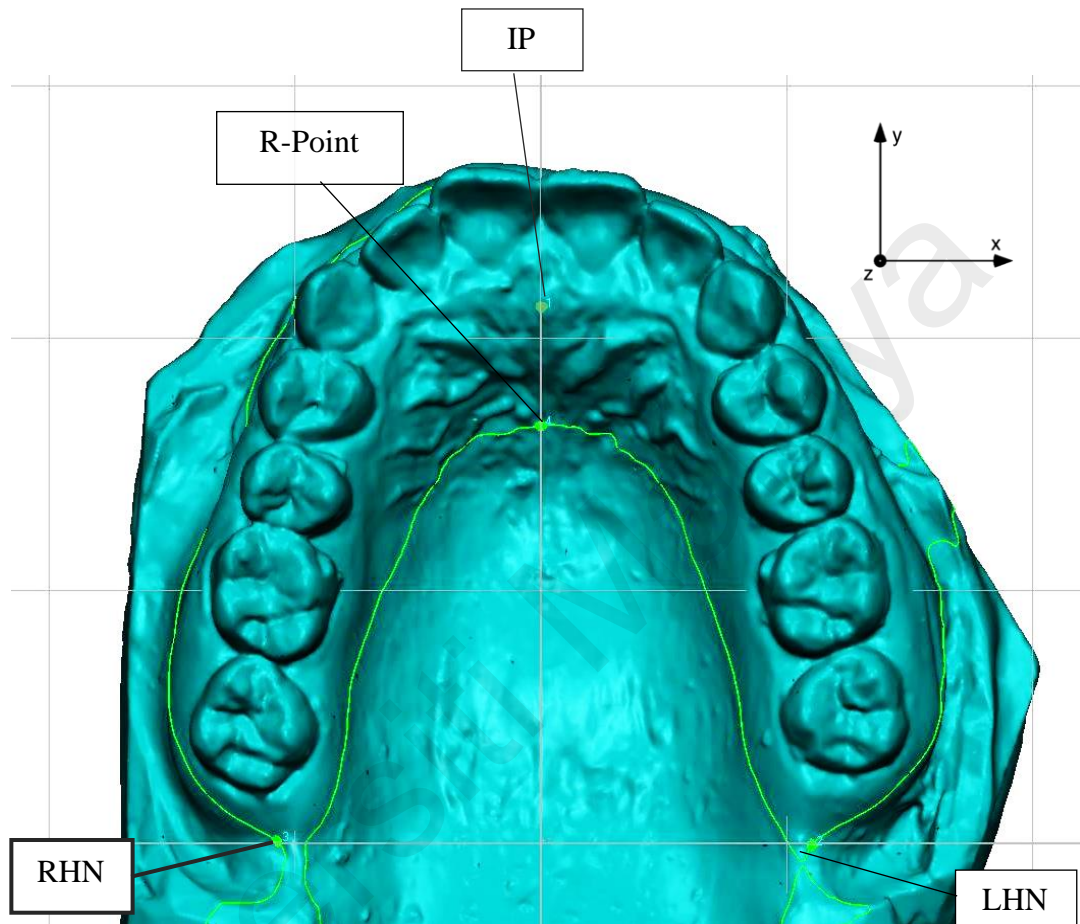


**Figure 3.38: Landmarks registration and HNR curve formation**

The view of the dental cast from an aspect perpendicular to the HNR curve is exported and saved as 2D image to digitise the HNR curve. The image is downloaded and calibrated in 2D image analysis application (GetData version 2.1) where:

33 uniformly distributed points along the HNR curve were selected to represent the curve form in the 2D Cartesian system (Figure 3.39).

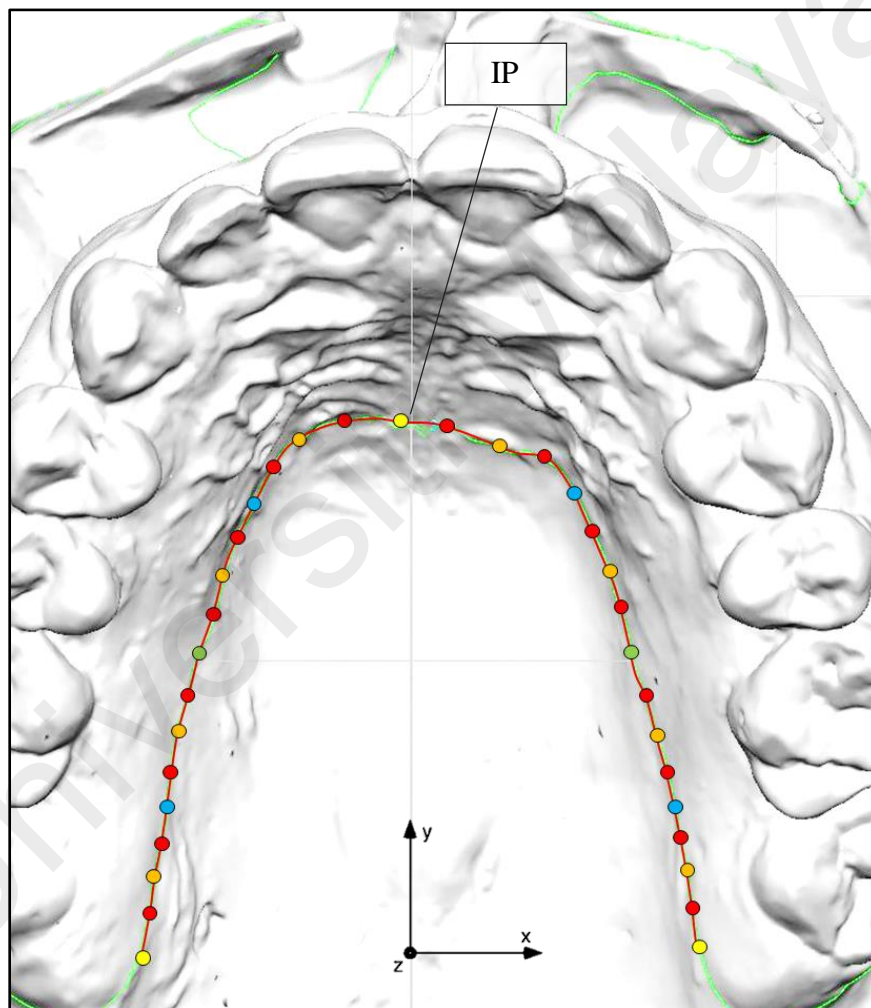


**Figure 3.39: Digitising HNR curve by making points to fit polynomial curve equation**

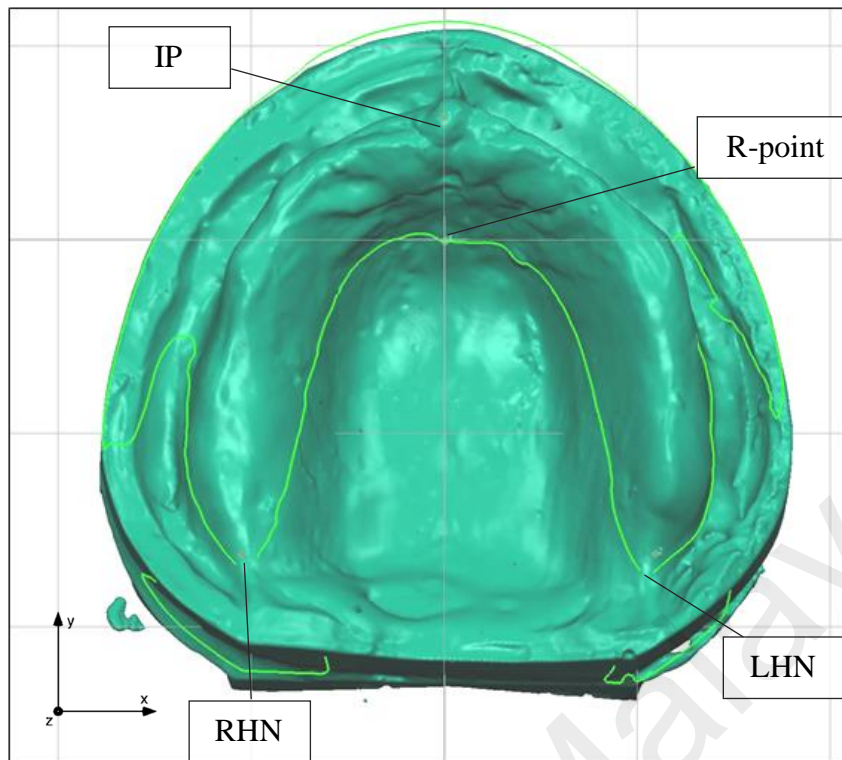


**Figure 3.40: Palatal vault curve (HNR curve) in edentulous maxillary cast**

Similarly, the palatal vault curve was registered and coordinates extracted in edentulous digital casts (Figure 3.40).

#### **3.6.4.2 The dental arch curves**

The dental arch curves were defined as three versions:

##### **(a) Buccal dental curve ( $T_1$ )**

A curve composed of 18 points extending through the middle of incisal edge of each anterior tooth and buccal cusp-tips (mesiobuccal and distobuccal) of each maxillary first and second molars (Figure 3.41-A).

(b) ***Fossae curve (T<sub>2</sub>)***

A curve composed of 18 points extending on a curve made through the middle fossae of the incisors and canine, first and second premolars and middle and mesial fossae of the maxillary first and second molars (resembling line of occlusion curve) (Figure 3.41-B).

(c) ***Palatal curve (T<sub>3</sub>)***

The curve that is joining the cingula of the anterior teeth and the palatal cusps of the posterior teeth i.e. mesiopalatal and distopalatal cusps of the first and second molars (18 points) (Figure 3.41-C).

Universiti Malaysia

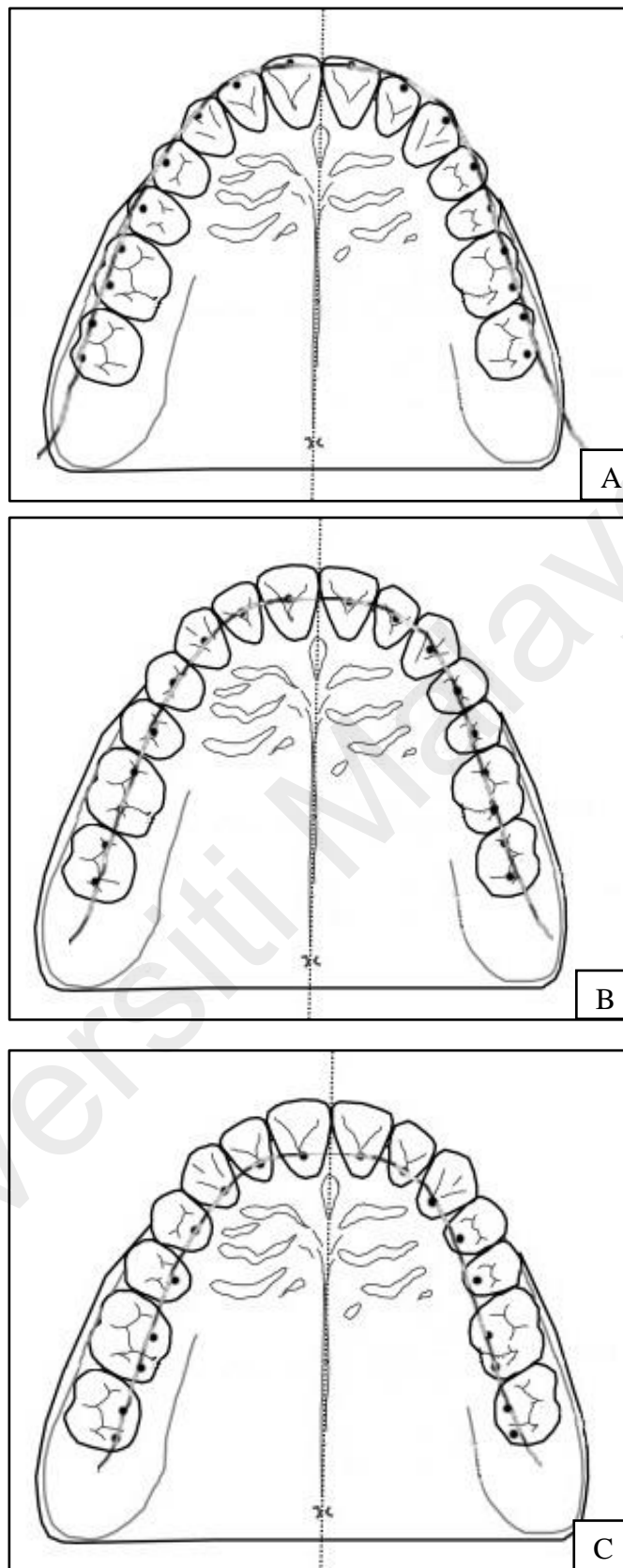


**Figure 3.41: Dental arch curves: (A) buccal cusps curve T<sub>1</sub>, (B) fossae curve T<sub>2</sub> and (C) lingual cusps curve T<sub>3</sub>**

### 3.6.5 Digitising the dental arch curves

An occlusal view perpendicular to the hamular notches-incisive papilla plane was exported from 3D analyser into two-dimensional plane image (.jpeg) format. The 2D images were downloaded into 2D image analysis application (GetData). The images were calibrated based on the 3D grid background provided originally by the 3D analyser. Each side of the squares in the grid is 20mm. Origin is defined as point joining the vertical line passing on the middle of incisive papilla (Y axis) and the horizontal line passing over the left and right hamular notches (X axis). The coordinates of the three dental arch curves along with the palatal arch (red) curve are shown in Figure 3.42, where each of the dental curves; the green, maroon and blue curves are the buccal, fossae and lingual curves respectively is composed of 18 points while the palatal curve is composed of 33 points and all are marked and extracted as (x. y) sets and tabulated in Excel spread sheet (Figures 3.39 and 3.43).

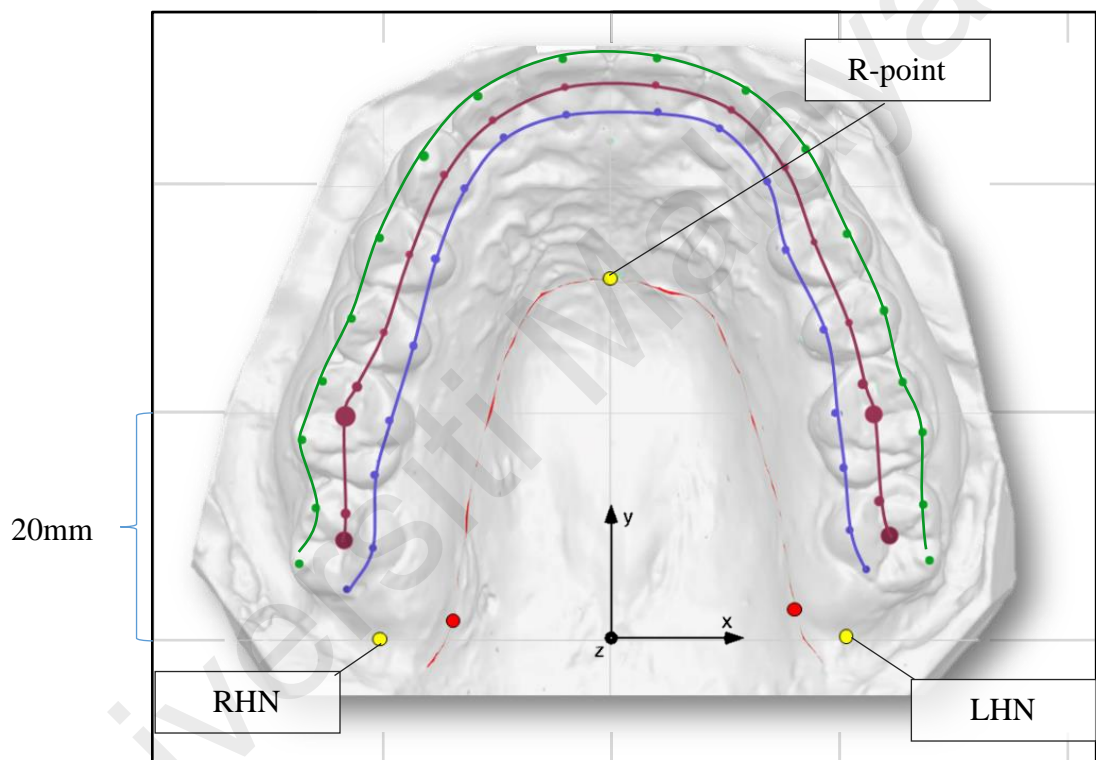


**Figure 3.42: Buccal dental curve (T<sub>1</sub>) in green, central fossae curve (T<sub>2</sub>) in maroon and lingual dental curve (T<sub>3</sub>) in blue**

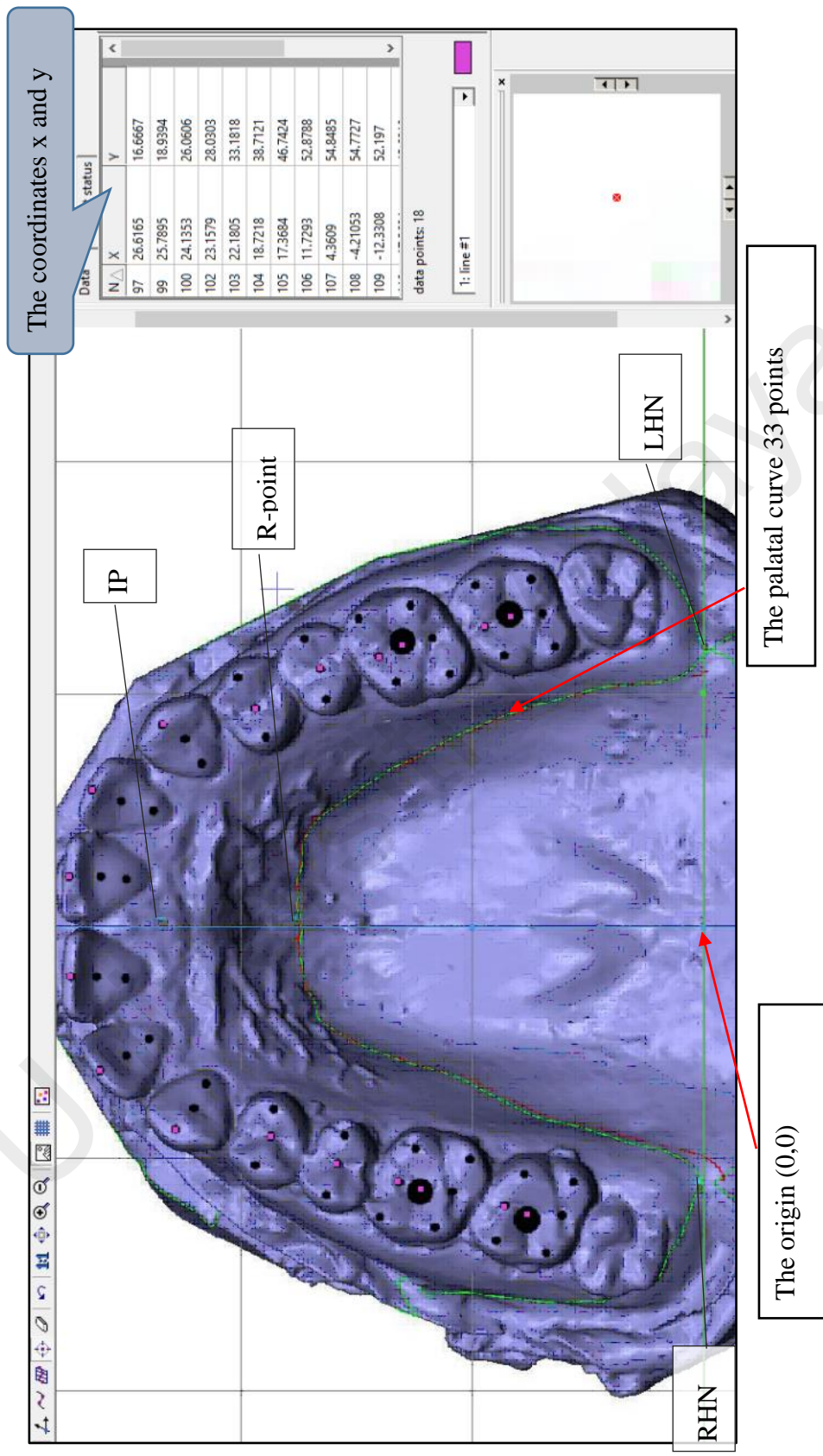


Figure 3.43: Digitising the palatal and dental curves in 2D image using GetData software

The coordinates collected were as the following:

- |  |   |   |
|--|---|---|
| 1. <b>33 points</b> from HNR curve     | } | Collected from 92 dentate and 34 edentulous casts |
| 2. <b>18 points</b> from Buccal curve  |   |   |
| 3. <b>18 points</b> from Fossae curve  | } | 92 dentate casts only                             |
| 4. <b>18 points</b> from Palatal curve |   |   |

The coordinates obtained were tabulated in Microsoft Excel sheet and used to generate 368 least squares polynomial fourth-degree equations that fit the above-mentioned curves.

### 3.6.5.1 Fitting mathematical functions to the dental arch curves

To be able to analyse and compare the dental cast curves, each curve was fitted to 4th degree polynomial function using Microsoft Excel and Matlab 2013b (Figure 3.44).

The quartic function equation was as the following:

$$y = a_0 + a_1 \cdot x + a_2 \cdot x^2 + a_3 \cdot x^3 + a_4 \cdot x^4$$

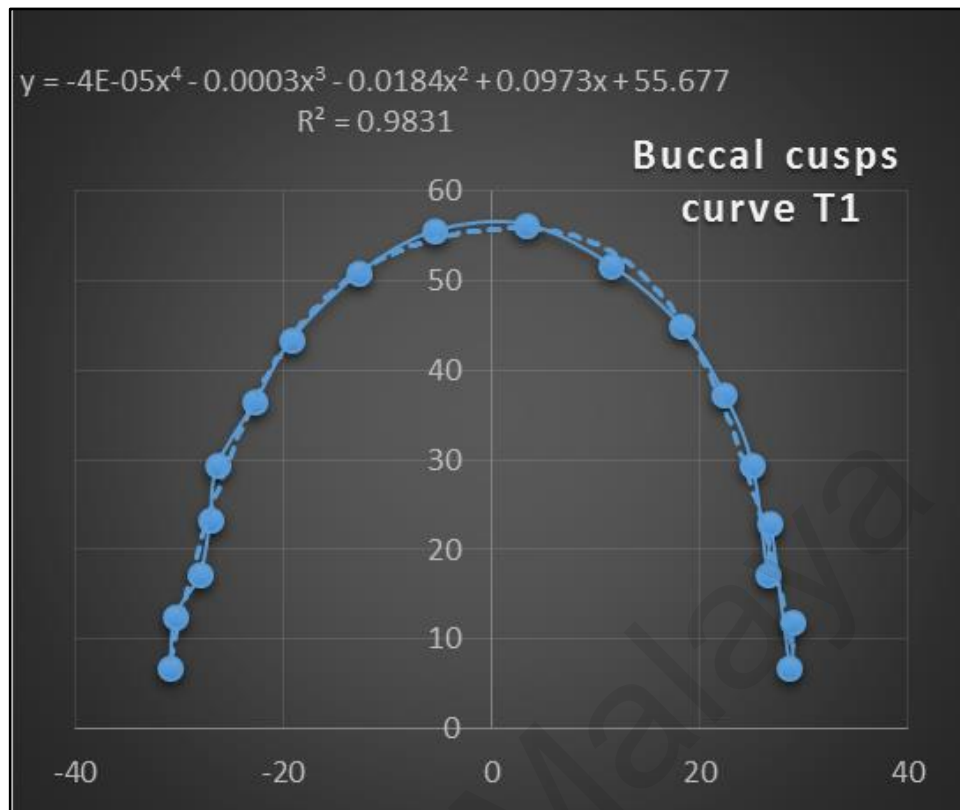


**Figure 3.44:** Example of fitting the buccal cusps curve (T<sub>1</sub>) to 4<sup>th</sup> degree polynomial equation.  $R^2$  is indicating the percentage of the curve fitting the 18 points

### 3.6.6 Similarity between the curves (hypothesis test)

The null hypothesis in this objective was “there is no significant difference between the forms of the compared curves” which means that the difference between them is always constant upon comparing the functions.

Using Microsoft Excel, modified *t*-test (*Z* values) were calculated for every case to test the significance in difference between the palatal curve form (HNR curve) and each of the 3 dental arch forms (T<sub>1</sub>, T<sub>2</sub> and T<sub>3</sub>). *Z* values compared palatal curves and the dental arch curves in the entire dentate sample (92).

$92 * 3 = 276$  *Z* values were obtained.

The *z* value is calculated as the following:

**Table 3.1 Modified *t*-tests applied to compare palatal curves and dental arches**

$Z_1$	Compares HNR curve with	T <sub>1</sub> dental arch curve
$Z_2$	Compares HNR curve with	T <sub>2</sub> dental arch curve
$Z_3$	Compares HNR curve with	T <sub>3</sub> dental arch curve

HNR curve:  $y_0=f(x) + \varepsilon_1$

Dental curve:  $y_1=g(x) + \varepsilon_2$

$H_0$ :  $g(x)= f(x) + c$

$\Rightarrow c = g(x)- f(x)$  or  $y_1 - y_0 = c + \varepsilon \sim N(0, \sigma^2)$

Test statistic  $Z = \frac{\bar{\hat{c}} - \bar{c}}{Se(\hat{c}_i)/(\sqrt{n-5}/\sqrt{n-1})}$  ( $\bar{\hat{c}} = \frac{\sum \hat{c}_i}{n}$ )

Reject  $H_0$  at the 5% level if  $|z| > 1.96$

### 3.6.7 Predicting the dental curve from the HNR curve

When similarity was verified, Matlab software was used to generate an artificial neural network (ANN) code that can be used after data training to predict the curves of the three dental arch forms (i.e., the T<sub>1</sub>, T<sub>2</sub> and T<sub>3</sub>) given the HNR-curve obtained from the digital dental cast (Figure 3.45). By providing enough training data to the neural network in the form of coordinates of the original curve data and the target curves coordinates: T<sub>1</sub>, T<sub>2</sub> or T<sub>3</sub>, the ANN should be able to predict the dental arch curves T<sub>1</sub>, T<sub>2</sub> or T<sub>3</sub> independently when original curve data is fed for new independent sample. The outcome data of the network prediction (coordinates of the curves) were compared with the real dental curve coordinates of the corresponding subjects

using paired  $t$ -test with significance of 0.05. The ANN should be able to propose the dental arch curves by the palatal curve data.

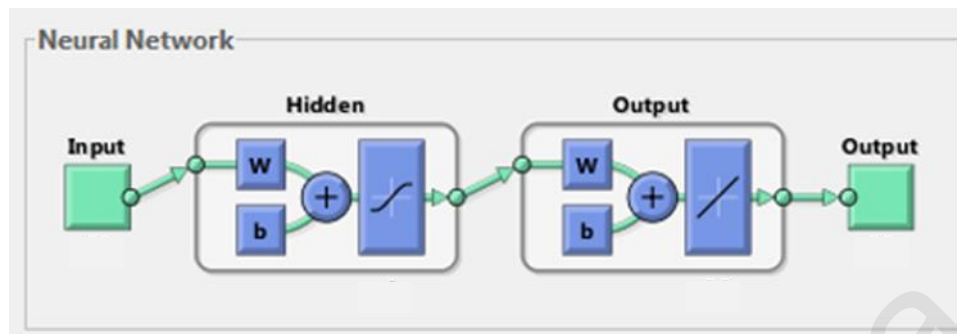


Figure 3.45: Neural network training tool flow

### 3.6.8 Predicting dental arch for dentate sample

The dentate sample was subdivided into 2 groups: training group and testing group. The training group helped the ANN to learn the relationship between the curves to be able to produce dental curve form for the new sample

Training data (70) were given to the computer input: original (HNR curve) and three targets ( $T_1$ ,  $T_2$  and  $T_3$  curves) as binary 2D data ( $x$ ,  $y$ ) of 18 points for each curve.

In the neural network, the tests for fitting the equations, the coefficients of determinations and the reproducibility were generated by the algorithm designed and the results.

### 3.6.9 Verification test of the method in second objective

Coordinates of the dental arch form predicted by the computer ANN for dental arches of new dentate sample (test group of 22 subjects) were compared with the existing dental arches for that sample. Paired  $t$ -test was used to

measure the statistical significance in difference. The null hypothesis was “there is no significant difference between the real and predicted arches within significance of 0.05”. The  $z$  test was used for this task, with the critical value of 1.96. If  $|z| < 1.96$  no significant difference in the forms of the arches can be concluded.

### **3.6.10 Predicting the form of maxillary dental arch for edentulous cases**

Artificial neural network (ANN) algorithm was designed to predict dental arch curves (buccal, middle and palatal) for each case based on input data from the palatal HNR curve. The ANN is verifying the outcome repeatedly and enhancing the fitting equations until it gets the best fitting and least error outcome (Rumelhart et al., 1988; Agatonovic-Kustrin & Beresford, 2000). The variables given to the ANN were 33 points representing the curve of palate HNR ( $T_0$ ) which is extending from the left to right hamular notches passing through R-point making a transactional plane through the palate, points representing the three dental arch curves: 18 points as Buccal curve ( $T_1$ ), 18 points as fossae curve ( $T_2$ ) and 18 points of lingual curve ( $T_3$ ) for each dental cast.

In the process of ANN training, each point's data composed of a pair of (x, y) coordinates were given to the computer. Each cast input was given as four sets of coordinates:  $T_0$  (33 pair),  $T_1$  (18 pair),  $T_2$  (18 pair) and  $T_3$  (18 pair). The data of 70 casts were introduced to the ANN to learn. The remaining 22 dentate casts went through verification of the method. In other words, ANN was given the  $T_0$  and asked to produce  $T_1$ ,  $T_2$  and  $T_3$  for the dental casts, the predicted values  $\bar{T}_1$ ,  $\bar{T}_2$  and  $\bar{T}_3$  were compared to the known  $T_1$ ,  $T_2$  and  $T_3$  values to check the reproducibility.

Finally, the computer was given data of  $T_0$  of edentulous sample to produce  $\bar{T}_1, \bar{T}_2$  and  $\bar{T}_3$  for the edentulous casts and fit or adjust to the predicted points of teeth positions by using the mathematical models from objective 1.

Universiti Malaya

# CHAPTER 4

---

## Results

---

Universiti Malaya

## CHAPTER 4: RESULTS

### 4.1 Introduction on results

The results in this chapter are composed of three main parts: the preliminary analysis pre-experimental results, experimental results and post-experimental results. description and descriptive statistics, the first objective results and the second objective results. In the first objective, the relationship models for geometric position of teeth in relation to the origin R-point were listed as separate elements; the radius, the azimuth angle and elevation angle.

### 4.2 3D position of maxillary teeth

The dentate study sample mean age (*SD*) was 22.61 (3.44). The positions of the teeth are presented in this chapter as three sections according to the coordinates: the radius, the azimuth and the elevation coordinates analyses.

#### 4.2.1 Descriptive statistics

##### 4.2.1.1 Cartesian coordinates

In the form of Cartesian coordinates, the positions of the predictors (biometric triangular pyramid) are presented in Table 4.1. The mean and standard deviation values of the Cartesian coordinates ( $x$ ,  $y$ ,  $z$ ) of the landmarks in the dentate sample were presented. The coordinate of 0 (0.00) for R-point was presented as the origin in this Cartesian system. Both the mean values of  $x$  coordinates of LHN and RHN were similar (21.58) and (-21.67) as the Y axis passes through the middle of IP, the negative sign is indicating the direction in

Cartesian plane not the true value (Figure 3.8). The uniformity of mean  $z$  coordinate of IP, RHN and LHN can be observed too due to standardisation of the casts position to have HNIP plane parallel to XY plane.

Table 4.2 displays the descriptive data for the 18 points of maxillary teeth observed in the control dentate sample ( $n = 70$ ). The left and right teeth similar mean  $x$  coordinates indicated similar positions in relation to R-point. For instance, the left central incisor (LCI) and right central incisor (RCI) had mean values of coordinates ( $x, y, z$ ), (4.25, 22.01, 16.4) and (-4.16, 22.04, 16.21) respectively means that they are at the same height, anterior-posterior position but on opposing left and right sides in relevance to R-point (Figures 4.1, 4.2 & 4.3).

**Table 4.1: Means and standard deviations of the Cartesian coordinates (x, y, z) of the biometric triangular pyramid points (in mm)**

Point	x mean (SD)	y mean (SD)	z mean (SD)
IP	0 (0.00)	12.71 (2.11)	10.16 (1.65)
R-point	0 (0.00)	0 (0.00)	0 (0.00)
LHN	21.58 (2.04)	-34.53(2.92)	10.16 (1.65)
RHN	-21.67(2.01)	-34.53(2.96)	10.16 (1.65)

**Table 4.2: Means and standard deviations of the Cartesian coordinates (x, y, z) (in mm) of the teeth and landmarks of the experiment dentate groups (n = 70)**

Point	x mean (SD)	y mean (SD)	z mean (SD)
LCI	4.25(0.61)	22.01(2.70)	16.14(2.27)
LLI	12.05(0.72)	18.79(2.64)	15.68(2.31)
LC	17.72(0.87)	13.48(2.66)	16.34(2.21)
RCI	-4.16(0.55)	22.04(2.64)	16.21(2.17)
RLI	-11.81(0.77)	18.80(2.52)	15.87(2.19)
RC	-17.45(1.00)	13.33(2.56)	16.68(2.12)
L1PM	21.74(1.02)	6.08(2.81)	16.77(2.19)
L2PM	24.45(1.32)	0.85(2.78)	16.82(2.22)
LMb1M	27.04(1.48)	-6.71(2.83)	16.08(2.27)
LDb1M	27.78(1.65)	-11.94(2.87)	16.41(2.16)
LMb2M	29.74(1.85)	-17.44(3.05)	15.00(2.18)
LDb2M	29.83(1.99)	-22.55(3.01)	14.39(2.32)
R1PM	-21.48(1.18)	6.06(2.61)	17.01(2.07)
R2PM	-24.16(1.59)	0.77(2.69)	17.09(2.07)
RMb1M	-26.58(1.75)	-6.75(2.61)	16.31(2.05)
RDb1M	-27.47 (1.86)	-12.01(2.64)	16.61(2.01)
RMb2M	-29.47(2.16)	-17.50(2.78)	15.22 (2.01)
RDb2M	-29.79(2.27)	-22.62(2.83)	14.51(2.15)

\*3D plotting of the points is illustrated and shown in figures 4.1, 4.2 & 4.3.

A visual representation for the average coordinates of teeth positions in dentate sample were plotted in 3D Cartesian system from occlusal, frontal and side views respectively in (Figures 4.1, 4.2 and 4.3).

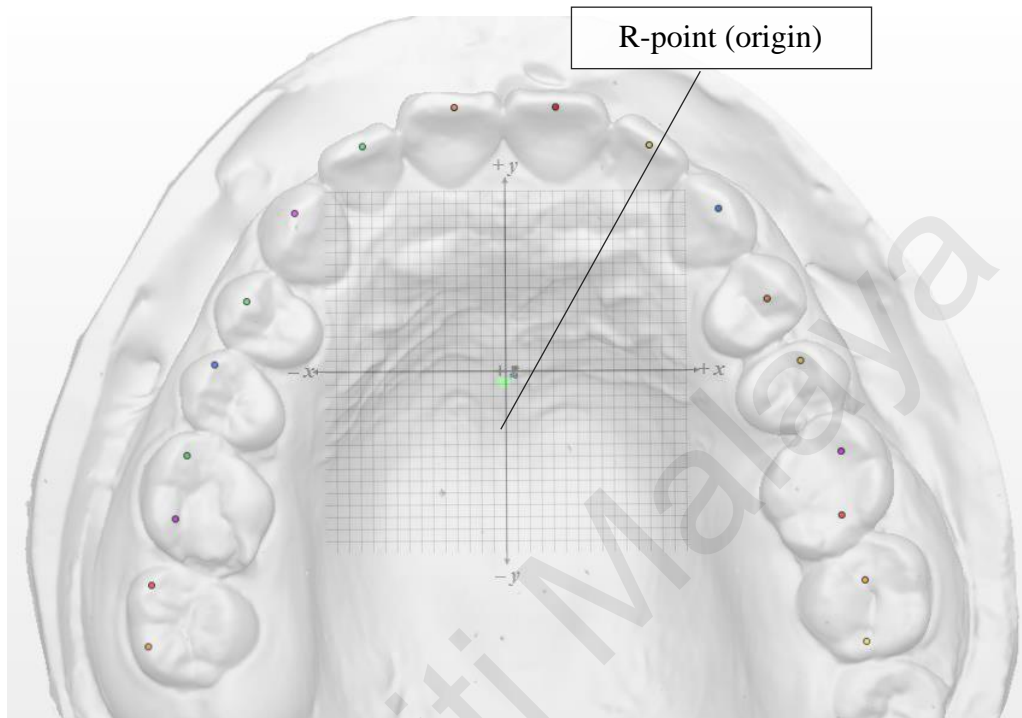


**Figure 4.1: Occlusal view of average 3D tooth position points for dentate sample plotted on Cartesian graph**

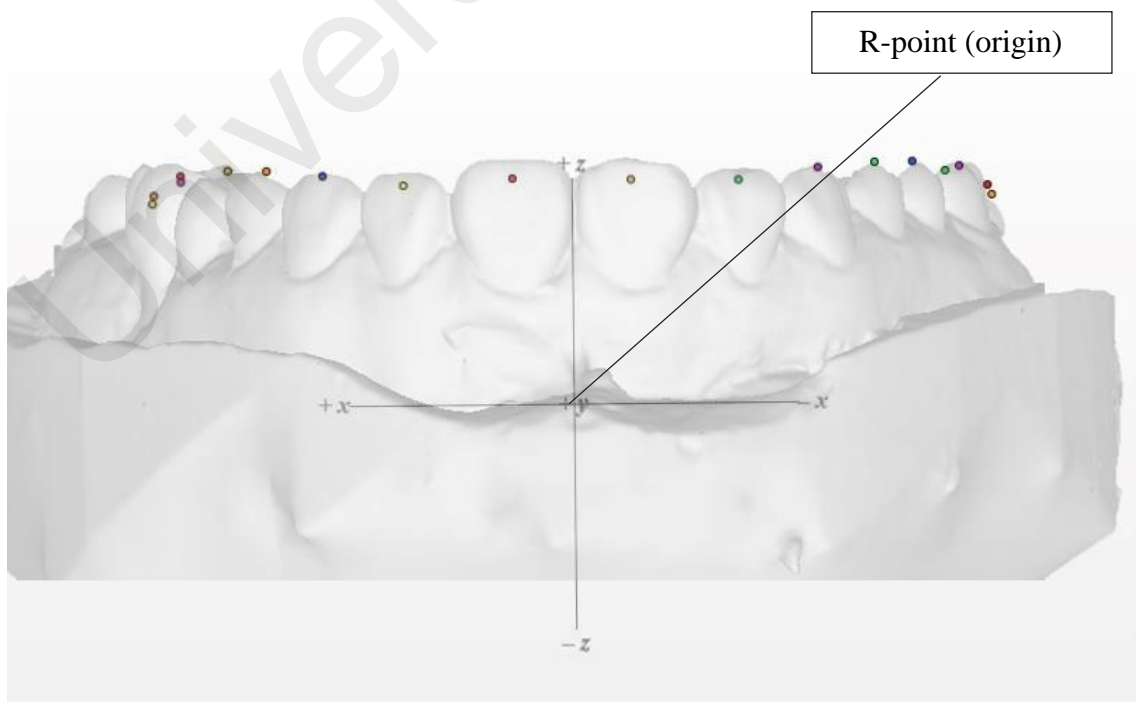


**Figure 4.2: Frontal view of average of 3D tooth position points for dentate sample plotted on Cartesian graph**

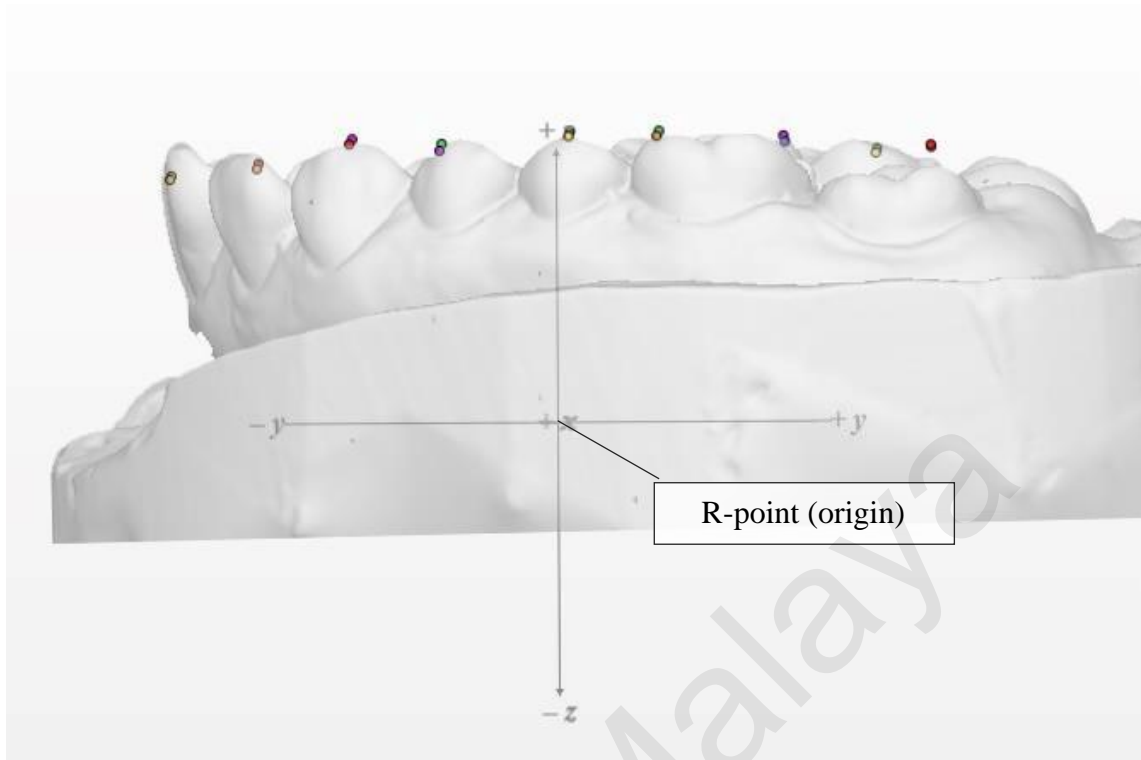


**Figure 4.3: Right side view of average 3D tooth position points for dentate sample plotted on Cartesian graph**

An interactive online visualisation of the mean values of Cartesian coordinates for teeth position in control dentate sample that is shown in (Table 4.2) and (Figures 4.1, 4.2 & 4.3) is plotted in a free 3D plotting website and are available online at the following online link:

< <https://bit.ly/2IolmmP> >.

#### 4.2.1.2 Spherical coordinates

Tables 4.3 and 4.4 are showing the same coordinates presented in Tables 4.1 and 4.2 but in spherical coordinates elements ( $\ell$ ,  $\theta$ ,  $\varphi$ ). The first element was measured by millimetres, while the second and third were measured by degrees for angles. These coordinates were representing the same points or location of the points in relation to the R-point as origin (0, 0, 0). The mean  $\ell$  for IP is 16.07 which represented the straight 3D (shortest real) distance between IP and

R-point, the mean  $\theta$  coordinate was 90 degrees as it should always be measured from +ve side of the X axis (Figure 4.4) and the  $\varphi$  coordinate which was measured in degree represented the elevation of the point from zenith (Figure 3.30). Both  $\theta$  angles of LHN and RHN were 301 and 237 degrees.

**Table 4.3: Means and standard deviations of the spherical coordinates ( $\ell$ ,  $\theta$ ,  $\varphi$ ) of the biometric triangular pyramid points**

Point	$\ell$ mm Mean (SD)	$\theta$ ° Mean (SD)	$\varphi$ ° Mean (SD)
IP	16.07 (2.20)	90 (0.00)	39.25 (5.67)
R-point	0 (0.00)	0 (0.00)	0 (0.00)
LHN	42.06 (2.58)	301.88 (3.14)	13.94 (2.51)
RHN	42.23 (2.55)	237.72 (3.07)	13.89 (2.50)
HNIP- height	10.16 (1.65)	0 (0.00)	90 (0.00)

**Table 4.4: Means and standard deviations of the spherical coordinates ( $\ell$ ,  $\theta$ ,  $\varphi$ ) that represent the location of the teeth and landmarks in relevance to the origin (R-point)**

Point	$\ell$ mm Mean (SD)	$\theta$ ° Mean (SD)	$\varphi$ ° Mean (SD)
LCI	27.50 (2.49)	78.81 (1.91)	36.12 (5.30)
LLI	27.21 (2.28)	56.72 (3.86)	35.32 (5.05)
LC	27.63 (1.98)	36.52 (5.50)	36.39 (4.60)
RCI	27.55 (2.44)	100.87 (1.85)	36.19 (5.18)
RLI	27.22 (2.24)	122.60 (3.65)	35.60 (4.87)
RC	27.61 (2.02)	143.08 (5.29)	36.95 (4.42)
L1PM	28.24 (1.51)	14.90 (6.51)	36.40 (4.49)
L2PM	29.85 (1.58)	357.60 (6.17)	34.15 (4.23)
LMb1M	32.32 (1.67)	345.86 (5.51)	29.78 (4.06)
LDb1M	34.53 (1.80)	336.64 (5.07)	28.25 (3.81)
LMb2M	37.75 (1.89)	329.56 (4.78)	23.37 (3.63)
LDb2M	40.28 (2.13)	322.89 (4.23)	21.04 (3.57)
R1PM	28.17 (1.65)	164.55 (6.13)	36.86 (4.37)

<b>R2PM</b>	29.76 (1.63)	181.87 (6.07)	34.69 (4.19)
<b>RMb1M</b>	32.11 (1.81)	194.02 (5.22)	30.28 (3.84)
<b>RDb1M</b>	34.46 (1.88)	203.34 (4.77)	28.53 (3.60)
<b>RMb2M</b>	27.74 (2.00)	210.30 (4.42)	32.66 (3.26)
<b>RDb2M</b>	40.38 (2.17)	216.76 (4.03)	21.04 (3.32)

\*The mean and standard deviation of the measurements (in mm) and angles (in degrees)

The rose chart in Figure 4.4 is showing visual representation of the statistical finding of the angular data of the control group in directions, quantity and range of minimum and maximum values. The colours are representing each tooth as the legend, the length of the petal or fan represents the number of sample and the width of the petal represents the range of the measured angles.

Universiti Malaysia

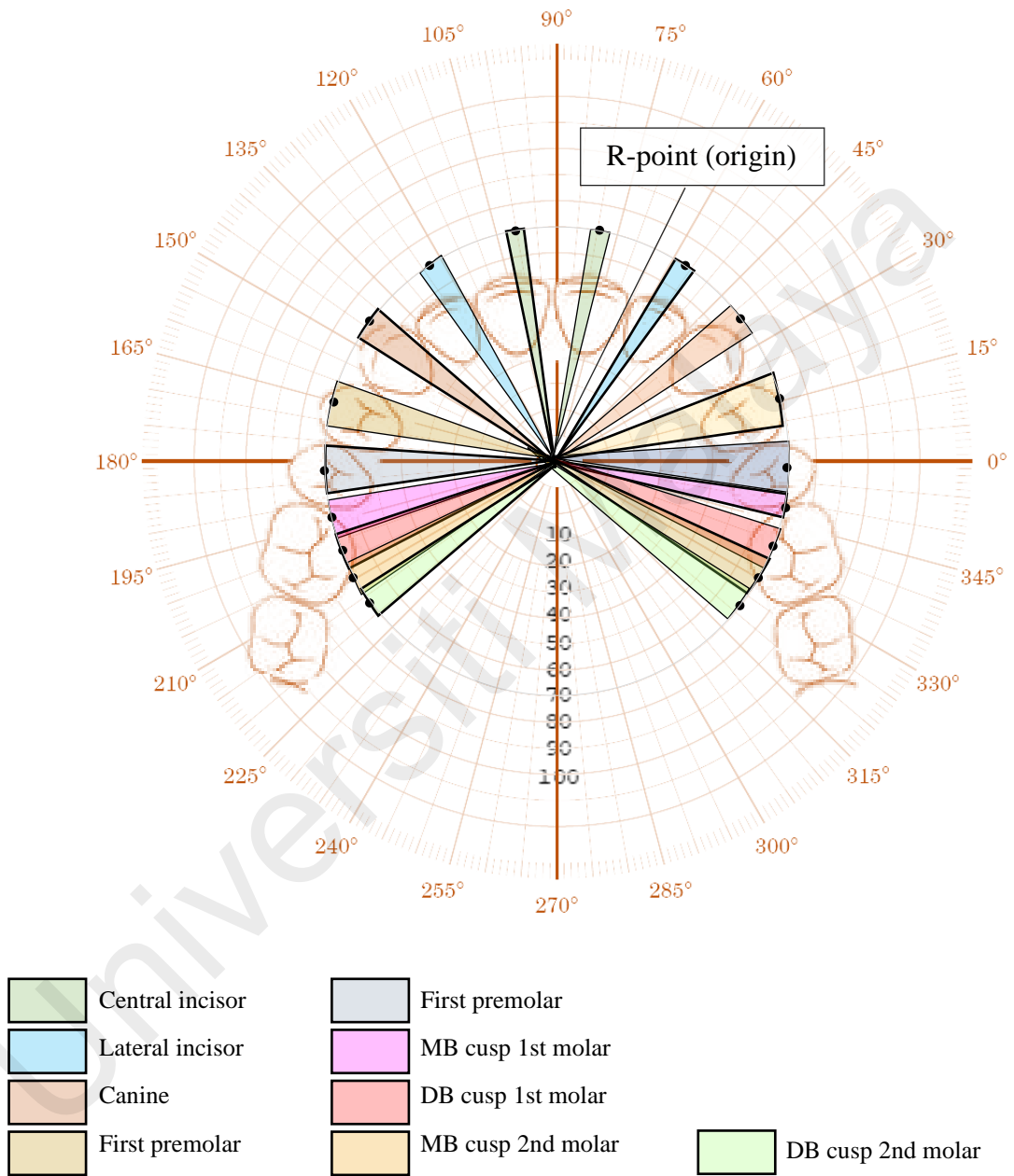


**Figure 4.4: Rose graph showing the means and standard deviations of the azimuth angles measured in experiment dentate group (n = 70)**

## 4.2.2 Analysis to determine position of teeth in dentate subjects

This section was described as three parts: the radius distance, the azimuth angle and the elevation angle determination analysis.

### 4.2.2.1 The radius coordinate analysis of the teeth

#### (a) *Testing correlations before regression*

Scatter plots and correlations between the variables were tested as described in chapter 3.

The high correlation coefficients may indicate relationships between the variables. Table 4.5 displayed correlations between the potential predictors (independent variables) and the dependent variables namely the teeth position radial distance parameter (first coordinate in spherical system). The correlations were evaluated based on the proximity of the coefficient to negative or positive 1 (i.e., the closer the value of correlation to 1, the stronger the correlation existing). The weak correlations were decided for those having  $p$  values less than 0.5. Therefore, Table 4.6 was created to specify the parameters that were showing acceptable correlations ( $p \geq 0.5$ ) only and may be used to further investigate the relationship by using regression analysis.

The correlations tested were also verified for any multicollinearity. The multicollinearity is able to identify if false position correlation exists between the variables through the value of VIF. Variables found with weak correlations or high (VIF > 4) in Table 4.6 were excluded and not selected for further investigation as they already projected weak relationships.

**Table 4.5: Pearson correlation coefficient values for correlation analysis between the teeth radial distance and landmarks measurements**

predictor toothℓ	IP-ℓ mm	LHN-ℓ mm	RHN-ℓ mm	HNIP- height mm
<b>LCI ℓ</b>	0.879 *	-0.157	-0.057	0.568 †
<b>LLI ℓ</b>	0.876 *	-0.138	-0.081	0.605 †
<b>LC ℓ</b>	0.831 *	-0.083	-0.032	0.653 †
<b>L1PM ℓ</b>	0.683 *	0.010	0.002	0.584 *
<b>L2PM ℓ</b>	0.343 †	0.251	0.197	0.536 *
<b>LMb1M ℓ</b>	0.151 †	0.390 *	0.367 †	0.406 *
<b>LDb1M ℓ</b>	0.026	0.496 *	0.464 †	0.349 *
<b>LMb2M ℓ</b>	-0.039	0.569 *	0.543 †	0.291 *
<b>LDb2M ℓ</b>	-0.080	0.605 *	0.579 †	0.261 *
<b>RCI ℓ</b>	0.899 *	-0.158	-0.063	0.584 †
<b>RLI ℓ</b>	0.888 *	-0.143	-0.036	0.616 †
<b>RC ℓ</b>	0.810 *	-0.088	0.025	0.612 †
<b>R1PM ℓ</b>	0.629 *	0.047	0.189	0.539 *
<b>R2PM ℓ</b>	0.347 †	0.209	0.338 *	0.458 *
<b>RMb1M ℓ</b>	0.149	0.332 †	0.469 *	0.381 *
<b>RDb1M ℓ</b>	0.057	0.423 †	0.566 *	0.327 *
<b>RMb2M ℓ</b>	0.046	0.505 †	0.663 *	0.294 *
<b>RDb2M ℓ</b>	-0.005	0.562 †	0.701 *	0.256 *

\* Statistically significant correlation ( $p < 0.05$ )

† Multicollinearity (high VIF)

In Table 4.3, some variables had weak correlations such as the radial distance of left central incisor (LCI ℓ) with the radial distance of right hamular notch (RHN-ℓ), their correlation coefficient was -0.057, while other pairs of variables were found with strong correlation such as LCI ℓ and radian distance of incisive papilla (IP-ℓ) who had correlation coefficient of 0.879 with no multicollinearity. Notice that the negative value

of coefficient indicates negative relationship and weakness in relationship is indicated by value close to 0.

**Table 4.6: Summary of one or more predictors out of Table 4.5 that are eligible and recommended to use for regression relationship analysis to find the radius ( $\ell$ ) values for the teeth**

predictor tooth $\ell$	IP- $\ell$	LHN- $\ell$	RHN- $\ell$	HNIP- height
LCI $\ell$	✓	-	-	-
LLI $\ell$	✓	-	-	-
LC $\ell$	✓	-	-	-
L1PM $\ell$	✓	-	-	✓
L2PM $\ell$	-	-	-	✓
LMb1M $\ell$	-	✓	-	✓
LDb1M $\ell$	-	✓	-	✓
LMb2M $\ell$	-	✓	-	✓
LDb2M $\ell$	-	✓	-	✓
RCI $\ell$	✓	-	-	-
RLI $\ell$	✓	-	-	-
RC $\ell$	✓	-	-	-
R1PM $\ell$	✓	-	-	✓
R2PM $\ell$	-	-	✓	✓
RMb1M $\ell$	-	-	✓	✓
RDb1M $\ell$	-	-	✓	✓
RMb2M $\ell$	-	-	✓	✓
RDb2M $\ell$	-	-	✓	✓

✓ Eligible variables to proceed with regression analysis concluded from Table 4.5

In Table 4.6, each posterior tooth radial coordinate except L2PM  $\ell$  was presented good correlation with at least two predictors for regression relationship analysis. While the coordinate of the anterior teeth and L2PM  $\ell$  were correlated with one predictor for each.

(b) *Performing regression analysis to determine the relationship*

Regression analyses were performed to investigate the relationship between the predictor variables and the radius coordinate of each tooth. Eighteen simple and multiple statistical regression models (equations) were produced (Tables 4.7 and 4.8) using the eligible predictor(s) listed in Table 4.6 to predict the first spherical coordinate ( $\ell$ ) for the teeth. The coefficients of determinations  $R^2$ s and Variation inflation factors (VIF) were also listed beside every regression equation for reference.

**Table 4.7: Weighted simple regression models, coefficients of determination and variance inflation factors for predicting the radial element ( $\ell$ ) of spherical coordinates for maxillary left and right of anterior teeth points in relevance to R-point**

Regression models of anterior teeth	$R^2$	VIF**
$LCI_{\ell} = 10.9784 + 1.024 IP. \ell$	0.9801 *	1.00
$LLI_{\ell} = 12.208 + 0.9315 IP. \ell$	0.9418 *	1.00
$LC_{\ell} = 14.869 + 0.7904 IP. \ell$	0.9581 *	1.00
$RCI_{\ell} = 11.453 + 1.0008IP. \ell$	0.9917 *	1.00
$RLL_{\ell} = 12.521 + 0.91126 IP. \ell$	0.9996 *	1.00
$RC_{\ell} = 15.726 + 0.7318 IP. \ell$	0.9724 *	1.00

$R^2$  is the coefficient of determination (% of predictability)

\*Regression  $p < 0.001$

\*\*individual VIF > 4 indicate multicollinearity

In Figure 4.7 the best regression models for anterior teeth are listed, after filtering the predictors that showed multicollinearity (high VIF value). Interestingly, the radial distance of IP exhibited the strongest predictor for the radial distances of anterior teeth. The power of regression model is measured by the coefficient of determination  $R^2$ , the  $R^2$ s in Table 4.7 were higher than 0.9 with highest in regression model of right lateral

incisor tooth RCI  $\ell$  (0.999). The model was accepted to be true when the VIF is not high and considered for further verification before implementation.

**Table 4.8: Weighted simple and multiple regression models, coefficients of determination and variance inflation factors for predicting the radial element ( $\ell$ ) of spherical coordinates for the maxillary left and right posterior teeth points in relevance to R-point**

Weighted multiple linear regression models for maxillary posterior teeth distance to R-point	$R^2$ *	VIF**
$L1PM_{\ell} = 20.508 + 0.3667 IP.\ell + 0.1759HNIP.R$	0.911 *	1.51 1.51
$L2PM_{\ell} = 24.486 + 0.5256 HNIP.R$	0.9117 *	1.00
$LMb1M_{\ell} = 19.202 + 0.3731 HNIP.R + 0.2219 LHN.\ell$	0.9213 *	1.00 1.00
$LDb1M_{\ell} = 17.598 + 0.3363 HNIP.R + 0.3232LHN.\ell$	0.8993 *	1.31 1.31
$LMb2M_{\ell} = 18.066 + 0.28255HNIP.R + 0.40042LHN.\ell$	0.9986 *	3.21 3.21
$LDb2M_{\ell} = 17.335 + 0.2899 HNIP.R + 0.475LHN.\ell$	0.9848 *	1.01 1.01
$R1PM_{\ell} = 20.721 + 0.3350 IP.\ell + 0.2037HNIP.R$	0.9075*	1.13 1.13
$R2PM_{\ell} = 16.056 + 0.4682 HNIP.R + 0.21359RHN.\ell$	0.8909 *	1.22 1.22
$RMb1M_{\ell} = 14.365 + 0.4554 HNIP.R + 0.3096 RHN.\ell$	0.9404 *	1.01 1.01
$RDb1M_{\ell} = 12.577 + 0.3798 HNIP.R + 0.42715 RHN.\ell$	0.9928 *	1.03 1.03
$RMb2M_{\ell} = 10.065 + 0.3512 HNIP.R + 0.5714 RHN.\ell$	0.9859 *	1.46 1.46
$RDb2M_{\ell} = 9.953 + 0.3606 HNIP.R + 0.6335 RHN.\ell$	0.9543 *	3.42 3.42

$R^2$  is the coefficient of determination (% of predictability)

\*Regression  $p < 0.001$

\*\*individual VIF > 4 indicate multicollinearity

In Table 4.8, all the generated models showed high coefficients of determinations values  $R^2$  (0.899 – 0.998). The closer the  $R^2$  value is to 1, the stronger the relationship and the more powerful the mathematical model to predict the dependent variable from the independent one. However, these relationships could be unreal until VIF is used to verify the true effect of the predictor to produce the dependent variable. Only the model that predicted the

radial coordinate of L2PM had a simple regression model; the abbreviation HNIP.R was used in models to represent the HNIP-height from R-point.

(c) *The verification of radial element prediction*

Tables 4.9 and 4.10 described the mean values and standard deviations of spherical coordinates of the biometric triangular pyramid and the teeth of the second subgroup of dentate sample (the verification group). This group of dentate data was used to perform the verification of the determined mathematical relationships to assure the reproducibility and accuracy of the models in predicting the radial coordinates.

**Table 4.9: Descriptive statistics, means and standard deviations of the spherical coordinates ( $\ell$ ,  $\theta$ ,  $\varphi$ ) of the biometric triangular pyramid points of the verification sample (n = 22)**

Point	$\ell$ mm Mean (SD)	$\theta$ ° Mean (SD)	$\varphi$ ° Mean (SD)
IP	15.16 (2.20)	90 (0.00)	40.76 (5.17)
R-point	0 (0.00)	0 (0.00)	0 (0.00)
LHN	42.05 (2.41)	302.06 (3.21)	13.66 (2.77)
RHN	42.60 (2.25)	237.36 (2.83)	13.46 (2.77)
HNIP-height	9.86 (1.73)	0 (0.00)	90 (0.00)

**Table 4.10: Descriptive statistics of the spherical coordinates ( $\rho$ ,  $\theta$ ,  $\phi$ ) that represent the location of the teeth and landmarks with relevance to the origin (R-point) in the verification sample (n = 22)**

Point	$\rho$ mm Mean (SD)	$\theta$ ° Mean (SD)	$\phi$ ° Mean (SD)
LCI	26.73(2.51)	78.39 (1.75)	37.07 (5.64)
LLI	26.54(2.34)	55.80 (3.84)	36.20 (5.13)
LC	27.18(1.93)	35.31 (5.57)	37.32 (5.46)
RCI	26.79(2.42)	101.04 (2.10)	37.05 (5.76)
RLI	26.60(2.26)	123.20 (3.63)	35.90 (5.50)
RC	27.27(2.18)	143.54 (5.16)	36.63 (5.17)
L1PM	27.97(1.51)	13.36 (5.74)	36.62 (5.22)
L2PM	29.76(1.51)	356.41 (4.99)	33.83 (5.16)
LMb1M	32.20(1.79)	345.02 (4.69)	29.68 (4.66)
LDb1M	34.35(1.91)	336.03 (3.98)	27.85 (4.60)
LMb2M	37.66(1.95)	329.16 (4.05)	23.22 (4.57)
LDb2M	40.39(2.20)	322.55 (3.81)	21.19 (4.14)
R1PM	27.95(1.75)	164.90 (5.65)	36.23 (5.54)
R2PM	29.67(1.35)	181.89 (5.26)	33.53 (5.11)
RMb1M	32.25(1.39)	193.49 (4.69)	29.28 (4.79)
RDb1M	34.59(1.45)	202.68(4.27)	27.31 (4.43)
RMb2M	38.04(1.34)	209.14(3.55)	22.96 (3.84)
RDb2M	40.71(1.63)	215.50 (3.28)	20.60 (3.81)

In order to confirm how feasible and how reasonable the prediction of the equations established in this study, coordinates of teeth positions were predicted for the independent sample (the verification group) composed of 22 dentate subjects and comparison between the predicted coordinates and the observed coordinates of the existing natural teeth were measured in the same sample. The predicted coordinates were calculated using the anatomical information/measurements obtained from the cast's biometric triangular pyramid. The comparison was set to test the hypothesis of having difference between the

means of predicted and measured coordinates = 0 within critical value of 0.05. Table 4.11 shows that all the calculated  $p$ -values were found larger than the critical values (0.05). therefore, conclusion can be driven to reject the null hypothesis and support the hypothesis that assumes the difference between the means = 0.

**Table 4.11: Means, standard deviations and  $p$ -values of paired  $t$ -tests comparing the predicted and measured radial coordinates ( $\ell$ ) values of the verification new dentate group (n = 22)**

Tooth	Measured $\ell mm$ mean (SD)	Predicted $\ell mm$ mean (SD)	$p$ -value*
<b><i>LCI<math>_{\ell}</math></i></b>	26.73(2.51)	26.51(2.20)	0.378
<b><i>LLI<math>_{\ell}</math></i></b>	26.54(2.34)	26.33(2.00)	0.388
<b><i>LC<math>_{\ell}</math></i></b>	27.18(1.93)	26.85(1.70)	0.196
<b><i>RCI<math>_{\ell}</math></i></b>	26.79(2.42)	26.63(2.15)	0.506
<b><i>RLI<math>_{\ell}</math></i></b>	26.60(2.26)	26.34(1.96)	0.315
<b><i>RC<math>_{\ell}</math></i></b>	27.27(2.18)	26.82(1.57)	0.147
<b><i>L1PM<math>_{\ell}</math></i></b>	27.97(1.51)	27.80(1.04)	0.431
<b><i>L2PM<math>_{\ell}</math></i></b>	29.76(1.51)	29.67(0.89)	0.780
<b><i>LMB1M<math>_{\ell}</math></i></b>	32.20(1.79)	32.21(0.72)	0.978
<b><i>LDb1M<math>_{\ell}</math></i></b>	34.35(1.91)	34.51(0.84)	0.646
<b><i>LMB2M<math>_{\ell}</math></i></b>	37.66(1.95)	37.69(0.95)	0.935
<b><i>LDb2M<math>_{\ell}</math></i></b>	40.39(2.20)	40.17(1.11)	0.552
<b><i>R1PM<math>_{\ell}</math></i></b>	27.95(1.75)	27.81(1.02)	0.625
<b><i>R2PM<math>_{\ell}</math></i></b>	29.67(1.35)	29.77(0.83)	0.654
<b><i>RMb1M<math>_{\ell}</math></i></b>	32.25(1.39)	32.05(0.92)	0.406
<b><i>RDb1M<math>_{\ell}</math></i></b>	34.59(1.45)	34.52(1.03)	0.787
<b><i>RMb2M<math>_{\ell}</math></i></b>	38.04(1.34)	37.87(1.28)	0.540
<b><i>RDb2M<math>_{\ell}</math></i></b>	40.71(1.63)	40.50(1.41)	0.525

\*  $p \geq 0.05$  indicates insufficient evidence to conclude that the means differ significantly at a critical value of 0.05

#### 4.2.2.2 The azimuth angle determination

**Table 4.12: Functional linear relationship models for predicting the azimuth angle ( $\theta$ ) spherical coordinate measured in radians for the left and right anterior and posterior maxillary teeth positions in relation to R-point**

<b>Tooth (abbrev)</b>	<b>Simple linear functional relationship models to find <math>\theta</math></b>
<b><i>LCI<math>_{\theta}</math></i></b>	<i>LCI <math>\theta = 2.3891 + LHN \theta \pmod{2\pi}</math></i>
<b><i>LLI<math>_{\theta}</math></i></b>	<i>LLI <math>\theta = 2.0061 + LHN \theta \pmod{2\pi}</math></i>
<b><i>LC<math>_{\theta}</math></i></b>	<i>LC <math>\theta = 1.6554 + LHN \theta \pmod{2\pi}</math></i>
<b><i>RCI<math>_{\theta}</math></i></b>	<i>RCI <math>\theta = 3.8918 + RHN \theta \pmod{2\pi}</math></i>
<b><i>RLI<math>_{\theta}</math></i></b>	<i>RLI <math>\theta = 4.2689 + RHN \theta \pmod{2\pi}</math></i>
<b><i>RC<math>_{\theta}</math></i></b>	<i>RC <math>\theta = 4.6271 + RHN \theta \pmod{2\pi}</math></i>
<b><i>L1PM<math>_{\theta}</math></i></b>	<i>L1PM <math>\theta = 1.2798 + LHN \theta \pmod{2\pi}</math></i>
<b><i>L2PM<math>_{\theta}</math></i></b>	<i>L2PM <math>\theta = 0.9760 + LHN \theta \pmod{2\pi}</math></i>
<b><i>LMb1M<math>_{\theta}</math></i></b>	<i>LMb1M <math>\theta = 0.7690 + LHN \theta \pmod{2\pi}</math></i>
<b><i>LDb1M<math>_{\theta}</math></i></b>	<i>LDb1M <math>\theta = 0.6069 + LHN \theta \pmod{2\pi}</math></i>
<b><i>LMb2M<math>_{\theta}</math></i></b>	<i>LMb2M <math>\theta = 0.4822 + LHN \theta \pmod{2\pi}</math></i>
<b><i>LDb2M<math>_{\theta}</math></i></b>	<i>LDb2M <math>\theta = 0.3655 + LHN \theta \pmod{2\pi}</math></i>
<b><i>R1PM<math>_{\theta}</math></i></b>	<i>R1PM <math>\theta = 2.7792 + RHN \theta \pmod{2\pi}</math></i>
<b><i>R2PM<math>_{\theta}</math></i></b>	<i>R2PM <math>\theta = 5.3065 + RHN \theta \pmod{2\pi}</math></i>
<b><i>RMb1M<math>_{\theta}</math></i></b>	<i>RMb1M <math>\theta = 5.5215 + RHN \theta \pmod{2\pi}</math></i>
<b><i>RDb1M<math>_{\theta}</math></i></b>	<i>RDb1M <math>\theta = 5.6850 + RHN \theta \pmod{2\pi}</math></i>
<b><i>RMb2M<math>_{\theta}</math></i></b>	<i>RMb2M <math>\theta = 5.8090 + RHN \theta \pmod{2\pi}</math></i>
<b><i>RDb2M<math>_{\theta}</math></i></b>	<i>RDb2M <math>\theta = 5.9225 + RHN \theta \pmod{2\pi}</math></i>

Simple linear functional relationship models were used with circular data to find the simplest effective relationship method that can predict the angles from each other. The relationship between the azimuth angles of the maxillary teeth and the azimuth angles of the biometric triangular pyramid points were determined and represented in Table 4.12. the left hamular notch azimuth angle  $LHN \theta$  was used to predict the left side teeth azimuth

angles and the right hamular notch angle RHN  $\theta$  to predict the right-side teeth angles  $\theta$  of teeth. The equations (models) are having their constants and the angles used for these questions must be in rad units. Therefore,  $\text{mod } 2\pi$  was used to adjust the angles to fit the models.

(a) *Verification of azimuth angles prediction*

In Table 4.13, the first column is showing the measured azimuth angles' ( $\theta$ ) mean values and the standard deviations for the of the teeth of the verification group as listed shown in Table 4.10 versus the mean of predicted corresponding values of azimuth angles ( $\theta$ ) for the same sample individuals using the predictors in equations listed in the middle column. Note the similarity between the mean values for each tooth. Paired  $t$ -test was performed to assure the similarity statistically and  $p$ - values were listed for each value in the third column of Table 4.13. if  $p$ -value for  $t$ -test was less than 0.05 the two means were considered having significant difference (difference between means  $\neq 0$ ).

**Table 4.13: Means, standard deviations and  $p$ -values of paired  $t$ -test comparing the predicted and measured values of the azimuth angle spherical coordinate ( $\theta$ ) of the verification new dentate group (n = 22)**

<b>Tooth</b>	<b>Measured <math>\theta^\circ</math> mean (SD)</b>	<b>Predicted <math>\theta^\circ</math> mean (SD)</b>	<b><math>p</math>-value*</b>
<b><math>LCI_\theta</math></b>	78.39 (1.75)	78.24 (2.92)	0.814
<b><math>LLI_\theta</math></b>	55.80 (3.84)	56.29 (2.92)	0.611
<b><math>LC_\theta</math></b>	35.31 (5.57)	36.20 (2.92)	0.500
<b><math>RCI_\theta</math></b>	101.04 (2.10)	100.35 (2.83)	0.331
<b><math>RLI_\theta</math></b>	123.20 (3.63)	121.95 (2.83)	0.173
<b><math>RC_\theta</math></b>	143.54 (5.16)	142.47 (2.83)	0.371
<b><math>L1PM_\theta</math></b>	13.36 (5.74)	14.68 (2.92)	0.337
<b><math>L2PM_\theta</math></b>	356.41 (4.99)	357.27(2.92)	0.405
<b><math>LMb1M_\theta</math></b>	345.02 (4.69)	345.41 (2.92)	0.737
<b><math>LDb1M_\theta</math></b>	336.03 (3.98)	336.12 (2.92)	0.927
<b><math>LMb2M_\theta</math></b>	329.16 (4.05)	328.98 (2.92)	0.844
<b><math>LDb2M_\theta</math></b>	322.55 (3.81)	322.29 (2.92)	0.784
<b><math>R1PM_\theta</math></b>	164.90 (5.65)	165.10 (2.29)	0.786
<b><math>R2PM_\theta</math></b>	181.89 (5.26)	188.39 (2.83)	0.680
<b><math>RMb1M_\theta</math></b>	193.49 (4.69)	193.72 (2.83)	0.827
<b><math>RDb1M_\theta</math></b>	202.68(4.27)	203.08(2.83)	0.671
<b><math>RMb2M_\theta</math></b>	209.14(3.55)	210.19(2.83)	0.199
<b><math>RDb2M_\theta</math></b>	215.50 (3.28)	216.69(2.83)	0.105

\*  $p \geq 0.05$  indicate insufficient evidence to conclude that the means differ at the 0.05 level of significance

Based on Table 4.13 ,none of the paired  $t$ -tests had a  $p$ -value equal or less than the critical value of the test (0.05).

#### 4.2.2.3 Elevation angle determination

Similar to the determination and calculation of the azimuth angle in 4.2.2.2, the relationship between the elevation angles ( $\varphi$ ) of the biometric triangular pyramid points were investigated and Simple linear functional relationship models were used for the circular data to find the effective relationship that can predict the elevation angles from the independent variables. As shown in Table 4.14, the left hamular notch elevation angle (LHN  $\varphi$ ) helped to predict the elevation angles of the left side teeth and the right hamular notch angle RHN  $\varphi$  to predict the angles for the right-side teeth angles  $\theta$  of teeth. The equations (models) must be using angles in rad units. Therefore,  $mod2\pi$  was also needed.

Universiti Malaysia

**Table 4.14: Functional linear relationship models for predicting the elevation angle ( $\varphi$ ) spherical coordinate measured in radians for the left and right anterior and posterior maxillary teeth positions in relation to R-point**

<b>Tooth</b>	<b>Simple linear functional relationship model to find <math>\varphi</math></b>
<b><i>LCI</i><sub><math>\varphi</math></sub></b>	<i>LCI</i> $\varphi = 0.3802 + LHN \varphi \pmod{2\pi}$
<b><i>LLI</i><sub><math>\varphi</math></sub></b>	<i>LLI</i> $\varphi = 0.3668 + LHN \varphi \pmod{2\pi}$
<b><i>LC</i><sub><math>\varphi</math></sub></b>	<i>LC</i> $\varphi = 0.3850 + LHN \varphi \pmod{2\pi}$
<b><i>RCI</i><sub><math>\varphi</math></sub></b>	<i>RCI</i> $\varphi = 0.3821 + RHN \varphi \pmod{2\pi}$
<b><i>RLI</i><sub><math>\varphi</math></sub></b>	<i>RLI</i> $\varphi = 0.3749 + RHN \varphi \pmod{2\pi}$
<b><i>RC</i><sub><math>\varphi</math></sub></b>	<i>RC</i> $\varphi = 0.4018 + RHN \varphi \pmod{2\pi}$
<b><i>L1PM</i><sub><math>\varphi</math></sub></b>	<i>L1PM</i> $\varphi = 0.3891 + LHN \varphi \pmod{2\pi}$
<b><i>L2PM</i><sub><math>\varphi</math></sub></b>	<i>L2PM</i> $\varphi = 0.3528 + LHN \varphi \pmod{2\pi}$
<b><i>LMb1M</i><sub><math>\varphi</math></sub></b>	<i>LMb1M</i> $\varphi = 0.2754 + LHN \varphi \pmod{2\pi}$
<b><i>LDb1M</i><sub><math>\varphi</math></sub></b>	<i>LDb1M</i> $\varphi = 0.2502 + LHN \varphi \pmod{2\pi}$
<b><i>LMb2M</i><sub><math>\varphi</math></sub></b>	<i>LMb2M</i> $\varphi = 0.1639 + LHN \varphi \pmod{2\pi}$
<b><i>LDb2M</i><sub><math>\varphi</math></sub></b>	<i>LDb2M</i> $\varphi = 0.1215 + LHN \varphi \pmod{2\pi}$
<b><i>R1PM</i><sub><math>\varphi</math></sub></b>	<i>R1PM</i> $\varphi = 0.4022 + RHN \varphi \pmod{2\pi}$
<b><i>R2PM</i><sub><math>\varphi</math></sub></b>	<i>R2PM</i> $\varphi = 0.3670 + RHN \varphi \pmod{2\pi}$
<b><i>RMb1M</i><sub><math>\varphi</math></sub></b>	<i>RMb1M</i> $\varphi = 0.2893 + RHN \varphi \pmod{2\pi}$
<b><i>RDb1M</i><sub><math>\varphi</math></sub></b>	<i>RDb1M</i> $\varphi = 0.2596 + RHN \varphi \pmod{2\pi}$
<b><i>RMb2M</i><sub><math>\varphi</math></sub></b>	<i>RMb2M</i> $\varphi = 0.1720 + RHN \varphi \pmod{2\pi}$
<b><i>RDb2M</i><sub><math>\varphi</math></sub></b>	<i>RDb2M</i> $\varphi = 0.1248 + RHN \varphi \pmod{2\pi}$

(a) *Verification study of elevation angle perdition*

Similar to the azimuth angle verification, the predicted elevation angles were verified by comparing them to the existing measured angles in the same sample. The left column has the measured elevation angles of the verification group.

Paired  $t$ -test was performed to test the similarity between the two mean values, the third column had  $p$ -values to compare with the critical value of 0.05 and conclude results. in Table 4.15, all the  $p$ -values were larger than 0.05 and there was no significant difference between the observed and measured means of elevation angles of all the 18 teeth tested.

Universiti Malaysia

**Table 4.15: Means (standard deviations) of the measured and predicted elevation angles for the teeth with  $p$ -values for paired  $t$ -test for each comparison between the angles  $\varphi$  with confidence interval of 95% for verification sample ( $n = 22$ )**

<b>Tooth</b>	<b>Measured <math>\varphi^\circ</math> mean (<i>SD</i>)</b>	<b>Predicted <math>\varphi^\circ</math> mean (<i>SD</i>)</b>	<b><math>p</math>-value*</b>
<b><i>LCI</i><math>\varphi</math></b>	37.07 (5.64)	35.44 (2.77)	0.098
<b><i>LLI</i><math>\varphi</math></b>	36.20 (5.13)	34.67 (2.77)	0.075
<b><i>LC</i><math>\varphi</math></b>	37.32 (5.46)	35.72 (2.77)	0.064
<b><i>RCI</i><math>\varphi</math></b>	37.05 (5.76)	35.36 (2.65)	0.098
<b><i>RLI</i><math>\varphi</math></b>	35.90 (5.50)	34.95 (2.65)	0.294
<b><i>RC</i><math>\varphi</math></b>	36.63 (5.17)	36.49 (2.65)	0.862
<b><i>L1PM</i><math>\varphi</math></b>	36.62 (5.22)	35.95 (2.77)	0.399
<b><i>L2PM</i><math>\varphi</math></b>	33.83 (5.16)	33.87 (2.77)	0.955
<b><i>LMb1M</i><math>\varphi</math></b>	29.68 (4.66)	29.43 (2.77)	0.709
<b><i>LDb1M</i><math>\varphi</math></b>	27.85 (4.60)	27.99 (2.77)	0.839
<b><i>LMb2M</i><math>\varphi</math></b>	23.22 (4.57)	23.05 (2.77)	0.787
<b><i>LDb2M</i><math>\varphi</math></b>	21.19 (4.14)	20.61 (2.77)	0.353
<b><i>R1PM</i><math>\varphi</math></b>	36.23 (5.54)	36.51 (2.65)	0.745
<b><i>R2PM</i><math>\varphi</math></b>	33.53 (5.11)	34.49 (2.65)	0.224
<b><i>RMb1M</i><math>\varphi</math></b>	29.28 (4.79)	30.04 (2.65)	0.281
<b><i>RDb1M</i><math>\varphi</math></b>	27.31 (4.43)	28.34 (2.65)	0.133
<b><i>RMb2M</i><math>\varphi</math></b>	22.96 (3.84)	23.32 (2.65)	0.519
<b><i>RDb2M</i><math>\varphi</math></b>	20.60 (3.81)	20.62 (2.65)	0.977

\*  $p \geq 0.05$  indicates insufficient evidence to conclude that difference between the means may exist at the level of 0.05 significance.

### 4.2.3 Determining maxillary teeth positions for the edentulous sample

The inclusion and exclusion criteria were verified for 34 patients (13 men and 21 women). The selected edentulous patient's mean and standard deviation age was 65.4( $\pm$ 7.2) years were found eligible and they agreed to participate in the study. Their age ranged between 42 and 81 years. The subjects' duration of being edentulous was 2 to 15 years (mean = 12.68 years). Descriptive statistics (mean and standard deviation) of spherical coordinates are shown in Table 4.16 for the biometric pyramid points used for predicting coordinates of the teeth. The same points are displayed in Table 4.18 but in Cartesian coordinates form.

Tables 4.16 -4.19 showed the mean (standard deviation) of the spherical and Cartesian coordinates of the predicted positions of the maxillary teeth for the edentulous group respectively.

**Table 4.16: Spherical coordinates of the biometric triangular pyramid of edentulous sample (n = 34) application sample**

<b>Point</b>	<b><math>\ell</math> mm Mean (SD)</b>	<b><math>\theta^\circ</math> Mean (SD)</b>	<b><math>\phi^\circ</math> Mean (SD)</b>
<b>IP</b>	13.85 (1.98)	90.00 (0.00)	31.40 (3.35)
<b>R-point</b>	0.00 (0.00)	0.00 (0.00)	0.00 (0.00)
<b>LHN</b>	41.46 (3.99)	304.08 (2.87)	10.04 (2.65)
<b>RHN</b>	41.29 (3.46)	236.34 (3.95)	10.09 (2.69)
<b>HNIP-height</b>	7.19 (1.85)	0.00 (0.00)	90 (0.00)

**Table 4.17: Predicted spherical coordinates for teeth position for edentulous sample (n = 34) application sample**

<b>Point</b>	<b><math>\ell</math> mm Mean (SD)</b>	<b><math>\theta^\circ</math> Mean (SD)</b>	<b><math>\phi^\circ</math> Mean (SD)</b>
<b>LCI</b>	25.16 (2.02)	80.96 (2.87)	31.81 (2.65)
<b>LLI</b>	24.83 (1.91)	59.02 (2.87)	31.05 (2.65)
<b>LC</b>	25.48 (1.61)	38.92 (3.87)	32.09 (2.65)
<b>RCI</b>	25.17 (2.06)	99.33 (3.95)	31.98 (2.69)
<b>RLI</b>	24.84 (1.88)	120.93 (3.95)	31.57 (2.69)
<b>RC</b>	25.37 (1.66)	141.46 (3.95)	33.11 (2.69)
<b>L1PM</b>	26.77 (1.10)	17.40 (2.87)	32.33 (2.65)
<b>L2PM</b>	28.31 (1.15)	359.99 (2.87)	30.25 (2.65)
<b>LMb1M</b>	31.10 (1.15)	348.14 (2.87)	25.82 (2.65)
<b>LDb1M</b>	33.33 (1.25)	338.85 (2.87)	24.37 (2.65)
<b>LMb2M</b>	36.61 (1.56)	331.71 (2.87)	19.42 (2.65)
<b>LDb2M</b>	39.06 (2.03)	325.02 (2.87)	16.99 (2.65)
<b>R1PM</b>	26.60 (1.22)	35.58 (3.95)	33.13 (2.69)
<b>R2PM</b>	28.04 (1.22)	180.38 (3.95)	31.11 (2.69)
<b>RMb1M</b>	30.44 (1.47)	192.71 (3.95)	26.66 (2.69)
<b>RDb1M</b>	32.74 (1.67)	202.07 (3.95)	24.96 (2.69)
<b>RMb2M</b>	35.62 (1.99)	209.18 (3.95)	19.94 (2.69)
<b>RDb2M</b>	38.69 (2.26)	215.68 (3.95)	17.24 (2.69)

**Table 4.18: Cartesian coordinates' means and standard deviations version of the biometric triangular pyramid for application sample (n = 34) of edentulous subjects**

Point	x mean (SD)	y mean (SD)	z mean (SD)
IP	0.01(0.32)	11.72(1.69)	7.22(1.83)
R	0 (0.00)	0 (0.00)	0 (0.00)
LHN	22.77(4.45)	-33.78(3.88)	7.19(1.86)
RHN	-22.36(4.38)	-33.78(3.88)	7.20(1.85)

**Table 4.19: Cartesian coordinates' means and standard deviations version of the predicted coordinates of teeth for application sample (n = 34) of edentulous subjects**

Point	x mean (SD)	y mean (SD)	z mean (SD)
LCI	3.34 (1.06)	21.03(1.36)	13.31 (1.91)
LLI	11.03 (1.06)	18.38(1.24)	12.99(1.81)
LC	16.95 (0.97)	13.70 (1.10)	13.74 (1.71)
RCI	-3.45 (1.43)	21.09 (1.35)	13.54 (1.91)
RLI	-10.95 (1.31)	18.29 (1.36)	13.2 (1.81)
RC	-16.86 (1.05)	13.44 (1.37)	14.15 (1.68)
L1PM	21.59 (0.56)	6.77 (1.09)	14.38 (1.51)
L2PM	24.35 (0.35)	-0.01 (1.22)	14.27 (1.58)
LMb1M	27.32 (0.95)	-5.76 (1.45)	13.55 (1.57)
LDb1M	28.32 (1.22)	-10.98 (1.67)	13.79 (1.65)
LMb2M	30.40 (1.42)	-16.40 (1.96)	12.20 (1.75)
LDb2M	30.56 (1.60)	-21.43 (2.22)	11.43 (1.86)
R1PM	-21.39 (0.59)	6.56 (1.49)	14.68 (1.53)
R2PM	-24.09 (0.87)	-0.19 (1.68)	14.61 (1.56)
RMb1M	-26.42 (1.05)	-6.00 (1.97)	13.67 (1.64)
RDb1M	-27.57 (1.28)	-11.23 (2.25)	13.91 (1.70)
RMb2M	-29.57 (1.62)	-16.58 (2.68)	12.34 (1.81)
RDb2M	-29.89 (1.76)	-21.55 (2.96)	11.47 (1.90)

Graphical 3D representation of the teeth positions' points was made available online in a free 3D plotting interactive website by plotting the points representing the measured positions of teeth for dentate from Table 4.2 and predicted points of teeth for edentulous that are shown in Table 4.19 (and Figures 4.5 - 4.7) in one graph at the following online link:

< <https://bit.ly/2WmyJsO> >

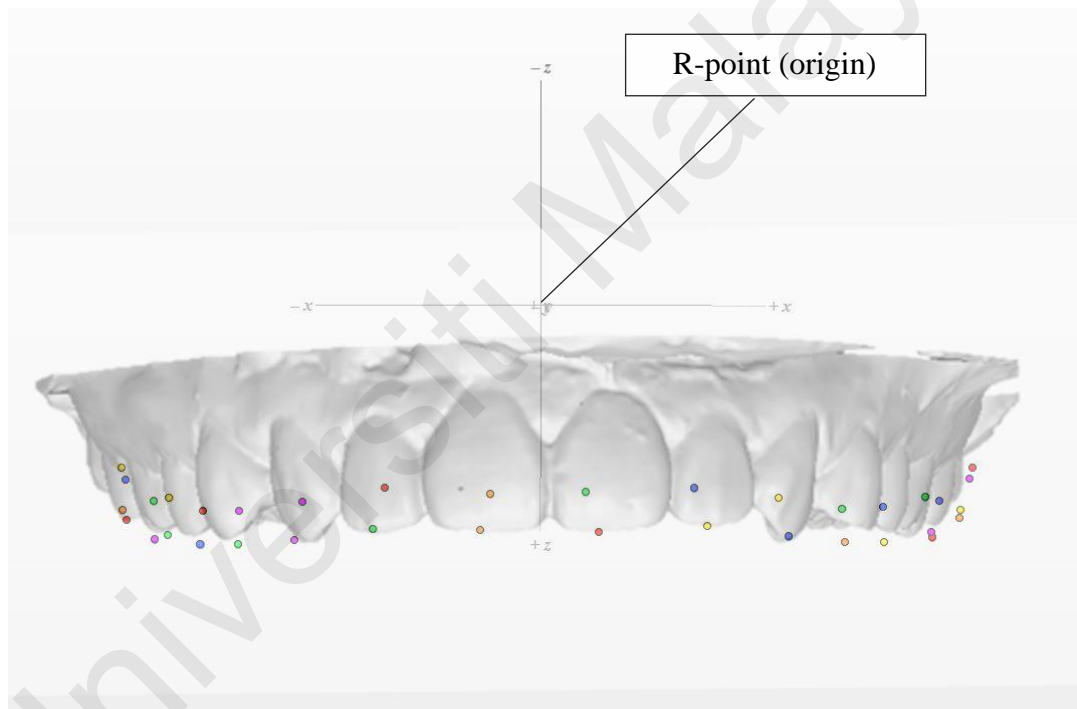


**Figure 4.5: Front view of average predicted 3D tooth position points for edentulous sample compared to dentate sample plotted on Cartesian graph**

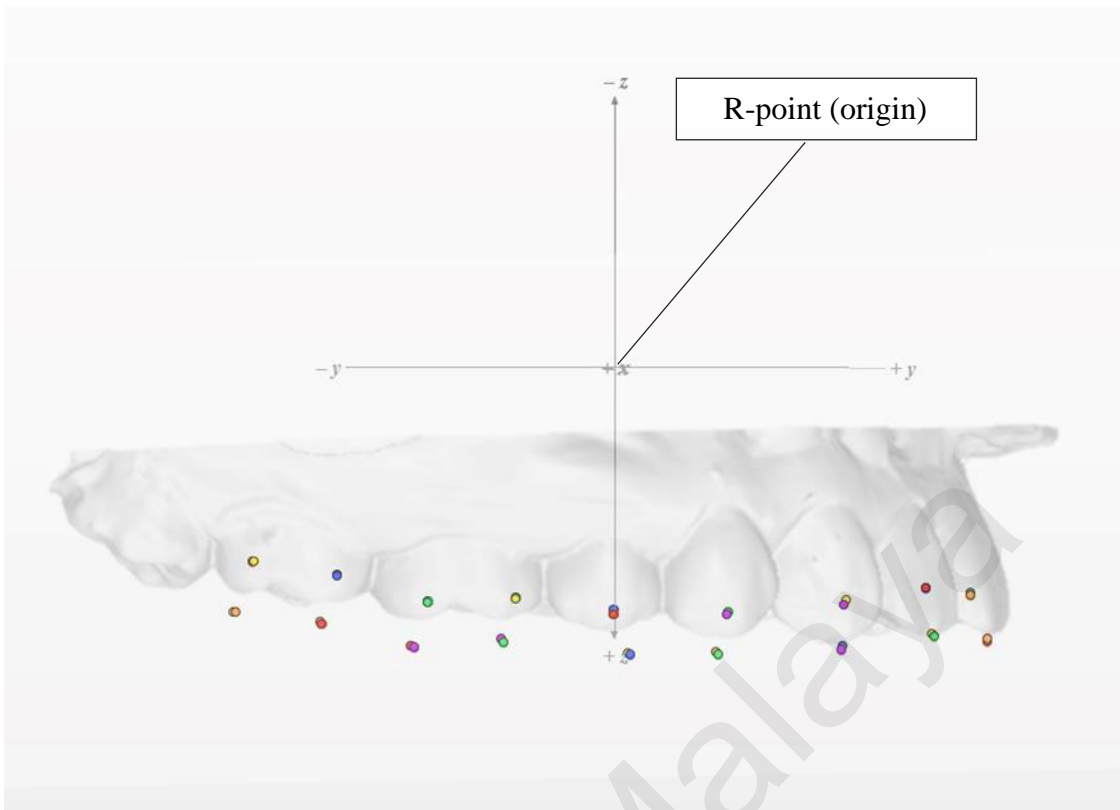


**Figure 4.6: Right side view of average predicted 3D tooth position points for edentulous sample compared to dentate sample plotted on Cartesian graph**

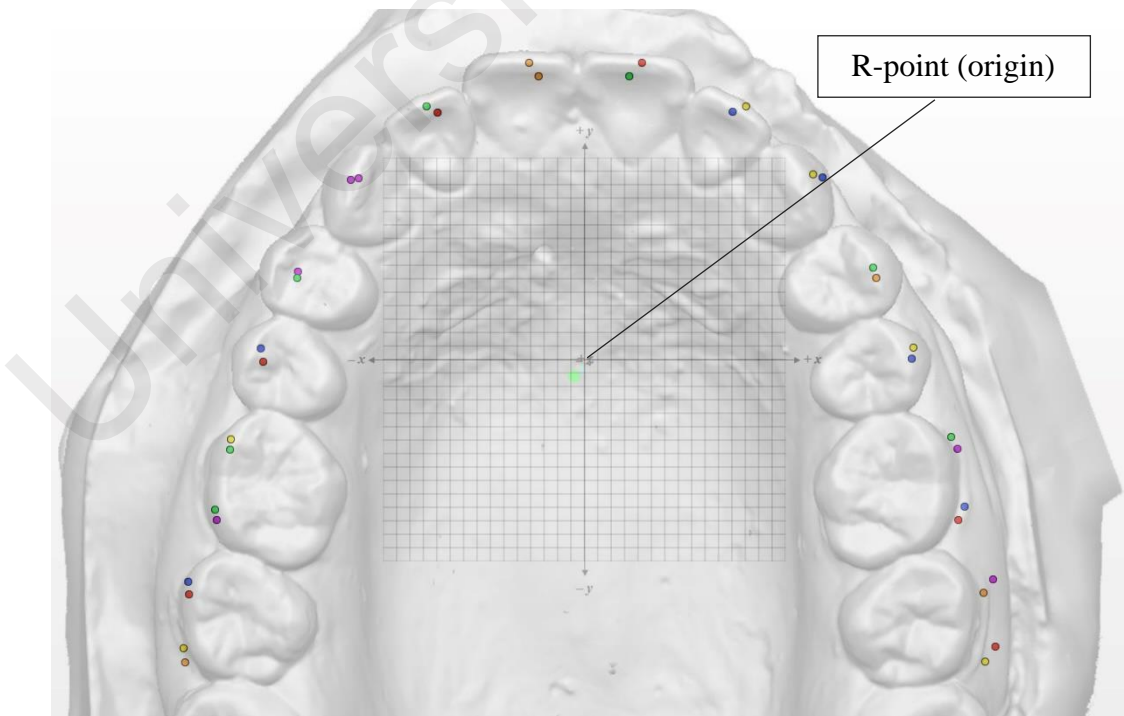


**Figure 4.7: Occlusal view of average predicted 3D tooth position points for edentulous sample compared to dentate sample plotted on Cartesian graph**

#### 4.2.4 Equivalence test results

To confirm that the predicted positions of the teeth for edentulous patients are realistic and within the range of the known natural teeth positions, the predicted values of the coordinates were compared with the measured values of coordinates of the entire dentate sample ( $n = 92$ ) to test whether the predicted values fall within the range limit of the observed teeth positions or not. Statistical equivalence test was performed to test whether or not the radial distances, azimuth angles and elevation angles predicted for edentulous patients were within the equivalent level compared to the dentate sample teeth. Minitab version 15 was used to perform the test. The test is checking the difference between the means of the two samples (mean dentate-mean edentulous). Null hypothesis was as the following:

Difference  $\leq$  lower limit (mean - minimum range of the dentate sample) or

Difference  $\geq$  upper limit (maximum range of the dentate sample – mean).

Assuming equal means, the alternative hypothesis was:

$0 - (\text{mean} - \text{minimum range}) < \text{Difference} < 0 + (\text{maximum range} - \text{mean})$ . In other words, the difference should be between the upper and lower limits.

The boxplots of the 54 equivalence tests (18 tooth points X 3 coordinates) are shown in Appendix G. Each equivalent test had two  $p$ -values produced and the significance level was set to  $\alpha = 0.1$  due to two tails test ( $0.05 * 2$ ). The  $p$ -values were compared to the critical value 0.1 and none of the  $p$ -values of the tests was found greater than 0.1. Hence, through the graphs for the tests and the test coefficient the claim of equivalence was valid in all the tests that compared

teeth positions of dentate sample with the predicted teeth positions for edentulous sample (Appendix G).

When comparing the predicted azimuth angles for edentulous patients to the measured azimuth angles in dentate sample the means and standard deviations of the predicted angle values were found in a range that is bounded within the

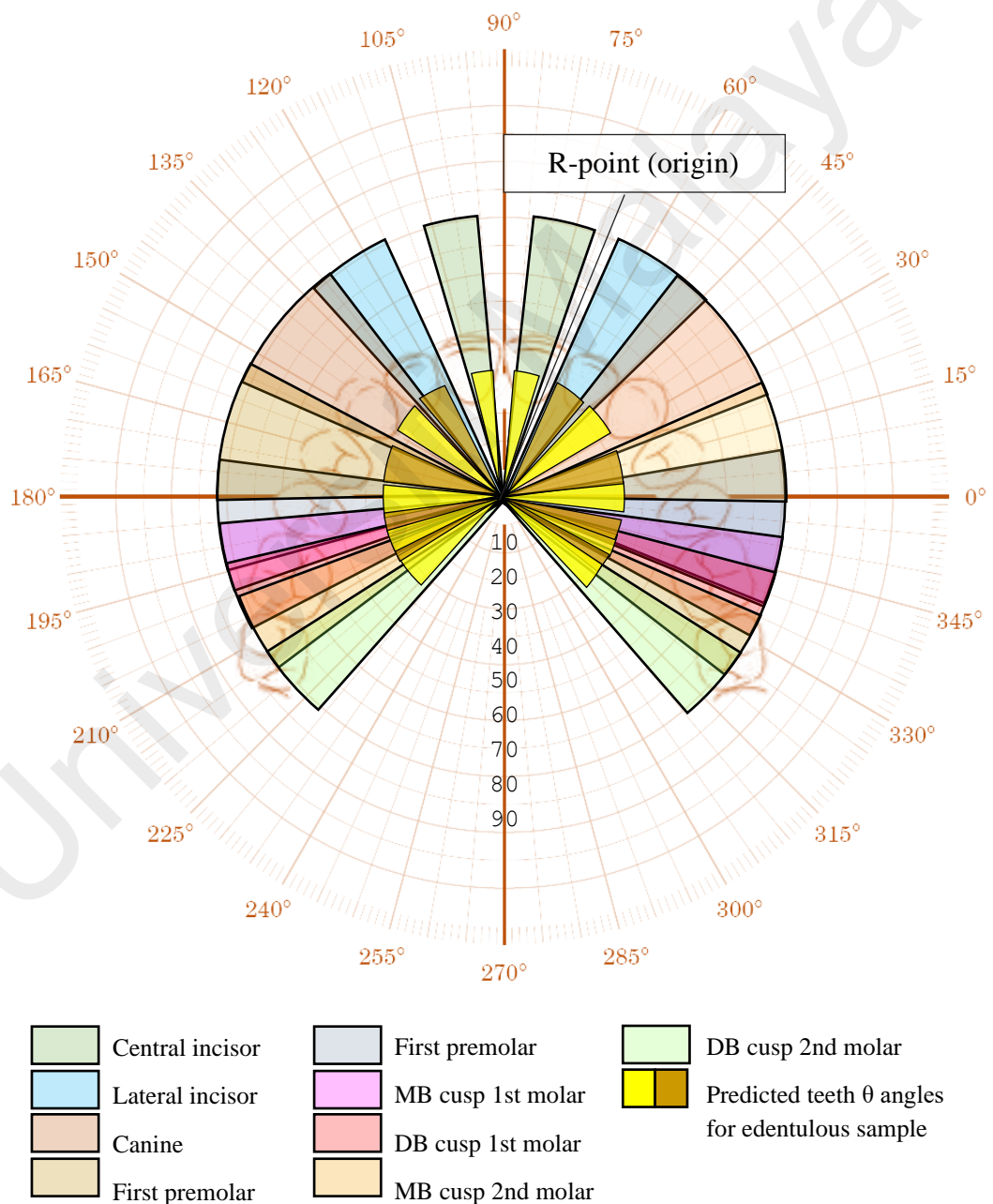


**Figure 4.8: Rose graph showing the range of azimuth angles of the maxillary teeth in dentate sample (n = 92) compared to the range of azimuth angles of the correspondent teeth predicted for edentulous sample (n = 34)**

range of the measured angles of dentate population. Visual representation for the angles is given in a rose graph (Figure 4.8).

#### 4.2.5 Results of integrity of study's digital measurements (error of measurements)

The mean (standard deviation) for the 41 intercanine distances measured by callipers was 35.197 (1.72) mm. When the same distance measured digitally using the 3D coordinates, the mean was 35.197 (1.74) mm.

The table in Appendix F displayed the straight distance measurements in millimetre between the left and right canine tips measured manually by digital calliper and repeated by obtaining the coordinates of the same points from the 3D cast and calculating the Euclidean distance between the points digitally. With relevance to Appendix F, Table 4.20 is disclosed the means and standard deviations of the calipers measured and the computer calculated intercanine distance. When  $p$ -value for paired  $t$ -test is higher than 0.05, it indicated that there is no evidence of significant difference between the two measurements. Therefore the computer calculated measurements can be safely used in the study testing the hypothesis suggesting difference between the two readings.

**Table 4.20: Means (standard deviations) and paired  $t$ -test value for the digital and manual measurement on Error! Reference source not found.**

Digital 3D		Manual		
Mean(mm)	SD	Mean(mm)	SD	$p$ -value
35.197	1.74	35.197	1.72	0.993

\*Paired  $t$ -test  $p = 0.99$  is indicating that there is no enough evidence to conclude that the means differ at the 0.05 level of significance. Null hypothesis of difference between the two means rejected.

### 4.3 Results of maxillary dental arch curve reconstruction

#### 4.3.1 Verification results

Appendix H listed the 4th degree polynomial equations for each dental cast tested.

The results of the Z-tests (Z values) testing the null hypothesis assumption “No significant difference between the forms of the compared curves” were found in the following tables:

#### 4.3.2 The comparison between the forms (form similarity test)

Ranges of Z values and the number of cases that were identified with significance difference in comparison in the form of the palatal curve (T<sub>0</sub>) and buccal central and lingual curves for the entire dentate sample using z-test are shown in Table 4.21.

**Table 4.21: Summary statistics of one sample z-test comparing the difference in the dentate sample between the palatal curve (T<sub>0</sub>) and buccal (T<sub>1</sub>), central (T<sub>2</sub>) and lingual (T<sub>3</sub>) dental arch curves by Z<sub>1</sub>, Z<sub>2</sub> and Z<sub>3</sub> respectively (n = 92)**

Z test value	Range of  Z  calculated	No. cases with significant difference (Z > 1.96)
Z <sub>1</sub> (T <sub>0</sub> VS T <sub>1</sub> )	0.01 – 2.88	7
Z <sub>2</sub> (T <sub>0</sub> VS T <sub>2</sub> )	0.00 – 2.32	1
Z <sub>3</sub> (T <sub>0</sub> VS T <sub>3</sub> )	0.00 – 1.83	0

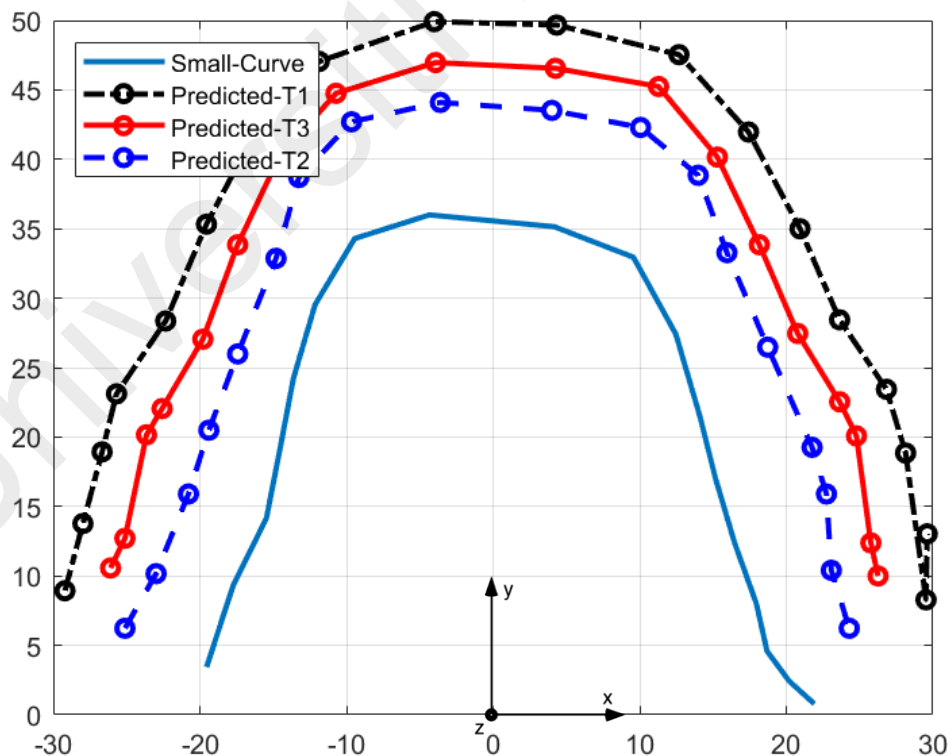
Critical value for 0.05 level is 1.96 was compared to z values; therefore, the null hypothesis (H<sub>0</sub>) can be rejected at 5% level if  $|z| > 1.96$

Comparing the output of the polynomial functions fitting the curves of the arch and the palatal curve, Z test results showed not enough evidence to claim difference between the form of the palatal cusps dental arch (T<sub>3</sub>) and the palatal curve (HNR-curve) in the entire sample tested.

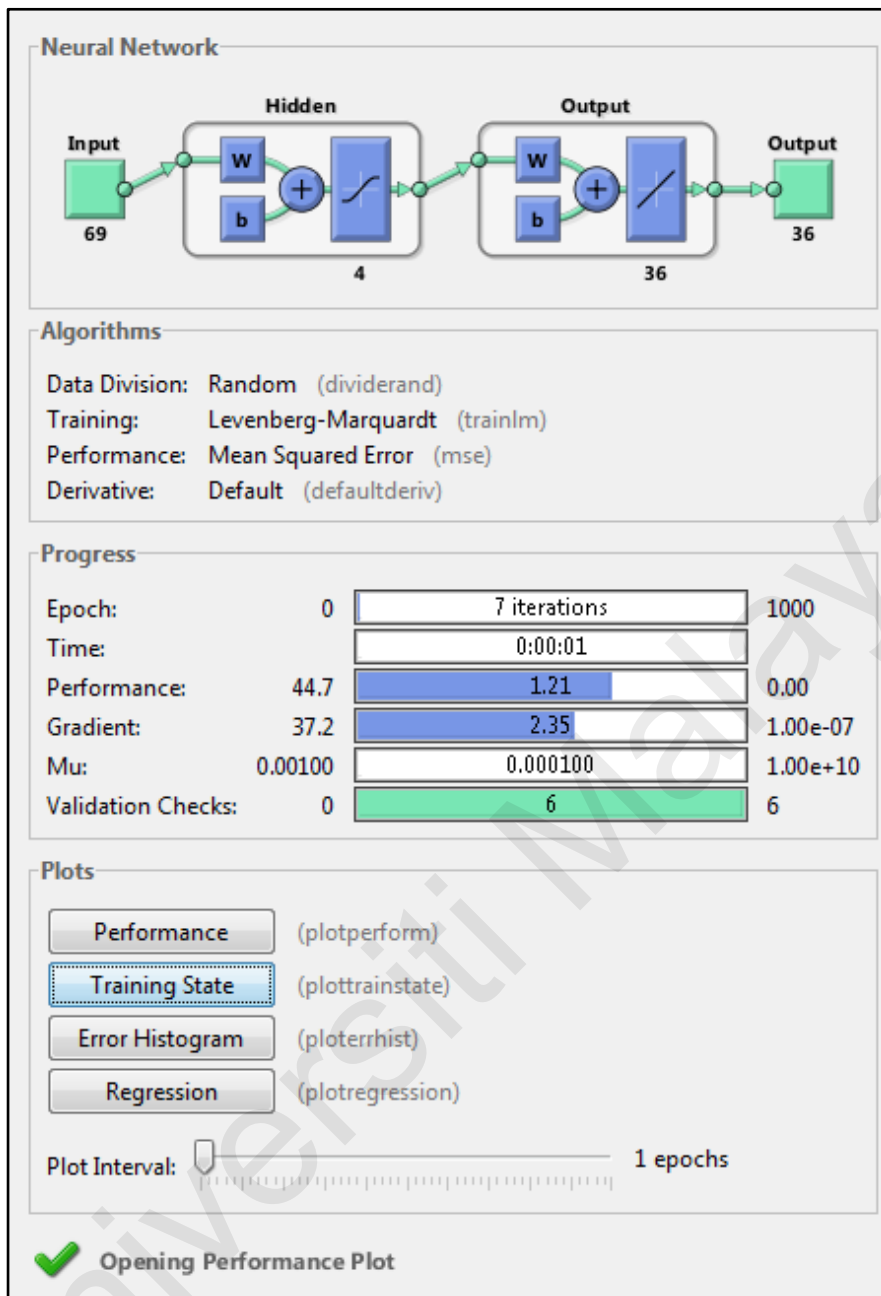
### 4.3.3 Prediction of dental arch curve based on palatal curve

Figure 4.9 shows the prediction of dental arch curve based on the palatal curve following ANN training.

Detection of the best validation performance is one of the essential steps to develop an algorithm that allows the ANN to predict and suggest the three dental arch curves ( $T_1$ ,  $T_2$  and  $T_3$ ) for a given palatal arch curve ( $T_0$ ) as input. When parameter regularisation was made by tuning the data to 33 coordinates as input points and 18 coordinates as output points representing each curve, it was found that at epoch 4, the mean square error (MSE) was decreased (best value of 0.65). Therefore, epoch 4 was considered as the best validation performance and appropriate for further regression and verification analysis (Figures 4.9, 4.10 and 4.11).



**Figure 4.9: The training data were given to the ANN as 2D coordinates in millimetre: 18 points of HNR curve ( $T_0$ ) as original curve; 18 points of  $T_1$ ; 18 points of  $T_2$  and 18 points for  $T_3$  as target curves**



**Figure 4.10: The neural network training dataset after training completion**

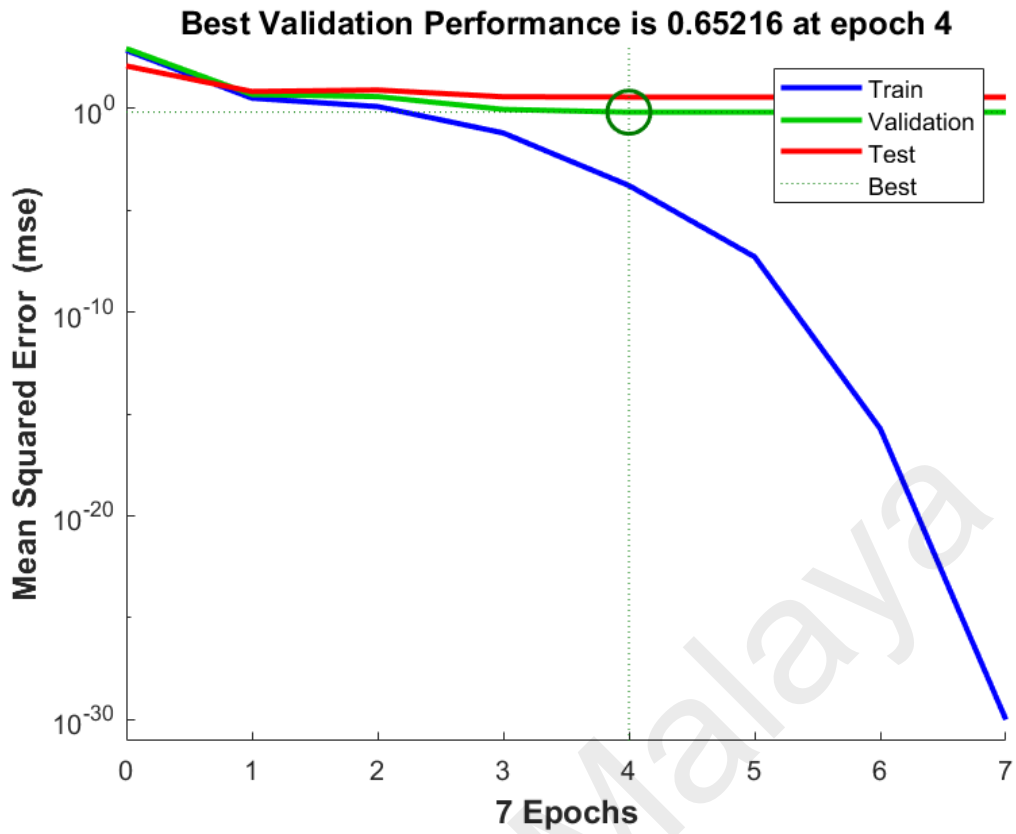
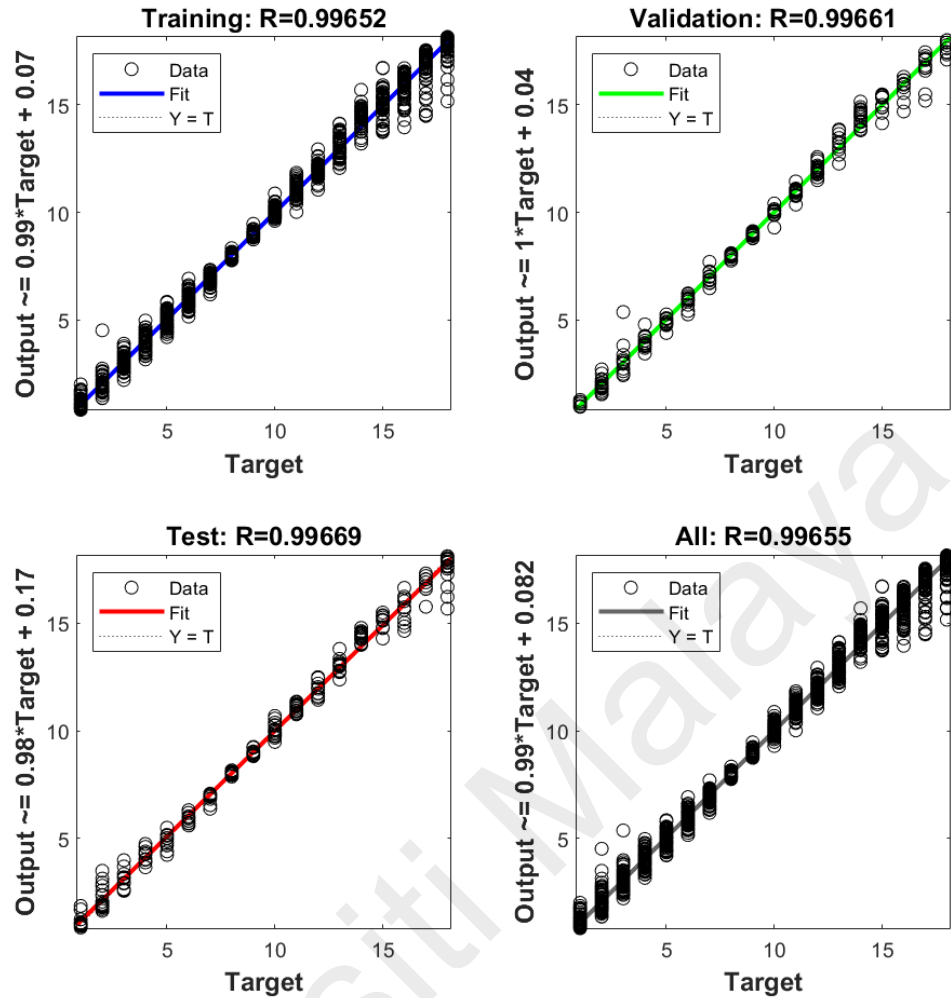


Figure 4.11: Performance plot for ANN with 7 Epochs showing the iteration at which the validation performance reached a minimum MSE as 0.65 at epoch 4



**Figure 4.12: Regression plots of training, validation, testing and total data and fitting lines with coefficients of determinations of the proposed ANN**

Figure 4.12 presented the second processing and analysis stage where the ANN fitted linear regression models as training on the given data and input (blue line), followed by validation test for the fitting models (green line) and finally a test was performed to assure the ANN ability to predict fitting model to the data (red line). The coefficients of determination  $R^2$  value is indicating the strength of relationship between the outputs and targets. If  $R^2 = 1$ , this indicates an exact linear relationship between outputs and targets. If  $R^2$  is close to zero, there is no linear relationship between outputs and targets. The coefficients in this step were found very close to 1 ( $R^2 > 0.98$ ) when the output

curve predicted by the ANN was compared to the target curve given. In other words, the ANN programme code predicted dental arch curves very close to the existing ones in the dentate subjects.

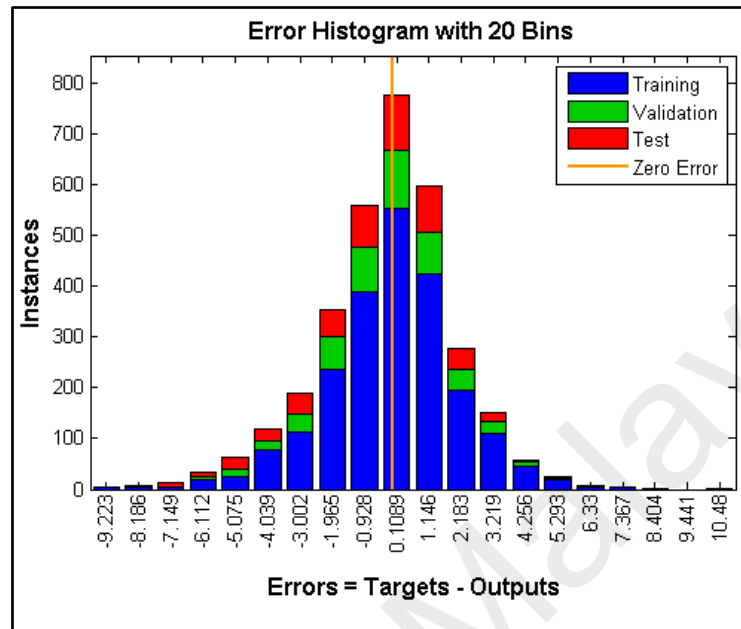


**Figure 4.13: Histogram showing the error instances between the predicted output and the target curves**

Figure 4.13 showed that the instance of having zero error has been increased through fitting the models; starting from training (blue) it was increased in the validation stage (green) and became highest in the testing stage (red).

The ANN predicted the three-target dental arch curves  $T_1$ ,  $T_2$  and  $T_3$  for edentulous casts based on the HNR curve input and the previously machine learnt information. Figure 4.15 displays the plotted HNR curve and the corresponding predicted dental arch curves  $T_1$ ,  $T_2$  and  $T_3$  respectively for edentulous case. The figures A and C are showing better fitting than B (Figure 4.14).

#### 4.3.4 Verification of the dental arch prediction method

As in the first objective, verification of the method is needed to ensure that the ANN code is able to suggest dental arch curves for a given HNR curve that are not different

from the existing dental arch curves of the given dentate cast. This time, the ANN need not have separated quantum of subjects that can investigate the relationship and other subjects to verify. The forms of the dental arch curves predicted by the ANN were compared individually with the corresponding existing dental arch curves of the casts (Figure 4.14).

According to Figure 4.12, the validation  $R^2$  was 0.99661; the dental arch curves were plotted for the validation purpose for the dentate subjects to confirm the reproducibility (Figure 4.14).

Universiti Malaysia

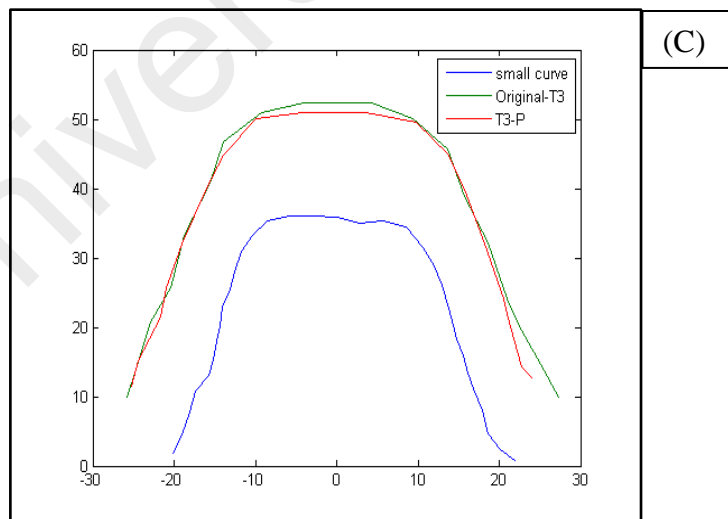
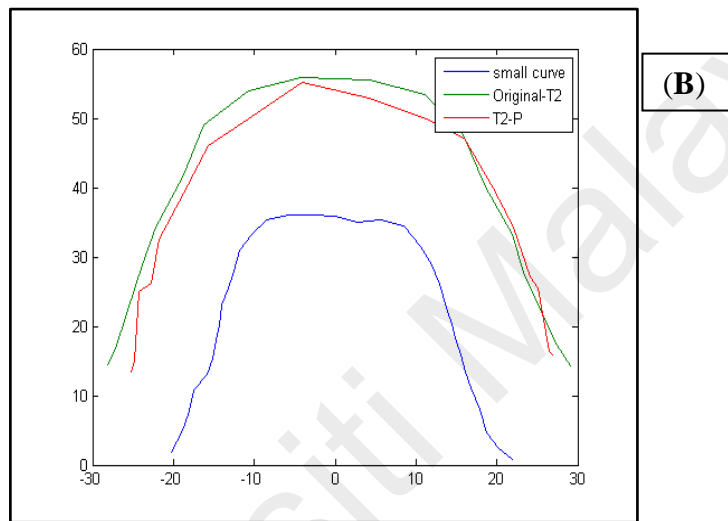
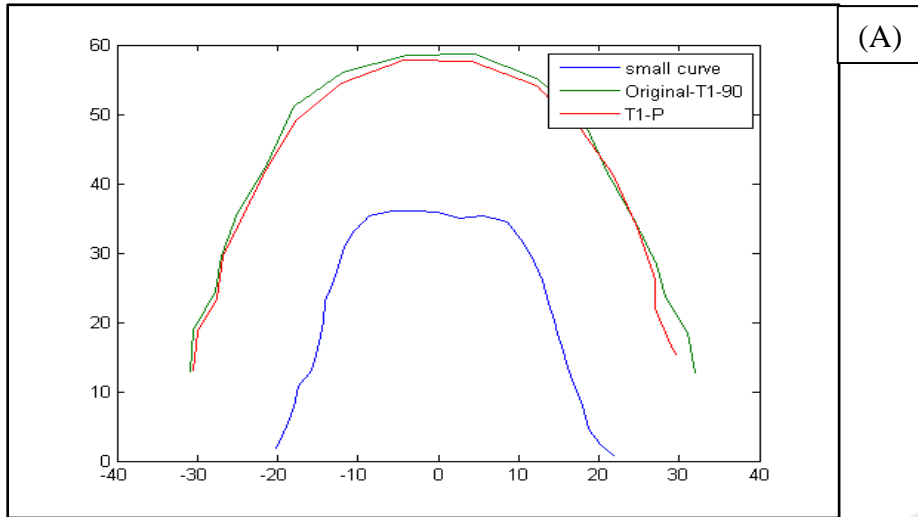


**Figure 4.14: Verification predicted dental arch curves (red) shown in comparison to the (green) actual dental arch curves (A)T<sub>1</sub> buccal cusps curve, (B)T<sub>2</sub> fossae curve and (C)T<sub>3</sub> Palatal cusps curve for dentate subjects predicted using the palatal vault curve, HNR-curve (blue) through the ANN**

### 4.3.5 Application on edentulous casts: prediction dental arch curves for edentulous cast

Figure 4.15 shows the predicted dental arch curves for edentulous cast.

Based on the results explained earlier, input data of edentulous casts' HNR curve

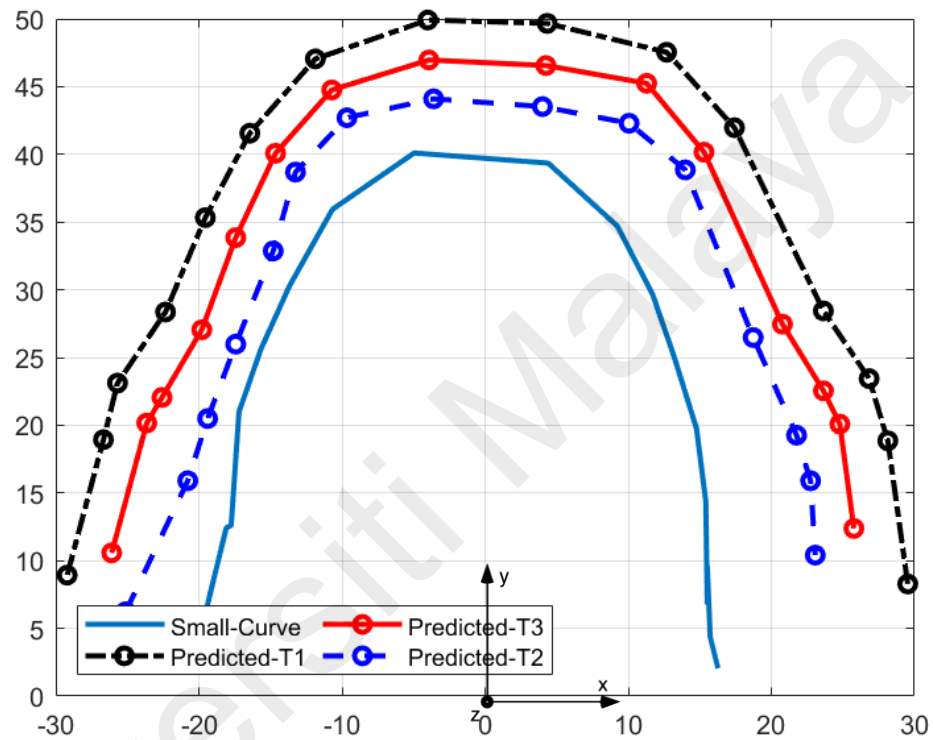


**Figure 4.15: Predicted dental arch curves for edentulous casts by given  $T_0$  curve,  $T_1$ ,  $T_2$  and  $T_3$  were predicted**

composed of coordinates of 18 points was given to the ANN to get the three dental arch curves predicted as shown in Figures 4.15: and 4.16.

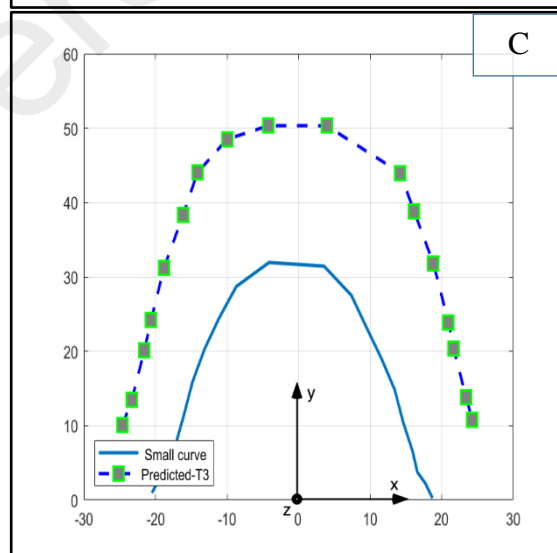
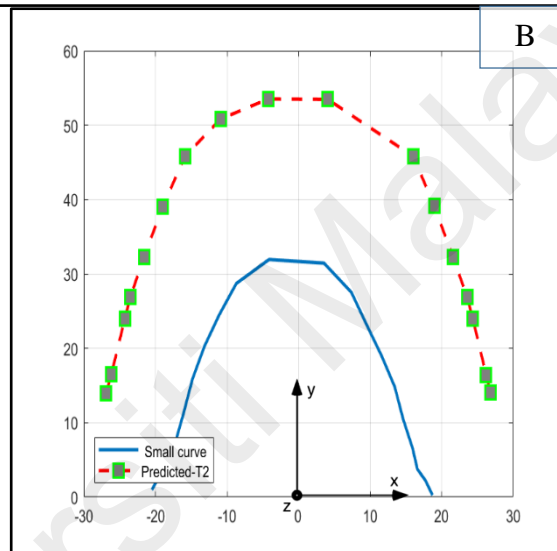
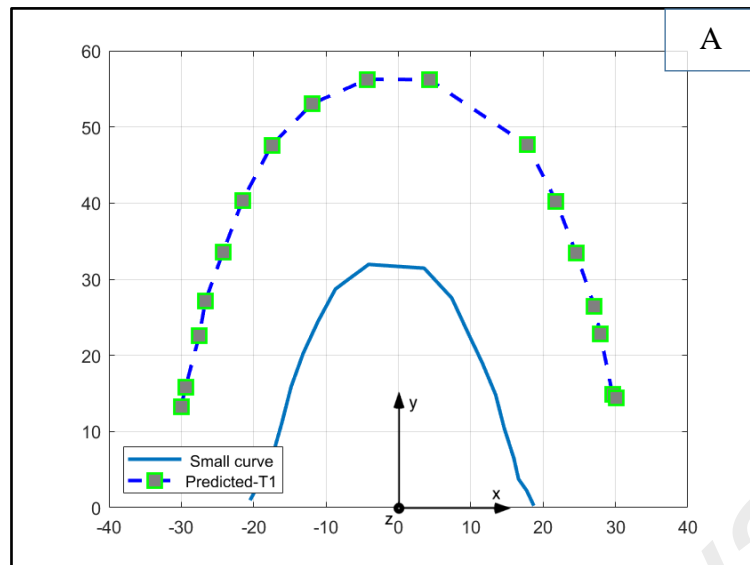


**Figure 4.16: ANN system application to predict dental arch curves for given HNR curve of edentulous cast. (A) predicting the buccal cusps curve  $T_1$ , (B) predicting the central fossae curve  $T_2$  and (C) predicting the lingual cusps curve  $T_3$**

# CHAPTER 5

---

## Discussion

---

Universiti Malaya

## CHAPTER 5: DISCUSSION

Most of edentulous patients would want to apply what dentate patients prefer for their restorations (Stockheimer & Waliszewski, 2012). The literature also showed that most of the currently known biometric guides stemmed from studies analysing dentate subjects' measurements or preferences and applying them on edentulous patients (Devlin & Hoad-Reddick, 2001; Waliszewski, 2005). In alignment with this concept, this study investigated the mathematical and geometrical relationship between the teeth positions as 3D coordinates and selected intraoral landmarks measurements in subjects having not less than full set of intact natural well aligned teeth in the maxillary and mandibular arches. The outcome of mathematical models was verified for the affordability of suggested values to predict teeth positions for given cast by testing the difference in teeth positions between the existing teeth in the dental cast and the predicted ones in an independent dentate sample.

A Few studies investigated the position of posterior teeth such as Watt & MacGregor (1976) and Keshvad et al. (2000). However, majority of the current tooth position guide studies are limited to maxillary central incisors and canines only (Schiffman, 1964; Ehrlich & Gazit, 1975; Lau & Clark, 1993; Amin et al., 2008; Misch, 2008). The positions of all the maxillary teeth were investigated in this study except for the third molars. Hence, the biometric guide in this study may have added value when compared to the existing guides.

In every geometric analysis, proper reference point of the reference plane that can be reliable for the analysis was determined (Hayashi et al., 2003). The

landmarks of HN and R-point area were reported to be very stable and independent of the teeth existence or aging as after 20 palatal sutures become heavily interdigitating, it is impossible to separate the maxillary bone halves without fracturing them (Reardon, 1976).

Determining the artificial teeth optimal positions for edentulous patient is a very crucial and time-consuming process. Within conventional complete denture limitations, the characteristic features of the lip and jaw relationships have made doubtful the likelihood of placing artificial teeth in the position of the natural teeth (Watson & Bhatia, 1989).

Using three-dimensional virtual dental casts and performing the measurements by 3D analysis software allows consistent, precise, and objective measurements that may not be possible using conventional methods. However, identifying a permanent and stable reference plane or reference point to standardise measurements is always the problem for such studies (Hayashi et al., 2003; Park et al., 2007).

This study aimed at investigating the three-dimensional positional relationships between selected intraoral landmarks and tooth position in healthy dentate subjects who have natural well aligned teeth and using these relationships to establish objective biometric guides that can predict with uniqueness the suitable individual tooth position for dentate and edentulous dental arches. This guide is composed of suggested point(s) for each tooth position and an overall dental arch form that can help limit the rotated position of the tooth in the dental arch. Stable landmarks were used to relate the teeth positions in the form of spherical coordinates representing the tooth position. Unlike the Cartesian coordinate system, the spherical coordinate system was

chosen because the elements of this system in three-dimensional space (the radius, azimuth angle and elevation angle) can allow meaningful comparison and analysis in order to predict each element by certain landmarks measurements (Fisher et al., 1993).

### **5.1 The selection of study sample**

The age range of the selected dentate subjects in this study was between 20 and 32 years. Similarly, the age range of subjects in previous studies that investigated biometric guides such as the incisive papilla or other markers to position teeth in denture were not much different from this study. A study by Ehrlich & Gazit (1975) had subjects with age range of 17 to 35 years, Sawiris (1977) had subjects age range between 20 to 35, Mavroskoufis & Ritchie (1981) had 19 to 28 and Park et al. (2007) had subjects with age range of 23 to 26 years. This is further supported by the fact that by the age of 20, full eruption of permanent teeth, complete cranial and palatal development and dental growth has already taken place. The dental arch achieve stability if no crowding or proximal restorations were made. Consequently, highest prevalence of permanent tooth retention among adults are expected (Carter & McNamara, 1998; Jonsson & Magnusson, 2010; Dye et al., 2015).

Having normal occlusion tend to be maintained longitudinally and can represent a role model in teeth positions for complete dentures (Solow & Tallgren, 1976; Dye et al., 2015). This was taken into consideration in this study inclusion criteria where the dentate subjects had naturally well aligned teeth, no temporomandibular disorder, normal class or class I occlusion with no history of extraction, restorations or orthodontic treatment done to the maxillary teeth. Similar criteria of selection with more or less the same

conditions were followed in several previous studies that investigated biometric guides to position teeth (Ehrlich & Gazit, 1975; Fu et al., 2007b; Misch, 2008; Panjwani et al., 2013).

As Malaysia is a multi-racial country, most of the subjects in this study represented the two main races namely the Malay and the Chinese ethnic groups. Both were from the Mongoloid ethnic group (Lu et al., 2017). This criteria for patient selection is in alignment with previous studies conducted in Malaysia (Mahmud, 2016).

## **5.2 Data collection**

As all of the manufacturers' guide were adhered during the impression making and stone casting process, the casts were deemed suitable for digitisation. The dental stone casts were collected and digitised into 3D digital dental casts as this method facilitated the scanning and improved its accuracy (Bootvong et al., 2010; Claus et al., 2018).

Data reading accuracy and repeatability was warranted by repeating the landmarks' identification in the dental cast two times on different occasions and conducting a statistical paired *t*-test to compare the readings obtained. The results showed no difference between the two readings ( $p < 0.000$ ). However, it is to note that testing the variables' measurements repeatability was not essential as all the measurements were calculated mathematically using the computer collected coordinates and mathematical equations to avoid measurement errors.

### **5.3 The variables used in the study**

The variables were measured in three (3) different parameters in this study to represent all the related aspects. Basically, measurements by millimetres were used between the landmarks, while the angles were measured by radians and degrees. In the mathematical analysis, the angles were presented in radians. However, the units of the angles were presented in the figures and tables by degrees for easy understanding and comparison with other studies such as in Runte et al. (2001) and Palaskar et al. (2020). The conversion of the angles was made using Microsoft Excel application.

To justify the validity of measurements used in this study, comparison was made between two measurements for the intercanine distance in randomly selected sample measured digitally using the coordinates and directly using manual digital calliper. Paired *t*-test was used to verify the difference. Appendix F showed the values measured by the two methods and Table 4.20 summarised the paired *t*-test results. The *p*-value was larger than 0.05, therefore it was proper to conclude that the mean difference between the two was measurements was not significantly different from 0.

#### **5.3.1 The landmarks selected for this study analysis**

##### **5.3.1.1 Hamular notches**

Hamular notch is a groove that lies between the maxillary tuberosity and the hamular process of the sphenoid bone on both left and right sides of the maxillary jaw (Rahn et al., 2009). The hamular notches are landmarks that are lifelong stable in position in adulthood regardless of the dentition status,

orthodontic teeth movement, or extraction unless subjected to surgical procedure or injury to its site, the tuberosity or pterygoid hamulus (Kerr et al., 1991; Nelson, 2014).

Hamular notches are well known as prosthodontic landmarks that give posterior limit for the maxillary denture extension and as part of the postdam for the complete dentures and distal extended removable partial dentures (Kolb, 1966). They were also used as landmarks in other applications, mostly for verifying the parallelism between the hamular incisive papilla plane and occlusal plane as it is believed that the virtual plane passes between the hamular notches and the incisive papilla is parallel to the occlusal plane (Cooperman, 1975; Rich, 1982; Fu et al., 2007a). The straight distance between the hamular notches was measured by Rijal et al. (2011) for dental arch dimensional clustering. Among six measurements, the inter-hamular width was measured (Baker et al., 2011) to investigate guides that help in selecting the proper teeth width for edentulous patients.

Baker et al. (2011) also reported the median (standard deviation) of the interhamular width as 41.00(4.4) mm and the straight distance from the left hamular notch to incisive papilla (LHN-IP) and right hamular notch to incisive papilla (RHN-IP) were 52.1(4.5) mm and 52.1(4.3) mm respectively in Caucasian edentulous casts. Similarly, in this study, the mean (standard deviation) of distances between the left and right hamular notches was 45.10(3.2) mm while LHN-IP and RHN-IP were 50.98(4.2) mm and 50.86(3.8) mm respectively. The slight differences can be due to the ethnicity included as dental arch in the Malaysian population was found to be wider than in the Caucasian population (Mohammad et al., 2011) and the overall head shape was

reported rounder in Asian (Mongoloid ethnic) population compared to the Caucasian population studied (Ball et al., 2010).

### **5.3.1.2 Incisive papilla**

Various studies focused on the incisive papilla as a stable and obvious intraoral anatomical landmark (Harper, 1948; Solomon & Arunachalam, 2012). The incisive papilla is considered as the most known and most frequently used landmark for dental cast analysis (Ortman & Tsao, 1979; Grave & Becker, 1987). Majority of studies on teeth positioning investigated the centre of the incisive papilla as a reference point for teeth positioning; others used the anterior part of the papilla or the posterior border of the papilla (Schiffman, 1964; Ehrlich & Gazit, 1975; Mavroskoufis & Ritchie, 1981; Isa & Abdulhadi, 2012). Based on this evidence, the centre of the incisive papilla was used in this study as the reference point in representing the IP position. The incisive papilla was used in standardising the dental cast position to be on a plane parallel to the hamular invasive papilla plane and in measuring the straight distance between the papilla and the R-point.

### **5.3.1.3 Rugae lines, midpalatal raphe and rugae point (R-point)**

The rugae lines are claimed to be lifelong stable in shape but not in position or dimensions (Almeida et al., 1995). In adulthood, the third rugae lines seem to be least affected by alterations in dentition if no orthodontic or surgical procedures occurred. However, in orthodontic treated patients, teeth movements may affect the lateral borders of rugae lines (Jang et al., 2009). In

contrast, Watt & Likeman (1974) found that, after teeth extraction, the area near the medial ends of the third and the fourth rugae pairs was the most stable and independent area. Longitudinal studies have confirmed this finding and proven that the area between the medial points of the third rugae lines are the most stable after extraction or orthodontic treatment (Almeida et al., 1995; Bailey et al., 1996; Abdel-Aziz & Sabet, 2001; Jang et al., 2009). The midpalatal suture and midpalatal raphe are identified as stable structures in dentate and edentulous patients regardless of teeth extraction or orthodontic movement (Allen, 1888; Kumar, 2019). Additionally, in partial and complete dentures, the rugae area and midpalatal raphe relief is always recommended whenever possible to avoid applying stress on these tissues and cause irritation or alterations to them (Winkler, 1988; Zarb et al., 2013; Özkan et al., 2018).

Hence this study introduced R-point as the specific and consistent landmark point that lies at the intersection between the midpalatal raphe and the straight line joining the left to right medial points of the third pair of primary rugae lines and it was aligned simultaneously with the line extending from the centre of the incisive papilla perpendicular to the line joining the left and right hamular notches. R-point in this study was similar to the reference point (point A): the midpoint of the line connecting the medial points of the right and left third palatal rugae lines used by Jang et al. (2009). However, R-point in this study was more consistent as it was always located on the midpalatal raphe regardless of being in the middle of the line joining the medial rugae point or not (Figure 3.7). Having one specific and consistent reference point could help to establish as a stable and accurate reference for teeth positions for dentate and edentulous patients.

#### 5.3.1.4 Points representing tooth position

In the literature, various points or landmarks were used to represent a tooth position. For instance, some studies used the mesioincisal angle of central incisors as reference point to determine the position of the central incisor in relevance to incisive papilla (Harper, 1948; Lau & Clark, 1993). Others used the labial surface of the central incisor as the reference (Mavroskoufis & Ritchie, 1981). In this study, the middle of the incisal edge of each incisor was selected to represent the tooth position rather than the incisal angles to minimise the tooth rotation effect and to keep optimum reasonable number of points that represent the dental arch curve for the curve-fitting polynomial equations and to obtain data comparable to that in previous studies (Watson & Bhatia, 1989; AlHarbi et al., 2008). Furthermore, in this study, the positions of all of the maxillary teeth excluding the third molars were investigated whereas the previous studies in the literature, except Watt & Likeman (1974) who investigated the horizontal distance between the teeth and the lingual gingival vestige, selected teeth positions such as the central incisors, the first molars or the canines only (Harper, 1948; Watson & Bhatia, 1989; Devlin & Hoad-Reddick, 2001; Fu et al., 2007a; Fu et al., 2007b).

In this study, two points were used to represent molar, the mesiobuccal and distobuccal cusp-tips were registered and considered in representing the position of each first and second molar tooth on the dental arch. In agreement to that, several dental arch analysis studies considered the molar's two buccal cusps in tooth position representation and had 18 points for teeth similar to this study (Braun et al., 1998; AlHarbi et al., 2008; Ardzijauskaitė, 2009; Akyalcin et al., 2011).

#### **5.4 Tooth position determination for dentate and edentulous arch**

Currently available biometric guides for complete dentures are indicating the positions of few teeth only and offering only observation average values from clinical cases such as the average horizontal distance from the centre of IP to the labial surface of central incisor tooth (Hickey et al., 1962; Waliszewski, 2005). According to Shaughnessy et al. (2000), many studies have fallen in a common misunderstanding when considering the statistical significance in the data as a power of relationship between the variables regardless of the power of the relationship or correlation itself. The confusion between the relationship strength and relationship importance have made the interpretations incorrect. This study attempted to find more reliable guides to determining the teeth positions in 3D based on more robust analyses.

As it is known that the human body is always in harmony in dimensions (Abu-Taieh & Al-Bdour, 2018), the oral structures, arch dimensions and teeth sizes are not an exception to this rule (Smith et al., 2000; Park et al., 2017). In this study, the positions of the teeth in reference to R-point were investigated as three separate coordinates that collectively offer the 3D position of the teeth. Anatomical measurements between landmarks in dental cast were believed to have a relationship with the position on the teeth in the dental arch.

In Table 4.1, the Cartesian coordinates' mean and standard deviation values of the selected maxillary anatomical landmarks used in this study were listed. The selection of the landmarks IP, LHN, RHN and R-point as predictors was made as the author believes that these palatal vault landmarks are representing the dimensions of the basal bones of the maxillary arch: the anteroposterior distance between the IP and the hamular notches represents the length of the

arch, the distance between the left and right hamular notches represents the width of the arch and the depth of the vault was represented by the depth of HNIP plane from R-point. In order to be able to compare the casts directly, visualise and describe the mean positions of the teeth and investigate the relationships between the measurements and landmark positions and the teeth positions, the dental casts had to be aligned in standardised manner before collecting any of the coordinates or measuring any value. When the digital dental casts were aligned in the Cartesian coordinates system in a standardised manner, the landmarks had standardised coordinates as they were aligned with the basic axes of the system; all the casts had the same Cartesian origin (0, 0, 0) in R-point and any landmarks had the same coordinates such as the  $z$  coordinates of the IP, LHN and RHN points were made parallel to the XY plane as described in chapter 3. The standardised coordinates of the landmarks have made it impossible to investigate and derive the tooth coordinates from landmarks' measurements. Thus, converting the Cartesian coordinates to spherical coordinates allowed the study to investigate the relationship between the coordinates and the predictor variables. Although the Cartesian and spherical coordinates are simply exchangeable systems, the value of affordability to analyse the spherical coordinates in this research have made the conversion valid.

In Tables 4.3 and 4.4, the descriptive statistics of the spherical coordinate for the landmarks used in the study were displayed. As the coordinates are composed of two angles and one distance for each point, these coordinates are representing measurable values such as distance or angle that can be unique for each tooth and its relationship to other parameters can be investigated.

In Figures 4.3 and 4.6, the curve of Spee can be noticed in the alignment of the teeth positions in reference to the origin. In a similar study, Fu et al. (2007b) measured the 3D distance of the maxillary anterior teeth with reference to IP as origin; they have only described the average horizontal distance between the centre of IP and the incisal edges of the studied teeth. HNIP plane was used as a reference for presenting the vertical distance of the teeth on the dental arch.

Figures 4.1, 4.2 and 4.3 present the average points of teeth positions in 3D Cartesian space in the dentate and Figures 4.5, 4.6 and 4.7 present the same earlier coordinates compared to the average points of predicted coordinates for edentulous subjects. The vertical difference between the mean dentate and edentulous points in Figure 4.6 is justified by the difference in average values of the predictors in the edentulous sample compared to the values of predictors in the dentate sample because the predicted positions of teeth for edentulous were found equivalent and within the range of the natural teeth. However, if the difference occurs only in vertical dimension, the verification of vertical dimension of occlusion is a standard step in the conventional and digital complete denture fabrication using other aiding means before issuing any denture (Yilmaz et al., 2017).

Pearson correlation tests were performed to investigate the potential between the predictors represented by the radial distances or distance from origin (R-point) of the biometric triangular pyramid points (IP-ℓ, LHN-ℓ, RHN-ℓ, HNIP-height) and the radial distances of the 18 points of teeth in this investigation part. This was done based on two factors, namely the Pearson coefficient value and the VIF. Table 4.5 shows some instances with weak correlation coefficient (less than 0.5) between the tested variables

such as the correlation between the radial distance of left hamular notch (LHN- $\ell$ ) and the radial distance of left first premolar (L1PM  $\ell$ ) having coefficient of 0.01. In other instance, the weakness was due to high variance inflation factor (VIF) found in the analysis indicating unreal relationship such as in correlation between the same predictor (LHN- $\ell$ ) and left central incisor radial distance (LCI  $\ell$ ). When the VIF was found acceptable (less than 1) and the correlation coefficient higher than 0.5, the correlation was considered strong.

The correlations in Table 4.5 were used as markers to indicate whether or not regression analysis can take place and make meaningful regression relationship analysis. Some of the  $p$ -values show significant correlations while others did not. Table 4.6 was designed to describe conclusive summary of Table 4.5 where a check-mark (✓) was placed in correspondence to the strong correlations found between the variables in the table. Some variables showed single and some showed multiple positive correlations which can be investigated in the next level of relationship investigation such as regression analysis.

In Table 4.7 and Table 4.8, the single and multiple regression equations are presented along with their corresponding values of coefficient of determination  $R^2$  and the variation inflation factor for each equation. The closer the  $R^2$  to 1, the stronger the relationship or fitting regression line suggested. All the values found of  $R^2$  were larger than 0.94 in anterior teeth and 0.89 for posterior teeth. Earlier studies that attempted to determine relationship between teeth positions and rugae lines, did not perform verification to the models, did not check the presence of multicollinearity and reported very weak coefficient of determination ( $R^2$  ranged between 0.04 and 0.23) as significant although they

had not shown practical application (Shaughnessy et al., 2000; Panjwani et al., 2013). In this study, the regression models that had VIF larger than 4 were investigated, the predictor variable that had no effective impact on the model was removed from the regression model before models were finalised to the setting listed in Tables 4.7 and 4.8. Multiple regression models with high coefficient of determinations could be considered as strong relationship models for prediction only if the standard assumptions (SA1 – SA6) and requirements for proper application of regression analysis were followed judiciously and the absence of multicollinearity of the predictors was verified in the models.

Strong coefficients of determination in the regression models can be justified if experimental verification was applied and mathematical test conducted to attest the accuracy of model's prediction. Therefore, a new group of 22 dentate subjects were randomly selected off the overall dentate population in the study under the same criteria of inclusion to help in the verification part of the study. The independent variables in the required regression models (biometric triangular pyramid) were taken from the verification subjects to fit in the regression models and predict radial distance coordinates for the maxillary teeth. These coordinates were then compared with the existing natural teeth coordinates. Tables 4.9 and 4.10 exhibited the mean, *SD* of the spherical coordinates of the biometric triangular pyramid and teeth points of the verification group respectively. In Table 4.11, the predicted radial coordinates for the verification group were listed in the first column against the corresponding real coordinates and the paired *t*-test *p*-values for each test. All *p*-values were larger than the critical value (0.05). Therefore, a conclusion can be made stating that the mean azimuth angles predicted by the equations had no significant difference statistically from the mean angles of the

existing teeth in the verification group of dental population studied within the set critical value.

In Tables 4.12 and 4.14, the simple functional linear relationship models that were derived from the control group were listed. The variables used for these models were angular measured by rad units, the data normality, distribution and correlations were tested before making the models. The modular arithmetic ( $\text{mod } 2\pi$ ) was used in the models to regulate all the odd-integer multiples of  $\pi$  in the angles used within  $2\pi$  ( $360^\circ$ ). the functional models were used to predict the circular second and third elements of spherical coordinates, the azimuth ( $\theta$ ) and the elevation angle ( $\varphi$ ) for the verification dentate group casts and the resulted mean values were compared with the corresponding existing measured values found in the natural teeth of the same individuals by paired  $t$ -test. The means and standard deviations of the angles predicted presented in degrees were listed along with the corresponding angles found in the same sample in Tables 4.13 and 4.15 for  $\theta$  and  $\varphi$  respectively. P values of paired  $t$ -tests in all the tests were larger than 0.05, indicating that there was no evidence to conclude significant difference between the difference of mean values and 0 (no evidence to support the null hypothesis suggesting mean difference  $\neq 0$ ).

The intraoral and extraoral guides suggested in the literature for positioning the teeth in dental arch are built on references and landmarks that are lacking long term stability in position after tooth orthodontic movement, wearing denture or extraction and alveolar ridge resorption (Waliszewski, 2005). These guides are also limited to mere average two-dimensional distances observed in certain population and limited only to central incisor (Fu et al., 2007b), canine

(Amin et al., 2008) or first molar (Foley & Latta, 1985). The change in the position of the incisive papilla relative to the stable area of the palate was observed in every case following extraction of the maxillary central incisors and changes in the papilla shape were also found to accompany the loss of these teeth. On average, the papilla moved forward about 1.6 mm (range 0.6 to 2.7 mm) and upwards about 2.3 mm (range 1.3 to 4.0 mm) according to Watt & Likeman (1974). To the best of the author's knowledge, there is no verified three-dimensional statistical guide that suggests the position of all the maxillary teeth for patient based on reliable reference landmarks. This study suggested R-point as the origin to standardise the alignment of the dentate and edentulous digital casts and as the main landmark to relate the teeth positions in 3D; this suggestion has given advantage to this study as the R-point is more stable than other landmarks because the area of R-point is in the relief zone off the denture stress sites and the area between the medial points of the third rugae lines have been reported as the most stable areas in the hard palate throughout longitudinal studies (Watt & Likeman, 1974; Jang et al., 2009).

#### **5.4.1 Determination of teeth positions for edentulous sample**

Having the regression and functional models established and verified would justify a further step in predicting artificial teeth positions for edentulous casts using the biometric triangular pyramid as predictors in the verified models. the application sample of the 34 edentulous subjects. Table 4.16 projected the means and *SD* for the spherical coordinates of the biometric triangular pyramid points of the edentulous sample. Referring to the fact that the edentulous casts are only having this information available, prediction of teeth would be made and compared to overall dentate range or teeth positions to test whether or not

the predicted teeth are within logical and normal range using equivalence test. Table 4.17 showed the means and *SD* of the spherical coordinates for the predicted teeth positions for edentulous sample, in order to directly compare and plot the predicted coordinates on virtual platform versus the natural teeth in dentate sample, Tables 4.18 and 4.19 were made to show the Cartesian coordinates version of the predictors and predicted points related to edentulous sample. Figures 4.5 - 4.7 were plotted to visually explore the means of predicted teeth for edentulous patients in Cartesian system along with the means of coordinates of the overall dentate sample ( $n = 92$ ). The URL in page 189 was provided to enable interactive 3D supportive projection.

The edentulous sample was collected to serve as the research testing group on which the verified mathematical models were applied to predict reconstruction measures for them. Applying the studied theories on edentulous cases was the ultimate objective of the study as the edentulous patients were the target in this study. Finally, the aim was to confirm that the predicted values for edentulous cases are falling within acceptable margin of error when compared to the values observed in dentate population. This final confirmation was conducted as there is a lack of benchmark or control to be compared with edentulous cases; only with that confirmation, application on edentulous cases can safely be offered as a reasonable outcome.

#### **5.4.2 The current CAD/CAM complete denture systems and their method for teeth selection**

When the technology for fabricating CAD/CAM dentures emerged, many challenges arose and hindered fast growth and progress of the industry. Recently, the maxillo-mandibular relationship recording visit time has been

improved and shortened as a single procedure by aligning the scans of edentulous maxillary and mandibular arches (Russo et al., 2019; Russo et al., 2020a, 2020b).

Digital impression using intraoral scans for removable dentures has been improved and no significant difference was shown when compared to the conventional impressions (Russo et al., 2020c).

Techniques for recording and deciding the vertical dimension of occlusion and fitting denture surfaces have been improved to a level that suits the rapidity and precision required in the CAD/CAM denture industry (Russo & Salamini, 2018; Steinmassl et al., 2018)

To the best knowledge of the researcher, the nine available CAD/CAM complete denture systems are still following the previously known simple biometric guides for determining teeth position. The weakness and limitations of the suggested two-dimensional guidelines were stressed in the literature review chapter. The CAD/CAM systems are in need of robust three-dimensional guides that can automatically predict the teeth positions in information level that are compatible with the three-dimensional printers and variance that can accommodate individuality of the prosthesis. This study investigated the biometric guides that produce the coordinates for the teeth for a given dentate or edentulous dental cast.

## **5.5 Reconstructing the maxillary dental arch form**

Although the dental arch form is not constant throughout life, in adulthood, changes in the dental arches will occur at a slower rate with no significant changes throughout adult life unless orthodontic treatment, extensive

restorations or teeth extraction were done (Bishara et al., 1996). The dental arch in young adults who had no treatment or extractions done is in the ideal situation; therefore, investigating the dental arch for this age group would help to predict the ideal dental arch for edentulous patients.

Various methods have been used to reconstruct the dental arch form in various studies. AlHarbi et al. (2008) compared several interpretations and found the fourth-degree polynomial as the most reasonable function to fit the dental arch when the objective is to describe the general smooth curvature of the arch. In this study, polynomial fourth-degree equation was used to fit the dental arch (Appendix H).

Figure 4.4 is displayed the average positions of the angles of the teeth in dentate sample as circular data graphically, each point is representing the mean, the length of the arm represents the number of subjects ( $n = 70$ ) while the width of the arm represents the range of the angle of each tooth respectively. While Figure 4.8 represents the entire sample of dentate subjects ( $n = 92$ ) versus the predicted azimuth angle values for the edentulous patients ( $n = 34$ ) which can show that the means and ranges of the predicted angles are not different from the mean and range of the natural teeth.

The form similarity was tested between each of the dental arches ( $T_1$ ,  $T_2$  and  $T_3$ ) in relation to the HNR curve tests' results represented by  $z$  values, and these results were summarised in Table 4.21.

### **5.5.1 Application on edentulous cases**

Zarb et al. (2013) found existence of similarity between the dental arch form and the form of the palatal vault, where the palatal vault form may give

indication to the original dental arch form. In this research not only was the relationship between the palatal vault form and the dental arch form investigated, reproducibility and effectiveness of the suggested methods were verified on an independent new sample of dentate subjects before application on edentulous sample. Furthermore, the ranges of predicted locations of teeth for edentulous patient were compared to the ranges of the measured locations of the natural teeth through equivalence test. The test showed that the predicted positions of the teeth for edentulous patients in reference to R-point of the edentulous subjects can be considered as equivalent to the measured positions of teeth in relevance to R-point in the dentate subjects Appendix G exhibited the equivalence test graphs for the three elements of the spherical coordinates comparing the predicted values of tooth position for edentulous with the range of the measured values found in the dentate subjects as control. All the predicted values were showing equivalence variables compared to the control (dentate) values that confirms the reality of the expected results for the edentulous within the normal known range of the teeth in humans.

# CHAPTER 6

---

## Conclusions

---

Universiti Malaya

## CHAPTER 6: CONCLUSIONS

### 6.1 Limitations of the study

This study investigated dentate and edentulous subjects with normal class I occlusal and skeletal relationships as models. However, the various occlusal or skeletal relationships may be investigated in future studies.

The edentulous arch may undergo severe resorption that made it impossible to position the teeth in the ideal or original position following this study method.

The study findings are not yet applied in clinical trials as implementation in vivo on dentate or edentulous patient's treatment.

The vertical dimensions and centric jaw relation were not investigated as general consensus is found in the literature on the concepts of recording and retrieving the OVD and CR.

The mandibular arch form and teeth position were not investigated as they should ideally follow the maxillary arch and teeth in various occlusal schemes and occlusal relationships.

The research findings may not help some edentulous cases with resorbed alveolar ridges, abnormality in the palatal mucosa especially in rugae area such as denture-induced hyperplasia or histopathological changes in palatal mucosa, history of extensive trauma or surgery in the palatal area (Figure 6.1). Allen (1889) considered fibrous tumours, over-pressure exerted by denture and nevi as causes of absence of rugae in the palate in some patients.

This study may offer limited help for children and teenagers below 18 who may need rehabilitation. According to Vasilakos et al. (2017), only the medial part of the third rugae lines and a small area on the mid-palatal suture posterior to that were considered stable in longitudinal studies for growing patients and produced accurate, reproducible, and precise results. In this case, predicting the teeth position would only be possible but predicting the form of the dental arch is not, due to the dimensional changes and growing area.

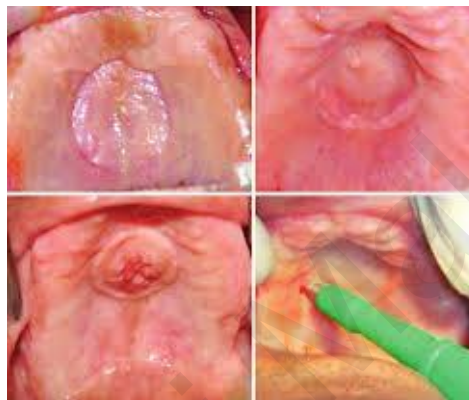


**Figure 6.1: Occlusal view for four cases showing extensive hyperplastic changes in the palatal mucosa. Image taken from Rao et al. (2014)**

## 6.2 Conclusions

Within the limitations of this study, the following conclusions were made:

### 1. In three-dimensional positions of teeth:

- a) In the control dentate group, strong relationships were found between the selected anatomical landmarks' measurements and the 3D positions (as coordinates) of maxillary teeth in relevance to R-point. Some 18 regression equations were concluded to predict the radial coordinate ( $\ell$ ); 18 simple circular relation equations to find the azimuth coordinate ( $\theta$ ) and 18 others for the elevation coordinate ( $\varphi$ ).
- b) The derived equations were verified by predicting teeth positions for the verification dentate group as a new group of dentate subjects and

comparing the predicted teeth positions with the existing positions. No significant difference was found between the predicted and the existing positions of the verification sample's teeth. This led to the conclusion that the relationship equations are having good reproducibility and may give an objective biometric guide for suggesting the teeth positions.

- c) The verified relationships equations were successfully applied to predict positions of artificial teeth for the application group of edentulous casts. The values of predicted teeth positions' coordinates were found mathematically equivalent to the values of the corresponding natural teeth positions' coordinates observed in studied dentate subjects.

## 2. In dental arch form:

- a) Shape similarity was found between the form of the palatal vault curve (HNR curve) and the three dental arch curves in dental cast. However, the lingual ( $T_3$ ) curve showed higher incidence of similarity to the HNR curve.
- b) An artificial neural network (ANN) code was developed, trained, verified on dentate and implemented to predict dental arch curve for edentulous cases using the HNR curve as input. When dental arch form prediction was tested, high reproducibility rates were found and concluded.

### **6.2.1 Summary and potential future benefits of this research**

The determination of dental arch form combined with the 3D teeth positions in the dental arch would complement each other to construct the dental arch that is biometrically suitable for the given cast. Considering the limitations of the study, the study findings may not only benefit prosthodontic rehabilitation

but they can also be used as guides in orthodontic, oral maxillofacial treatment planning (Ho et al., 2016) and forensic dentistry.

In contemporary dental implantology, the planning should be influenced by the desired position of the artificial teeth and the type of definitive prosthesis that suits the patient not by the amount of available bone and the number of implant fixtures that the patient can afford. As widely agreed in dental literature, the best position for the artificial tooth is the natural tooth position; knowing the position of the natural tooth and the dental arch form using the patient's own clinical guide would help in utilising the latest technology such as tissue engineering and guided bone regeneration to plan and decide the number and location of the implant fixtures and amount and direction of the bone to regenerate. This study attempted to provide mapping to suggest the ultimate individualised biometric position of maxillary teeth that can serve best the patient's mouth. The findings of this study may help the prosthodontist, surgeon and orthodontist to plan for their patient's rehabilitation such as the amount and directions of bone or tissue regeneration, the amount and direction of surgical correction needed and the form and dimensions of the lingual orthodontic arch wire that suits the patient in the fastest way and for more efficient outcome.

The type of data produced in this study and the level of accuracy of variables may be of significant help and compatibility with computer related or robotic treatment modalities such as CECD or CAD/CAM prosthodontics. The computerised systems need coordinates for the teeth position and form of dental arch; the three-dimensional coordinates that may suggest teeth positions in close approximation to the original position would facilitate suggesting teeth

positions for given cases better than currently possible. In addition, the predicted teeth positions of this study are derived from the patient's own anatomical features and have been verified on samples before application on edentulous cases and they showed values equivalent to natural teeth positions.

### **6.3 Recommendations for further study**

Implementation of the research concept on patient cases with fixed complete dentures using CAD/CAM technology may be suggested for future study. Testing the clinical trial on cases may necessitate additional improvement to the outcome in future works. Integration with the current established concepts of the CAD/CAM industry could be made to produce a better outcome.

The study sample of this research was composed of Malaysian subjects from Malay and Chinese ethnic background as Malays and Chinese are the largest ethnic groups in Malaysia, making up 50.1% and 22.6% of the population of Malaysia, respectively (Ibrahim & Siri, 2014). Established guides were not tested on other ethnic groups to investigate whether or not it is feasible for them. Different ethnic groups may have different dental arch dimensions and facial proportions that may necessitate establishing new regression models to accommodate the sample of the study.

## REFERENCES

- Abdel-Aziz, H. M., & Sabet, N. E. (2001). Palatal rugae area: A landmark for analysis of pre- and post-orthodontically treated adult Egyptian patients. *Eastern Mediterranean Health Journal*, 7(1-2), 60-66.
- Abu-Taieh, E., & Al-Bdour, H. S. (2018). A human body mathematical model biometric using golden ratio: A new algorithm. *Machine Learning and Biometrics*, 113.
- Adaškevičius, R., & Vasiliauskas, A. (2009). Evaluation of dental arch form using 3D dental cast scanning technology. *Elektronika ir Elektrotechnika*, 93(5), 99-102.
- Adell, R., Lekholm, U., Rockler, B., & Brånemark, P.-I. (1981). A 15-year study of osseointegrated implants in the treatment of the edentulous jaw. *International Journal of Oral Surgery*, 10(6), 387-416.
- Agatonovic-Kustrin, S., & Beresford, R. (2000). Basic concepts of artificial neural network (ANN) modeling and its application in pharmaceutical research. *Journal of Pharmaceutical and Biomedical Analysis*, 22(5), 717-727.
- Akyalcin, S., Erdinc, A. E., Dincer, B., & Nanda, R. S. (2011). Do long-term changes in relative maxillary arch width affect buccal-corridor ratios in extraction and nonextraction treatment? *American Journal of Orthodontics and Dentofacial Orthopedics*, 139(3), 356-361.
- Alhaji, M. N., Khalifa, N., Abduo, J., Amran, A. G., & Ismail, I. A. (2017). Determination of occlusal vertical dimension for complete dentures patients: An updated review. *Journal of Oral Rehabilitation*, 44(11), 896-907.
- AlHarbi, S., Alkofide, E. A., & AlMadi, A. (2008). Mathematical analyses of dental arch curvature in normal occlusion. *The Angle Orthodontist*, 78(2), 281-287.
- AlHelal, A., AlBader, B., Kattadiyil, M., Garbacea, A., & Proussaefs, P. (2016). CAD-CAM implant-supported fixed complete dental prosthesis with titanium milled molars: A clinical report. *The Journal of Prosthetic Dentistry*, 117(4), 463-469.
- AlHelal, A., AlRumaih, H. S., Kattadiyil, M. T., Baba, N. Z., & Goodacre, C. J. (2017a). Comparison of retention between maxillary milled and conventional denture bases: A clinical study. *The Journal of Prosthetic Dentistry*, 117(2), 233-238.
- AlHelal, A., Goodacre, B. J., Kattadiyil, M. T., & Swamidass, R. (2017b). Errors associated with digital preview of computer-engineered complete dentures and guidelines for reducing them: A technique article. *The Journal of Prosthetic Dentistry*, 119(1), 17-25.
- Allen, H. (1888). The palatal rugae in man. *Proceedings of the Academy of Natural Sciences of Philadelphia*, 254-272.

- Almeida, M. A., Phillips, C., Kula, K., & Tulloch, C. (1995). Stability of the palatal rugae as landmarks for analysis of dental casts. *The Angle Orthodontist*, 65(1), 43-48.
- Amin, S. (2010). Mechanical factors and bone health: Effects of weightlessness and neurologic injury. *Current Rheumatology Reports*, 12(3), 170-176.
- Amin, W. M., Taha, S. T., Al-Tarawneh, S. K., Saleh, M. W., & Ghzawi, A. (2008). The relationships of the maxillary central incisors and canines to the incisive papilla in Jordanians. *The Journal of Contemporary Dental Practice*, 9(5), 42-51.
- Araújo, M. G., & Lindhe, J. (2005). Dimensional ridge alterations following tooth extraction. An experimental study in the dog. *Journal of Clinical Periodontology*, 32(2), 212-218.
- Ardzijauskaitė, V. (2009). *Approximation of maxillary arch shape by mathematical functions*. Paper presented at the 2009 IEEE International Workshop on Intelligent Data Acquisition and Advanced Computing Systems: Technology and Applications.
- Atwood, D. A. (1971). Reduction of residual ridges: A major oral disease entity. *The Journal of Prosthetic Dentistry*, 26(3), 266-279.
- Atwood, D. A. (1979). Bone loss of edentulous alveolar ridges. *Journal of Periodontology*, 50(4s), 11-21.
- Atwood, D. A., & Coy, W. A. (1971). Clinical, cephalometric, and densitometric study of reduction of residual ridges. *The Journal of Prosthetic Dentistry*, 26(3), 280-295.
- Bailey, L. T. J., Esmailnejad, A., & Almeida, M. A. (1996). Stability of the palatal rugae as landmarks for analysis of dental casts in extraction and nonextraction cases. *The Angle Orthodontist*, 66(1), 73-78.
- Baker, P. S., Morris, W. J., Lefebvre, C. A., Price, G. A., & Looney, S. W. (2011). Relationship of denture cast measurements to width of maxillary anterior teeth. *The Journal of Prosthetic Dentistry*, 105(1), 44-50.
- Ball, R., Shu, C., Xi, P., Rioux, M., Luximon, Y., & Molenbroek, J. (2010). A comparison between Chinese and Caucasian head shapes. *Applied Ergonomics*, 41(6), 832-839.
- Bansode, S. C., & Kulkarni, M. M. (2009). Importance of palatal rugae in individual identification. *Journal of Forensic Dental Sciences*, 1(2), 77.
- Basker, R. M., Davenport, J. C., & Thomason, J. M. (2011). *Prosthetic treatment of the edentulous patient* (5th ed., pp. 286). West Sussex, UK: Wiley-Blackwell.
- Begole, E. A. (1980). Application of the cubic spline function in the description of dental arch form. *Journal of Dental Research*, 59(9), 1549-1556.

- BeGole, E. A., & Lyew, R. C. (1998). A new method for analyzing change in dental arch form. *American Journal of Orthodontics and Dentofacial Orthopedics*, 113(4), 394-401.
- Bell, R. A. (1978). The geometric theory of selection of artificial teeth: Is it valid? *The Journal of the American Dental Association*, 97(4), 637-640.
- Beresin, V. E., & Schiesser, F. J. (2006). The neutral zone in complete dentures. *The Journal of Prosthetic Dentistry*, 95(2), 93-100.
- Bewick, V., Cheek, L., & Ball, J. (2003). Statistics review 7: Correlation and regression. *Critical Care*, 7(6), 451-459.
- Bhorgonde, D., Nandakumar, K., Khurana, P. R., Kumari, V. S., Reddy, M. S., & Siddique, S. (2014). An evaluation of the position of the neutral zone in relation to the crest of mandibular alveolar ridge: An in-vivo study. *Journal of International Oral Health*, 6(2), 45.
- Bidra, A. S., Farrell, K., Burnham, D., Dhingra, A., Taylor, T. D., & Kuo, C.-L. (2016). Prospective cohort pilot study of 2-visit CAD/CAM monolithic complete dentures and implant-retained overdentures: Clinical and patient-centered outcomes. *The Journal of Prosthetic Dentistry*, 115(5), 578-586.e571.
- Bidra, A. S., Taylor, T. D., & Agar, J. R. (2013). Computer-aided technology for fabricating complete dentures: Systematic review of historical background, current status, and future perspectives. *The Journal of Prosthetic Dentistry*, 109(6), 361-366.
- Biggerstaff, R. (1972). Three variations in dental arch form estimated by a quadratic equation. *Journal of Dental Research*, 51(5), 1509-1509.
- Bilgin, M. S., Baytaroglu, E. N., Erdem, A., & Dilber, E. (2016). A review of computer-aided design/computer-aided manufacture techniques for removable denture fabrication. *European Journal of Dentistry*, 10(2), 286-291.
- Bilgin, M. S., Erdem, A., Aglarci, O. S., & Dilber, E. (2015). Fabricating complete dentures with CAD/CAM and RP technologies. *Journal of Prosthodontics*, 24(7), 576-579.
- Bishara, S. E., Treder, J. E., Damon, P., & Olsen, M. (1996). Changes in the dental arches and dentition between 25 and 45 years of age. *The Angle Orthodontist*, 66(6), 417-422.
- Bissasu, M. (1992). Copying maxillary anterior natural tooth position in complete dentures. *The Journal of Prosthetic Dentistry*, 67(5), 668-669.
- Bissasu, M. (2004). Pre-extraction records for complete denture fabrication: A literature review. *The Journal of Prosthetic Dentistry*, 91(1), 55-58.
- Bootvong, K., Liu, Z., McGrath, C., Hägg, U., Wong, R. W. K., Bendeus, M., & Yeung, S. (2010). Virtual model analysis as an alternative approach to plaster model

analysis: Reliability and validity. *European Journal of Orthodontics*, 32(5), 589-595.

- Boronat, A., Carrillo, C., Peñarrocha, M., & Peñarrocha, M. (2010). Dental implants placed simultaneously with bone grafts in horizontal defects: A clinical retrospective study with 37 patients. *International Journal of Oral & Maxillofacial Implants*, 25(1), 189-196.
- Braun, S., Hnat, W. P., Fender, D. E., & Legan, H. L. (1998). The form of the human dental arch. *The Angle Orthodontist*, 68(1), 29-36.
- Buduru, S., Gulei, D., Zimta, A.-A., Tigu, A., Cenariu, D., & Berindan-Neagoe, I. (2019). The potential of different origin stem cells in modulating oral bone regeneration processes. *Cells*, 8(1), 29.
- Carter, G. A., & McNamara, J. A. (1998). Longitudinal dental arch changes in adults. *American Journal of Orthodontics and Dentofacial Orthopedics*, 114(1), 88-99.
- Cassidy, K. M., Harris, E. F., Tolley, E. A., & Keim, R. G. (1998). Genetic influence on dental arch form in orthodontic patients. *The Angle Orthodontist*, 68(5), 445-454.
- Cawood, J., & Howell, R. (1988). A classification of the edentulous jaws. *International Journal of Oral and Maxillofacial Surgery*, 17(4), 232-236.
- Chen, G., Chen, S., Zhang, X. Y., Jiang, R. P., Liu, Y., Shi, F. H., & Xu, T. (2011). Stable region for maxillary dental cast superimposition in adults, studied with the aid of stable miniscrews. *Orthodontics and Craniofacial Research*, 14(2), 70-79.
- Christou, P., & Kiliaridis, S. (2008). Vertical growth-related changes in the positions of palatal rugae and maxillary incisors. *American Journal of Orthodontics and Dentofacial Orthopedics*, 133(1), 81-86.
- Chuck, G. C. (1934). Ideal arch form. *The Angle Orthodontist*, 4(4), 312-327.
- Claus, D., Radeke, J., Zint, M., Vogel, A. B., Satravaha, Y., Kilic, Fatih, . . . Lapatki, B. G. (2018). Generation of 3D digital models of the dental arches using optical scanning techniques. *Seminars in Orthodontics*, 24(4), 416-429.
- Cooperman, H. (1975). HIP plane of occlusion in oral diagnosis. *Dental Survey*, 51(11), 60.
- Craddock, F. (1956). *Prosthetic dentistry: A clinical outline* (3rd ed.). London: Henry Kimpton.
- Cucchi, A., Vignudelli, E., Napolitano, A., Marchetti, C., & Corinaldesi, G. (2017). Evaluation of complication rates and vertical bone gain after guided bone regeneration with non - resorbable membranes versus titanium meshes and resorbable membranes. A randomized clinical trial. *Clinical Implant Dentistry and Related Research*, 19(5), 821-832.

- Currier, J. H. (1969). A computerized geometric analysis of human dental arch form. *American Journal of Orthodontics*, 56(2), 164-179.
- Dayan, C., Guven, M. C., Gencel, B., & Bural, C. (2019). A color stability comparison of conventional and CAD/CAM polymethyl methacrylate denture base materials. *Acta Stomatologica Croatica*, 53(2), 158-167.
- de Mendonça, A. F., Furtado de Mendonça, M., White, G. S., Sara, G., & Littlefair, D. (2016). Total CAD/CAM supported method for manufacturing removable complete dentures. *Case Reports in Dentistry*, 2016, 1-5.
- De Menezes, M., Rosati, R., Baga, I., Mapelli, A., & Sforza, C. (2011). Three-dimensional analysis of labial morphology: Effect of sex and age. *International Journal of Oral and Maxillofacial Surgery*, 40(8), 856-861.
- Devlin, H. (2002). *Complete dentures: A clinical manual for the general dental practitioner* (1st ed.). Berlin: Springer.
- Devlin, H., & Hoad-Reddick, G. (2001). Biological guides to the positioning of the artificial teeth in complete dentures. *Dental Update*, 28(10), 492-495.
- Dielman, T. E. (2001). *Applied regression analysis for business and economics* (3rd ed.). Boston: PWS-Kent.
- Divaris, K., Ntounis, A., Marinis, A., Polyzois, G., & Polychronopoulou, A. (2012). Loss of natural dentition: Multi - level effects among a geriatric population. *Gerodontology*, 29(2), e192-e199.
- Donovan, T. E., Sulaiman, T. A., Oliveira, G. M. S., Bayne, S. C., & Thompson, J. Y. (2019). 13 - Dental Biomaterials. In A. V. Ritter, L. W. Boushell, & R. Walter (Eds.), *Sturdevant's Art and Science of Operative Dentistry* (pp. 453-510). St. Louis: Elsevier.
- Douglass, C. W., Shih, A., & Ostry, L. (2002). Will there be a need for complete dentures in the United States in 2020? *The Journal of Prosthetic Dentistry*, 87(1), 5-8.
- Doundoulakis, J. H., Eckert, S. E., Lindquist, C. C., & Jeffcoat, M. K. (2003). The implant-supported overdenture as an alternative to the complete mandibular denture. *The Journal of the American Dental Association*, 134(11), 1455-1458.
- Draper, N. R., & Smith, H. (2014). *Applied regression analysis* (3rd ed.). New York: Wiley.
- Dryden, I. L., & Mardia, K. V. (2016). *Statistical shape analysis: With applications in R*. Chichester, UK: Wiley.
- Dye, B., Thornton-Evans, G., Li, X., & Iafolla, T. (2015). Dental caries and tooth loss in adults in the United States, 2011-2012. *NCHS Data Brief* (197), 197.
- Ehrlich, J., & Gazit, E. (1975). Relationship of the maxillary central incisors and canines to the incisive papilla. *Journal of Oral Rehabilitation*, 2(3), 309-312.

- Elaskary, A. (2008). *Fundamentals of esthetic implant dentistry*. Berlin: Wiley.
- Emami, E., de Souza, R. F., Kabawat, M., & Feine, J. S. (2013). The impact of edentulism on oral and general health. *International Journal of Dentistry*, 2013.
- Fahmi, F. (1992). The position of the neutral zone in relation to the alveolar ridge. *The Journal of Prosthetic Dentistry*, 67(6), 805-809.
- Feine, J. S., & Carlsson, G. E. (2003). *Implant overdentures: The standard of care for edentulous patients*. Chicago: Quintessence.
- Ferrario, V. F., Sforza, C., Miani, A., Jr., & Tartaglia, G. (1994). Mathematical definition of the shape of dental arches in human permanent healthy dentitions. *European Journal of Orthodontics*, 16(4), 287-294.
- Fish, E. W. (1933). Using the muscles to stabilize the full lower denture. *The Journal of the American Dental Association*, 20(12), 2163-2169.
- Fisher, N. I., Lewis, T., & Embleton, B. J. (1993). *Statistical analysis of spherical data*. Cambridge: Cambridge University Press.
- Foley, P., & Latta, G. (1985). A study of the position of the parotid papilla relative to the occlusal plane. *The Journal of Prosthetic Dentistry*, 53(1), 124-126.
- Fonseca, R. J. (2017). *Oral and maxillofacial surgery: 3-volume set* (3rd ed.). New York: Elsevier.
- Fu, P. S., Hung, C. C., Hong, J. M., & Wang, J. C. (2007a). Three-dimensional analysis of the occlusal plane related to the hamular-incisive-papilla occlusal plane in young adults. *Journal of Oral Rehabilitation*, 34(2), 136-140.
- Fu, P. S., Hung, C. C., Hong, J. M., Wang, J. C., Tsai, C. F., & Wu, Y. M. (2007b). Three-dimensional relationship of the maxillary anterior teeth to the incisive papilla in young adults. *The Kaohsiung Journal of Medical Sciences*, 23(10), 519-525.
- Fujita, K., Takada, K., QianRong, G., & Shibata, T. (2002). Patterning of human dental arch wire blanks using a vector quantization algorithm. *The Angle Orthodontist*, 72(4), 285-294.
- Gali, S. (2020). Digital technology and Artificial Intelligence in prosthodontics. *Journal of Dental & Oro-facial Research* 16(1), 15-19.
- Ganzer, N., Feldmann, I., Liv, P., & Bondemark, L. (2017). A novel method for superimposition and measurements on maxillary digital 3D models: Studies on validity and reliability. *European Journal of Orthodontics*, 40(1), 45-51.
- Gasteiger, J., & Zupan, J. (1993). Neural networks in chemistry. *Angewandte Chemie International Edition in English*, 32(4), 503-527.
- Gonzalez, J. (2014). The evolution of dental materials for hybrid prosthesis. *The Open Dentistry Journal*, 8, 85-94.

- Goodacre, B. J., Goodacre, C. J., Baba, N. Z., & Kattadiyil, M. T. (2018). Comparison of denture tooth movement between CAD-CAM and conventional fabrication techniques. *The Journal of Prosthetic Dentistry*, 119(1), 108-115.
- Goodacre, C. J., Garbacea, A., Naylor, W. P., Daher, T., Marchack, C. B., & Lowry, J. (2012). CAD/CAM fabricated complete dentures: Concepts and clinical methods of obtaining required morphological data. *The Journal of Prosthetic Dentistry*, 107(1), 34-46.
- GPT-9. (2017). The glossary of prosthodontic terms (9th ed.). *The Journal of Prosthetic Dentistry* 117(5S), e1-e105.
- Grave, A. M., & Becker, P. J. (1987). Evaluation of the incisive papilla as a guide to anterior tooth position. *The Journal of Prosthetic Dentistry*, 57(6), 712-714.
- Guldag, M. U., Sentut, F., & Buyukkaplan, U. S. (2008). Investigation of vertical distance between incisive papilla and incisal edge of maxillary central incisors. *European Journal of Dentistry*, 2(3), 161-166.
- Hämmerle, C. H., Jung, R. E., Yaman, D., & Lang, N. P. (2008). Ridge augmentation by applying bioresorbable membranes and deproteinized bovine bone mineral: A report of twelve consecutive cases. *Clinical Oral Implants Research*, 19(1), 19-25.
- Harper, R. N. (1948). The incisive papilla: The basis of a technique to reproduce the positions of key teeth in prosthodontics. *Journal of Dental Research*, 27(6), 661-668.
- Hass, J., Heil, C., & Weir, M. D. (2018). *Thomas' calculus: Early transcendentals* (14th ed.). New York: Pearson.
- Hassan, W. N. W., Othman, S. A., Chan, C. S., Ahmad, R., Ali, S. N. A., & Rohim, A. A. (2016). Assessing agreement in measurements of orthodontic study models: Digital caliper on plaster models vs 3-dimensional software on models scanned by structured-light scanner. *American Journal of Orthodontics and Dentofacial Orthopedics*, 150(5), 886-895.
- Hawkinson, R. T. (2005). A prosthodontic wake - up call: Reaffirming the complete denture, implants alone do not solve the problems: The old principles are still important. *Journal of Prosthodontics*, 14(4), 294-295.
- Hayashi, K., Uechi, J., & Mizoguchi, I. (2003). Three-dimensional analysis of dental casts based on a newly defined palatal reference plane. *The Angle Orthodontist*, 73(5), 539-544.
- Haykin, S. (1999). *Neural networks: A comprehensive foundation* (2nd ed.). Hamilton, Canada: Pearson.
- Hickey, J. C., Boucher, C. O., & Woelfel, J. B. (1962). Responsibility of the dentist in complete dentures. *The Journal of Prosthetic Dentistry*, 12(4), 637-653.

- Hirayama, H. (2019). Digital Removable Complete Denture (DRCD). In F. Tamimi, & H. Hirayama (Eds.), *Digital restorative dentistry: A guide to materials, equipment, and clinical procedures* (pp. 115-136). Cham: Springer.
- Ho, D. C., Li, J., Chang, C. M., Yuan, P., Teichgraeber, J., Gateno, J., & Xia, J. (2016). A new approach of generating object reference frame for maxillary dental arch. *Journal of Oral and Maxillofacial Surgery*, 74(9), e26-e27.
- Hoggan, B. R., & Sadowsky, C. (2001). The use of palatal rugae for the assessment of anteroposterior tooth movements. *American Journal of Orthodontics and Dentofacial Orthopedics*, 119(5), 482-488.
- Huang, S.-J., Chou, T. M., Lee, H. E., Wu, Y. C., Yang, Y. H., Ho, C.-D., & Huang, P.-S. (2004). Exploring the distance between upper central incisor edge and incisive papilla in Taiwanese population. *Taiwan Journal of Oral Medicine Sciences*, 20, 4-10.
- Ibrahim, R. I., & Siri, Z. (2014). *Analysis of mortality trends by specific ethnic groups and age groups in Malaysia*. Paper presented at the AIP Conference Proceedings.
- Infante, L., Yilmaz, B., McGlumphy, E., & Finger, I. (2014). Fabricating complete dentures with CAD/CAM technology. *The Journal of Prosthetic Dentistry*, 111(5), 351-355.
- Isa, Z. M., & Abdulhadi, L. M. (2012). Relationship of maxillary incisors in complete dentures to the incisive papilla. *Journal of Oral Science*, 54(2), 159-163.
- Isa, Z. M., Tawfiq, O. F., Noor, N. M., Shamsudheen, M. I., & Rijal, O. M. (2010). Regression methods to investigate the relationship between facial measurements and widths of the maxillary anterior teeth. *The Journal of Prosthetic Dentistry*, 103(3), 182-188.
- Ismail, Y. H., & Bowman, J. F. (1968). Position of the occlusal plane in natural and artificial teeth. *The Journal of Prosthetic Dentistry*, 20(5), 407-411.
- Jahangiri, L., Devlin, H., Ting, K., & Nishimura, I. (1998). Current perspectives in residual ridge remodeling and its clinical implications: A review. *The Journal of Prosthetic Dentistry*, 80(2), 224-237.
- Jain, A., Sridevi, U., & Kumar, U. V. (2015). Effect of duration of edentulism on neutral zone position in relation to alveolar crest ridge. *Saudi Journal of Oral Sciences*, 2(2), 79.
- Jain, P., & Rathee, M. (2019). *Stability in mandibular denture*. Treasure Island, FL: StatPearls.
- Jammalamadaka, S. R., & Sengupta, A. (2001). *Topics in circular statistics*. Singapore: World Scientific.
- Jan, S.-L., & Shieh, G. (2019). Sample size calculations for model validation in linear regression analysis. *BMC Medical Research Methodology*, 19(1), 54.

- Jang, I., Tanaka, M., Koga, Y., Iijima, S., Yozgatian, J. H., Cha, B. K., & Yoshida, N. (2009). A novel method for the assessment of three-dimensional tooth movement during orthodontic treatment. *The Angle Orthodontist*, 79(3), 447-453.
- Jayachandran, S., Ramachandran, C. R., & Varghese, R. (2008). Occlusal plane orientation: A statistical and clinical analysis in different clinical situations. *Journal of Prosthodontics*, 17(7), 572-575.
- Jazayeri, H. E., Kang S., Masri, R. M., Kuhn, L., Fahimipour, F., Vanevenhoven, R., . . . Tayebi, L. (2018). Advancements in craniofacial prosthesis fabrication: A narrative review of holistic treatment. *The Journal of Advanced Prosthodontics*, 10(6), 430-439.
- Jivraj, S., Chee, W., & Corrado, P. (2006). Treatment planning of the edentulous maxilla. *British Dental Journal*, 201(5), 261-279.
- Jo, W. (1970). The influence of wearing dentures on residual ridges: A comparative study. *The Journal of Prosthetic Dentistry*, 24(2), 137-144.
- Johnson, W. W. (1959). The history of prosthetic dentistry. *The Journal of Prosthetic Dentistry*, 9(5), 841-846.
- Jonsson, T., & Magnusson, T. E. (2010). Crowding and spacing in the dental arches: Long-term development in treated and untreated subjects. *American Journal of Orthodontics and Dentofacial Orthopedics*, 138(4), 384.e381-384.e387.
- Kapur, K. K., Lestrel, P. E., & Chauncey, H. H. (1982). Development of prosthodontic craniofacial standards: Occlusal plane location. *The Journal of Prosthetic Dentistry*, 48(6), 646.
- Kasai, K., Richards, L. C., Townsend, G. C., Kanazawa, E., & Iwasawa, T. (1995). Fourier analysis of dental arch morphology in South Australian twins. *Anthropological Science*, 103(1), 39-48.
- Kassebaum, N. J., Arora, M., Barber, R. M., Bhutta, Z. A., Brown, J., Carter, A., . . . Murray, C. J. L. (2016). Global, regional, and national disability-adjusted life-years (DALYs) for 315 diseases and injuries and healthy life expectancy (HALE), 1990–2015: A systematic analysis for the Global Burden of Disease Study 2015. *The Lancet*, 388(10053), 1603-1658.
- Katagiri, W., Osugi, M., Kawai, T., & Hibi, H. (2016). First-in-human study and clinical case reports of the alveolar bone regeneration with the secretome from human mesenchymal stem cells. *Head & Face Medicine*, 12(1), 5.
- Katsoulis, J., Pazera, P., & Mericske - Stern, R. (2009). Prosthetically driven, computer - guided implant planning for the edentulous maxilla: A model study. *Clinical Implant Dentistry and Related Research*, 11(3), 238-245.
- Kattadiyil, M., Goodacre, C., & Baba, N. (2013). CAD/CAM complete dentures: A review of two commercial fabrication systems. *Journal of the California Dental Association*, 41(6), 407-416.

- Kattadiyil, M. T., & AlHelal, A. (2017). An update on computer-engineered complete dentures: A systematic review on clinical outcomes. *The Journal of Prosthetic Dentistry*, 117(4), 478-485.
- Kattadiyil, M. T., AlHelal, A., & Goodacre, B. J. (2017). Clinical complications and quality assessments with computer-engineered complete dentures: A systematic review. *The Journal of Prosthetic Dentistry*, 117(6), 721-728.
- Kawahata, N., Ono, H., Nishi, Y., Hamano, T., & Nagaoka, E. (1997). Trial of duplication procedure for complete dentures by CAD/CAM. *Journal of Oral Rehabilitation*, 24(7), 540-548.
- Kawai, M., Kataoka, Y. H., Sonobe, J., Yamamoto, H., Inubushi, M., Ishimoto, Takuya, . . . Yamamoto, T. (2018). Non-surgical model for alveolar bone regeneration by bone morphogenetic protein-2/7 gene therapy. *Journal of Periodontology*(0), 1-18.
- Kerr, W., Kelly, J., & Geddes, D. (1991). The areas of various surfaces in the human mouth from nine years to adulthood. *Journal of Dental Research*, 70(12), 1528-1530.
- Keshvad, A., Winstanley, R., & Hooshmand, T. (2000). Intercondylar width as a guide to setting up complete denture teeth. *Journal of Oral Rehabilitation*, 27(3), 217-226.
- Khojasteh, A., Kheiri, L., Motamedian, S. R., & Khoshkam, V. (2017). Guided bone regeneration for the reconstruction of alveolar bone defects. *Annals of Maxillofacial Surgery*, 7(2), 263.
- Kim, J.-T., & Lee, J.-W. (2011). Three dimensional structural analysis between dental arch and basal bone in normal occlusion. *Korean Journal of Orthodontics*, 41(4), 224-236.
- Kim, Y., Oh, T. J., Misch, C. E., & Wang, H. L. (2005). Occlusal considerations in implant therapy: Clinical guidelines with biomechanical rationale. *Clinical Oral Implants Research*, 16(1), 26-35.
- Kojima, T., Sohmura, T., Nagao, M., Wakabayashi, K., Nakamura, T., & Takahashi, J. (2003). A preliminary report on a computer - assisted dental cast analysis system used for the prosthodontic treatment. *Journal of Oral Rehabilitation*, 30(5), 526-531.
- Kolb, H. (1966). Variable denture-limiting structures of the edentulous mouth: Part I. Maxillary border areas. *The Journal of Prosthetic Dentistry*, 16(2), 194-201.
- Kumar, G. S. (2019). *Orban's oral histology and embryology* (15th ed.). Gurgaon: Elsevier.
- Kumar, L. (2014). Biomechanics and clinical implications of complete edentulous state. *Journal of Clinical Gerontology and Geriatrics*, 5(4), 101-104.

- Kutkut, A., Bertoli, E., Frazer, R., Pinto-Sinai, G., Fuentealba Hidalgo, R., & Studts, J. (2018). A systematic review of studies comparing conventional complete denture and implant retained overdenture. *Journal of Prosthodontic Research*, 62(1), 1-9.
- Lam, R. V. (1960). Contour changes of the alveolar processes following extractions. *The Journal of Prosthetic Dentistry*, 10(1), 25-32.
- Lammie, G. (1956). Aging changes and the complete lower denture. *The Journal of Prosthetic Dentistry*, 6(4), 450-464.
- Lammie, G. (1959). The position of the anterior teeth in complete dentures. *The Journal of Prosthetic Dentistry*, 9(4), 584-586.
- Lau, G., & Clark, R. (1993). The relationship of the incisive papilla to the maxillary central incisors and canine teeth in Southern Chinese. *The Journal of Prosthetic Dentistry*, 70(1), 86-93.
- LaVere, A. M., Marcroft, K. R., Smith, R. C., & Sarka, R. J. (1992a). Denture tooth selection: An analysis of the natural maxillary central incisor compared to the length and width of the face. Part I. *The Journal of Prosthetic Dentistry*, 67(5), 661-663.
- LaVere, A. M., Marcroft, K. R., Smith, R. C., & Sarka, R. J. (1992b). Denture tooth selection: An analysis of the natural maxillary central incisor compared to the length and width of the face: Part II. *The Journal of Prosthetic Dentistry*, 67(6), 810-812.
- Lee, S.-W., & Kim, S.-G. (2014). Membranes for the guided bone regeneration. *Maxillofacial Plastic and Reconstructive Surgery*, 36(6), 239.
- Likeman, P. R., & Watt, D. M. (1974). Morphological changes in the maxillary denture bearing area: A follow up 14 to 17 years after tooth extraction. *British Dental Journal*, 136(12), 500-503.
- Ling, J. Y., & Wong, R. W. (2009). Dental arch widths of Southern Chinese. *The Angle Orthodontist*, 79(1), 54-63.
- Linkow, L. I. (1977). *Maxillary implants: A dynamic approach to oral implantology*. New Haven, CT: Glarus.
- Littlewood, S. J., & Mitchell, L. (2019). *An introduction to orthodontics* (5th ed.). New York: Oxford University Press.
- Lorenz, J., Blume, M., Korzinskas, T., Ghanaati, S., & Sader, R. A. (2019). Short implants in the posterior maxilla to avoid sinus augmentation procedure: 5-year results from a retrospective cohort study. *International Journal of Implant Dentistry*, 5(1), 3.
- Lu, T. Y., Kadir, K., Ngeow, W. C., & Othman, S. A. (2017). The prevalence of double eyelid and the 3D measurement of orbital soft tissue in Malays and Chinese. *Scientific Reports*, 7(1), 14819.

- Lundquist, D. O., & Luther, W. W. (1970). Occlusal plane determination. *The Journal of Prosthetic Dentistry*, 23(5), 489-498.
- Lysell, L. (1955). Plicae palatinae transversae and papilla incisiva in man: A morphologic and genetic study. *Acta Odontologica Scandinavica*, 13(Suppl. 18), 5-137.
- MacConaill, M., & Scher, E. (1949). The ideal form of the human dental arcade, with some prosthetic application. *The Dental Record*, 69(11), 285-302.
- MacEntee, M. I., & Walton, J. N. (1998). The economics of complete dentures and implant-related services: A framework for analysis and preliminary outcomes. *The Journal of Prosthetic Dentistry*, 79(1), 24-30.
- Mack, M. R. (1996). Perspective of facial esthetics in dental treatment planning. *The Journal of Prosthetic Dentistry*, 75(2), 169-176.
- Maeda, Y., Minoura, M., Tsutsumi, S., Okada, M., & Nokubi, T. (1994). A CAD/CAM system for removable denture. Part I: Fabrication of complete dentures. *International Journal of Prosthodontics*, 7(1), 17-21.
- Mahmud, A. (2016). National population and family development board (NPFDB), 2016.
- Makzoumé, J. E. (2004). Morphologic comparison of two neutral zone impression techniques: A pilot study. *The Journal of Prosthetic Dentistry*, 92(6), 563-568.
- Markiewicz, M. R., Allareddy, V., & Miloro, M. (2020). *Orthodontics for oral and maxillofacial surgery patient, part II*. New York: Elsevier.
- Masri, R., & Driscoll, C. F. (2015). *Clinical applications of digital dental technology*. Ames, IA: Wiley.
- Mavroskoufis, F., & Ritchie, G. (1981). Nasal width and incisive papilla as guides for the selection and arrangement of maxillary anterior teeth. *The Journal of Prosthetic Dentistry*, 45(6), 592-597.
- May, R., Dandy, G., & Maier, H. (2011). Review of input variable selection methods for artificial neural networks *Artificial neural networks: Methodological advances and biomedical applications*. InTech.
- McGarry, T. J., Nimmo, A., Skiba, J. F., Ahlstrom, R. H., Smith, C. R., & Koumjian, J. H. (1999). Classification system for complete edentulism. *Journal of Prosthodontics*, 8(1), 27-39.
- McLaughlin, J. B., & Ramos, V. (2015). Complete denture fabrication with CAD/CAM record bases. *The Journal of Prosthetic Dentistry*, 114(4), 493-497.
- Mersel, A., & Ehrlich, J. (1981). Connection between incisive papilla, central incisor and rugae canina. *Quintessence International, Dental Digest*, 12(12), 1327-1329.

- Mina, M., Borzabadi-Farahani, A., Tehranchi, A., Nouri, M., & Younessian, F. (2017). Mathematical beta function formulation for maxillary arch form prediction in normal occlusion population. *Odontology*, *105*(2), 229-236.
- Minitab-Blog. (2013). Enough Is Enough! Handling Multicollinearity in Regression Analysis. Retrieved from <http://blog.minitab.com/blog/understanding-statistics/handling-multicollinearity-in-regression-analysis>
- Minitab-Blog. (2016). How to identify the most important predictor variables in regression models. Retrieved from <http://blog.minitab.com/blog/adventures-in-statistics-2/how-to-identify-the-most-important-predictor-variables-in-regression-models>
- Misch, C. E. (2008). Guidelines for maxillary incisal edge position—a pilot study: The key is the canine. *Journal of Prosthodontics*, *17*(2), 130-134.
- Misch, C. E. (2014). *Dental implant prosthetics* (2nd ed.). St. Louis, MO: Mosby.
- Mohammad, H., Hassan, M. I. A., & Hussain, S. (2011). Dental arch dimension of Malay ethnic group. *American Journal of Applied Sciences*, *8*(11), 1061-1066.
- Monteith, B. D. (1985). A cephalometric method to determine the angulation of the occlusal plane in edentulous patients. *The Journal of Prosthetic Dentistry*, *54*(1), 81-87.
- Murray, C. G. (1977). Anterior tooth positions in prosthodontics. *Australian Dental Journal*, *22*(2), 113-119.
- Nag, P. V. R., Sarika, P., Bhagwatkar, T., & Dhara, V. (2020). Angulated implants: A novel concept for the rehabilitation of severe atrophic maxilla with 3 years follow up supported by Finite Element Analysis. *Journal of Osseointegration*, *12*(1), 39-44.
- Nelson, S. J. (2014). *Wheeler's dental anatomy, physiology and occlusion*. St. Louis, MO: Elsevier.
- Nissan, J., Barnea, E., Zeltzer, C., & Cardash, H. (2003). Relationship between occlusal plane determinants and craniofacial structures. *Journal of Oral Rehabilitation*, *30*(6), 587-591.
- Nomura, S., Miura, J., Kaneko, Y., Hoshino, T., & Ishioka, K. (1991). The study on the application of the biometric trays for Japanese edentulous patients. Measurements of the Japanese bucco-lingual breadth of the dentulous alveolar process. *Nihon Hotetsu Shika Gakkai Zasshi*, *35*(4), 789-793.
- Noroozi, H., Nik, T. H., & Saeeda, R. (2001). The dental arch form revisited. *The Angle Orthodontist*, *71*(5), 386-389.
- O'Brien, R. M. (2007). A caution regarding rules of thumb for variance inflation factors. *Quality & Quantity*, *41*(5), 673-690.

- Ohkubo, C., Shimpo, H., Tokue, A., Park, E.-J., & Kim, T. H. (2018). Complete denture fabrication using piezography and CAD-CAM: A clinical report. *The Journal of Prosthetic Dentistry*, *119*(3), 334-338.
- Olofsson, H., Ulander, E. L., Gustafson, Y., & Hörnsten, C. (2018). Association between socioeconomic and health factors and edentulism in people aged 65 and older: A population-based survey. *Scandinavian Journal of Public Health*, *46*(7), 690-698.
- Omar, R. A. (2004). *Maxillary arch dimensions and stock tray design* (Unpublished M. Dent. Sc. thesis, University of Malaya, Kuala Lumpur).
- Ono, M., Oshima M., Ogawa M., Sonoyama, W., Hara, E. S. , Oida, Yasutaka, . . . Hayano, S. (2017). Practical whole-tooth restoration utilizing autologous bioengineered tooth germ transplantation in a postnatal canine model. *Scientific Reports*, *16*(7), 1-11.
- Ortman, H. R., & Tsao, D. H. (1979). Relationship of the incisive papilla to the maxillary central incisors. *The Journal of Prosthetic Dentistry*, *42*(5), 492-496.
- Özkan, Y. K., Evren, B., & Kauffman, A. (2018). Anatomical landmarks and age-related changes in edentulous patients. In Y. K. Özkan (Ed.), *Complete denture prosthodontics: Planning and decision-making* (pp. 3-48). Cham: Springer.
- Palaskar, J. N., Joshi, N., Gullapalli, P., & Shah, P. (2020). Comparative evaluation of sagittal inclination of the occlusal plane with Frankfort horizontal plane in facebow transfers to semiadjustable and fully adjustable articulators. *The Journal of Prosthetic Dentistry*, *123*(2), 299-304.
- Panjwani, B., Cable, C., Flores-Mir, C., & Bhargava, K. (2013). Palatal rugae: A potential reference to determine key anterior maxilla dimensions and tooth positions. *International Journal of Prosthodontics*, *26*(3), 227-229.
- Park, S.-J., Leesungbok, R., Song, J.-W., Chang, S. H., Lee, S.-W., & Ahn, S.-J. (2017). Analysis of dimensions and shapes of maxillary and mandibular dental arch in Korean young adults. *The Journal of Advanced Prosthodontics*, *9*(5), 321-327.
- Park, Y. S., Lee, S. P., & Paik, K. S. (2007). The three-dimensional relationship on a virtual model between the maxillary anterior teeth and incisive papilla. *The Journal of Prosthetic Dentistry*, *98*(4), 312-318.
- Peavy, D. C., Jr., & Kendrick, G. S. (1967). The effects of tooth movement on the palatine rugae. *The Journal of Prosthetic Dentistry*, *18*(6), 536-542.
- Pellacani, G., & Seidenari, S. (1999). Variations in facial skin thickness and echogenicity with site and age. *Acta Dermato-Venereologica*, *79*, 366-369.
- Peroz, I., Leuenberg, A., Haustein, I., & Lange, K.-P. (2003). Comparison between balanced occlusion and canine guidance in complete denture wearers: A clinical, randomized trial. *Quintessence International*, *34*(8), 607-612.

- Petersen, P. E., Bourgeois, D., Ogawa, H., Estupinan-Day, S., & Ndiaye, C. (2005). The global burden of oral diseases and risks to oral health. *Bulletin of the World Health Organization*, 83, 661-669.
- Petre, A., Drafta, S., Stefanescu, C., & Oancea, L. (2019). Virtual facebow technique using standardized background images. *The Journal of Prosthetic Dentistry*, 121(5), 724-728.
- Polzer, I., Schimmel, M., Müller, F., & Biffar, R. (2010). Edentulism as part of the general health problems of elderly adults. *International Dental Journal*, 60(3), 143-155.
- Porwal, A., Satpathy, A., Jain, P., & Ponnanna, A. A. (2016). Association of neutral zone position with age, gender, and period of edentulism. *Journal of Prosthodontics*, 27(3), 232-239.
- Preti, G., Pera, P., & Bassi, F. (1986). Prediction of the shape and size of the maxillary anterior arch in edentulous patients. *Journal of Oral Rehabilitation*, 13(2), 115-125.
- Prithviraj, D. R., Madan, V., Harshamayi, P., Kumar, C. G., & Vashisht, R. (2014). A comparison of masticatory efficiency in conventional dentures, implant retained or supported overdentures and implant supported fixed prostheses: A literature review. *Journal of Dental Implants*, 4(2), 153.
- Qi, X. (2008). *Report of the third national oral health survey in China* (pp. 60-61). Beijing: People's Medical Publishing House.
- Rahn, A. O., Ivanhoe, J. R., & Plummer, K. D. (2009). *Textbook of complete dentures*. Shelton, CT: PMPH.
- Rangarajan, V., & Padmanabhan, T. (2017). *Textbook of prosthodontics*. New Delhi, India: Elsevier.
- Rao, Y., D'souza, M., Porwal, A., Yadav, P., Kumar, S., & Aggarwal, A. (2014). Clinical and histopathological changes in palatal mucosa following two treatment modalities in patients wearing maxillary complete dentures with suction cup. *Contemporary Clinical Dentistry*, 5(2), 150.
- Rapp, B. E. (2017). Vector calculus. In B. E. Rapp (Ed.), *Microfluidics: Modelling, mechanics and mathematics* (pp. 137-188). Oxford: Elsevier.
- Razavi, R., Zena, R. B., Khan, Z., & Gould, A. R. (1995). Anatomic site evaluation of edentulous maxillae for dental implant placement. *Journal of Prosthodontics*, 4(2), 90-94.
- Reardon, T. (1976). *Short term histological changes in the palatal sutures and the periodontal ligaments resulting from rapid palatal expansion in the Rhesus monkey*. (Master of Science, Loyola University, Chicago).
- Resnik, R. (2020). *Misch's contemporary implant dentistry*. St. Louis, MO: Elsevier.

- Rich, H. (1982). Evaluation and registration of the HIP plane of occlusion. *Australian Dental Journal*, 27(3), 162-168.
- Ricketts, R. (1990). *Provocations and perceptions in craniofacial orthopedics: Dental science and facial art/parts 1 and 2* (1st ed.). Denver: Rocky Mountain Orthodontics.
- Rijal, O. M., Abdullah, N. A., Isa, Z. M., Davaei, F. A., Noor, N. M., & Tawfiq, O. F. (2011). *A novel shape representation of the dental arch and its applications in some dentistry problems*. Paper presented at the 2011 Annual International Conference of the IEEE Engineering in Medicine and Biology Society.
- Rumelhart, D. E., Hinton, G. E., & Williams, R. J. (1988). Learning representations by back-propagating errors. *Cognitive Modeling*, 5(3), 1.
- Runte, C., Lawerino, M., Dirksen, D., Bollmann, F., Lamprecht-Dinnesen, A., & Seifert, E. (2001). The influence of maxillary central incisor position in complete dentures on /s/ sound production. *The Journal of Prosthetic Dentistry*, 85(5), 485-495.
- Russo, L. L., Caradonna, G., Salamini, A., & Guida, L. (2020a). Intraoral scans of edentulous arches for denture design in a single procedure. *The Journal of Prosthetic Dentistry*, 123(2), 215-219.
- Russo, L. L., Caradonna, G., Salamini, A., & Guida, L. (2020b). A single procedure for the registration of maxillo-mandibular relationships and alignment of intraoral scans of edentulous maxillary and mandibular arches. *Journal of Prosthodontic Research*, 64(1), 55-59.
- Russo, L. L., Caradonna, G., Troiano, G., Salamini, A., Guida, L., & Ciavarella, D. (2020c). Three-dimensional differences between intraoral scans and conventional impressions of edentulous jaws: A clinical study. *The Journal of Prosthetic Dentistry*, 123(2), 264-268.
- Russo, L. L., Ciavarella, D., Salamini, A., & Guida, L. (2019). Alignment of intraoral scans and registration of maxillo-mandibular relationships for the edentulous maxillary arch. *The Journal of Prosthetic Dentistry*, 121(5), 737-740.
- Russo, L. L., & Salamini, A. (2018). Removable complete digital dentures: A workflow that integrates open technologies. *The Journal of Prosthetic Dentistry*, 119(5), 727-732.
- Sabir, S., Regragui, A., & Merzouk, N. (2019). Maintaining occlusal stability by selecting the most appropriate occlusal scheme in complete removable prosthesis. *Japanese Dental Science Review*, 55(1), 145-150.
- Sagat, G., Yalcin, S., Gultekin, B. A., & Mijiritsky, E. (2010). Influence of arch shape and implant position on stress distribution around implants supporting fixed full-arch prosthesis in edentulous maxilla. *Implant Dentistry*, 19(6), 498-508.

- Salzmann, J. (1955). Review of Lysell, L.: Plicae palatinae transversae and papillae incisiva in man. A morphologic and genetic study. *American Journal of Orthodontics and Dentofacial Orthopedics*, 41, 879-880.
- Sampson, P. D. (1983). Statistical analysis of arch shape with conic sections. *Biometrics*, 411-423.
- Sawiris, M. M. (1977). The role of anthropometric measurements in the design of complete dentures. *Journal of Dentistry*, 5(2), 141-148.
- Scandrett, F. R., Kerber, P. E., & Umrigar, Z. R. (1982). A clinical evaluation of techniques to determine the combined width of the maxillary anterior teeth and the maxillary central incisor. *The Journal of Prosthetic Dentistry*, 48(1), 15-22.
- Scheaffer, R. L., & McClavei, J. T. (1990). *Probability and statistics for engineers* (3rd ed.). Boston: PWS-Kent.
- Scheid, R. C., & Weiss, G. (2017). *Woelfel's dental anatomy* (9th ed.). Philadelphia, PA: Wolters Kluwer.
- Schiffman, P. (1964). Relation of the maxillary canines to the incisive papilla. *The Journal of Prosthetic Dentistry*, 14(3), 469-472.
- Schimmel, M., Genton, L., & McKenna, G. (2019). Masticatory function and nutritional status: Considerations for an ageing population. In A. Mersel (Ed.), *Oral rehabilitation for compromised and elderly patients* (pp. 81-96). Cham: Springer.
- Sellen, P., Jagger, D., & Harrison, A. (1998). Computer-generated study of the correlation between tooth, face, arch forms, and palatal contour. *The Journal of Prosthetic Dentistry*, 80(2), 163-168.
- Sharry, J. J. (1974). *Complete denture prosthodontics* (3rd ed., pp. xvi, 378). New York: McGraw-Hill.
- Shaughnessy, J. J., Zechmeister, E. B., & Zechmeister, J. S. (2000). *Research methods in psychology* (10th ed., pp. 512). Boston: McGraw-Hill.
- Sheikh, Z., Qureshi, J., Alshahrani, M. A., Nassar, H., Ikeda, Y., Glogauer, M., & Ganss, B. (2017). Collagen based barrier membranes for periodontal guided bone regeneration applications. *Odontology*, 105(1), 1-12.
- Shigli, K., Chetal, B., & Jabade, J. (2005). Validity of soft tissue landmarks in determining the occlusal plane. *The Journal of Indian Prosthodontic Society*, 5(3), 139.
- Shillingburg, H. T., Hobo, S., Whitsett, L. D., & Brackett, S. E. (1997). Fundamentals of fixed prosthodontics. *Learning*, 10, 40.
- Shirani, M., Mosharraf, R., & Shirany, M. (2014). Comparisons of patient satisfaction levels with complete dentures of different occlusions: A randomized clinical trial. *Journal of Prosthodontics*, 23(4), 259-266.

- Shuai, Y., Ma, Y., Guo, T., Zhang, L., Yang, R., Meng, Qi, . . . Yan, J. (2018). Dental stem cells and tooth regeneration *Cell Biology and Translational Medicine* (Vol. 3, pp. 41-52). Cham: Springer.
- Smith, S. S., Buschang, P. H., & Watanabe, E. (2000). Interarch tooth size relationships of 3 populations: "Does Bolton's analysis apply?". *American Journal of Orthodontics and Dentofacial Orthopedics*, 117(2), 169-174.
- Solomon, E., & Arunachalam, K. (2012). The incisive papilla: A significant landmark in prosthodontics. *The Journal of Indian Prosthodontic Society*, 12(4), 236-247.
- Solow, B., & Tallgren, A. (1976). Head posture and craniofacial morphology. *American Journal of Physical Anthropology*, 44(3), 417-435.
- Soycan, A., & Soycan, M. (2019). Perspective correction of building facade images for architectural applications. *Journal of Engineering Science and Technology*, 22(3), 697-705.
- Srinivasan, M., Schimmel, M., Naharro, M., O' Neill, C., McKenna, G., & Müller, F. (2019). CAD/CAM milled removable complete dentures: Time and cost estimation study. *Journal of Dentistry*, 80, 75-79.
- Staley, R. N., Stuntz, W. R., & Peterson, L. C. (1985). A comparison of arch widths in adults with normal occlusion and adults with Class II, Division 1 malocclusion. *American Journal of Orthodontics*, 88(2), 163-169.
- Steinmassl, O., Dumfahrt, H., Grunert, I., & Steinmassl, P. A. (2018). CAD/CAM produces dentures with improved fit. *Clinical Oral Investigations*, 22(8), 2829-2835.
- Steinmassl, P.-A., Klaunzer, F., Steinmassl, O., Dumfahrt, H., & Grunert, I. (2017). Evaluation of currently available CAD/CAM denture systems. *International Journal of Prosthodontics*, 30(2), 116-122.
- Stewart, J., Redlin, L., & Saleem, W. (2016). *Precalculus: Mathematics for calculus* (7th ed.). Boston, MA: Cengage Learning.
- Stockheimer, C., & Waliszewski, M. P. (2012). A survey of dentulous and edentulous patient preference among different denture esthetic concepts. *Journal of Esthetic and Restorative Dentistry*, 24(2), 112-124.
- Sun, Y., Lü, P., & Wang, Y. (2009). Study on CAD&RP for removable complete denture. *Computer Methods and Programs in Biomedicine*, 93(3), 266-272.
- Takahashi, K., Kiso, H., Saito, K., Togo, Y., Tsukamoto, H., Huang, B., & Bessho, K. (2013). Feasibility of gene therapy for tooth regeneration by stimulation of a third dentition *Gene Therapy-Tools and Potential Applications*. InTech.
- Taneva, E., Evans, C., & Viana, G. (2017). 3D evaluation of palatal rugae in identical twins. *Case Reports in Dentistry*, 2017, 1-6.

- Tayşi, N. (2010). Application of Neural Network models on analysis of prismatic structures. *Scientific Research and Essays*, 5(9), 978-989.
- Thompson, C. G., Kim, R. S., Aloe, A. M., & Becker, B. J. (2017). Extracting the variance inflation factor and other multicollinearity diagnostics from typical regression results. *Basic and Applied Social Psychology*, 39(2), 81-90.
- Tsai, C. L., Cai, Z., & Wu, X. (1998). The examination of residual plots. *Statistica Sinica*, 8, 445-465.
- Urban, I. A., Nagursky, H., Lozada, J. L., & Nagy, K. (2013). Horizontal ridge augmentation with a collagen membrane and a combination of particulated autogenous bone and anorganic bovine bone-derived mineral: A prospective case series in 25 patients. *International Journal of Periodontics & Restorative Dentistry*, 33(3), 299-307.
- Valenzuela, A., Pardo, M. A., & Yezioro, S. (2001). Description of dental arch form using the Fourier series. *The International Journal of Adult Orthodontics & Orthognathic Surgery*, 17(1), 59-65.
- Van der Weijden, F., Dell'Acqua, F., & Slot, D. E. (2009). Alveolar bone dimensional changes of post - extraction sockets in humans: A systematic review. *Journal of Clinical Periodontology*, 36(12), 1048-1058.
- Vasilakos, G., Schilling, R., Halazonetis, D., & Gkantidis, N. (2017). Assessment of different techniques for 3D superimposition of serial digital maxillary dental casts on palatal structures. *Scientific Reports*, 7(1), 5838.
- Wakabayashi, K., Sohmura, T., Takahashi, J., Kojima, T., Akao, T., Nakamura, Takashi, . . . Maruyama, T. (1997). Development of the computerized dental cast form analyzing system: Three dimensional diagnosis of dental arch form and the investigation of measuring condition. *Dental Materials Journal*, 16(2), 180-190.
- Waliszewski, M. (2005). Restoring dentate appearance: A literature review for modern complete denture esthetics. *The Journal of Prosthetic Dentistry*, 93(4), 386-394.
- Walls, A., & Steele, J. (2004). The relationship between oral health and nutrition in older people. *Mechanisms of Ageing and Development*, 125(12), 853-857.
- Watson, R., & Bhatia, S. (1989). Tooth positions in the natural and complete artificial dentitions, with special reference to the incisor teeth: An interactive on - line computer analysis. *Journal of Oral Rehabilitation*, 16(2), 139-153.
- Watt, D. (1987). Good design, the secret of successful complete denture prostheses. *Nihon Hotetsu Shika Gakkai Zasshi*, 31(6), 1327-1334.
- Watt, D. M. (1978). Tooth positions on complete dentures. *Journal of Dentistry*, 6(2), 147-160.

- Watt, D. M., Durran, C. M., & Adenubi, J. O. (1967). Biometric guides to the design of complete maxillary dentures. *The Dental Magazine and Oral Topics*, 84(3), 109-111.
- Watt, D. M., & Likeman, P. R. (1974). Morphological changes in the denture bearing area following the extraction of maxillary teeth. *British Dental Journal*, 136(6), 225-235.
- Watt, D. M., & MacGregor, A. R. (1976). *Designing complete dentures*. Philadelphia: Saunders.
- Weinberg, L. A. (1958). Tooth position in relation to the denture base foundation. *The Journal of Prosthetic Dentistry*, 8(3), 398-405.
- Welc, J., & Esquerdo, P. J. R. (2017). *Applied regression analysis for business: Tools, traps and applications*. Cham: Springer.
- Werbos, P. J. (1990). Backpropagation through time: What it does and how to do it. *Proceedings of the IEEE*, 78(10), 1550-1560.
- Winkler, S. (1988). *Essentials of complete denture prosthodontics* (2nd ed., pp. xvi, 464). St. Louis, MO: Mosby.
- Yamamoto, S., Kanazawa, M., Iwaki, M., Jokanovic, A., & Minakuchi, S. (2014). Effects of offset values for artificial teeth positions in CAD/CAM complete denture. *Computers in Biology and Medicine*, 52, 1-7.
- Yeh, Y.-L., Pan, Y.-H., & Chen, Y.-Y. (2013). Neutral zone approach to denture fabrication for a severe mandibular ridge resorption patient: Systematic review and modern technique. *Journal of Dental Sciences*, 8(4), 432-438.
- Yilmaz, B., Azak, A. N., Alp, G., & Ekşi, H. (2017). Use of CAD-CAM technology for the fabrication of complete dentures: An alternative technique. *The Journal of Prosthetic Dentistry*, 118(2), 140-143.
- Yoon, S.-J., Wang, R.-F., Hwang, H.-S., Kang, B.-C., Lee, J.-S., & Palomo, J. M. (2011). Application of spherical coordinate system to facial asymmetry analysis in mandibular prognathism patients. *Imaging Science in Dentistry*, 41(3), 95-100.
- Yoon, S.-J., Wang, R.-F., Na, H. J., & Palomo, J. M. (2013). Normal range of facial asymmetry in spherical coordinates: A CBCT study. *Imaging Science in Dentistry*, 43(1), 31-36.
- Yoon, S.-J., Wang, R.-F., Ryu, S.-Y., Hwang, H.-S., Kang, B.-C., Lee, J.-S., & Palomo, J. M. (2014). Use of spherical coordinates to evaluate three-dimensional facial changes after orthognathic surgery. *Imaging Science in Dentistry*, 44(1), 15-20.
- Zarb, G. A., Hobkirk, J., Eckert, S., & Jacob, R. (2013). *Prosthodontic treatment for edentulous patients: Complete dentures and implant-supported prostheses* (13th ed.). St. Louis, MO: Elsevier.

- Zarb, G. A., & Schmitt, A. (1990). The longitudinal clinical effectiveness of osseointegrated dental implants: The Toronto study. Part I: Surgical results. *The Journal of Prosthetic Dentistry*, 63(4), 451-457.
- Zeitlin, B. D. (2020). Banking on teeth: Stem cells and the dental office. *Biomedical Journal*, 43(2), 124-133.
- Zhang, Y.-D., Zhao, Z.-F., Lu, P.-J., Wang, Y., Song, R.-J., & Lu, J.-L. (2002). Robotic system approach for complete denture manufacturing. *IEEE/ASME Transactions on Mechatronics*, 7(3), 392-396.
- Zia, M., Azad, A. A., & Ahmed, S. (2009). Comparison of distance between maxillary central incisor and incisive papilla in dentate individuals with different arch forms. *Journal of Ayub Medical College*, 21(4), 125-128.
- Živković, S., Majstorović, N., Glišić, B., & Kramar, D. (2019). *New improved method of setting the jaw's coordinate system*. Paper presented at the International Conference on Measurement and Quality Control-Cyber Physical Issue.